DOE/ET/10463-T1(Vol.2)

HOT GAS DESULFURIZATION

Volume 2. Use of Gasifier Ash in a Fluidized-Bed Process

Final Report

By
J. Thomas Schrodt

February 1, 1981

Work Performed Under Contract No. AS05-76ET10463

University of Kentucky
Lexington, Kentucky

U. S. DEPARTMENT OF ENERGY

DISCLAIMER

DISCLAIMER

Available from the National Technical Information Service, U. S. Department of Commerce, Springfield, Virginia 22161.

Price: Printed Copy A15
Microfiche A01

DOE/ET/10463-T1(Vol.2)
Distribution Category UC-90c

HOT GAS DESULFURIZATION

II. USE OF GASIFIER ASH IN A FLUIDIZED-BED PROCESS

FINAL REPORT

J. THOMAS SCHRODT

DEPARTMENT OF CHEMICAL ENGINEERING
UNIVERSITY OF KENTUCKY
LEXINGTON, KENTUCKY 40506

February 1, 1981

Prepared for the United States Department of Energy
under Contract No. DE-AS05-76ET05076

ABSTRACT

Three gasifier coal ashes were used as reactant/sorbents in batch fluidized-beds to remove hydrogen sulfide from hot, made-up fuel gases. It is predominantly the iron oxide in the ash that reacts with and removes the hydrogen sulfide; the sulfur reappears in ferrous sulfide. Sulfided ashes were regenerated by hot, fluidizing streams of oxygen in air; the sulfur is recovered as sulfur dioxide, exclusively.

Ash sorption efficiency and sulfur capacity increase and stablize after several cycles of use. These two parameters vary directly with the iron oxide content of the ash and process temperature, but are independent of particle size in the range 0.01 - 0.02 cm. A western Kentucky No. 9 ash containing 22 weight percent iron as iron oxide sorbed 4.3 weight percent sulfur at 1200^{o}F with an ash sorption efficiency of 0.83 at ten percent breakthrough.

A global, fluidized-bed, reaction rate model was fitted to the data and it was concluded that chemical kinetics is the controlling mechanism with a predicted activation energy of 19,600 BTU/lb mol.

Iron oxide reduction and the water-gas-shift reaction were two side reactions that occurred during desulfurization.

The regeneration reaction occurred very rapidly in the

fluid-bed regime, and it is suspected that mass transfer is the controlling phenomenon.

TABLE OF CONTENTS

	Page
ABSTRACT	ii
TABLE OF CONTENTS	iv
LIST OF TABLES	vii
LIST OF FIGURES & GRAPHS	viii
SUMMARY	xii
CHAPTER	1
1 INTRODUCTION	1
1A SCOPE OF THE RESEARCH	6
2 A LITERATURE REVIEW OF HIGH-TEMPERATURE H_2S REMOVAL PROCESSES USING IRON OXIDE BASED SORBENTS	8
2.1 General Discussions	8
2.2 High-Temperature H_2S Removal Processes	10
2.2.1 Iron Oxide Based Processes	11
2.2.1.1 Appleby-Frodingham Process	11
2.2.1.2 Babcock-Wilcox Process	15
2.2.1.3 U.S. Bureau of Mines Process	16
2.2.1.4 Coal Ash Process	28
3 REVIEW OF CHEMISTRY, THERMODYNAMICS AND KINETICS OF THE COAL ASH PROCESS	38
3.1 General Considerations	38
3.2 Chemistry and Thermodynamics of Iron Oxide Processes	40

3.2.1 Iron Oxide Reduction 40
3.2.2 Desulfurization 44

3.2.2.1 Secondary Reactions During Desulfurization 51

3.2.3 Regeneration Reactions 54

3.3 Review of Kinetic Studies 57

3.3.1 Desulfurization 57
3.3.2 Regeneration 64

4 EQUIPMENT AND OPERATING PROCEDURES 66

4.1 Description of Experimental Setup 66

4.2 Procedure 77

4A PRELIMINARY RESULTS 81

5 THEORY OF GAS-SOLID REACTIONS AND REACTION MODELING IN A FLUIDIZED-BED 85

5.1 General Considerations 85

5.2 Single-Particle Reactions 85

5.2.1 Nature of Gas-Solid Reactions 85
5.2.2 Single-Particle Analysis 87

5.2.2.1 Nonporous Particles 88
5.2.2.2 Porous Particles 95

5.3 Gas-Solid Reactions in Fluidized-beds 99

5.3.1 General Considerations 99
5.3.2 Reactor Models 101

5.3.2.1 Pseudo-homogeneous Model 101
5.3.2.2 Unreacted-core Models 108

6 RESULTS AND DISCUSSIONS 112

6.1 Preliminary Fluidization Runs 112

6.2 General Discussion of Process Studies 114

6.2.1 Ash Capacity and Sorption Efficiency Results 118

6.2.1.1 Initial Increase of Capacity and Efficiency of Fresh Ash 123

6.2.1.2 Change in Capacity and Sorption Efficiency of Stabilized Ash Immediately following a Temperature Reduction 127
6.2.1.3 Effect of Process Variables on Capacity of Stabilized Ash 131

6.3 Secondary Effects 137

6.4 Discussion of Reaction Rate 150

6.4.1 Effect of Process Variables on Reaction Rate 151
6.4.2 Development of Rate Model 156
6.4.3 Comparison of Rate Data with the Results of Other Investigators 169

6.5 Continuous Desulfurization-Regeneration System 175

7 CONCLUSIONS AND SIGNIFICANCE 179

NOMENCLATURE 181

APPENDIX A MINERAL ANALYSES OF GASIFIER ASHES 185

APPENDIX B DATA TABLES SHOWING GAS COMPOSITIONS FOR SELECTED RUNS 189

APPENDIX C REDUCED DATA 196

APPENDIX D COMPUTER PROGRAM FOR DATA REDUCTION 261

APPENDIX E COMPUTER PROGRAMS FOR MODELS 266

APPENDIX F SUMMARY OF MODEL PARAMETERS AND DETERMINATION OF PARAMETERS BY CURVE MATCHING 276

APPENDIX G CONTINUOUS DESULFURIZER-REGENERATOR COMPUTER SIMULATION 293

APPENDIX H ROTAMETER CALIBRATION CURVE 306

BIBLIOGRAPHY 308

CURRICULUM VITA 316

LIST OF TABLES

TABLE		Page
2.1	Typical low-BTU gas composition	9
3.1	Thermodynamic parameters for iron oxide process	45
6.1	Preliminary fluidization results (room conditions)	113
6.2	Minimum fluidizing velocity at 1000°F (1 atm)	113
6.3	Capacity change on reduction of temperature for Western Kentucky #9 Ash	128
6.4	Capacity and Breakthrough-efficiency of stabilized ash	132
6.5a	Summary of kinetic constants for Western Kentucky #9 Ash	162
6.5b	Summary of kinetic constants for Elkhorn and Montana Ashes	164
6.6	Statistical analysis of rate data for Western Kentucky Ash	166
6.7	Comparison of reported activation energies for the iron oxide-hydrogen sulfide reaction	171
APPENDIX A	Mineral analyses of gasifier ashes	185
APPENDIX B	Data tables showing gas compositions for selected runs	189
APPENDIX C	Reduced Data	196
APPENDIX F	Summary of model parameters	276

LIST OF FIGURES-GRAPHS

FIGURE		Page
1.1	Combined-cycle power plant with hot-gas cleanup	3
2.1	APCI regeneration sulfur breakthrough curve	26
2.2	Effect of Fe_2O_3 concentration on ash capacity for packed-bed studies	34
3.1(a) & 3.1(b)	Desulfurization potential of candidate solids	39 39
3.2(a)	Iron-Carbon-Oxygen equilibrium diagram	42
3.2(b)	Iron-Carbon-Hydrogen equilibrium diagram	43
3.3	Desulfurization equilibrium constant	49
3.4	Equilibrium constants for the reduction of iron oxides and CO_2	53
3.5	Phase diagram for iron oxides and sulfur with respect to oxygen partial pressures	56
4.1	Experimental setup	67
4.2	A picture of the experimental setup	68
4.3	Reactor setup	70
4.4	Arrangement of valves and columns	73
4.5	The analysis sequence	74
4.6	CDS 111 program	76
4.7	A typical chromatographic output	80
4A.1	Preliminary regeneration curves for W. Ky. #9 Ash	82

4A.2	Preliminary regeneration curves for W. Ky. #9 Ash	83
5.1(a)	Concentration profile for a nonporous solid reactant with diffuse reaction zone	89
5.1(b)	Concentration profile for a nonporous, spherical particle with narrow reaction zone	89
5.2	Mass balance for nonporous particles	92
5.3(a)	Schematic diagram of concentration profile in the first stage	97
5.3(b)	Schematic diagram of concentration profile in the second stage	97
5.4	Schematic representation of the grain model	98
5.5	Reactor mass balance	104
6.1	Reproducibility of rate data	115
6.1(a)	Regeneration breakthrough curves for W. Ky. #9 Ash	117
6.2	Perfect sorption	121
6.3	Effect of temperature on desulfurization	122
6.4(a)	Initial increase of H_2S capacity with number of cycles	124
6.4(b)	Initial increase of sorption efficiency with number of cycles	125
6.5	Efficiency and capacity change on reduction of temperature for W. Ky. #9 Ash	129
6.6	Ash capacity vs. temperature for W. Ky. #9 Ash	134
6.7	Effect of iron oxide concentration on H_2S capacity	136
6.8	Composition change (of exit gas) during desulfurization for W. Ky. #9 Ash	139

6.9	Variation of H_2S and COS during desulfurization	140
6.10(a)	Check of equilibrium for water gas shift reaction $CO + H_2O = CO_2 + H_2$	142
6.10(b)	Check of equilibrium in relation to the COS hydrogenation reaction, $COS + H_2 = H_2S + CO$	143
6.10(c)	Check of equilibrium in relation to COS hydrolysis reaction, $COS + H_2O = H_2S + CO_2$	144
6.11	Examination of catalytic effect of ash for the reaction, $CO + H_2O = CO_2 + H_2$	145
6.12	Dissociation of H_2S to COS	147
6.13	Effect of u/u_{mf}	153
6.14	Effect of inlet H_2S concentration	154
6.15	Unreacted-core model with reaction rate controlling	157
6.16	Unreacted-core model with product layer diffusion controlling	158
6.17	Estimation of K_k by curve matching	161
6.18	Plot of residual vs. predicted k_v values	168
6.19	Plot of observed vs. predicted k_v values	170
6.20	Comparison of absolute reaction rates predicted for packed-bed and fluidized-bed studies	174
6.21	Continuous desulfurization-regeneration fluid-bed system	176

APPENDIX F Figures showing curve matching procedure 276

APPENDIX H Rotameter calibration curve 306

SUMMARY

This research program has focused upon determining the operating characteristics and the technical feasibility of two high temperature, coal-derived fuel gas desulfurization processes that both use gasifier coal ash as chemisorbents.

The first phase of the project dealt with a fixed-bed process that uses tanden reactors for desulfurization, and regeneration of the sulfided ash. During regeneration, large exothermic heats can elevate the temperature of fixed-beds to unacceptable levels unless dilute streams of oxygen are used. The sulfur is recovered as a mixture of sulfur dioxide and elemental sulfur.

This report, "Hot Gas Desulfurization, Vol. 2: Use of Gasifier Ash in a Fluid-Bed Process" documents the second phase of this project conducted under the U.S. DOE Contract DE-AS05-76ET05076 (formerly EY-76-S05-5076). The University of Kentucky's Institute for Mining and Minerals Research contributed financially and technically to this project also.

The fluid-bed process also uses tanden reactors; however, these are operated, exchanging regenerated and sulfide ash, in a continuous fashion. The ash beds are no deeper than necessary to bring about the desired gas sulfide removal within the contraints of acceptable heat removal and solids exchange. During regeneration in the fluid-bed mode, the problem of temperature is not severe; however, the sulfur is recovered

exclusively as sulfur dioxide at a concentration suitable for sulfuric acid manufacture or direct reduction to sulfur.

FUEL-GAS DESULFURIZATION AT HIGH-TEMPERATURES IN FLUIDIZED-BEDS USING GASIFIER BOTTOMS ASH

DISSERTATION

A dissertation submitted in partial fulfillment of the requirements for the degree of Doctor of Philosophy at The University of Kentucky

By

CHAT PARAMESWARAN MOHAN

Lexington, Kentucky

Director: Dr. J. Thomas Schrodt,
Professor of Chemical Engineering

Lexington, Kentucky

1980

CHAPTER 1

INTRODUCTION

Coal has emerged as a major energy source for the future as a result of the energy crisis brought about by an acute shortage of crude oil. Major efforts are currently underway to produce liquid and gaseous fuels from coal; however, the sulfur contained in coal presents a serious technological challenge in view of today's stringent environmental regulations on sulfur emissions.

The production of synthesis gas and low-BTU fuel gas for power generation both require a substantial removal of the sulfur present in coal. Synthesis gas hydrogenation catalysts are particularly susceptible to poisoning by sulfur, and for this reason the total sulfur content of this gas should not exceed 0.1 grain per 100 cubic feet (Sand and Schmidt (1950)). The bulk of U.S. coals belong to the high sulfur class with up to 5% total sulfur present (Meyers (1977)). To consider an example of the magnitude of the sulfur emission problem at this high sulfur level for a plant producing about 400 million cubic feet of gas per day, the sulfur to be removed would amount to about 200 tons per day.

Two ways in which coal can be used to generate power are (1) direct combustion and (2) gasification

prior to combustion. Following direct combustion, flue gases must be treated to remove sulfur dioxide. One drawback to this is that enormous quantities of gas must be treated, because of dilution by air in the combustion step. The removal of sulfur from such dilute streams is economically prohibitive. The high cost of sulfur removal associated with the direct combustion process has led to recent investigations on more efficient and less expensive overall power generation processes. Gasification of coal prior to combustion offers one such alternative; currently, gasification and gas cleaning are being considered jointly. One of the techniques under investigation is the gasification of coal to produce low-Btu gas which can be utilized in combined-cycle power plants. Such a gas has a nominal heating value of about 100-175 BTU/SCF. At gasifier exit conditions it contains about 10-20% more energy in the form of sensible heat; a gas turbine system in the combined-cycle power plant can transform a portion of this energy into electricity. A conceptual combined-cycle plant is shown in Figure 1.1. The sulfur compounds and alkali-metal compounds can cause severe corrosion of the gas turbine blades and therefore must be removed from the fuel gas stream.

During gasification, sulfur in coal is transformed to hydrogen sulfide, carbonyl sulfide, carbondisulfide, etc. with H_2S being the predominant species. These sul-

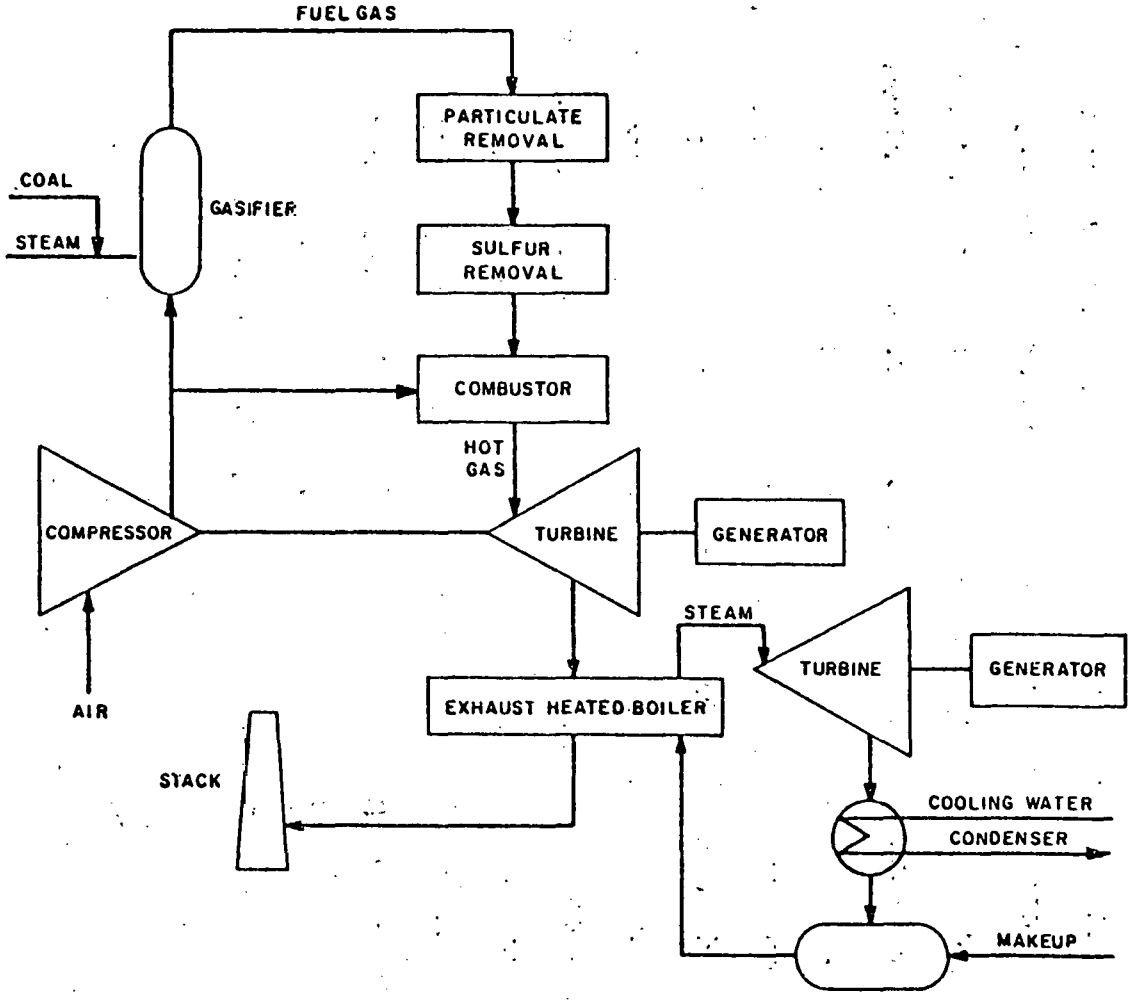

Figure 1.1 Combined-cycle power plant with hot-gas cleanup (Stone & Webster (1974)).

fur gases along with the low-BTU gas leave the gasifier at a temperature of over 1500°F. The traditional H_2S removal processes operate below 250°F necessitating the cooling of the fuel gas. The removal of H_2S from the coal gas at gasifier exit temperature and pressure results in an improved thermal efficiency of the combined-cycle plant. Comparisons between high and low temperature sulfur removal processes in combined-cycle power systems have revealed that hot processes promise a typical increment in thermal efficiency of about 4%; this increased efficiency will save about 20 tons/hr. of coal at 1000 MW capacity (Zabolotny (1976)). Capital requirements of the hot and cold processes have been estimated to be equal.

The feasibility of recovering sulfur as a by-product of gas cleaning operations is another important advantage of precombustion gas cleanup. Sulfur is a very important industrial raw material. As the naturally occuring elemental sulfur deposits become depleted, in the future, sulfur recovered from process streams such as fuel gases should become a very attractive by-product.

While gasification technology has developed to the commercial scale, high-temperature desulfurization technology has lagged behind. This dissertation represents an effort to contribute to this urgently needed technology.

In the present investigation, kinetic studies are performed on the process of high-temperature hydrogen

sulfide removal from low-BTU producer gas streams using gasifier bottom ash as a sulfur acceptor. The studies are conducted in a laboratory-scale fluidized-bed. The specific objective is to elucidate the effects of the various process parameters on the desulfurization process and represent the data in the form of a global reaction rate model which could be directly used in a process design network. The scope of the research project is presented in Chapter 1A.

CHAPTER 1A

SCOPE OF RESEARCH

In this study, the reaction between coal ashes and a hot simulated low-BTU gas containing H_2S are conducted in a fluidized bed reactor. Three coal ashes, namely, (1) Western Kentucky #9, (2) Montana Rosebud and, (3) Elkhorn #3 are studied. The H_2S absorbing capacity and sorption efficiency are measured.

The Western Kentucky ash is investigated for the following range of experimental conditions.

Temperature	900 - 1400°F
Mean particle size	0.01065-0.01935 cm
Superficial linear velocity of fluid	312 - 607 cm/min
Ratio of actual to minimum fluidizing velocity, u/u_{mf}	1.92 - 4.01
Inlet H_2S concentration	1.0, 1.25, 1.4 vol. %

The effect of the process variables on the capacity and efficiency are analyzed. The findings are incorporated into a global reaction rate model which expresses the global rate as a function of important process variables. The regimes of control are examined. The effect of the number of cycles (frequency of regeneration) on desulfurization

behavior is also studied. Elkhorn #3 and Montana Rosebud ashes are studied for the following experimental conditions.

Temperature	1000°F
Mean particle size	0.01935 cm
Superficial linear velocity	410 cm/min
u/u_{mf}	2.12
Inlet H_2S concentration	1.0 vol. %

Sorption capacities and efficiencies are evaluated for these two ashes.

Regeneration reaction is examined at oxygen concentrations of 3-5%. The secondary reactions of water-gas shift, COS formation etc. are also considered.

A computer program is developed using the predictive rate equation to predict the steady-state material and energy balances for a coupled, fluid-bed desulfurization-regeneration reactor system.

CHAPTER 2

A LITERATURE REVIEW OF HIGH-TEMPERATURE HYDROGEN SULFIDE REMOVAL PROCESSES USING IRON OXIDE BASED SORBENTS

2.1 General Discussion

A high percentage of the sulfur present in coal is transformed to hydrogen sulfide during gasification. Depending on the nature of this raw material and the gasification process, coal gas typically contains about 0.3 to 1.5% of H_2S; also present is organic sulfur (up to 20-50 grains/100 SCF) in the form of carbon disulfide, thiophene, mercaptans and carbonyl sulfide (Bhatia (1971)). The composition of low-BTU gas is variable depending on the particular gasifier. A typical product gas stream from an air-blown fluid-bed gas producer ought to have composition similar to that listed in Table 2-1. Due to their relatively higher concentrations, H_2S and COS are the only sulfur bearing gases that warrant concern in meeting environmental regulations and gas turbine corrosion guidelines. Many of the hot gas treatment systems currently under development do not remove ammonia or hydrogen cyanide (Morrison (1979)). If this results in NO_x emissions in excess of the EPA standard of 0.7 $lb/10^6$ BTU for coal-fired power plants, separate NO_x treatment steps should be included.

Table 2-1

TYPICAL LOW-BTU GAS COMPOSITION

component	concentration mole %
CO	20
CO_2	17
H_2	10
H_2S	1
N_2	49
CH_4	3
CS_2	0.001
COS	0.03
C_4H_4S (thiophene)	0.01
mercaptans	0.003
NH_3	0.3
HCN	-- 20 ppb

Many exhaustive general references are available on desulfurization and gas purification: (Meyers (1977), Crynes (1977), Kohl and Riesenfeld (1960). Ferguson (1975) presents an excellent review of hydrogen sulfide removal processes with emphasis on low-temperature techniques. Schrodt and Hahn (1976) give a general review of high-temperature H_2S removal processes. Meyers and Edwards (1978) make a detailed survey of processes for high-temperature, high-pressure gas purification. Edwards (1979) analyzes H_2S removal processes with particular reference to low-BTU coal gas and presents a brief section on high-temperature iron oxide processes. Recently, Morrison (1979) presented a concise review of the latest developments in hot gas cleanup processes. The U.S. Bureau of Mines (1959) published a bibliography of processes for removing H_2S from industrial gases covering the period of

1950-1957.

2.2 High-temperature H_2S Removal Processes

A high-temperature fuel-gas desulfurization process ideally should satisfy the following requirements:

a) High capacity and reaction rates for the sorbent material.

b) Favorable thermodynamic equilibrium and high sulfur removal efficiency to meet EPA standards.

c) Operating temperature and pressure ranges should be as close to gasifier exit conditions as possible.

d) It should be easy to regenerate the spent sorbent; sulfur recovery in the form of elemental sulfur is desirable.

e) The sorbent material should be both mechanically and chemically stable so that only minimum replacement is needed.

f) The desulfurization process itself should not significantly change the heating value of the fuel gas.

g) Operating cost, energy requirements and capital investment needed should be relatively low.

No process has been developed that meets all of the above desired characteristics. Some potentially promising processes which meet many of the above requirements are well summarized by Morrison (1979). Particularly noteworthy

are the calcium and copper oxide based processes. Only the iron oxide based processes will be considered here.

2.2.1. Iron Oxide Based Processes:

The reactivity of iron oxides and other metal oxides towards H_2S has long been known. In the rest of this chapter, the following processes based on iron oxide will be discussed: (1) Appleby-Frodingham process, (2) United States Bureau of Mines (USBM) process, (3) Babcock & Wilcox process and (4) IMMR ash process. Detailed review of chemistry, thermodynamics and chemical kinetics of the iron oxide process will be made in Chapter 3. The emphasis of the remainder of this chapter will be on the developmental findings of the four processes. All are based on the reaction of H_2S with iron oxides to form iron sulfides. Regeneration of the spent solid is achieved by reacting the sulfides with air to produce SO_2 in a concentrated form, or with water vapor to produce elemental sulfur (Bhatia (1971)).

2.2.1.1. Appleby-Frodingham Process:

This is the earliest known high-temperature iron oxide process that has been commercialized. Reeve (1958) describes the development that led to the installation and testing of a large pilot plant. The initial tests were carried out in laboratory-scale fixed and fluidized bed reactors using -16 mesh iron oxide particles. These were performed at the Appleby-Frodingham Steel Company at Scun-

thrope, England in 1946. The process outlined from these tests was covered by British Patent Specification 719,056 (1950). The desulfurization reaction was carried out at 620-750°F and space velocities up to 3000. The reaction rate was observed to increase with temperature. At a space velocity of 3000, the H_2S removal efficiency ranged from 71.0% at 617°F to 94.7% at 750°F. Sulfided oxide was regenerated by roasting in air at temperatures up to 1470°F. Some reduction in the rate of desulfurization reaction was noted after regeneration, but not to any significant extent.

The results were confirmed in a larger reactor (6 inch diameter) before the installation of a pilot plant in 1956. The plant was capable of treating 2.5 million cu. ft. of coke-oven gas containing about 600 grains of H_2S per 100 cu. ft. of gas per day and was designed as a steady state fluidized system with continuous circulation of the oxide between desulfurizer and regenerator. Sulfided oxide was regenerated at 1100-1500°F by air, the sulfur being removed as SO_2 plus some SO_3; the exothermic heat of reaction was sufficient to maintain the regeneration bed at these temperatures. The desulfurizer was maintained at about 700°F. Cold coke oven gas was preheated to about 480°F by heat exchange with the hot desulfurized gas. No external heat input was necessary for the whole process; and the process was self-sustaining

once properly adjusted.

It was noticed that the effect of increasing the desulfurizer bed depth was less than linear. Ultimately, the bed was divided into two shallow beds which resulted in H_2S removal efficiencies of 95 to 99%. While Reeve does not attempt to explain the nonlinear effect of bed height in his paper, it could have been due to the growth of bubble-size along the reactor length. The effect of particle size on the process was not evaluated; only constant-size particles of -16+100 mesh were used. Oxide replacement of 1 lb. per 5000 cu. ft. of gas treated were found necessary due to slow breakdown of particles. Both laboratory and pilot plant runs indicated that iron oxide acted as a catalyst towards the decomposition of organic sulfur in the gas to H_2S which was then absorbed by the hot oxide. It was concluded that the process was capable of removing 99% of the hydrogen sulfide together with 90% of all organic sulfur compounds other than thiophene of which 20% would be removed. The pilot plant did not include a facility to convert the sulfur dioxide in the regenerator exit gas into sulfuric acid.

Based on the overall success of the Frodingham pilot plant operation, a commercial size plant was installed at Exeter, England having a capacity of 32 million cu. ft. daily of crude coke-oven gas (Bureau and Olden 1967). A dry contact type sulfuric acid unit was included

in the scheme. The plant was designed to achieve bench-scale efficiency reported above, in a two-bed absorber with the final equivalent production of 98% sulfuric acid. Removal of hydrogen sulfide was substantially better than the design value, often reaching 99.9%. Removal of organic sulfur was found to be more temperature sensitive than that of hydrogen sulfide removal. When desulfurizer was maintained above 750°F, removal of thiophene and other organic sulfur exceeded the design figures. It was found that the plant was self-supporting in heat requirements even when the crude gas H_2S concentration was much below 350 grains per 100 cu. ft. Operation of the desulfurizer at temperatures below 570°F was avoided as this caused the formation of elemental sulfur. The sulfur dioxide concentration in the regenerator exit gas was only about 5%, but the sulfuric acid plant operated well at these levels. Oxide loss was greater than that from the pilot study and amounted to about twice the loss predicted.

Although the plant met all the technical design objectives, economic reasons caused its closure in 1965. During this period a new technology of producing clean gas at far less cost was introduced using light distillates as the fuel. Also the Frodingham process suffered economically due to the fact that the anticipated revenue from the sale of sulfuric acid did not materialize. Nevertheless, it established the feasibility of a hot iron

oxide process for temperatures up to 750°F. However, current approaching gasification technology will demand viable H_2S removal processes capable of operating at temperatures well over 1000°F.

2.2.1.2. Babcock-Wilcox Process:

Bhada and Sage (1970) and Kertamus (1973) have described the laboratory and pilot scale testing of this process. Initially, sintered iron powder packed in a reactor, and plain carbon steel were used as the reactant materials. The iron was first oxidized in a stream of air to generate a layer of iron oxide. This oxide surface was then used to remove the hydrogen sulfide present in a synthetic gas stream containing 1% H_2S, 12% CO, 8% CO_2, 1% CH_4 and the balance N_2. At the end of the desulfurization cycle, the sulfided iron layer was once again regenerated with air. The exit stream H_2S concentration during desulfurization, and the SO_2 concentration during regeneration were continuously analyzed. Later, more laboratory-scale tests were done using 1/8 inch carbon steel pellets as the reactants. Water vapor and hydrogen were also included in the synthetic gas for these tests. Larger-scale experiments were performed in a pilot plant reactor designed with iron grids.

Initial laboratory tests were performed at temperatures of 825-1600°F and gas velocities of 7 to 20 fps. The large-scale system was operated at temperatures in

excess of 1200°F to avoid fouling by carbon deposits; carbon deposition was noticed in the bench-scale runs. It was inferred from these tests that diffusive transport would be the controlling design parameter since rates of regeneration and desulfurization were both found to be rapid. The later tests with steel pellets were more extensive in nature. H_2S removal efficiency was found to increase with temperature, with 95% at 675°F to greater than 98% at 1200°F. Sulfur removal capacities were also found to increase with temperature; at space velocities of 2000-2500 per hour, the capacities were: 3.5 scf H_2S per 100 sq. ft. of surface area at 675°F and 13.8 at 1200°F. It was observed during the steel pellet runs that desulfurization below 1000°F caused an initial concentration spike of SO_2; after this spike, the SO_2 concentration dropped to a low value which remained until breakthrough. Kertamus suggested that low temperature regeneration ($<$1000°F) caused some formation of $FeSO_4$ in the solid which then reacted with H_2S during desulfurization to form SO_2 initially.

Based on these results Babcock & Wilcox designed a large-scale "regenerative desulfurizer" using steel plates. Further development efforts have not been reported.

2.2.1.3. U.S. Bureau of Mines Process:

The USBM conducted laboratory testing of 48 dif-

ferent materials to evaluate their performance for removal of H_2S from hot simulated producer gas. These tests were discussed by Abel et al. (1974), Lewis et al. (1973), and Shultz and Berber (1970). Initially these solids were tested at temperatures up to 1500°F using a simulated producer gas (without steam, tar vapor or dust) of the following composition: 50.5% N_2, 26.0% CO, 17.0% H_2, 5.0% CO_2 and 1.5% H_2S. The sorbents were packed in a stainless steel tubular reactor. Desulfurization was stopped when the H_2S concentration in the exit gas reached about 0.15%. The sorbent was then regenerated at 1000-1500°F in a stream of air. Among the various materials tried were: Fe_2O_3, fly-ash, red and brown mud, fly ash-red mud, pumice-Fe_2O_3, fly ash-Fe_2O_3, fly ash-metal oxides (other than Fe_2O_3), and gasifier bottom ash. All except the bottom ash were used in the form of sintered pellets. Based on the absorption capacity, durability, and ease of regeneration, the material found to be the best was sintered pellets of 75 percent fly ash-25 percent Fe_2O_3. Further tests were performed with this sorbent to determine the effects of sorbent composition, temperature, and steam, tar and dust concentrations in producer gas on H_2S removal. The use of fly ash-Fe_2O_3 sorbent for producer gas desulfurization was awarded a U.S. patent (Shultz et al. (1971)).

The selected fly ash-Fe_2O_3 pellets were formed by

extrusion of a thick water paste of the fine-size ingredients and sintering at furnace temperature of 1900°-2000°F for 10 to 15 minutes. The approximate composition of this material was 36% Fe_2O_3, 35% silica, 18% alumina, and small percentages of calcium, magnesium, sodium, potassium and titanium. They suggested that all oxides except iron oxide were inactive materials and did not contribute to the desulfurization process. Pellets of ¼ inch diameter and ½ to ½ inch length were tested through 175 regeneration cycles using simulated producer gas and bed temperatures of 1000°, 1250° and 1500°F with a space veolocity of 1000 per hr.

Average sorption capacities during the 175 cycle runs were lower than those for the newly sintered sorbents. The decrease was more pronounced at 1500°F than at 1000° and 1250°F. This finding was attributed to a decrease in the pore volume of the sorbent during the first 30 sorption-regeneration cycles.

Addition of steam was found to reduce the capacity of the sorbent; a 7 percent addition reduced the capacity by 25 percent at 1500°F. Runs made with tar vapor and dust showed some carbon deposition on the pellets from cracking of tar vapors; also considerable accumulation of dust was noticed. It was however concluded that tar and dust present in producer gas did not significantly affect the sorption capacity or the general performance

of the process.

The sorbent removed over 95% of the H_2S for extended periods at temperatures of 1100-1300°F and gas space velocities of 500-1000 per hr. Sorption capacities (including H_2S absorbed by the wall of the reactor) ranged from 4 grams of sulfur at 1100°F to over 6 grams of sulfur per 100 grams of sorbent at 1300°F in producer gas containing 10 percent steam and about 1 pound of tar and ½ pound of dust per 1000 scf. Up to 86 percent utilization of sorbent theoretical capacity was obtained. Water gas shift reaction $CO+H_2O = CO_2+H_2$ was found to be catalyzed by the sorbent, resulting in a reduction of the dry base heating value of the fuel gas due to dilution by CO_2. Increased temperature favored higher carbon monoxide concentration at equilibrium. The regeneration reaction rate did not increase when the bed temperature was increased above 1000°-1200°F. At an air space velocity of 1000 per hr. and bed temperatures of 1000° to 1500°F, SO_2 concentrations of regenerator exit gas were between 6 and 10 percent before oxygen breakthrough; regeneration in pure oxygen gave an effluent of 100 percent SO_2. It was recommended that temperatures over 1500°F be avoided to prevent fusion of the sorbent pellets. Some elemental sulfur formation during the regeneration reaction was noticed. At 1500°F some formation of CH_4 (not present in influent gas) was found during desulfurization. Spec-

trographic analysis of desulfurization reaction products revealed the formation of troilite (FeS); stoichiometric calculations indicated an empirical composition of $FeS_{1.3}$. It was suggested that the products of reaction were ferric sulfide (Fe_2S_3) and pyrite (FeS_2) (Shultz and Berber (1970)). No attempt was made to define the stoichiometry precisely. Oldaker et al. (1975a) had later suggested that the empirical composition was $FeS_{1.5}$ with FeS and FeS_2 being the sulfides.

In addition to the laboratory-scale tests described above, larger-scale tests were performed using a 6-inch-diameter, 4-foot-high stainless steel reactor (Oldaker et al. (1975a)). Actual producer gas from an experimental stirred, fixed-bed, air-blown gasifier (of 3.5 feet diameter) was used for these studies. The gas producer and the desulfurizer were coupled. The desulfurizer was loaded with 73 pounds of 3/16-inch-diameter sorbents. The complete system was maintained above 1000°F to prevent tar condensation. A gas space velocity of 1900 per hr. was maintained. Carbon deposition increased the pressure drop from 1.5 psig initially to 8 psig at the end of the runs. This material was removed during the regeneration reaction with air.

Four 15-hour sorption runs were conducted at 1100°F; the runs removed 90 to 94 percent of the inlet H_2S which was about 0.5 percent. The H_2S removal efficiencies

were calculated by averaging the H_2S outlet concentrations up to a value of 50 grains/100 scf. Prior to breakthrough, the exit H_2S concentration was steady at about 25 grains/100 scf. Tars and particulates did not adversely affect the process. Maintaining the regeneration bed temperature below 1500°F, the temperature limit to avoid particle fusion, was a major problem; regeneration air flow had to be kept very low to protect the sorbent.

Oldaker et al. (1975b and 1975c) and Farrior et al. (1976) have described the next stage of USBM tests to improve the crushing strength, sorption capacity, sorption efficiency and fusion temperature of the sorbent. Fly ash supported sorbent, as described above imposed a temperature limitation of 1500°F. This upper limit was increased to about 1750°F by the use of silica as the supporting material; the silica supported sorbent also allowed higher iron oxide additions (45%) without the problems of reduced crushing strength as exhibited by the fly ash-Fe_2O_3 pellets when total Fe_2O_3 exceeded 37 percent. The higher iron oxide content increased the H_2S sorption capacity of the silica based sorbents.

Air Products and Chemicals, Inc. (APCI) was awarded a contract by the U.S. Energy Research and Development Administration (currently Department of Energy) to extend the research on the USBM process. The APCI work included sorbent development and kinetic studies. Joshi

and Leuenberger (1977) have described in detail the results of the studies conducted by APCI. Most process studies were done in packed beds with 42% iron oxide in fly ash sorbent. The range of the process variables studied for desulfurization runs were: Temperature 600°F to 1400°F, pressure 20 to 400 psig, Space velocity 1300 to 3600, hydrogen sulfide concentration 0.6 to 1.2%, sorbent pellet diameter 1/8 and 1/4 inch, and iron oxide content of sorbent 8 to 63%. Sulfided sorbent was regenerated at 1000°F and 1200°F, 20 psig and 150 psig pressures, 700, 1300 and 6500 per hr. space velocities. Air concentrations of 15 and 20% (rest being steam) were used to regenerate the sorbent. For regeneration studies, only the 21% and 42% iron oxide pellets were used.

Simulated producer gas (free of tar and particulates) of the following nominal composition was used for the desulfurization studies: 48.6% N_2, 20.5% CO, 14.9% H_2, 6.5% CO_2, 1.9% CH_4, 0.6% H_2S and 7.0% H_2O. Dynamic desulfurization and regeneration were analyzed by plotting percent H_2S breakthrough vs. sorption efficiency. Sorption efficiency was defined as the ratio of sorber onstream time for actual operation to sorber onstream time for perfect sorption. The definition of perfect sorption is discussed in more detail in Chapter 6, Section 6.2.1. The slope and breakthrough point obtained from the above curve are influenced by the rate of reaction; the

sorption efficiency is therefore an indication of rate of reaction. The qualitative conclusions from the APCI kinetic studies are summarized below; the quantitative results are outlined in Chapter 3.

Desulfurization:

Change of linear velocity from 1.2 fps to 2.3 fps was found to result in increased bed efficiency. However, at constant linear velocity, increase in space velocity decreased the efficiency. It was postulated that the reaction wave would display a constant pattern after formation. Sorption efficiency was found to improve rapidly with temperature in the range 600°-900°F; the improvement was less rapid up to 1200°F; identical efficiencies were obtained at 1200 and 1400°F. Sorbent performance appeared to be better at lower H_2S concentration level; however the effect was considered small. Reduction of sorbent pellet diameter from ¼ inch to 1/8 inch improved the sorption efficiency by 5-10 percent; this effect was even more pronounced at higher pressures. No significant difference in performance was noticed between silica supported and fly ash supported sorbents. Performance curves for sorbents prepared with more than 42% added iron oxide indicated a decrease in performance; it was suggested that this effect was due to the change in controlling mechanism caused by the decrease in porosity of the sorbent. A sulfur capacity of 0.37 grams of sulfur per gram of iron

oxide at 1200°F indicated an empirical sulfided product of $Fe_{0.9}S$ close to that of pyrrhotite. An increase in pressure was, in general, found to improve sorbent performance the effect being considerably greater on a low performance sorbent. The authors have cautioned that these conclusions were based on sulfidation of fresh sorbent; effect of number of cycles of regeneration on sorbent performance was not evaluated.

Regeneration:

Many regeneration schemes were evaluated with overall process economy in mind and steam-air mixture was selected for the experimental studies; a 85% steam-15% air mixture was used in the experimental studies. Due to water vapor condensation problems, a dry gas analysis was performed using gas chromatography to obtain oxygen breakthrough curves. Adiabatic gas temperature rises of 400 to 500°F were predicted but observed values were lower. During regeneration, 80-95% of the absorbed sulfur was removed. Wet tests on regenerated sorbent showed that residual sulfur might be present as sulfate or some compound other than sulfide; however, X-ray diffraction analyses did not reveal any significant sulfate. Elemental sulfur, SO_3 and SO_2 were the sulfur products of reaction; high elemental sulfur formation, 20 to 30%, occured in the initial periods of regeneration. it was pointed out that, since elemental sulfur formation was ob-

served on sorbents sulfided in reducing atmospheres during desulfurization as well as sorbents sulfided in inert atmospheres, the sulfur forming phenomenon did not seem to depend on sorbent history. Figure 2.1 gives the regenerator effluent concentration of SO_2, SO_3 and S as a function of time on stream. Very high space velocities (6500 per hr.) were found to significantly reduce the fraction of elemental sulfur formed. Carbon deposition on the sorbent during desulfurization was found to be small (0.7% by weight) when there was water vapor present. Significant deposition of carbon (12% by weight) occured in the absence of water vapor.

Increased iron sulfide content in the sulfided sorbent increased the regeneration efficiency for oxygen breakthrough. Increase of space velocity from 200 to 1300 per hr. decreased the efficiency at 10% oxygen breakthrough from 1.0 to 0.88; and perfect sorption time decreased from 11.69 hrs. to 6.9 hrs. As previously discussed this amounts to a decrease in the observed rate due to increased space velocity. Increase in pressure increased the efficiency at 10% breakthrough slightly and seemed to give higher observed rates but the extent of regeneration percent removal of absorbed sulfur decreased significantly. When the bed temperature was increased from 1000 to 1200°F (with ½-inch-diameter pellets), regeneration efficiency increased significantly.

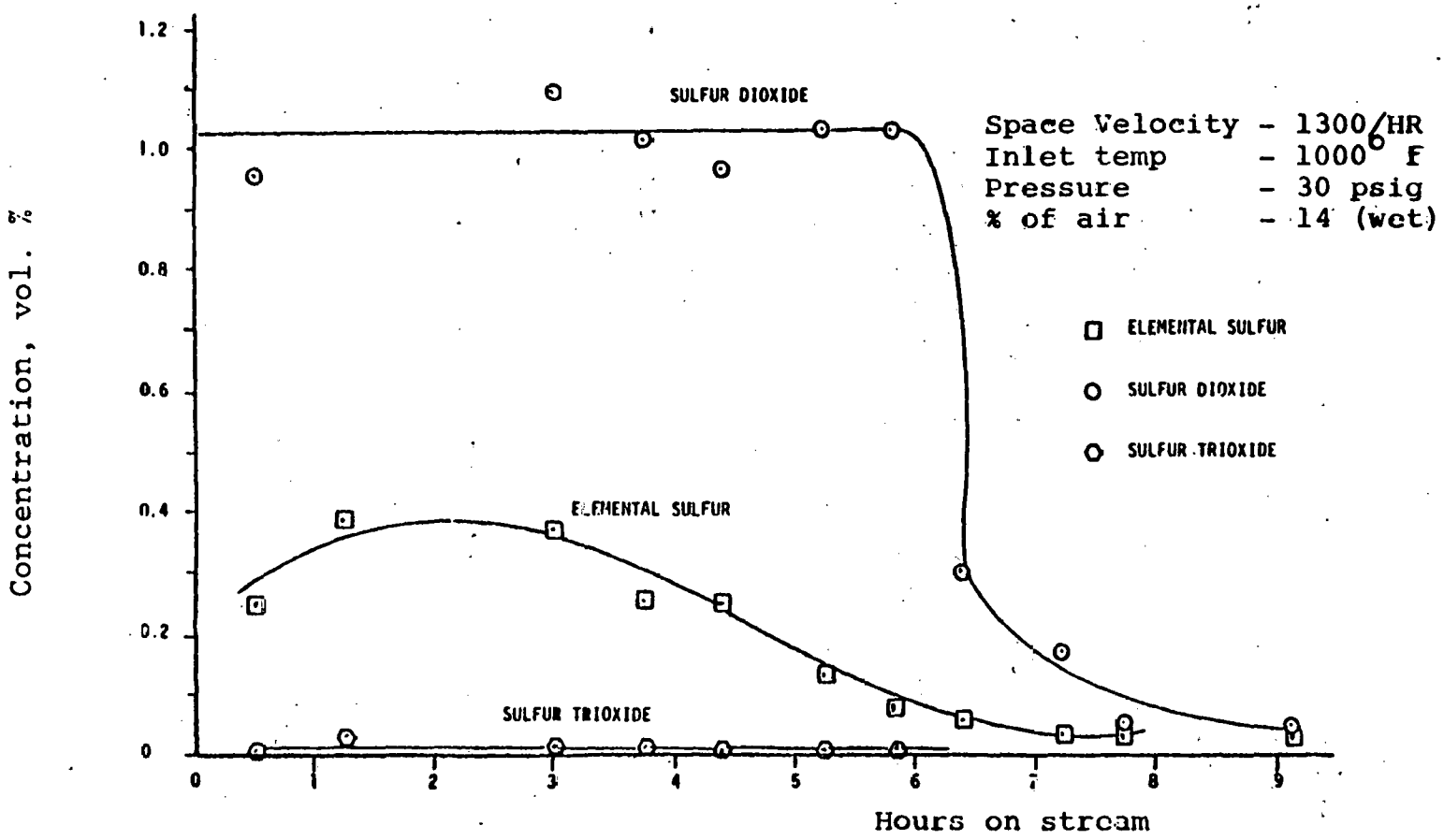

Figure 2.1 APCI Regeneration sulfur breakthrough curve (from Joshi and Leuenberger (1977)).

Increasing velocity at a constant space velocity increased the regeneration efficiency slightly; this effect was more pronounced for desulfurization. As in the case of desulfurization, 1/8-inch-diameter pellets displayed much higher efficiencies as compared with the ½-inch pellet. Two runs were conducted at different oxygen concentrations, namely 2.9% and 3.9%. Efficiency of regeneration increased slightly with increase in oxygen concentration; however, the adiabatic temperature rise was 258°F for 3.9% oxygen and 320°F for 2.9% oxygen. This was explained as being due to the greater extent of the endothermic elemental sulfur forming reaction ($SO_3 \rightarrow S_2$) at higher oxygen concentrations.

APCI also measured the change in physical characteristics of the sorbent pellet from fresh to sulfided to regenerated. Pellet true density increased by about 3 to 5% after sulfiding but decreased back to fresh sorbent value after regeneration. Crushing strengths of sulfided and regenerated sorbent pellets were 300 to 400 percent higher than those of fresh sorbent. Surface area of the sorbent decreased slightly after sulfiding but increased after regeneration. Total pore volume of the fresh sorbent decreased by about 34% after sulfiding; and increased slightly on regeneration. Pellets were also analyzed for X-ray diffraction patterns. These results will be discussed in Chapter 3.

2.2.1.4. Coal Ash Process:

The early stages of development of this process were done at the Institute for Mines and Minerals Research (IMMR), University of Kentucky and is referred to in literature citings as the IMMR process. The process utilizes coal gasifier-bottom ash as the sorbent material for H_2S. Results of these initial investigations were reported by Schrodt (1975b) and Schrodt and Hahn (1976). Based on the favorable results of these investigations, the second phase of process studies, supported by the U.S. Department of Energy, was started late in 1976. This dissertation work forms part of this study. Coal ash was one of the several solid sorbents considered by the U.S. Bureau of Mines during the initial evaluation of sorbents for the USBM process (Abel et al. (1974)). However, the material was not investigated further; the reason for this action was not discussed. Hamrin and Maa (1975), during their investigations on the use of bottom-ash to prevent coal agglomeration, also noticed the ability of the ash to absorb hydrogen sulfide. One of the earliest references to the use of coal ash as a high-temperature H_2S acceptor was in a U.S. Patent to desulfurize synthesis gas, assigned to Jahnig et al. (1950). The process described in this patent used coal ash with 10-40% carbon (referred to in the patent as spent char) to desulfurize synthesis gas at temperatures of 400 to 1000°F. About

2.5 to 5 volumes of air per volume of equivalent H_2S to be treated were added. It was claimed that the oxygen admitted into the desulfurizer (in the form of air) oxidized the hydrogen sulfide to free sulfur which deposited on the carbon in the spent char. Although it was claimed in the patent that the ferrous constituents in the ash aided the sulfur removal, no desulfurization chemical reactions pertaining to the process were discussed.

The mineral matter present in coal is non-combustible in nature and ends up as ash when coal is gasified. Coal contains typically 10-20 percent ash forming material. The ash itself contains 5-35 percent iron oxides. It is this iron oxide that is mainly responsible for the reactivity of coal ash towards hydrogen sulfide. Actual chemical analyses of ashes used in this work from four U.S. coals are listed in Appendix A. The ashes contain, besides iron oxide, silica (about 50%) as the major constituent, about 20% of alumina, about 5% of calcium oxide and smaller quantities of other oxides.

Initial feasibility studies of the coal ash process were conducted using Western Kentucky No. 9 ash packed in a 304 S.S. reactor of 2 inch diameter and 48 inch length. These fixed-bed experiments were described in detail by Hilton (1974). Experiments were carried out using synthesized producer gas (without water vapor and tars) at temperatures of 700-1450°F, pressures of 80 to

150 psi, space velocities of 800-2000 per hr. and inlet hydrogen sulfide concentrations of 0.5 to 1.5%. Hydrogen sulfide breakthrough curves were obtained for the range of variables mentioned above. H_2S removal of greater than 99% were obtained. A strong influence of the operating variables on ash capacity was noticed. Increased space velocities increased the sorption capacity but decreased the efficiency. Increasing the temperature, pressure and hydrogen sulfide concentration increased the observed ash capacity. Water-gas shift reaction was found to reach equilibrium concentrations. Methane decomposition resulting in carbon deposition occured above 800°F in the absence of water vapor in the preheater section. However, no carbon deposition was observed on the sorbent itself. An increase in methane composition was noticed, supporting similar observations made by Shultz and Berber (1970) while working on the USBM process. The hot ash process was later tried in a fluidized bed and found to work satisfactorily (DeBoer (1975)). It must be mentioned that sorption capacities reported in these two initial studies include H_2S absorbed by the ash and stainless steel reactor walls themselves.

Efforts were focused during the second phase of the process development studies, on obtaining quantitative reaction rate data. Effects of process variables on ash capacity and efficiency were investigated. The kinetic

rate expressions developed will be outlined in Chapter 3. Experiments were conducted in quartz reactor tubes of inside diameter 35.0 m.m (1.38 inch). Schrodt (1976 and 1977b) has described the experimental setup in detail. Four different ashes--Western Kentucky No. 9, Kentucky Elkhorn No. 3, Montana Rosebud and Virginia Sprint--were evaluated in the fixed-bed mode. Three different sizes--Tyler mesh 20/35, 10/20 and 4/8--of ash particles were tested. At the start of the desulfurization tests, rapid reduction of iron oxide took place as evidenced by decreases in the levels of the reducing gases CO and H_2 and increases in the CO_2 and H_2O levels. Carbon oxysulfide was formed by the reaction of CO with H_2S, but was apparently removed by the ash along with the input H_2S. Surprisingly, the capacity and efficiency of the ash were found to increase with the number of regenerations up to about 10 cycles. This effect is in apparent contradiction to the USBM findings (Abel et al. 1974). This was discussed in Section 2.2.1.3. The USBM effect was explained to be due to the reduction of pore volume of the sorbent, while in the case of the ash, progressive migration of iron towards the surface took place. This fact was verified by EDAX electron scans on the ash particles. With ten cycles, the iron concentration near the particle surface increased from 18.6 to 73.7% w/w and appeared to be concentrated in a layer of thickness

20-50 microns. These facts and the experimentally observed effects of operating variables on the hot ash process were discussed in detail by Schrodt (1977b, 1977c). The process variables effects on desulfurization are summarized in the following paragraph.

Presence of water vapor in the synthesized low-BTU gas did not significantly change the efficiency or ash capacity. However, presence of water vapor caused a measurable H_2S concentration in the reactor effluent gas prior to breakthrough, while none was detected in the absence of influent water vapor. Temperature effects were evaluated at 800, 1000, 1200 and 1400°F. Increase of temperature increased both the capacity and the efficiency markedly; ash performance was very poor at 800°F. Increase of ash particle-size generally decreased the capacity and efficiency. A slight increase of ash capacity was noticed at a space velocity of 2000 per hr. as compared with those obtained at 3000 and 4000 per hr. The ash bed effectively removed carbon-oxysulfide from the gas either directly or indirectly. A run conducted with 0.73% H_2S, 0.175% COS and 2.7% H_2O in the influent gas resulted in no measurable COS or H_2S in the effluent gas prior to breakthrough. The presence of COS did not affect the ash capacity. Carbon-oxysulfide was found to react with H_2 and/or H_2O to form H_2S which resulted in higher than input concentration of H_2S in the effluent gas, after

saturation of the ash bed. Effect of H_2S inlet concentration was studied at concentrations of 0.47%, 0.95% and 1.68%, all at a space velocity of 2000 per hr., 1000°F and 2% inlet water vapor content. The 1.68% H_2S run gave slightly higher ash capacity. The breakthrough curve for the 0.47% run appeared steeper than the other two. It was concluded that the effect of H_2S concentration on ash capacity was not great. When the carbon forming gases CO, CO_2 and CH_4 were excluded from the influent gas mixture a lower ash capacity resulted (see Morrison (1979) and Schrodt (1977b)). Four different ashes were tested that had iron oxide concentrations of approximately 5 to 22% by weight; results show that the ash capacity increases with increasing iron oxide concentration. Figure 2.2 illustrates the increase of capacity due to iron oxide concentration with temperature as the parameter. The Western Kentucky No. 9 ash exhibited a greater capacity and a greater (66%) utilization of its iron content at 1400°F as compared to 22% for Virginia ash at the same temperature. Addition of carbon-disulfide to the inlet gas showed an effect very similar to that of COS--CS_2 was not noticeable in the effluent stream prior to breakthrough. However, unlike COS, CS_2 was not detected in the effluent gas even after breakthrough; this was explained by the fact that the equilibrium concentration of CS_2, according to the reaction $COS+H_2S = CS_2+H_2O$, would

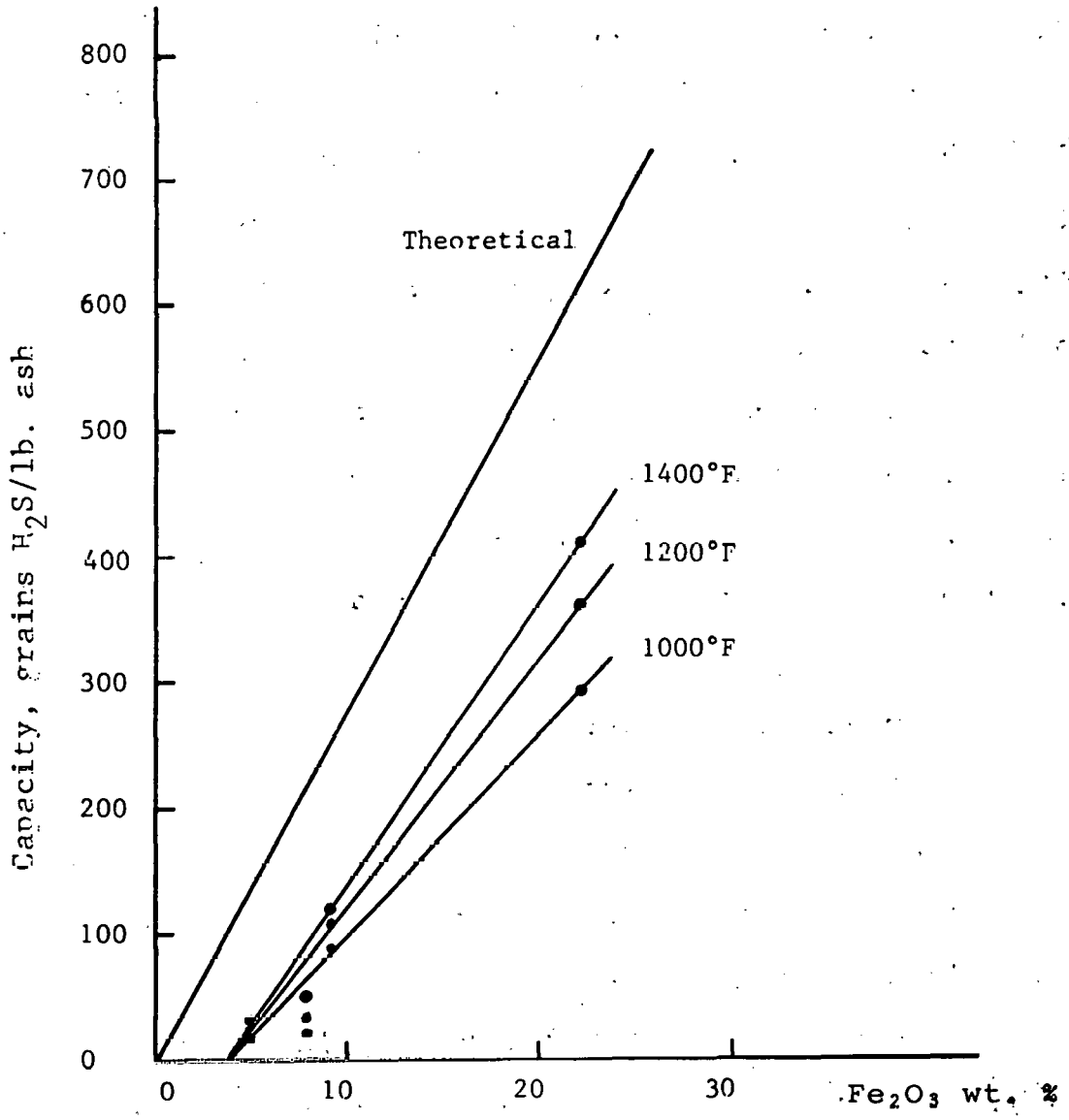

Figure 2.2 Effect of Fe_2O_3 concentration on ash capacity for packed bed studies (from Schrodt 1977c).

be below the detection level of the gas chromatograph. Also, no significant effect of CS_2 on ash capacity, efficiency or reaction rate was found. Since the Inconel 600 metal reactor used to test pressure effects reacted with the H_2S in the fuel gas, the only conclusion that could be reached was that pressure increases had a positive effect on the capacity of the ash. Test runs with the empty metal reactor showed that the sorption capacity of the metal wall increased with the number of regenerations in the same fashion as the ash, reaching a constant value after 8 to 10 cycles. The secondary effects of metal corrosion by H_2S, carbon deposition, water-gas shift reaction, and tar vapors were studied by Evans (1978) and summarized by Schrodt (1978). The theoretical and quantitative findings from these studies will be described in Chapter 3. The carbon deposition measured was quite small with only 2 to 7% of the theoretically predicted values. Since measured/predicted values increased with temperature while thermodynamics predicted an opposite effect, it was concluded that rate factors controlled the amount of carbon deposited. Iron oxide, cementite and iron sulfides, the iron compounds present in gasifier environment, were not found to catalyze the decomposition of CO. No adverse effect due to carbon deposition on the performance of the ash was observed. Carbon deposition from cracking of tars was found to be

significant (for example 0.1 gram of carbon/gram of tar injected at 1300°F) and increased with temperature; however, sulfidation tests indicated that this carbon did not affect the ash sulfur capacity. Some residual sulfur (up to 0.8% by weight) was still present in the regenerated ash samples during these tests. The investigation on the water-gas shift reaction revealed that this reaction proceeded to a significant extent approaching equilibrium composition. The reaction was found to be catalyzed by the minerals present in ash and highly temperature dependent. The metal corrosion studies revealed that metals with low nickel content and traces of aluminum and silicon showed good corrosion resistance.

Regeneration:

Regeneration studies with air were carried out on Western Kentucky No. 9 ash of 10/20 Tyler mesh particle size. Experiments were carried out at 800, 1000 and 1200°F with inlet air space velocities of 50, 90 and 134 per hour. High oxygen utilization efficiencies (0.8 to 0.95 measured at 15% breakthrough) were obtained. Reaction rate was found to be very rapid. Increases in temperature and air inlet velocities were found to improve efficiency. Maximum adiabatic temperature rises of the regeneration bed did not exceed 200°F. Typically 60 to 85% of the sulfur was recovered as SO_2, 10 to 20% as pure elemental sulfur and the balance remained on the ash in

an unidentified form. It was suggested that the elemental sulfur formed during the early stages of regeneration in the downstream section of the bed by the reaction of SO_2 with FeS in the bed. Low gas velocities were said to favor high elemental sulfur formation.

CHAPTER 3

REVIEW OF CHEMISTRY, THERMODYNAMICS AND KINETICS OF THE COAL ASH PROCESS

3.1 General Considerations

It has long been known that many metal oxides can react with hydrogen sulfide at elevated temperatures. Westmoreland and Harrison (1976) made a systematic thermodynamic screening of several metal oxides, using the method of free energy minimization, to evaluate their potential for desulfurization and to define the range within which the sorbent oxides would be effective. They identified oxides of Fe, Zn, Mo, Mn, V, Ca, Sr, Ba, Co, Cu, and W as showing thermodynamic feasibility for high-temperature desulfurization of low-BTU gas. The authors examined the gasification mixtures reported by various workers and concluded that their results would be applicable to a broad range of low-BTU gas compositions. Equilibrium fractional desulfurization for the various metal oxides at different temperatures (633°K to 1773°K) and 20 atmospheres pressure are reported in their work in the form of graphs which are reproduced here as Figures 3.1(a) and 3.1(b). The authors have also presented a table that predicts the stable solid phases for the different oxides as a function of temperature. A recent

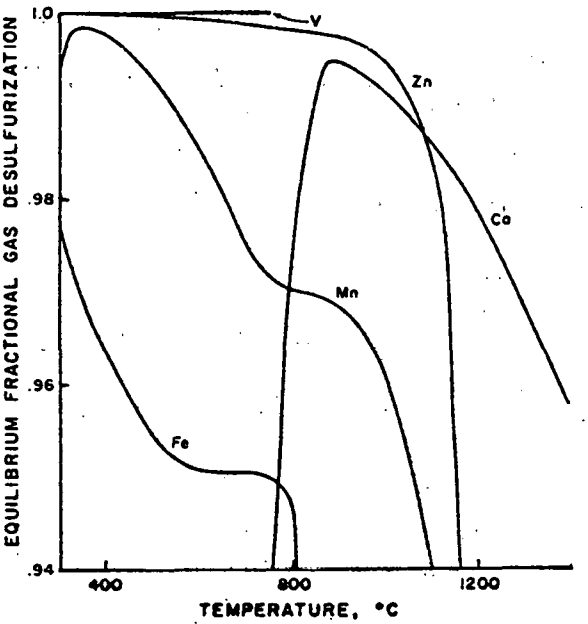

3.1(a)

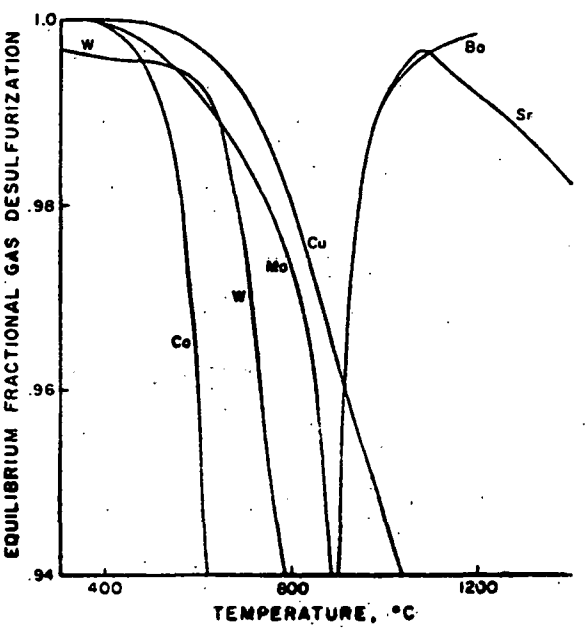

3.1(b)

Figures 3.1(a) and 3.1(b) Desulfurization potential of candidate solids (from Westmoreland and Harrison (1976)).

paper by Attar (1978) gives an exhaustive review of the chemistry, thermodynamics and kinetics of reactions of sulfur in coal-gas reactions. Though this paper does not directly deal with the iron oxide desulfurization reactions, it provides an excellent overview of the many sulfur-related reactions associated with coal pyrolysis and gasification. The rest of this chapter will be devoted to discussion of the iron oxide sorbent.

3.2 Chemistry and Thermodynamics of Iron Oxide Processes

3.2.1. Iron Oxide Reduction:

During the course of the regeneration reaction, the sulfided iron oxide is oxidized to the stable form Fe_2O_3 which is then recycled to the desulfurizer for further service. The strong reducing atmosphere present in low-BTU gas desulfurizers makes several reduction reactions possible, one of them being the reduction of iron oxide. Iron oxide may be reduced by both hydrogen and carbon monoxide that form part of the low BTU gas. These reactions may be represented as follows:

$$3Fe_2O_3+H_2 = 2Fe_3O_4+H_2O \quad (3.1)$$

$$Fe_3O_4+H_2 = 3FeO+H_2O \quad (3.2)$$

$$FeO+H_2 = Fe+H_2O \quad (3.3)$$

$$3Fe_2O_3+CO = 2Fe_3O_4+CO_2 \quad (3.4)$$

$$Fe_3O_4+CO = 3FeO+CO_2 \quad (3.5)$$

$$FeO+CO = Fe+CO_2 \quad (3.6)$$

These reactions have been studied in great detail due to

their importance in the iron and steel industry and extensive thermodynamic and kinetic data are available. Reduction rates of Fe_2O_3 are generally known to be much higher than desulfurization rates and, therefore, it appears that iron oxide reduction precedes the H_2S removal reaction. The hydrogen sulfide in the fuel gas would then react with the reduced iron oxide which may be Fe_3O_4, FeO or Fe. The degree of reduction of Fe_2O_3 is dictated by the temperature and, CO/CO_2 and H_2/H_2O ratios. These equilibriums are shown in Figures 3.2(a) and 3.2(b). It should also be noted that phase transformation of Fe_2O_3 from alpha form to beta occurs at 953°K and from beta to gamma at 1053°K. Figures 3.2(a) and 3.2(b) may be used to predict the different solid phases that may exist during the iron oxide reduction step. For example, for the reaction $\frac{1}{4}Fe_3O_4+CO = 3/4Fe+CO_2$ to proceed at 1000°F leading to the formation of elemental iron, Figure 3.2(a) shows that the ratio CO/CO_2 should be greater than 1.0. Figure 3.2(b) shows that for elemental iron formation by the reaction $\frac{1}{4}Fe_3O_4+H_2 = 3/4Fe+H_2O$ at 1000°F, the H_2/H_2O ratio should be greater than 4.0. Figure 3.2(a) also includes the equilibrium compositions for the carbon deposition reaction, $2CO = C+CO_2$ which will be discussed later. Westmoreland and Harrison (1976) conclude from their thermodynamic studies (mentioned in Section 3.1) that iron oxide is a suitable desulfurizing material at tempera-

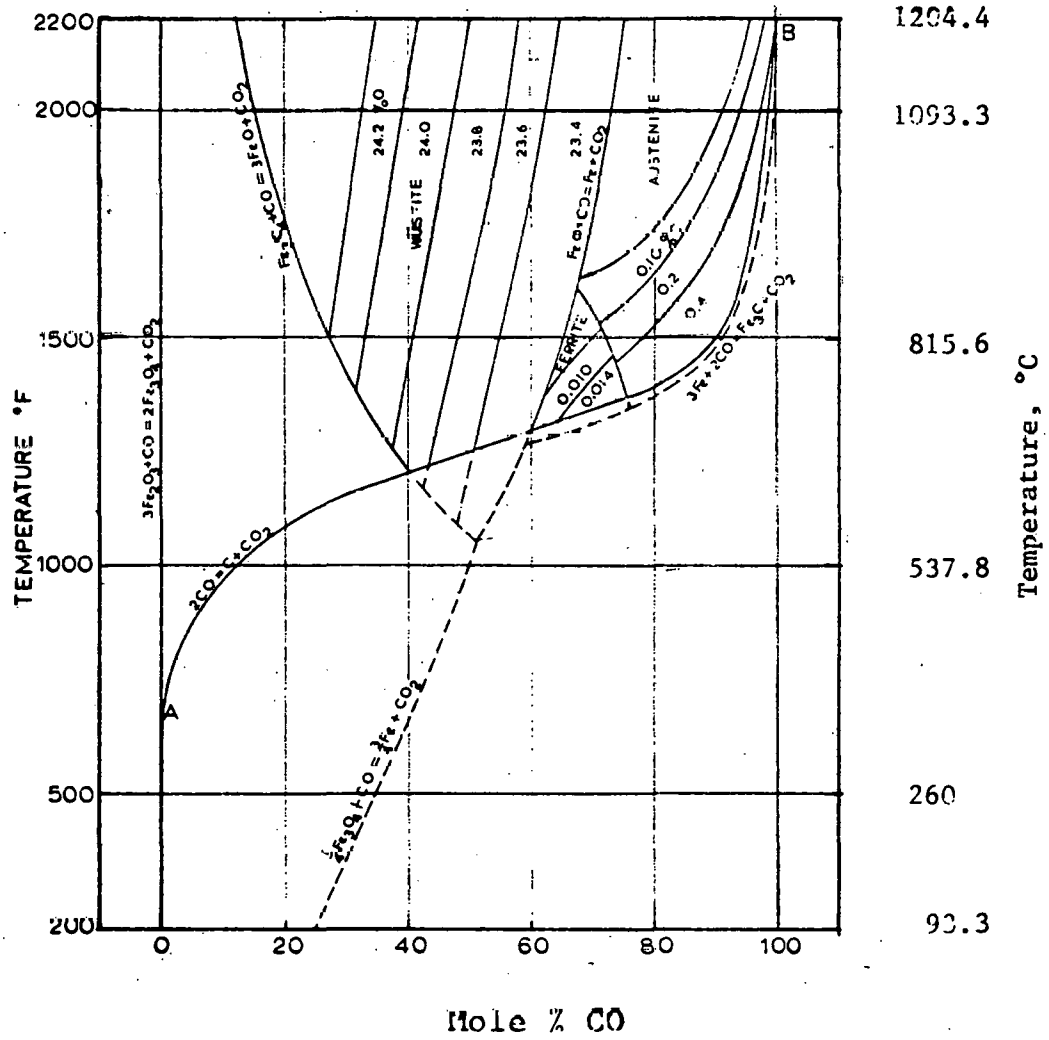

Figure 3.2(a) Iron Carbon-Oxygen equilibrium diagram (from Kirklady and Ward (1964)).

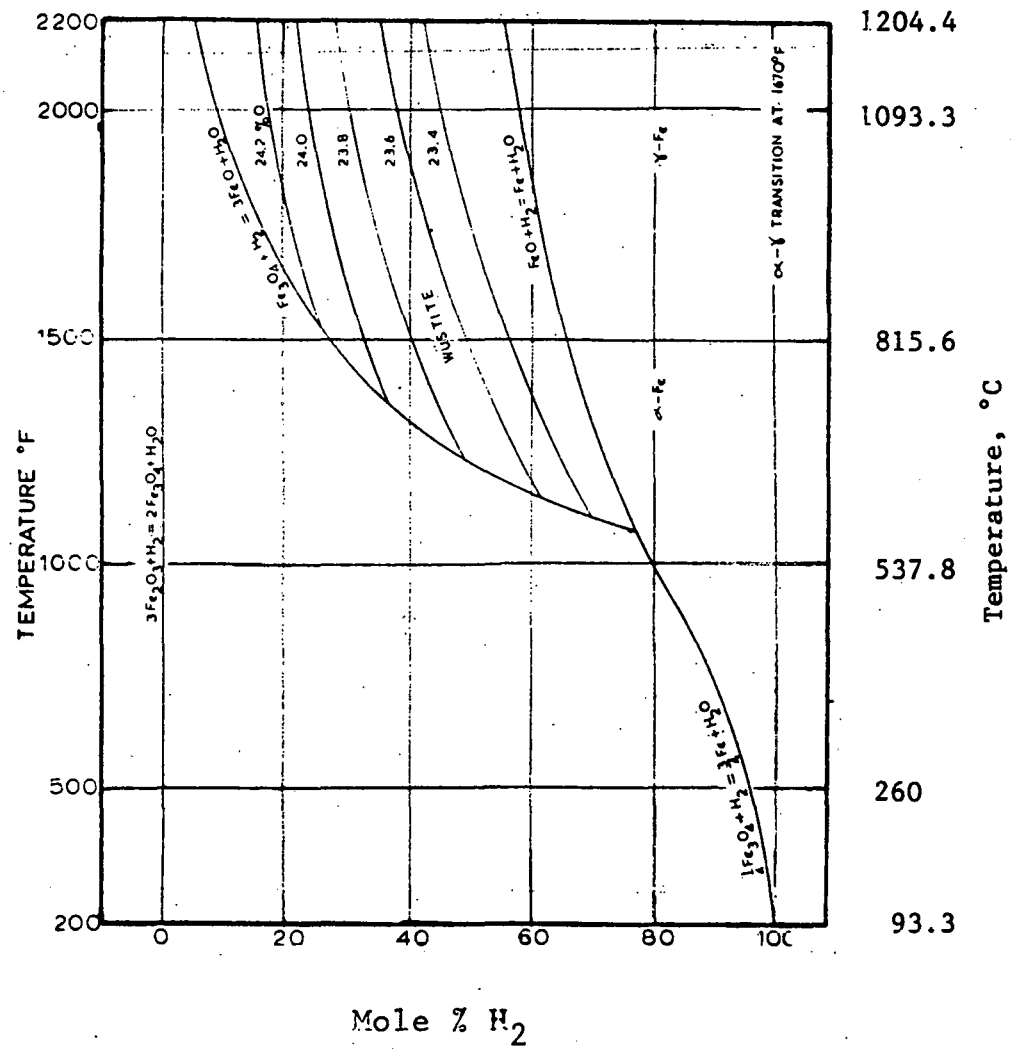

Figure 3.2(b) Iron-Carbon-Hydrogen equilibrium diagram (from Kirklady and Ward (1964)).

tures up to 973°K (1292°F). Beyond this temperature, the Fe_3O_4 phase starts transforming to (in low BTU gas atmospheres) FeO which results in a rapid decrease in fractional desulfurization. This decrease, an examination of Figure 3.1(a) reveals, becomes very large at about 1088°K (1500°F); therefore, a temperature of 1500°F may represent the upper limit for iron oxide based processes imposed by thermodynamic equilibrium considerations. The studies of Westmoreland and Harrison reported above also predict the stable phase of Fe_3C at temperatures 1073°K-1225°K and the formation of elemental iron above 1225°K. The $\Delta G°$, $\Delta H°$ and equilibrium constants for some of the reactions of interest in this chapter are listed in Table 3.1. Equilibrium constants for the iron formation reactions are also included in Figure 3.4.

3.2.2. Desulfurization:

During desulfurization, the oxides of iron may react with the hydrogen sulfide in the low-BTU gas to form solid sulfides according to the following chemical reactions:

$$Fe_2O_3+2H_2S+H_2 = 2FeS+3H_2O \quad (3.7)$$

$$Fe_2O_3+4H_2S = 2FeS_2+3H_2O+H_2 \quad (3.8)$$

$$Fe_3O_4+H_2+3H_2S = 3FeS+4H_2O \quad (3.9)$$

$$Fe_3O_4+H_2S = FeS_2+2FeO+H_2O \quad (3.10)$$

$$FeO+H_2S = FeS+H_2O \quad (3.11)$$

$$FeO+2H_2S = FeS_2+H_2O+H_2 \quad (3.12)$$

Table 3.1

THERMODYNAMIC PARAMETERS
FOR IRON OXIDE PROCESSES

Reaction[a]	$3Fe_2O_3 + H_2 = 2Fe_3O_4 + H_2O$			
Temperature, °K	650	800	950	1100
-ΔH, kcal	1.258	0.602	1.454	2.723
-ΔG°, kcal	14.649	17.830	21.009	23.994
K	8.43×10^5	7.43×10^5	6.81×10^4	5.86×10^4
Reaction[a]	$Fe_2O_3 + 2H_2S + H_2 = 2FeS + 3H_2O$			
Temperature, °K	650	800	950	1100
-ΔH, kcal	9.930	11.239	12.742	13.683
-ΔG°, kcal	24.260	27.435	30.337	33.036
K	1.43×10^8	3.13×10^7	9.54×10^6	3.66×10^6
Reaction[a]	$Fe_2O_3 + 4H_2S = 2FeS_2 + 3H_2O + H_2$			
Temperature, °K	650	800	950	1100
-ΔH, kcal	41.327	42.156	42.376*	44.224
-ΔG°, kcal	24.942	21.121	17.069	12.848
K	2.78×10^9	5.89×10^5	8.45×10^3	3.57×10^2
Reaction[a]	$4FeS + 7O_2 = Fe_2O_3 + 4SO_2$			
Temperature, °K	650	800	950	1100
-ΔH, kcal	593.650	591.888	589.720	588.629
-ΔG°, kcal	500.028	478.594	457.548	436.776
K	10^{100}	10^{100}	10^{100}	6.1×10^{86}
Reaction[a]	$4FeS_2 + 11O_2 = 2Fe_2O_3 + 8SO_2$			
Temperature, °K	650	800	950	1100
-ΔH, kcal	792.742	791.009	788.675	787.213
-ΔG°, kcal	743.942	732.847	722.149	711.763
K	10^{100}	10^{100}	10^{100}	10^{100}

*This number should correctly be 43.376.

Table 3.1 continued

Reaction[a]	$6FeS + 4SO_2 = 2Fe_3O_4 + 5S_2$			
Temperature, °K	650	800	950	1100
-ΔH, kcal	-32.743	-36.333	-38.739	-38.915
-ΔG°, kcal	-37.802	-38.582	-38.757	-38.731
K	1.94×10^{-13}	2.88×10^{-11}	1.21×10^{-9}	2.01×10^{-8}
Reaction[a]	$3FeS_2 + 2SO_2 = Fe_3O_4 + 4S_2$			
Temperature, °K	650	800	950	1100
-ΔH, kcal	-126.813	-126.586	-129.836	-130.077
-ΔG°, kcal	-61.552	-46.302	-30.746	-15.079
K	2.00×10^{-21}	2.21×10^{-13}	8.43×10^{-8}	1.01×10^{-3}
Reaction[b]	$FeS + H_2S = FeS_2 + H_2$			
Temperature, °K	500	645	1000	
-ΔG°, kcal	4.2	0.0	-7.5	
K	68.2	1	0.023	
Reaction[b]	$CO + H_2S = COS + H_2$			
Temperature, °K	500	800	1000	1200
-ΔG°, kcal	-0.301	-5.41	-6.84	-8.19
K	4.8×10^{-2}	3.3×10^{-2}	3.2×10^{-2}	3.2×10^{-2}
Reaction[b]	$CO_2 + H_2S = COS + H_2O$			
Temperature, °K	500	800	1000	1200
-ΔG°, kcal	-7.91	-7.70	-7.57	-7.45
K	3.5×10^{-4}	7.9×10^{-3}	2.2×10^{-2}	4.4×10^{-2}
Reaction[b]	$2FeS + SO_2 = FeO + 1.5S_2$			
Temperature, °K	1000			
-ΔH, kcal	-35.0			
-ΔG°, kcal	-22.5			
Reaction[b]	$3FeS + 5O_2 = Fe_3O_4 + 3SO_2$			
Temperature, °K	1000			
-ΔH, kcal	406			
-ΔG°, kcal	350			
K	-			

Table 3.1 continued

Reaction[b]	$3FeS + 2O_2 = Fe_3O_4 + 3/2S_2$		
Temperature	1000		
-ΔH, kcal	150		
-ΔG°, kcal	120		
K	-		
Reaction[b]	$3FeO + 2SO_2 = Fe_3O_4 + 1/2S_2 + SO_3$		
Temperature, °K	500	100	1500
-ΔH, kcal			
-ΔG°, kcal	0.0	-21.4	-34.5
K	-	-	-
Reaction[b]	$1/3Fe_2O_3 + SO_2 + 1/2O_2 = 1/3Fe_2(SO_4)_3$		
Temperature, °K	500	1000	1200
-ΔH, kcal			
-ΔG°, kcal	14.0	3.2	-9.4
K	-	-	-

[a] - from Schrodt and Hahn (1976)

[b] - from Case (1978)

$$Fe+H_2S = FeS+H_2 \quad (3.13)$$

$$Fe+2H_2S = FeS_2+2H_2 \quad (3.14)$$

$$FeS+H_2S = FeS_2+H_2 \quad (3.15)$$

Equations 3.7 and 3.8 represent the overall desulfurization reactions and may be obtained by combining the iron oxide reduction reactions (equations 3.1 to 3.6) with the equations 3.9 to 3.14 appropriately. Equilibrium constants for the overall desulfurization reactions are reported by Hilton (1974), Schrodt (1975b) and Schrodt and Hahn (1976). Data from these sources are used to plot Figure 3.3 giving equilibrium constants for reactions 3.7 and 3.8 as a function of temperature. It may be noted from this figure that the equilibrium constants are large in the temperature range of interest (700-1100°K), indicating favorable desulfurization. For many low-BTU gas compositions, the product to reactant ratios for reactions 3.7 and 3.8 are such that the ferric disulfide formation is not favored. The equilibrium constants for the desulfurization reactions are large enough to allow removal of H_2S consistently below the EPA standards of approximately 0.001 mole fraction for temperatures of up to 1200°K. Since there is no net change in moles of the gaseous species in reactions 3.7 to 3.15, total pressure will not affect equilibrium compositions. Desulfurization reactions are mildly exothermic with a $-\Delta H°$ value of about 8 kcal/mole H_2S.

A discussion on the stability regions of different

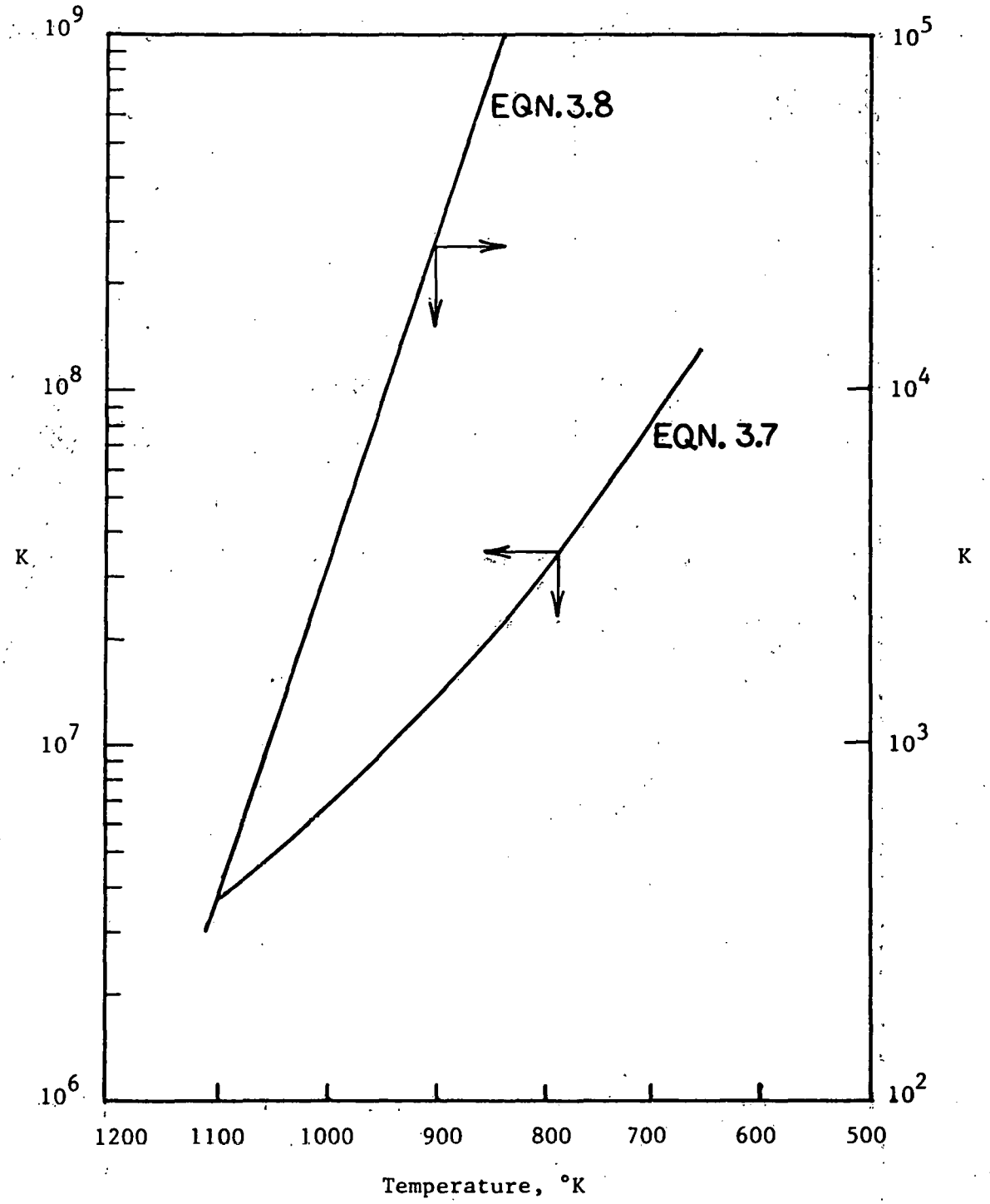

Figure 3.3 Desulfurization equilibrium constant.

iron sulfides is appropriate at this point. Only two iron sulfides are known to exist in a stable form at temperatures above 573°K, based on thermodynamic studies on iron-sulfur system. They are pyrrhotite and pyrite. Pyrrhotite is a nonstochiometric compound with varying degrees of iron deficiencies represented by $Fe_{1-x}S$ with x values of 0 to 0.34 (Hass and Khalafalla (1974)). The iron deficiency is caused by vacancies in the lattice. Pyrrhotite is similar in this respect to wustite ($Fe_{1-x}O$). Stoichiometric FeS with x=0, is known as troilite. Pyrite (cubic) is one of the two crystalline forms of iron disulfide, the other being the orthorhombic form called marcasite. Hass and Khalafalla (1974) found that at temperatures higher than about 573°K pyrite decomposed to pyrrhotite. Inspection of the equilibrium constants reported for equation 3.15 in Table 3.1 shows that above 630°K, the decomposition of FeS_2 is favored. Maa et al. (1975) have reported that pyritic sulfur was completely transformed to ferrous sulfide at about 873°K under hydrogen and at 1013°K under nitrogen. Similar observations were reported by Ganguly and Banerjee (1973) while studying recovery of elemental sulfur from pyrite by reaction with hydrogen and carbon monoxide. Attar (1978) also reported that the reduction of FeS_2 by H_2 to FeS and H_2S was favorable above 760°K. The empirical formula of $FeS_{1.5}$ reported from the preliminary work on the USBM

process (Abel (1974)) discussed previously in Section 2.2.3.3, was later found to overestimate the amount of sulfur absorbed by iron (Case (1978)) due to the inclusion of corrosion products; revisions indicated no sulfide of higher order than $FeS_{1.1}$. Schrodt (1977b) made a thermodynamic analysis using free energy minimization computer code; he also constructed Fe-S-O diagrams for comparing the computer predictions. These studies indicated that for standard low-BTU gas compositions in the temperature range 810°-1033°K, the solid sulfided reaction product was ferrous sulfide. This conclusion was strengthened by X-ray studies on ash particles. Based on the facts discussed in this section it may be concluded that iron sulfide (pyrrhotite) is the primary solid sulfur product of interest for desulfurization studies of low-BTU gas. Due to the lack of reliable thermodynamic data on nonstochiometric FeS, it is customary to use the data for troilite. Wustite and pyrrhotite are represented in this chapter by FeO and FeS respectively.

3.2.2.1. Secondary Reactions During Desulfurization:

Because of the presence of various gases in the low-BTU producer gas, several secondary reactions may take place during desulfurization. Some of the important ones are listed below.

$$CO+H_2O = CO_2+H_2 \qquad (3.16)$$

(Water-gas shift reaction)

$$2CO = C+CO_2 \quad (3.17)$$

(Boudouard reaction)

$$CH_4 = C+2H_2 \quad (3.18)$$

(Methane decomposition reaction)

$$CO+H_2S = COS+H_2 \quad (3.19)$$

$$CO_2+H_2S = COS+H_2O \quad (3.20)$$

$$RSH+H_2 = RH+H_2S \quad (3.21)$$

(Mercaptans)

$$C_4H_4S+4H_2 = C_4H_{10}+H_2S \quad (3.22)$$

(Thiophene)

$$CS_2+4H_2 = CH_4+2H_2S \quad (3.23)$$

Hydrolysis of the organic sulfur compounds in presence of water vapor may also be taking place according to the following reactions:

$$CS_2+2H_2O = CO_2+2H_2S \quad (3.24)$$

$$COS+H_2O = CO_2+H_2S \quad (3.25)$$

The free energy change, heat of reaction and equilibrium constants for some of these reactions are listed in Table 3.1. The first three reactions are undesirable since they tend to reduce the heating value of the fuel gas. Equilibrium constants for these reactions are shown in a graphical form in Figure 3.4, where it may be noted that reaction 3.16 is feasible in the temperature range of interest to the hot ash desulfurization process; the reaction is known to be catalyzed by iron and oxides of iron as discussed in Chapter 2. The reaction velocity has been found to be sufficient to allow attainment of equilibrium.

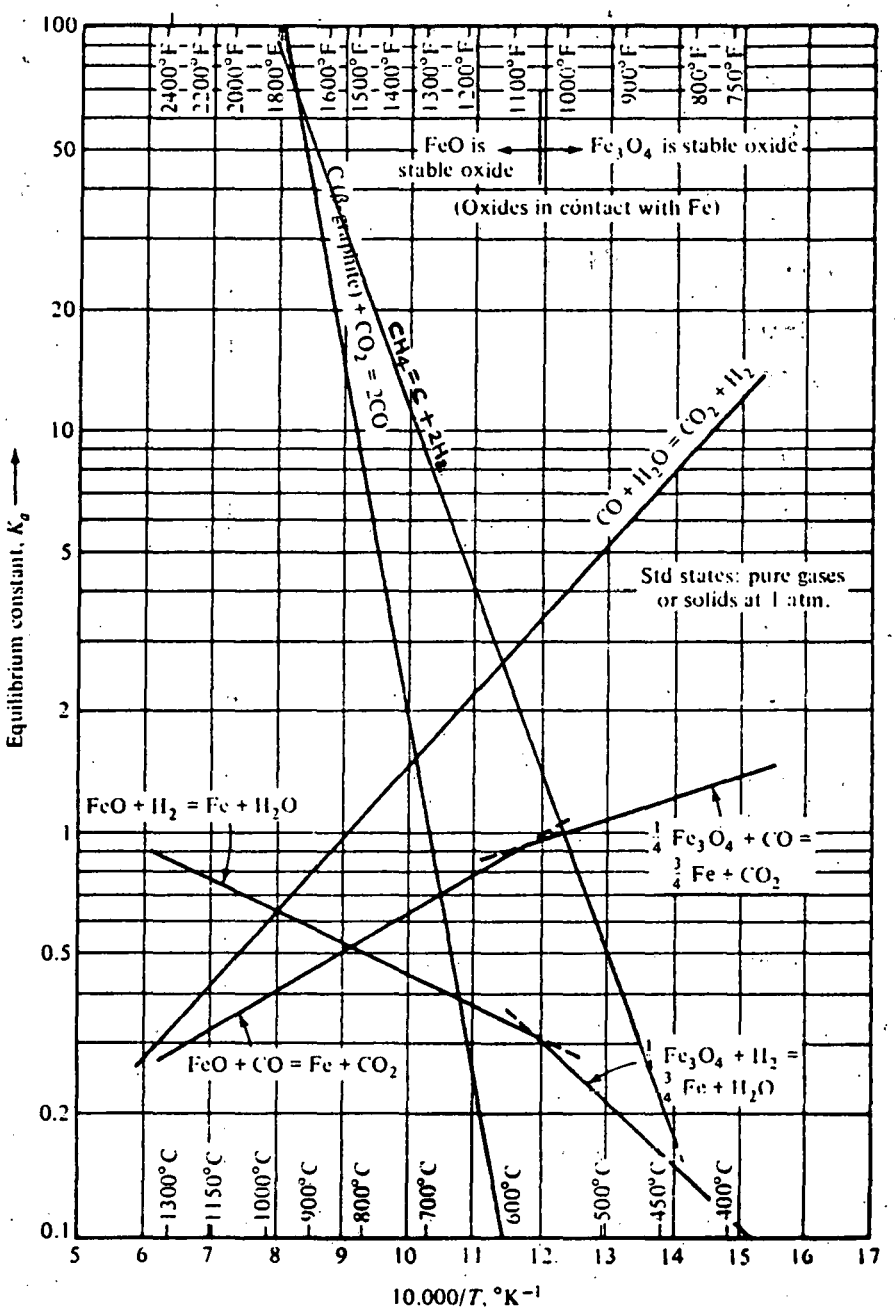

Figure 3.4 Equilibrium constants for the reduction of iron oxides and CO_2 (from Balzhiser et al. (1972)).

Reactions 3.17 and 3.18 may also be analyzed relative to Figure 3.4. Reaction 3.17 is favored by a decrease in temperature while 3.18 is favored by an increase. As pointed out in Chapter 2, the reaction velocities of these two reactions appear to be small; equilibrium predictions of the amount of carbon deposited are not observed in practice.

Reactions 3.19 to 3.24 are of great interest to the desulfurization process, as the inability to control the emission of organic sulfur may make the process unsuitable. Bhatia (1971) studied the catalytic promotion of these reactions to hydrogen sulfide and the subsequent removal of the H_2S using iron oxide containing "Luxmasse". It was mentioned in Chapter 2 that the iron oxide sorbents were found to remove these organic sulfur compounds satisfactorily. Metal oxides are known to catalyze the organic sulfur reactions.

3.2.3. Regeneration Reactions:

Regeneration of spent sorbent may be accomplished by roasting the sulfide with oxygen. Some of the reactions of interest to the regeneration step are listed below.

$$4FeS+7O_2 = Fe_2O_3+4SO_2 \quad (3.26)$$

$$4FeS_2+11O_2 = 2Fe_2O_3+8SO_2 \quad (3.27)$$

$$6FeS+4SO_2 = 2Fe_3O_4+5S_2 \quad (3.28)$$

$$3FeS+2O_2 = Fe_3O_4+3/2S_2 \quad (3.29)$$

$$3FeS+5O_2 = Fe_3O_4+3SO_2 \quad (3.30)$$

$$2FeS+SO_2 = 2FeO+1.5S_2 \quad (3.31)$$

The standard free energies, enthalpies and equilibrium constants for some of the regeneration reactions are included in Table 3.1. It is to be noted that all the regeneration reactions are highly exothermic and sensitive to total pressure. A phase diagram for iron oxides and sulfur with respect to oxygen prepared by Case (1978) is given in Figure 3.5. This phase diagram may be used to determine the resulting solid phases during regeneration. Figure 3.5 indicates that oxygen-starved regeneration will produce Fe_3O_4 and S_2 at proper conditions. Reaction 3.26 proceeds to completion (due to the large equilibrium constants) in excess air. It may be noted from the phase diagram that S_2 vapor cannot coexist with Fe_2O_3. Oxygen-limited regeneration results in the reaction of FeS with SO_2 according to reaction 3.28. According to the thermodynamic investigations of Case (1978), the maximum possible S_2 yield is 15-20% regardless of temperature; the S_2 yield increases from 4.7% of the total sulfur gases at 1000°K to a value of 10% at 1200°K. Obviously, the production of elemental sulfur is desirable. Regeneration with steam reported by Ganguly and Banerjee (1973) deserves consideration. They reacted pyrite with steam to produce elemental sulfur at temperatures of 1173-1373°K. It was suggested that FeS_2 converted to FeS with further release of sulfur from the latter. The unfavorable equilibrium restrictions were overcome by maintaining a high mole ratio

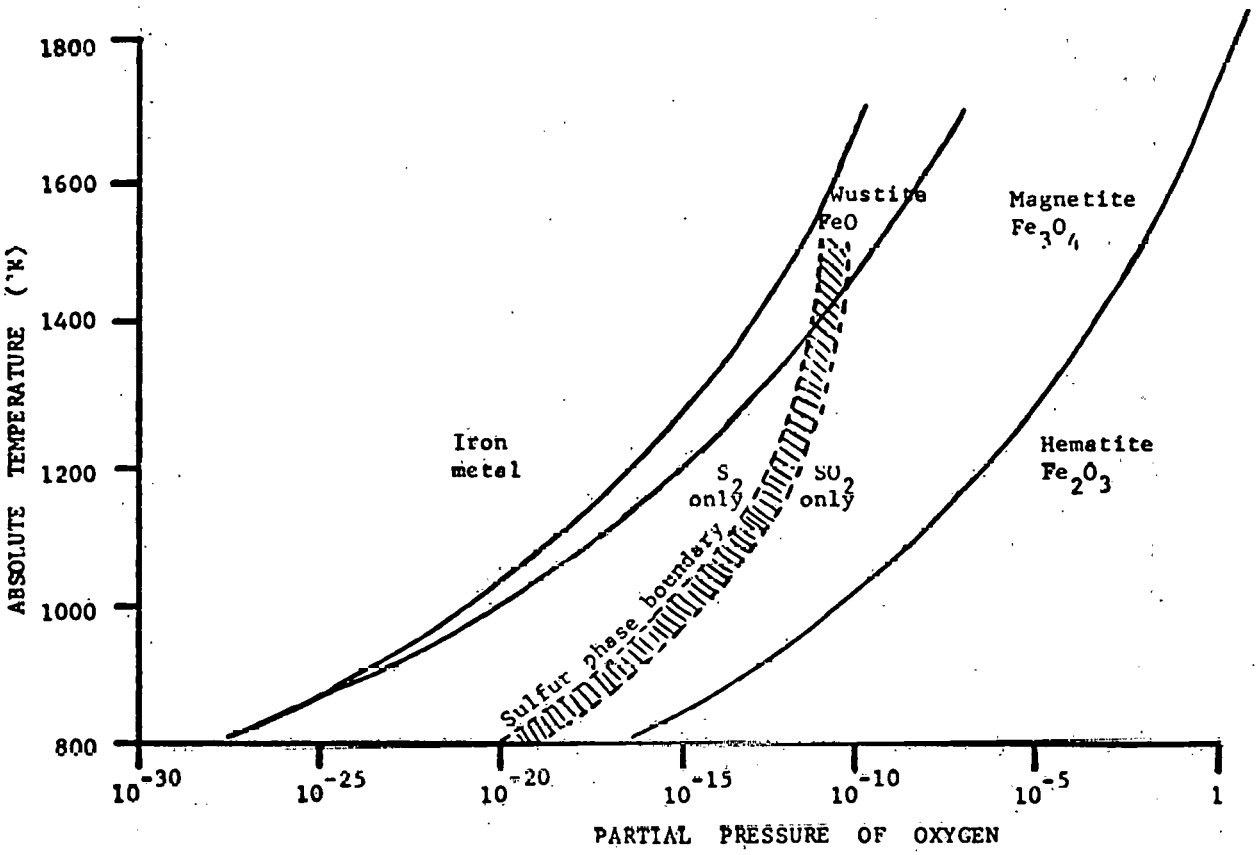

Figure 3.5 Phase diagram for iron oxides and sulfur with respect to oxygen partial pressure (from Case (1978)).

of steam to sulfur vapor. In this process, the yields of elemental sulfur and sulfur evolved as hydrogen sulfide and sulfur dioxide were, respectively 84.5 and 13.7% of total sulfur at 1273°K. The calcine contained ferrous oxide, ferroferric oxide, silica and 1.3% sulfur.

Since it was established in Section 3.2.2 that pyrrhotite is the only sulfide phase of interest during desulfurization, regeneration of FeS_2 is not considered here.

3.3 Review of Kinetic Studies

3.3.1. Desulfurization:

In spite of the fact that iron oxide has been used for H_2S purification since 1849, no quantitative kinetic data has been reported for the high-temperature reaction of H_2S with iron oxides prior to 1970. Westmoreland et al. (1977) reported comparative kinetics of high-temperature reaction between H_2S and oxides of Mn, Ca, Zn and V over the range 573-1073°K. All reactions were found to be first order with respect to H_2S and obeyed the Arrhenius equation. The relative magnitude of reaction rates determined was $MnO > CaO \gtrsim ZnO > V_2O_3$. Activation energies of 5690-8834 cal/mole were found.

Brandon (1973) evaluated the kinetics of the desulfurization reaction for iron oxide. He correlated his data according to the rate expression: $R_s = -k_v C_A^{.85} C_S$ where C_A and C_S refer to the H_2S and iron oxide concen-

trations respectively. The following values of k_v were reported.

Temperature (°C)	k_v moles H_2S / liter-min
623	25.4
673	50.7
723	77.7
773	55.0

It is to be noted that the units of k_v are not consistent with the rate expression used; no explanation is found in the work for this apparent discrepancy. Brandon explained the decrease of the rate constant as due to structural changes within the solid. No activation energy was reported. Since the activation energy is independent of the units used for the rate constant, a value may be obtained for the range 623-723°K as follows:

$$\ln \frac{25.4}{77.7} = - \frac{E}{R} \left\{\frac{1}{623} - \frac{1}{723}\right\}$$

Therefore, E = 9972 cal/mole.

Unfortunately, Brandon studied the reaction in the absence of CO and H_2, the reducing gases normally present in low-BTU producer gas; hydrogen sulfide in nitrogen streams were used for the studies. The effect of the absence of reducing gases on Fe_2O_3-H_2S kinetics is not known.

Gavrilova (1972) studied the H_2S removal reaction with iron oxide containing ore using thermogravimetric ap-

paratus. Dry fuel gas streams with about 0.42-1.0% H_2S were reacted with iron oxide particles of 0.5 to 1.0 mm. diameter. No dependence of reaction rate with linear velocity was found in the temperature range 628-783°K and linear velocities around 3.4 m/sec. Reaction was found to be first order with respect to H_2S concentration when the concentration was varied from 0.3 to 1.0% at 773°K. The kinetic data were correlated using the following expressions

$$y^n = K_o t \quad \text{for} \quad 628\text{-}783°K$$

$$y = K_1 t \quad \text{for} \quad 873\text{-}1073°K$$

where y is the thickness of the sulfided layer in mm., t the time and K_o, K_1 the rate constants. An activation energy of 11,800 cal/mole was obtained for the temperature range 628-783°K. In the higher temperature range of 873-1073°K, the activation energy was 1800 cal/mole indicating external mass transfer control. The linear velocity was 0.53 m/sec for the higher temperature range experiments.

The APCI packed bed data ((Joshi and Leuenberger (1977)) previously discussed in Section 2.2.3.3 was correlated to obtain kinetic expressions useful for scaleup. The regime of control was found to change from kinetic to diffusional as the solid was converted. A semi-empirical model was proposed to predict the breakthrough curves. The following rate parameters were obtained.

Activation energy, E = 7771 cal/ g mole

Arrhenius frequency factor, A = 4.52×10^7 $\frac{cm^3}{(min)(g\ mole\ Fe_2O_3)}$

The rate equation proposed was,

$$-R_A = A\ e^{-E/RT} I f y$$

where,

$-R_A$ = rate of consumption of H_2S, ((g mole)/ (cm^3 pellet)(min))

I = sorbent Fe_2O_3 concentration (g moles/ cm^3 solid)

f = gas molar density (g mole/cm^3)

y = H_2S mole fraction in gas phase of porous pellet

T = temperature (°K)

R = gas constant cal/(g mole-°K)

Schrodt (1978) developed kinetic models based on the packed bed studies using coal ash reported in Section 2.2.3.4. As in the case of the APCI studies it was found that the regime of control shifted from kinetic to pore diffusion as the solid converted. The solid conversion at which this change occured was determined to be approximately 0.8. For the kinetic regime, the following kinetic factors were evaluated:

Activation energy, E = 2740 cal/g mole

Arrhenius frequency factor, A = 6.74×10^6 cm^3/g mol-min

The rate equation is the same as the one given previously for APCI study. Pore diffusivities were observed to be of magnitude 10^{-1} to $10^{-2} cm^2/hr$.

Hasatani and Wen (1977) studied the reactivity of iron oxide sorbents (pelletized composition of 45 wt% Fe_2O_3 and 55% silica) in a hot simulated low-BTU gas containing H_2S at temperatures between 873-1173°K using a thermogravimetric analyzer. The iron oxide was first reduced in separate reduction runs by reacting with H_2 and CO; the reduced sorbent was then sulfided in a low-BTU gas stream. A limited number of runs were also conducted involving simultaneous reduction-sulfurization, and direct reaction of H_2S with iron oxide in the absence of reducing gases. Iron oxide reduction experiments revealed that (1) a spongy metal iron formed as a result of reduction; (2) intrinsic chemical reaction rate controlled reduction rate of pellets smaller than 0.2 mm (activation energy of 12.3 kcal/mole); (3) diffusion became increasingly important as particle size increased beyond 0.2mm. Sulfurization results revealed that (1) the reaction was first order with respect to H_2S; (2) the sulfurization rate exhibited the same trends as seen for reduction; (3) the activation energy was 2.65 kcal/mole. It was suggested that sulfurization and iron oxide reduction occured simultaneously during the first period of the reaction. It was found that a spongy metal iron formed as a result of

the reduction reaction was found to be more reactive with H_2S than iron oxide itself. The chemical composition of the final sulfurized iron oxide at equilibrium was determined to be close to $FeS_{1.1}$. The presence of water vapor was found to have no effect on the sulfurization rate. The direct sulfurization of iron oxide pellets with (H_2S+N_2) gas containing no reducing gases appeared slower in comparison with the situation when reducing gases were present. It was also concluded that the weight change curve of the simultaneous reduction-sulfurization reactions could be derived by simply adding the two curves obtained from that of the separate reduction and sulfurization. Unfortunately, Hasatani & Wen seem to have drawn this conclusion from tests conducted at over 1100°K. Recalling here the work of Gavrilova (1972) that was discussed earlier, it is interesting to note that he reported activation energies of 11800cal/ mole for the temperature range 628-783°K and 1800 cal/ mole for the range 873-1073°K. On the other hand, Hasatani and Wen conducted all their studies above a temperature of 873°K. Since Gavrilova reported that mass transfer was controlling in the range 873-1073°K, it raises the question whether Hasatani and Wen were not entirely in the transport controlled regime.

Korobeinichev (1967) studied the mechanism of the reactions of H_2S and COS with Fe_2O_3 taking place during the removal of sulfur compounds from fuel gases using the

calorimetric method. The solid, iron oxide containing material was either bauxite or pure Fe_2O_3. At 423-623°K the only solid reaction products of the interaction between Fe_2O_3 and H_2S were FeS and FeS_2. The reaction rate and the product composition were found to depend on the degree of solid phase conversion. With the increase of conversion, the ratio between H_2 and H_2O in the reaction products first increased and then decreased. The reaction was found to take place at temperatures above 593°K only. In the presence of H_2S, the reaction between COS and bauxite was strongly accelerated; this was not the case in the reaction of COS with pure Fe_2O_3. The reaction of COS with bauxite in the presence of H_2S was found to be zero order in COS and first order in H_2S. The mechanism was explained as follows: a slow reaction $1/3Fe_2O_3+H_2S = 1/3FeS_2+1/3FeS+H_2O$ and a fast reaction catalyzed by the Al_2O_3 in the bauxite, $COS+H_2O = H_2S+CO_2$, which regenerated the H_2S. In Chapter 2, it was mentioned while discussing the Appleby-Frodingham process that Reeve (1958) suggested that iron oxide catalyzed the conversion of organic sulfur to H_2S; however, the work of Korobeinichev (1967) discussed above contradicts this finding. This apparent disagreement may be explained as follows: The catalytic effect observed by Reeve might have really been due to the oxides other than Fe_2O_3 that were present in the iron ore he used. Also, Reeve did not make a systematic

study on this subject.

3.3.2 Regeneration:

The kinetics of the roasting reaction of ferrous sulfide by air was studied by Niwa et al. (1957) by means of the spring balance and X-ray diffraction analysis over the temperature range 773 to 973°K. At the initial stage of oxidation no evolution of SO_2 was found. This was interpreted as follows: iron ion reacted with oxygen by migrating from the interior of FeS crystal to the surface until the deficiency of iron attained a limiting value. Above 600°C the rate of oxidation did not change with temperature; gas phase diffusion was found to be the rate-determining factor.

Shakhtahtinskii (1974) has reported the formal kinetics of the fluidized bed roasting of ferrous sulfide. The reaction was carried out at 733-1093°K in air. At 1093°K, 93% of the sulfur was removed in 60 sec. The roasting process was a first order reaction which was kinetic below 808°K, translational from 808-959°K, and diffusional above 959°K, with activation energies respectively of 60.55, 14.99 and 3.2 kcal/mole. Kinetics of the oxidation of FeS were also reported by Calistru et al. (1965). Study of the reaction of water vapor with iron sulfide at high temperatures were reported by Montilo et al. (1975).

Vanyukov (1973) used differential thermal analysis

to study the oxidation kinetics of ferrous sulfide. Defects in ferrous sulfide were found to markedly affect their oxidation kinetics. As observed by Niwa (1957), the oxidation of FeS and $Fe_{0.83}S$ was found to proceed with an induction period (no SO_2 evolved). The effective activation energies found were 91.1 kcal/mole for FeS and 4.41 kcal/mole for $Fe_{0.83}S$.

Wen et al. (1978) studied the reaction of SO_2 with ferrous sulfide in a thermogravimetric analyzer. The initial rate of reaction was found to be first order with respect to the concentration of sulfur dioxide in the gaseous phase. Apparent activation energy of 6660 cal/mole was obtained. It was felt that intraparticle diffusion might play an important role in the rate controlling step.

For the packed bed air regeneration of sulfided coal ash, Schrodt (1978) reported the following rate constant:

$$k = 1.10 \times 10^{7} \exp(-799/RT)$$

The units are the same as for desulfurization.

Joshi and Leuenberger (1977) report the following rate parameters for the regeneration reaction with air and steam obtained from the APCI studies:

$$k = 4.33 \times 10^{8} \exp(-15542/RT)$$

units being the same as for the desulfurization rate constant. For regeneration, oxygen should be used instead of H_2S while defining concentrations.

CHAPTER 4

EQUIPMENT AND OPERATING PROCEDURES

4.1 Description of Experimental Setup

Figure 4.1 is a sketch of the equipment and Figure 4.2 is a picture of the experimental setup.

Pure gases from cylinders were used to obtain the simulated low-BTU gas used for the experiments. Each gas cylinder was equipped with a pressure regulator in order to obtain steady gas flows. Prior to mixing, the gases passed through individual rotameters. The mixed low-BTU gas passed through a calibrated rotameter (5) before entering the reactor. This rotameter (with Matheson 602 tube) was used to monitor the actual volumetric gas flow into the reactor. Calibration curve for this rotameter is given in Appendix H. Where necessary, the gas lines were heat-traced to keep the gas streams above the dew point of water vapor. Water vapor could be added to the inlet reactor fluid stream using the vapor generator shown in Figure 4.1. Nitrogen was bubbled through the heated water in the vapor generator to obtain a water vapor-saturated nitrogen stream. Water vapor concentration in nitrogen was regulated by controlling the energy input to the electrical heater that was installed inside the vapor

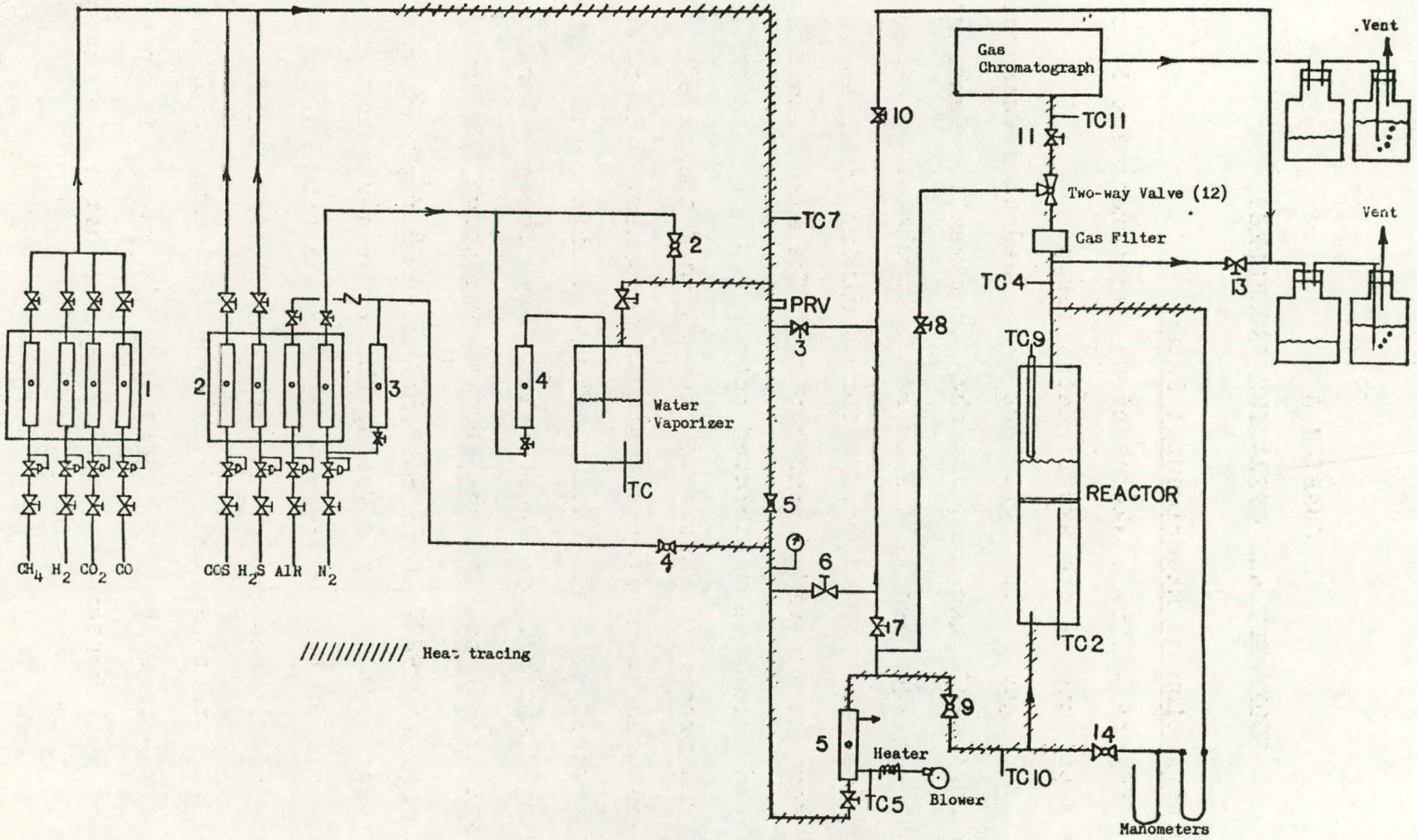

Figure 4.1 Experimental Setup

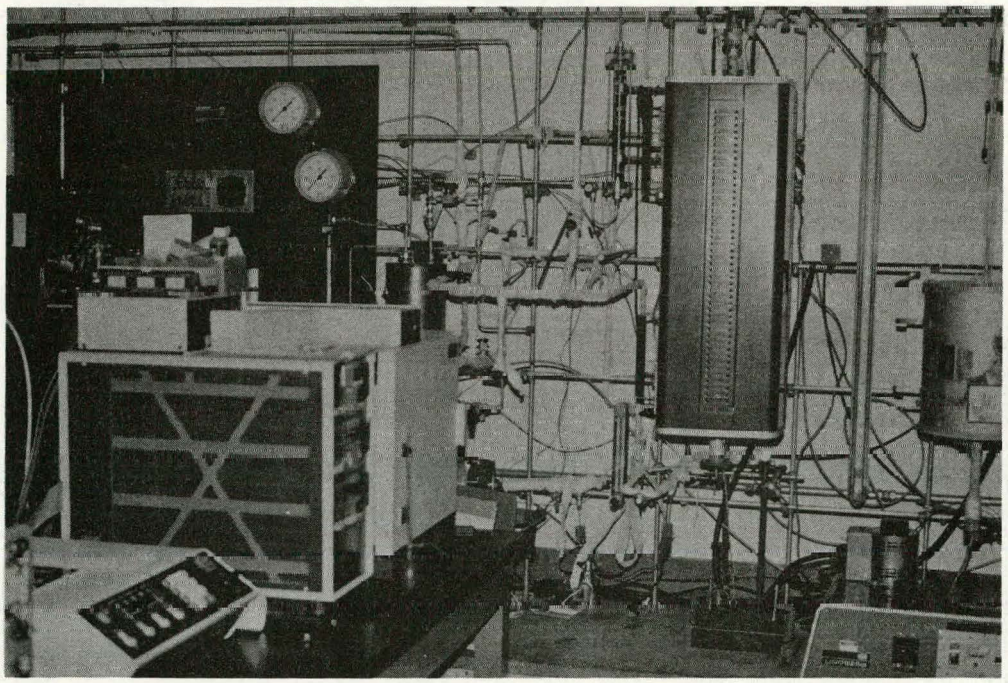

Figure 4.2 A picture of the experimental set up.

generator. For runs requiring no water vapor input, the vapor generator was bypassed using the by-pass valves. The nitrogen (nitrogen saturated with water vapor when water vapor was included in inlet stream) stream was mixed with the stream containing other gases (CH_4, H_2, CO_2, CO, H_2S) prior to entering rotameter-5. For regeneration, only air was mixed with nitrogen to obtain the desired oxygen concentration in the stream. Using the two-way valve (12) shown in Figure 4-1, either the reactor inlet or the exit gas streams could be sampled for the chromatographic analysis.

Due to the relatively high reaction temperatures, quartz tube was selected for reactor construction. The inside diameter of the reactor tube was 20 mm (0.787 inch) while the length was about 102 cm (40 inches). A porous quartz disc was fused inside the tube at approximately 22 inches from one end. This disc served the dual purpose of a support for the ash bed and a gas distributor. The portion below the quartz disc was filled with inert ceramic chips to preheat the gas stream to the reaction temperature. A thermowell made of quartz tube of ¼" diameter (nominal) was installed as shown in Figure 4.3. The well was so placed that the bottom tip made contact with the fluidized ash bed without hindering the process of fluidization. The reactor assembly was placed inside a Lindberg Model 54251 single-zone tube furnace equipped with a Model

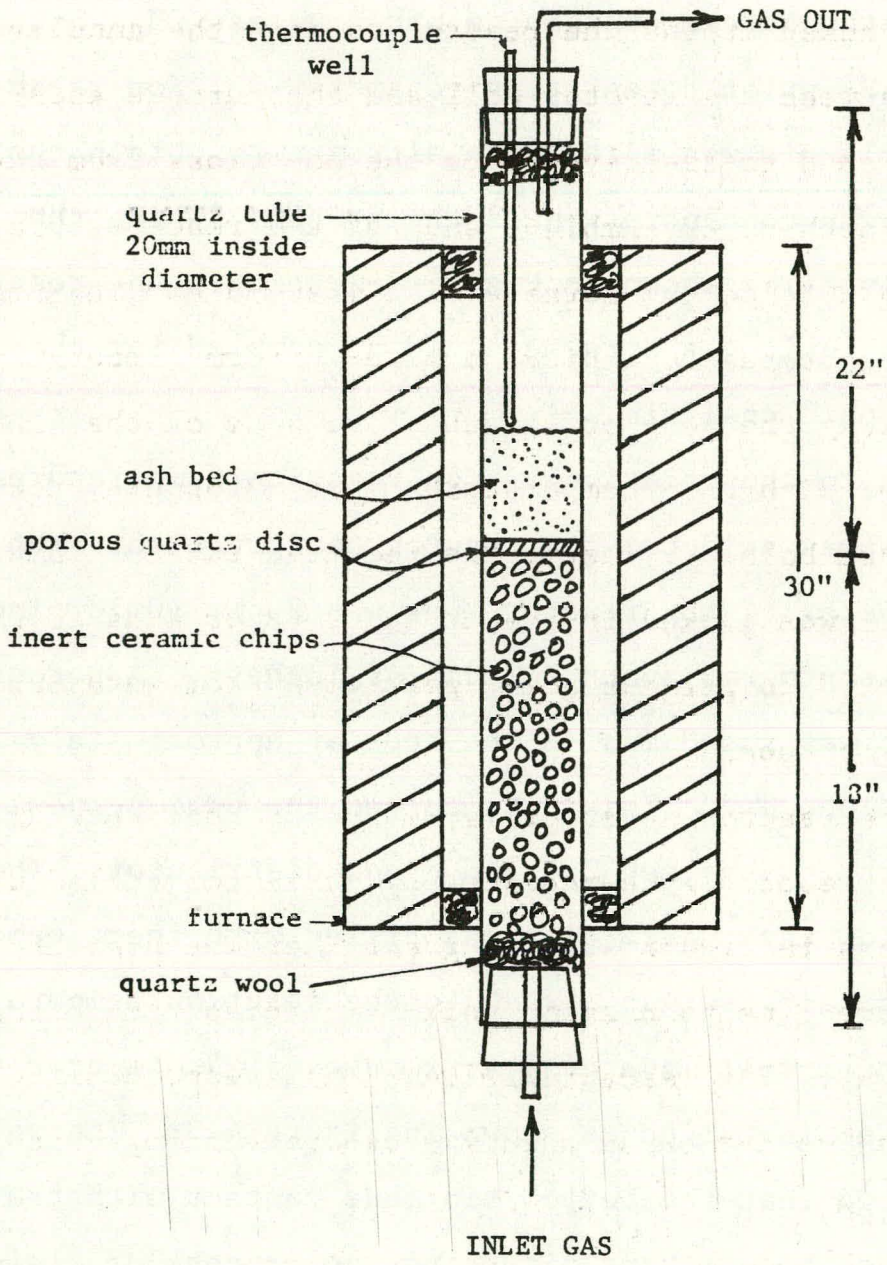

Figure 4.3 Reactor setup.

59344-S temperature controller. The furnace system offered excellent temperature control, the deviation range being about ±3°F from the set point. The furnace tube-cavity measured 2 inches i.d. by 31 inches long. Quartz wool was packed around the reactor to seal the annular spacing between the reactor wall and the furnace ends; this was found to greatly reduce the heat loss from the system. Further, the ambient ends of the reactor tubes protruding outside the furnace were wrapped and heated with heating tapes to achieve a more uniform temperature profile along the reactor length. The ends of the reactor were sealed with high-temperature rubber stoppers; the stoppers had holes to insert the required tubes. Some quartz wool was packed inside at the reactor ends as shown in Figure 4.3 to prevent solid particles from entering the gas-carrying tubes.

The reactor inlet pressure and the pressure drop across the reactor were measured by the water-filled manometers shown in Figure 4.1. A gas filter was provided on the GC purge line to prevent solid particles from being carried over. The reactor effluent gases were bubbled through sodium hydroxide solution before venting into the exhaust hood.

The isothermality of the reaction zone was tested using a thermocouple inserted from the reactor tube bottom extending to the bottom surface of the quartz support

plate. Comparison of this temperature with the one obtained from the thermocouple near the surface of the ash bed (explained earlier) showed that the temperature was uniform in the reaction zone.

A Varian Model 3700 gas chromatograph was used for gas composition analysis. The GC was controlled by a Chromatographic Data System (Varian CDS-111) that also processed the peak data. A thermal conductivity detector was used for peak sensing. Two different chromatographic columns were used in series for separating the gas components: A molecular sieve 5A, 30/60 column; and a Chromosorb 107, 100/120 column. Both columns were made of 1/8 inch diameter by 6 feet long stainless steel tube. A sampling loop located inside the GC oven was used to inject gas samples; the sampling loop had an approximate gas volume of 200 microliters. Columns were switched during the analysis by two automatic valves. The sampling and column-switching valves responded to time-programmed commands from the CDS-111. Figure 4.4 shows the arrangement of these valves and the columns; Figure 4.5 gives the analysis sequence. The position shown in Figure 4.4 was the normal arrangement (before sample injection) of the valves and the columns.

The analysis is started at a temperature of 100°C. Position-1 in Figure 4.5 indicates the sample injection. At this point, both the columns are in series. As seen in

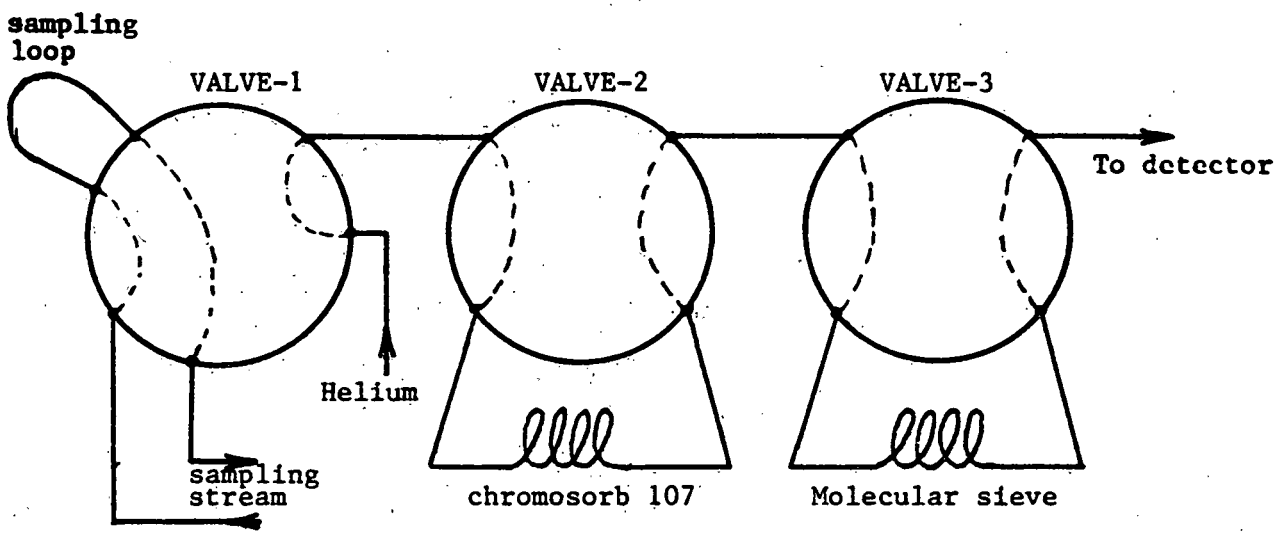

Figure 4.4 Arrangement of valves and columns.

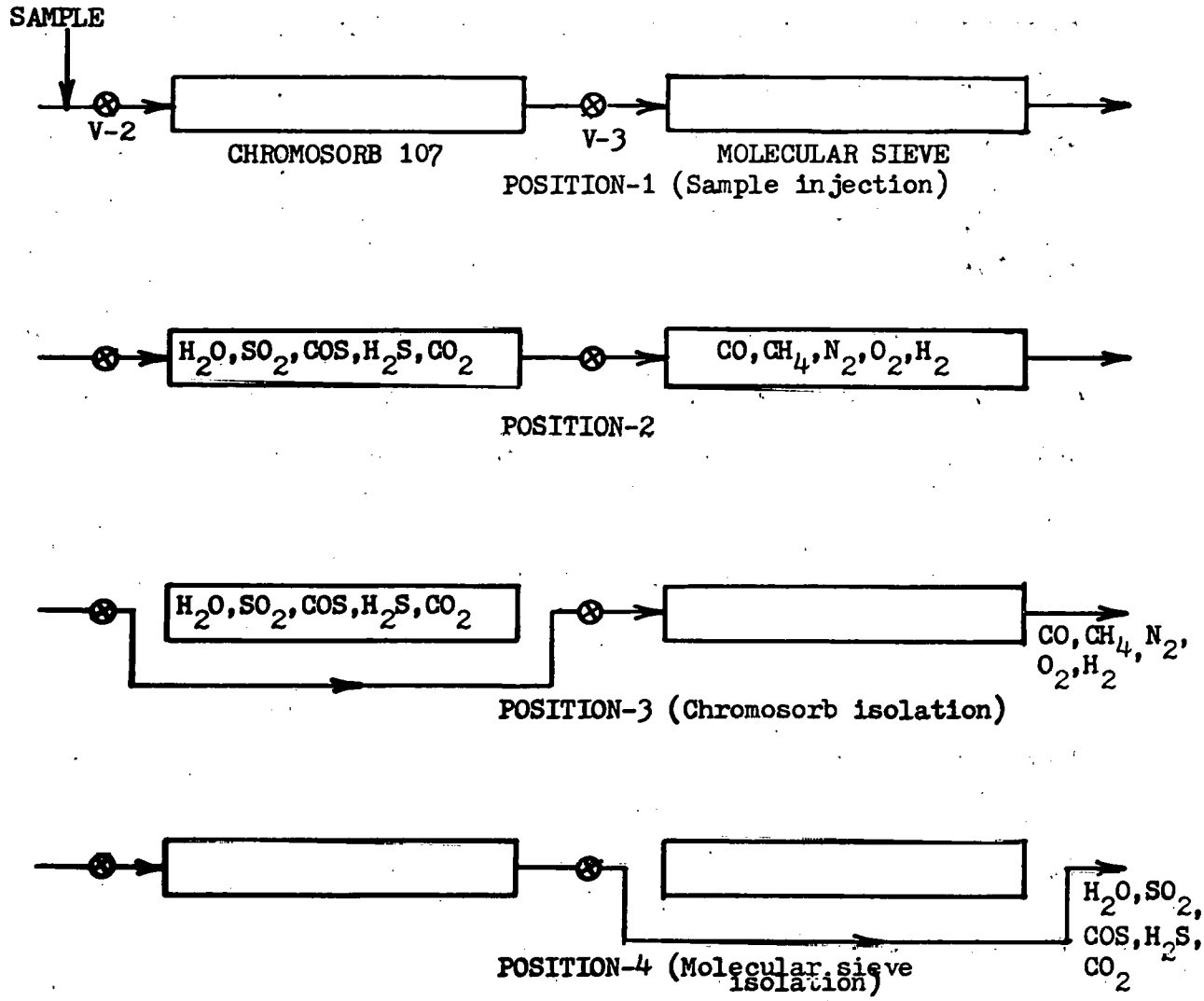

Figure 4.5 The analysis sequence.

Position-2, the gases have been separated with their relative positions inside the columns as indicated. The molecular sieve column separates CO, CH_4, N_2, O_2 and H_2 while the chromosorb 107 column separates H_2O, SO_2, COS, H_2S and CO_2. Since molecular sieve is easily inactivated by the latter gases due to irreversible adsorption, care must be exercised not to expose this column to these gases. A helium carrier gas flow rate of 30 ml/min each is used for analysis and reference columns. The situation depicted by Position-2 happens at about 1.40 minutes after sample injection. At this time, the Chromosorb column is isolated by valve switching as shown in Position-3 and the gases departed by the molecular sieve column are allowed to elute. This position is maintained until carbon monoxide is eluted out. When this happens (at 4.60 mins.) the valves V2 and V3 are switched again to isolate the molecular sieve column as indicated in Position-4. The gases separated by the Chromosorb column now elute. Also, at 7.00 minutes the temperature programming sequence is started with a rate of 20°C per minute, the maximum temperature being 150°C. Water peak elutes at about 12 minutes and the analysis is ended at 13.0 minutes. The setup returns to Position-1 automatically for the next sample injection. Figure 4.6 shows the programming on the CDS-111.

Internal normalization was the analysis method

SECTION 1

1	ID#	28#
2	S/N	2N
3	IPW	8S
4	TAN%	1.60%
5	AREJ	50A
6	STOP	13.00N

SECTION 2

LINE	TIME	EVT	VALUE
1	.00	8D1	.50
2	.00	2FB	.09
3	.01	6XE	.08
4	.10	6XE	.00
5	.10	2FB	1.34
6	1.30	6XE	.02
7	1.50	4S	.75
8	4.47	2FB	4.48
9	4.48	2FB	4.60
10	4.50	6XE	.04
11	4.51	5T%	.00
12	6.00	5T%	1.60
13	6.00	2FB	6.05
14	6.50	7PR	20
15	6.05	4S	2.00
16	9.02	7PR	00
17	9.50	4S	.75
18	10.50	4S	2.00

SECTION 3

1	CALC	1#
2	VIAL	1#
3	SEND	0#
4	LINK	0#
5	DCML	4#
6	UPF	.000000#
7	REF	5%
8	MUST	0A
9	MUST	0%
10	DATA	5%
11	DATA	.00N
12	FACT	10%
13	ALRM	0#

SECTION 4

	PK.	TIME	AMOUNT	AVE.FACT
H_2	1	1.43	.000000	77.69200
O_2	2	1.79	.000000	1.011760
N_2	3	2.05	.000000	1.000000
CH_4	4	2.97	.000000	1.013470
CO	5	3.33	.000000	.821178
CO_2	6	4.97	.000000	.695190
H_2S	7	6.85	.000000	.688418
COS	8	7.25	.000000	.642914
SO_2	9	10.60	.000000	.468300
H_2O	10	11.10	.000000	1.304000

SECTION 6

1	VOL	0
2	CAL	1
3	SAMP	1
4	ESP	2
5	R/O	0
6	DRFT	60
7	TEMP	100

Figure 4.6 CDS-111 Program.

employed. Response factors were calculated using standard gas mixtures relative to nitrogen; the nitrogen response factor was arbitrarily chosen to be unity. Care was exercised to obtain a positive hydrogen peak. Hydrogen is a difficult gas to analyze chromatographically; at certain H_2 concentrations negative and M shaped peaks may occur (Purcell and Ettre (1965)).

4.2 Procedure

Ash preparation: The original ash samples obtained from gasification plants consisted of varying sizes with some lumps measuring as big as 3-4 inches. First, the larger lumps were broken into smaller sizes (about ¼"). The latter were then broken down further using a rotating-plate crusher and sieved using a Rotap siever into varying cuts. The fluidizing characteristics of these cuts were studied. The results are discussed in Chapter 6. Based on these results, the choice of the proper ash particle sizes for reaction studies was made. The selected ash particles were prepared for reaction studies by heating in a muffle furnace at 800°F for 24 hours. This was done to burn off the carbonaceous and volatile components that might be present in the coal ash. This ash was sieved again and the proper cut was weighed to obtain a static bed length of 1 to 2 inches. The weighed ash was then charged into the reactor and fluidized overnight at 1200°F with air. Desulfurization studies were conducted using

this ash bed.

Experimental Procedure:

The oxidized ash bed was continuously purged using a nitrogen stream while heating to reaction temperature. The exit gas was analyzed using the GC to make sure that all the oxygen was purged out of the reactor. The reactor was then isolated by closing valve-9, valve-13 and changing the position of the three-way-valve-12. With the reactor isolated, the gas flow for H_2S adsorption reaction was started. The individual gas flows were set using rotameters 1 and 2. The total flow rate of the mixed gases was set using rotameter-5. The three-way-valve-12 admitted the analysis stream to the GC. Valve-10 and Valve-7 were open during this period. The appropriate gas-line heating tapes were turned on. The simulated low-BTU gas stream was continuously analyzed till the compositions and flow rate stabilized. Usually, this procedure took about three hours. Upon reaching stable conditions, the gas was admitted into the reactor by opening valves 13 and 9 and closing valves 8, 7 and 10. The position of the three-way-valve-12 was changed so that the reactor exit gas now passed through the GC sampling loop. Valve-13 was adjusted so that the desired flow rate of about 20 CC/minute was obtained through the GC sampling line. A stopwatch was used to follow the reaction time. When the H_2S adsorption reaction was over as indicated by the GC, the gas flow was stopped by closing

the gas lines at the gas cylinders. The reactor was purged free of low-BTU gas using nitrogen and was monitored by GC.

When purging was complete the reactor was isolated once again. Valves-7, 8, 10 and 12 were set for inlet flow analysis and air flow diluted with nitrogen was started. The oxygen concentration was again monitored by the GC. When the oxygen concentration and total-stream flow rate had stabilized, the regeneration reaction was started and monitored by following the same procedures as for adsorption. After the regeneration reaction was over, air flow through the ash bed was maintained overnight.

Figure 4.7 shows a sample chromatogram.

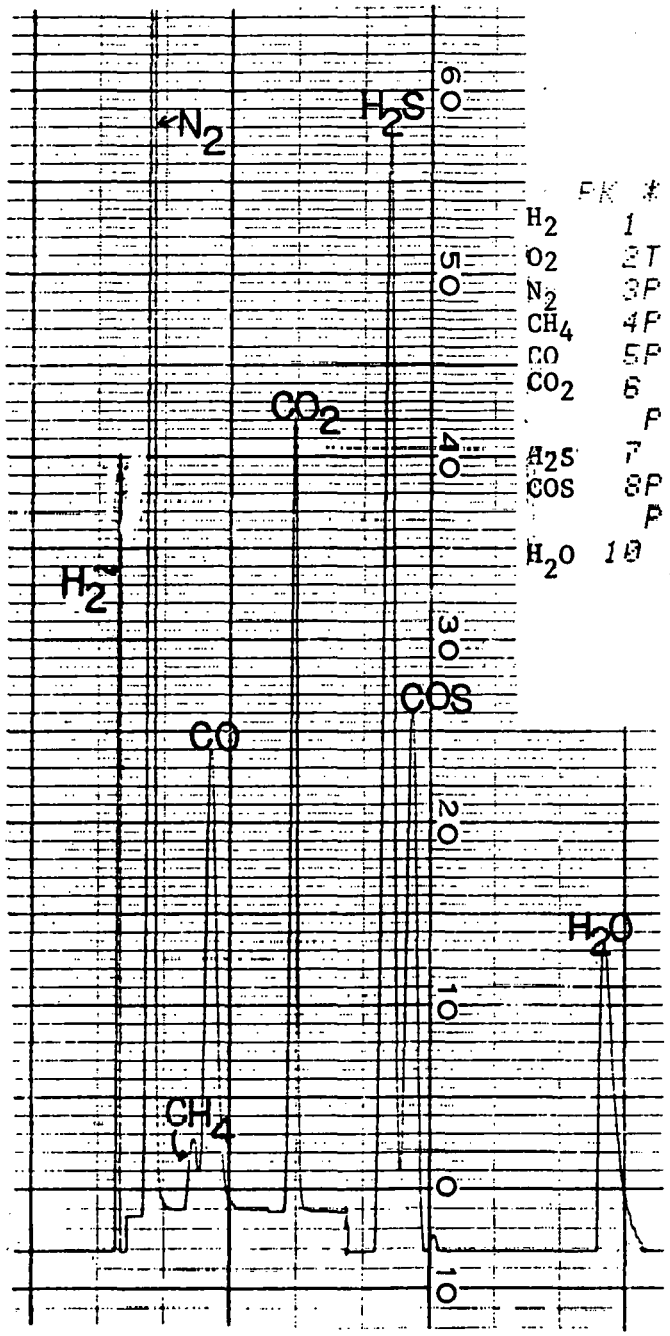

V# 1 INJ. A
FILE 1 ID# 47

PK	#	TIME	AREA	NORM
H_2	1	1.43	5838	9.2042
O_2	2T	1.79	602	.0127
N_2	3P	2.06	2454637	49.8121
CH_4	4P	2.97	144168	2.9650
CO	5P	3.38	1203654	20.0479
CO_2	6	4.97	1148720	16.2056
	P	5.42	538	.0000
H_2S	7	6.85	52952	.7357
COS	8P	7.33	20638	.2693
	P	7.77	2375	.0000
H_2O	10	11.21	28092	.7404
		TOTAL	5061615	99.9999

SCALAR 1.000000

Figure 4.7 A typical chromatographic output.

CHAPTER 4A

PRELIMINARY RESULTS

A few desulfurization and regeneration runs were carried out to determine the nature of the breakthrough curves. Initial runs were carried out at 900-1200°F. These preliminary results were needed to proceed with mathematical modeling and data analysis. A typical desulfurization curve obtained for Western Kentucky ash is given in Figure 4A.1. The regeneration curve is given by Figure 4A.2. During desulfurization as seen in Figure 4A.1, no measurable H_2S was noticed in the reactor effluent till the time of breakthrough. The concentration then increased with time and the bed was ultimately saturated. Some of the hydrogen sulfide was converted to carbonyl sulfide. This is more thoroughly discussed in Chapter 6, section 6.3. A strong temperature dependency was also noticed.

During regeneration of the spent ash bed some oxygen was measured, prior to breakthrough, in the exit gas stream; this concentration remained constant till breakthrough occured. The breakthrough curve was nearly vertical indicating extremely rapid reaction rates even at 3% oxygen concentration. It was suspected then that the

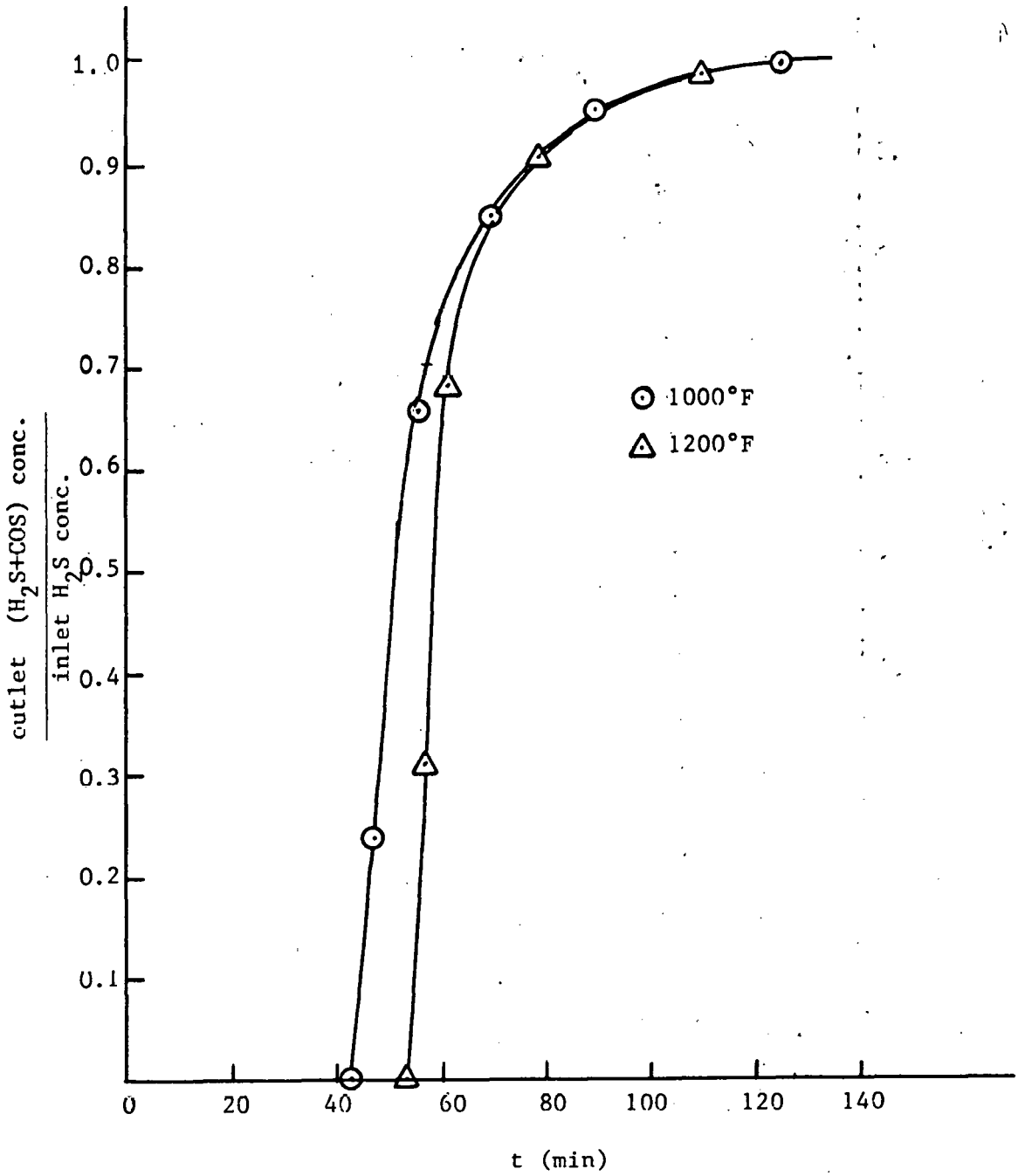

Figure 4A.1 Preliminary desulfurization breakthrough curves for W. Ky #9 ash, d_p = 0.01935 cm.

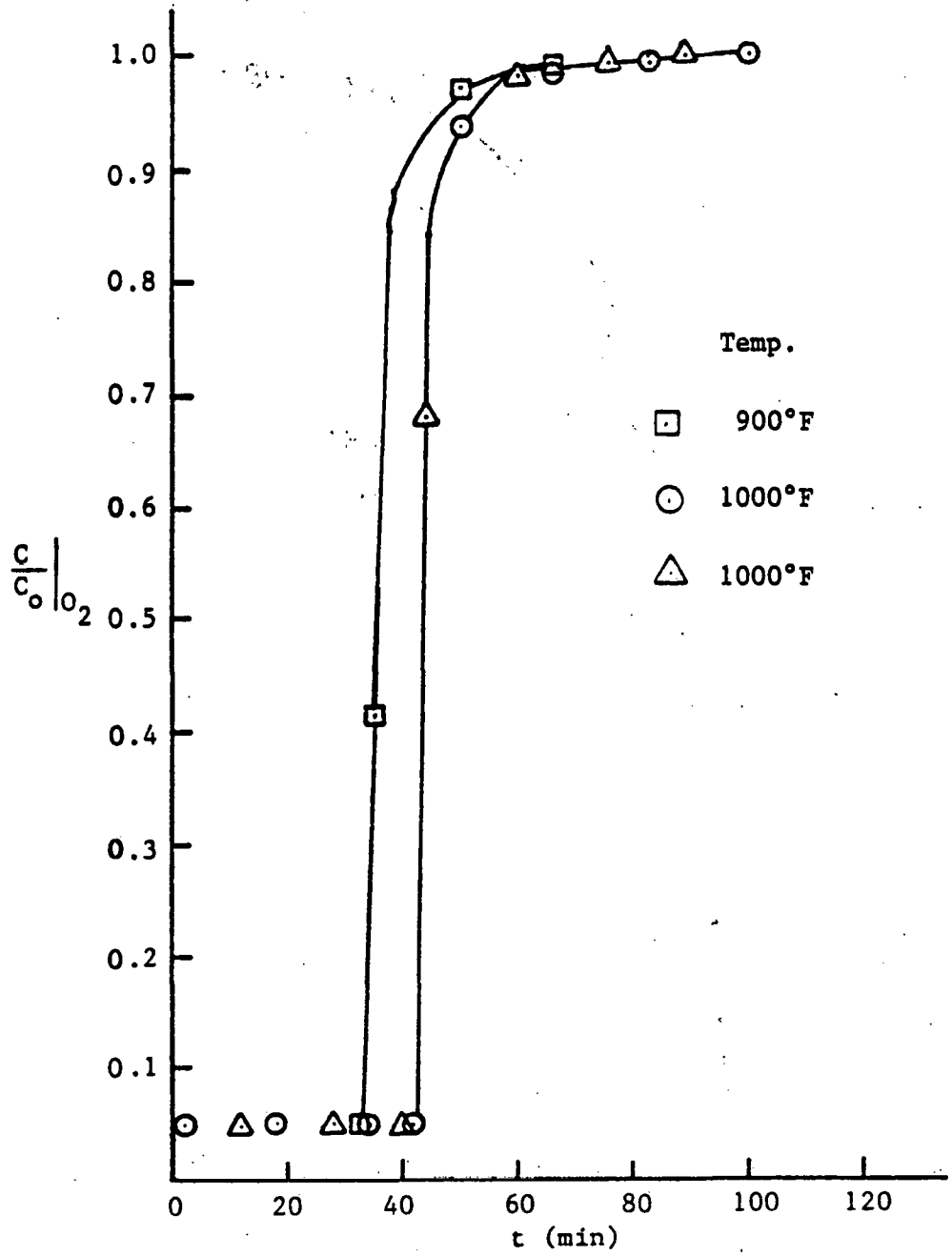

Figure 4A.2 Preliminary regeneration curves for W. Ky. No.9 Ash.

regeneration rates would probably be governed by mass transfer considerations.

These and other results are discussed in details in Chapter 6. These preliminary results formed the basis for the mathematical models developed in Chapter 5. The models were tested and continually refined as more data were accumulated.

CHAPTER 5

THEORY OF GAS-SOLID REACTIONS AND REACTION MODELING IN A FLUIDIZED-BED

5.1 General Considerations:

The desulfurization and regeneration reactions associated with the coal-ash iron oxide process are heterogeneous in nature since a solid is reacting with a gas. In this chapter, discussions will be centered on gas-solid reaction. Models will be developed, based on phenomenological considerations, which may be used in the extraction of rate parameters from experimental data obtained in a transient fluidized-bed. First, the theory for a single reactant solid particle will be developed in Section 5.2. The single-particle developments will then be incorporated in fluid-bed reactor models in Section 5.3 so that the reaction phenomena in the multiparticle (fluid-bed) system may be defined in terms of mathematical models.

5.2 Single-particle reactions:

5.2.1 Nature of gas-solid reactions:

Gas-solid reactions are of considerable importance to the chemical and metallurgical industries; gasification of coal, iron oxide reduction, halogenation of metals and metal and metal oxides, production of cyanamide etc. are

a few of the examples. Many of the features of heterogeneous catalysis also apply to gas-solid noncatalytic reactions. However, the latter is more complicated in the sense that the solid reactant is actually consumed during the reaction; this results in a transient behavior that is inherently more difficult to treat. Physical steps of heat and mass transfer are invariably associated with the process and proper care should be exercised to account for the effect of these steps on the overall reaction process.

When boundary-layer and intra-particle resistances are small the overall rate is controlled by surface reaction. In such a case it is possible, as for heterogeneous catalysis, to postulate different mechanisms based on adsorption, dissociation, surface reaction and desorption to get an insight into the correct mechanism. Unfortunately, the complex and transient nature of noncatalytic gas-solid reactions renders this investigative process unsuitable for all but the most elementary examples. The nth-order rate equation,

$$-r_A = kC_A^{n}W^{m} \qquad (5\text{-}1)$$

has been found to describe satisfactorily the surface reaction in many gas-solid reacting systems (Wen (1968)); n and m are the reaction orders with respect to gas and solid reactants respectively. The value of m depends on the structure of the solid and the distribution of the

solid-reactant in the solid and as such has no theoretical significance. The term W^m accounts for the change in the reaction rate as the solid is consumed. In cases where the change in the reaction surface area can be directly predicted as a function of solid conversion, the rate may be defined per unit surface area; the solid concentration term is not needed in such a case.

5.2.2. Single-particle Analysis:

Models for unchanging particle size are developed in this section with reference to the irreversible reaction given by,

$$A(g) + bB(s) \rightarrow eE(g) + sS(s) \qquad (5\text{-}2)$$

where both gaseous and solid products are formed. Porosity of the solid is an important variable in gas-solid reactions, since it generally dictates the manner in which the reaction takes place. Highly porous and non-porous reactant particles represent the two extremes that are encountered. In the case of the non-porous reactant, the product layer formed allows diffusion of the gaseous reactants and products; and a core consisting of unreacted reactant is formed. On the other hand, when the solid is highly porous, the consumption of the solid reactant is uniform throughout the particle. Accordingly, the analysis of gas-solid reactions may be classified under two groups--porous and nonporous; this classification is used in the discussions that follow.

5.2.2.1 Nonporous particles:

When the solid reactant does not permit the diffusion of gaseous species, a reaction zone is formed between the product layer (shell) and the reactant core. Many gas-solid reactions have been successfully analyzed based on the assumption that the reaction zone is very narrow so that the reaction may be assumed to take place at a sharp interface between the reactant core and the product shell. Figure 5.1(a) and 5.1(b) illustrate the concentration gradients that may exist based on this model. When the reaction zone is very narrow, the concentrations of C_{A1} and C_{A2} are about equal and may be represented by C_{Ac}, the gas concentration of reactant A at the surface of the unreacted core; Figure 5.1(b) illustrates this for a spherical particle. This model is generally referred to in the literature as the unreacted-core or shrinking-core model. The simpler case of the unreacted-core model involving a sharp interface between the core and the shell is examined below for a spherical particle. The theory is discussed by Smith (1970), Levenspiel (1972) and Carberry (1976) among others. It is clear from Figure 5.1 that the concentration of gaseous reactant A in the reaction zone or at the reaction interface (C_{Ac}) is different from the bulk concentration C_{Ab}. The actual value of C_{Ac} is determined by the transport resistances offered by the gas film and the product layer.

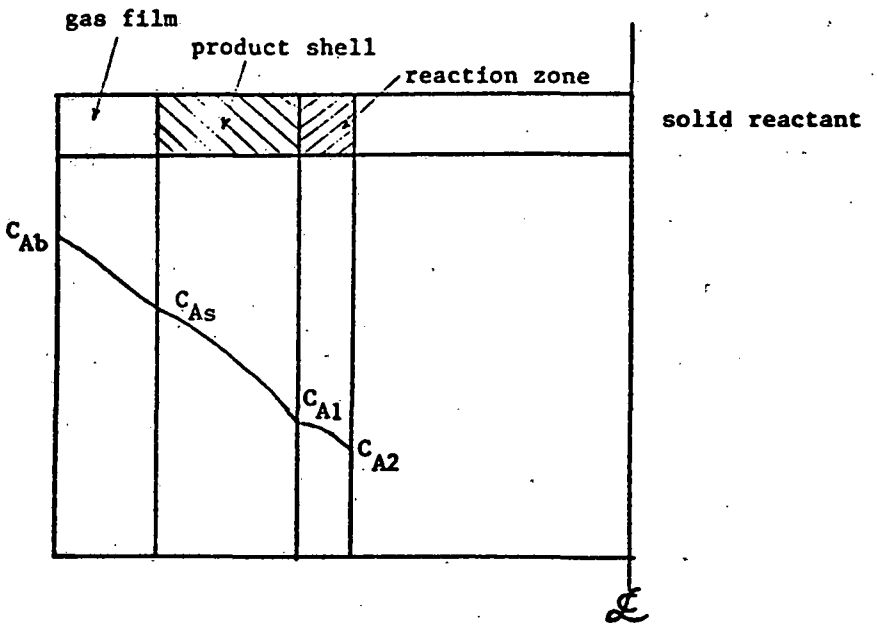

Figure 5.1(a) Concentration profile for a nonporous solid reactant with diffuse reaction zone.

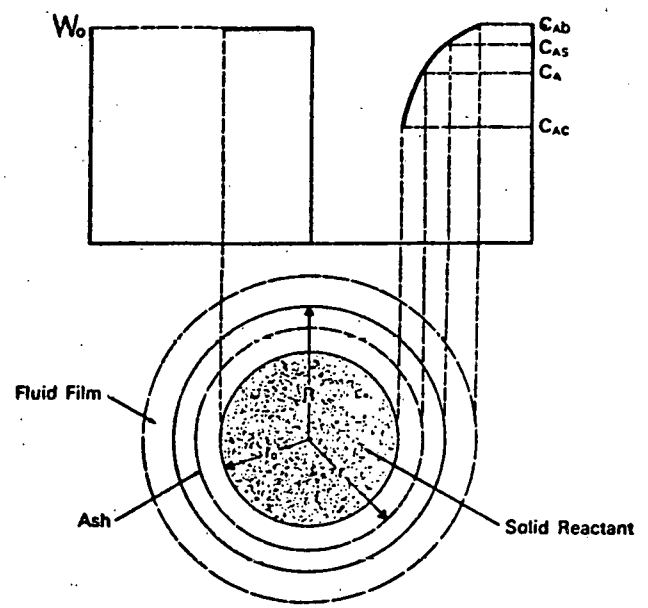

Figure 5.1(b) Concentration profile for a nonporous, spherical particle with narrow reaction zone (from Wen (1968)).

It is useful to define the physical and chemical rates explicitly at this point while noting that the rate of chemical reaction is proportional to the surface area of the unreacted-core.

Chemical reaction:

Rate per particle (moles A/time) for reaction (5-2),

$$-r_A = -\frac{1}{b} r_B = -\frac{dN_A}{dt} = -\frac{1}{b}\frac{dN_B}{dt}$$

$$-r_A = 4\pi r_c^2 k_s C_{Ac} \qquad (5\text{-}3)$$

Here, the assumption is made that the reaction is first order with respect to A. The literature review on kinetics of iron oxide process in Chapter 3 reveals that the reaction order may be taken to be unity with respect to the gaseous reactants H_2S during desulfurization, and O_2 during regeneration. Higher orders complicate the mathematics considerably. The unreacted-core radius is r_c.

Boundary-layer (gas film) diffusion:

Rate of mass transfer (moles A/time/particle) = $-\frac{dN_A}{dt}$

$$-\frac{dN_A}{dt} = 4\pi R^2 k_m [C_{Ab} - C_{As}] \qquad (5\text{-}4)$$

where k_m is the mass transfer coefficient and R the particle radius.

Diffusion through product layer (shell):

Rate of diffusion (moles A/time/particle) = $-\frac{dN_A}{dt}$

$$-\frac{dN_A}{dt} = 4\pi r_c^2 D_e \left(\frac{dC_A}{dr}\right)_{r=r_c} \qquad (5\text{-}5)$$

where D_e is the effective diffusivity of A through the porous product layer; the gradient is evaluated at $r = r_c$.

Since the concentrations C_{Ac} and C_{As} cannot be measured in general, it is expedient to express them in terms of the measurable quantity C_{Ab}, the bulk concentration. To do this one has to examine the relation between the chemical and physical steps involved; the following individual steps may be identified with reference to Figure 5.1.

1. Diffusion of gaseous reactant A through the boundary layer surrounding the particle.

2. Intraparticle diffusion of A through the solid product layer.

3. Chemical reaction at the reaction interface leading to the formation of the solid product E and gaseous product F.

4. Diffusion of F through the product shell to the particle external surface.

5. Diffusion of F through the gaseous boundary layer back into the bulk fluid stream.

Since both the desulfurization and regeneration reactions are essentially irreversible, steps 4 and 5 need not be considered (Levenspiel (1972)). If the rate of advancement of the reaction interface is assumed slow in relation to fluid diffusion inside the particle, the steps 1 to 3 may be considered to occur in series and in a pseudo-steady manner. Bischoff (1963) analyzed the validity of this assumption and came to the conclusion that the pseudo-steady-state assumption was reasonable if the

density of the gas in the pores of the product layer is small with respect to the density of the solid reactant B. This is true in the case of the iron oxide process. Assuming pseudo-steady state to prevail one may proceed to eliminate the immeasurable quantities and express the reaction rate in terms of measurables.

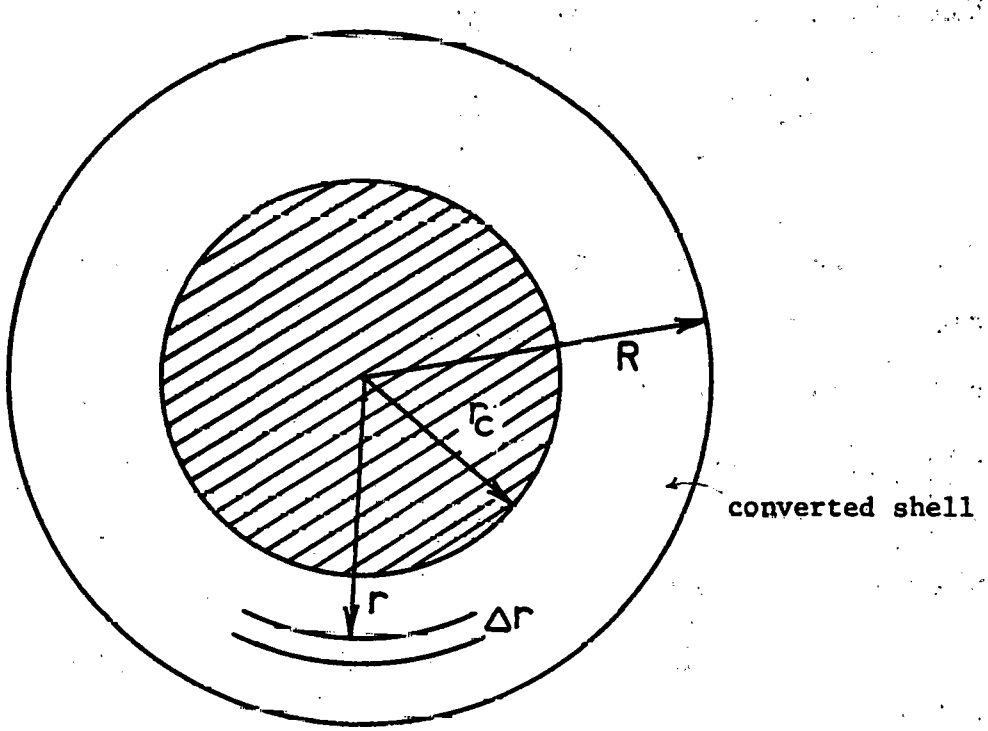

Figure 5.2 Mass balance for non-porous particles

Making a mass balance for reactant A on a thin shell in the product layer as shown in Figure 5.2 above with the assumptions of pseudo-steady state gives (Smith (1972)),

$$\frac{d}{dr}\left(r^2 D_e \frac{dC_A}{dr}\right) = 0 \qquad (5\text{-}6)$$

With the boundary conditions

$$C_A = C_{Ab} \text{ at } r = R$$

$$C_A = C_{Ac} \text{ at } r = r_c$$

integration of (5-6) twice with respect to r gives

$$C_A - C_{As} = (C_{As} - C_{Ac}) \frac{(\frac{R}{r} - 1)}{(\frac{r_c}{R} - 1)} \qquad (5\text{-}7)$$

Differentiation of (5-7) gives,

$$\left.\frac{dC_A}{dr}\right|_{r=r_c} = \frac{C_{As} - C_{Ac}}{r_c(1-\frac{r_c}{R})} \qquad (5\text{-}8)$$

Since the applicability of the pseudo-steady-state assumption allows one to consider the three steps represented by equations (5-3) to (5-5) to occur in series, they may be equated to each other to eliminate the unobservables C_{As} and C_{Ac}. First, the derivative in equation (5-5) is replaced by the identity on the right-hand side of equation (5-8). Equating equation (5-5) to (5-3) after this operation results in

$$C_{Ac} = \frac{C_{As}}{1 + (1-\frac{r_c}{R}) \frac{k_s r_c}{D_e}} \qquad (5\text{-}9)$$

which expresses C_{Ac} in terms of C_{As}. C_{As} in turn may now be expressed in terms of C_{Ab} by using (5-9), (5-4) and (5-3). The result is

$$C_{As} = \frac{C_{Ab}}{I + \frac{r_c^2 k_s}{R^2 k_m} \frac{1}{1 + (^1-\frac{r_c}{R}) \frac{k_s r_c}{D_e}}} \qquad (5\text{-}10)$$

Substitution of this in equation (5-9) gives

$$C_{Ac} = \frac{C_{Ab}}{1 + (1-\frac{r_c}{R})\frac{k_s r_c}{D_e} + \frac{r_c^2 k_s}{R^2 k_m}} \qquad (5\text{-}11)$$

It is convenient to define the following dimensionless quantities at this time.

$$\text{Da} = \text{Damkohler number} = \frac{k_s R}{D_e}$$

$$\text{Bi} = \text{Biot number} = \frac{k_m R}{D_e}$$

Substituting equation (5-11) in equation (5-3) and expressing the result in terms of the dimensionless groups just defined gives:

$$\text{Rate per particle} = -r_A = -\frac{dN_A}{dt} = 4\pi R^2 k_o C_{Ab} = 4\pi r_c^2 k_s C_{Ac}$$

$$= \frac{4\pi r_c^2 k_s C_{Ab}}{1+\text{Da}(1-\frac{r_c}{R})\frac{r_c}{R} + \frac{\text{Da}}{\text{Bi}}\frac{r_c^2}{R^2}} \qquad (5\text{-}12)$$

where k_o is the overall rate constant.

$$k_o = \frac{\frac{r_c^2}{R^2} k_s}{1 + \text{Da}(1 - \frac{r_c}{R})\frac{r_c}{R} + \frac{\text{Da}}{\text{Bi}}\frac{r_c^2}{R^2}}$$

or

$$\frac{1}{k_o} = \frac{R^2}{r_c^2}\frac{1}{k_s} + \text{Da}(1-\frac{r_c}{R})\frac{R}{r_c}\frac{1}{k_s} + \frac{\text{Da}}{\text{Bi}}\frac{1}{k_s} \qquad (5\text{-}13)$$

In this form, each of the terms on the right-hand side represents respectively, the fractional resistance of interfacial reaction, pore diffusion and external mass transfer. The radius of the unreacted core r_c is related to the solid concentration W and solid conversion X_e as follows.

Dimensionless solid concentration,

$$X = \frac{W}{W_o}$$

$$= \frac{\frac{4}{3}\pi r_c^3 \rho_p W_o}{\frac{4}{3}\pi R^3 \rho_p W_o}$$

$$= \left(\frac{r_c}{R}\right)^3 \qquad (5\text{-}14)$$

Conversion of solid, $X_c = 1 - X \qquad (5\text{-}15)$

The single-particle reaction rate model developed above will be applied to the fluid-bed reactor model in Section 5.3.2.

5.2.2.2 Porous Particles

When the solid is porous, the reaction may be considered to occur in a pseudo-homogeneous fashion throughout the particle. This concept is extensively employed in heterogeneous catalysis. Detailed discussions of the porous pellet models are presented by Richter and Hoffman (1977), and Wen (1968). When the rate equation (5-1) is employed, analytical solution is possible only for n = 1 and m = 0; numerical solution should be resorted to in

other cases. The treatment of non-catalytic gas-solid reactions is more complicated than gas reactions over heterogeneous catalysts, since a product layer with no reactive solid develops after a certain time as the solid is consumed. The reaction is said to have reached the second stage when this happens. Concentration profiles for the two stages are given in Figures 5.3(a) and 5.3(b). The work of Richter and Hoffman (1977), and Wen (1968) referred to above were based on the assumption that, on a macroscopic scale, the reactant was distributed throughout the solid in a homogeneous fashion.

In recent years, models for porous reactants have been developed that take into consideration the fact that the solid reactant may be distributed as grains in the solid. These models are generally known as grain models and extensive discussion of them may be found in Szekely et al. (1976). Figure 5.4 is a schematic representation of the grain model. Unfortunately, the grain model requires prior knowledge of the grain parameters--grain size, size distribution, shape factor, etc. Since these additional parameters are included, care must be exercised in the application of the grain models to multiparticle systems where scatter of the experimental data is inherently greater than for single particle studies. It must be pointed out here that the present study is made in a fluidized-bed, where the actual gas-solid contacting pattern

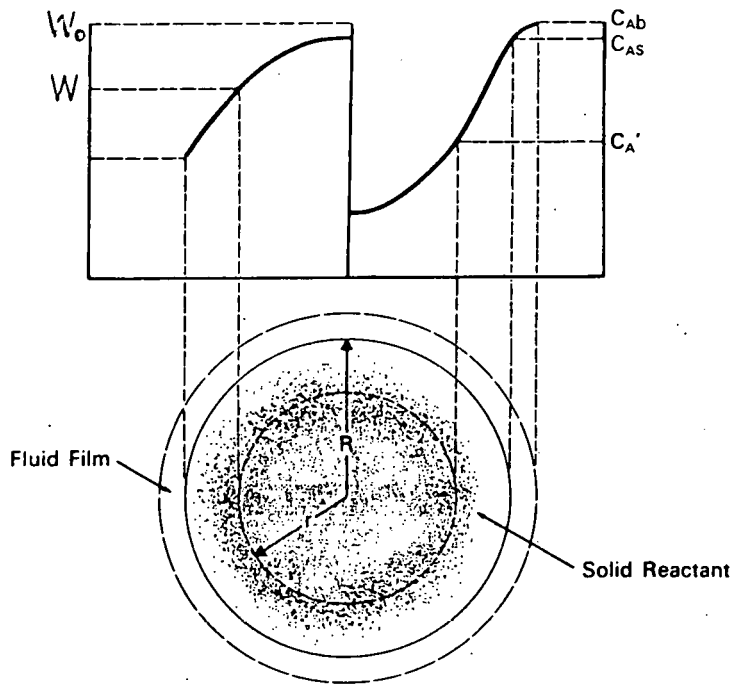

Figure 5.3(a) Schematic diagram of concentration profile in the first stage (from Wen (1968).

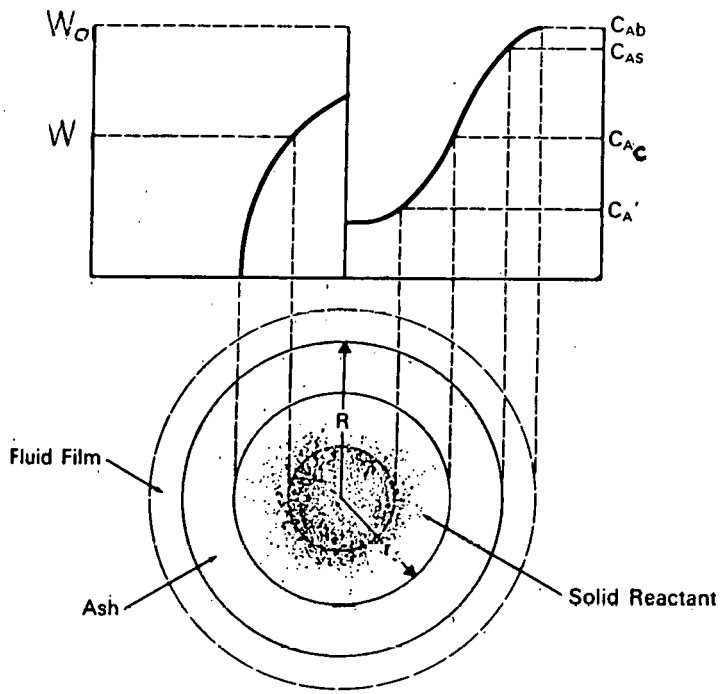

Figure 5.3(b) Schematic diagram of concentration profile in the second stage (from Wen (1968)).

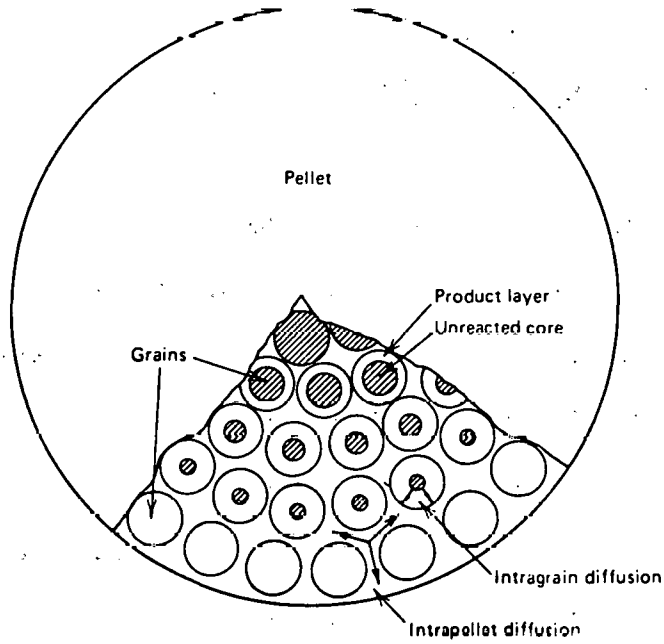

Figure 5.4 Schematic representation of the grain model (Sohn and Szekely (1972)).

is complex and not easily defined. Also, it must be emphasized that, the main objective of this research project is to evaluate the apparent (not intrinsic) kinetics useful for scaleup. The use of complicated gas-solid reaction models for the present case, therefore, is not justified. Only the pseudo-homogeneous model with no intraparticle concentration gradient will be tested among porous-solid models.

5.3 Gas-solid reactions in fluidized-beds

5.3.1 General considerations:

Fluid-beds are generally used to carry out heterogeneous reactions where there is a need to move the solids through the reaction vessel in a continuous fashion, and/or where high heat transfer rates are involved. The regeneration reaction of sulfided iron oxide is highly exothermic with a heat of reaction of about 150 kcal per g mole of FeS at normal regeneration temperatures. The temperature control requirements in the regeneration step make the continuous fluid-bed desulfurization-regeneration scheme a very practical choice.

Fluidization in gas-fluidized beds is termed "aggregative" since a significant portion of the fluidizing gas tends to travel through the bed in the form of bubbles. This behavior results in nonideal fluid-solid contacting patterns. The gas bubbles travel through the bed with a higher velocity than the gas in the emulsion phase. Be-

cause of poor contact between the gas and the solid in the bubbles, the overall rate of reaction in a fluid-bed is usually less than that observed in a packed-bed. The inherently complex fluid flow patterns that prevail in fluid-beds complicate the design and scaleup of fluidized-bed chemical reactors. In recent years, models have been proposed that attempt to account for the nonideal contacting pattern so that the fluidized-reactor may be designed from intrinsic kinetic data obtained from other types of reaction systems. Although these models have contributed significantly to the knowledge of the fluid-bed phenomena, they are not yet reliable enough to warrant their use in practical design. The accepted practice is to study the reaction first in a small-scale (2-4 cms. diameter) reactor, and then scale-up in two stages (Jordan 1968).

The usual purpose of laboratory investigations of chemical kinetics in a fluidized-bed is to deduce kinetic parameters that may be directly used in the design of a larger-scale fluid-bed reactor. Intrinsic reaction rate measurements are seldom performed in fluid-beds due to the complex flow regimes existing in these devices. It should be recalled here that the main objective of this study is to evaluate the kinetic parameters useful for process design. Therefore, a detailed review and analysis of the models that account for the nonideal flow regimes present in fluid-beds are not made. Yates (1975) gives an excellent

review of many existing fluidized-bed models which assume the bed to be a two-phase system consisting of a dense emulsion or interstitial phase, and a lean or bubble phase. After analyzing the various models available, Yates concludes that no one model is currently able to predict accurately the performance of a large-scale fluidized-bed reactor. Kunii and Levenspiel (1969) have presented a detailed analysis of fluid-bed models based on bubble dynamics. Detailed treatment of the fluid-mechanical aspects of fluidized-beds may be found in Leva (1959), Othmer (1956) Zenz and Othmer (1960) and Zabrodsky (1966). These are not discussed here since they are irrelevent to the principal thrust of this work.

5.3.2 Reactor Models

5.3.2.1 Pseudo-homogeneous Model:

The following assumptions are made.

1. Particle offers no diffusional resistance; the reactant diffuses to all the reaction sites readily. This is equivalent to saying that no intraparticle concentration gradient exists.
2. Isothermal conditions prevail.
3. Reaction is first order with respect to the reacting gas. The validity of this assumption was considered in Section 5.2.2.1.
4. Superficial linear velocity in the reactor remains unchanged during the course of the reaction.

This is generally valid when the reactant gas concentrations are small. This is the case during desulfurization.

5. The solids in the reactor are perfectly mixed. This assumption is very widely used in the treatment of batch fluidized-beds.

6. Axial dispersion is negligible.

7. Particles are spherical; structural and physical properties of the solid do not change during conversion of the solid.

8. It is assumed that the gas is in plug flow.

Assumption of a specific flow regime is necessary in order to evaluate apparent rate constants. Many researchers have assumed plug flow for gas especially for treatment of data obtained in small-diameter reactors (Jordan (1960)). Jordan, after analyzing the results of Gilliland et al. (1953) and other workers, concludes that fluid-beds with L/D (length to diameter) ratios greater than 1-2 are likely to approach plug flow behavior. Investigators have generally used the assumption of perfect mixing for the gas phase only when the beds were very shallow. When the reaction is very fast, the axial concentration profile cannot be neglected; perfect gas phase mixing would not be a reasonable assumption for such cases especially when the bed is not shallow.

The pseudo-homogeneous model is developed with reference to the stoichiometry indicated by equation (5-2) and the rate equation (5-1). As explained earlier, the order with respect to the gaseous reactant is assumed to be unity (n = 1). The rate of reaction is a function of both the position in the reactor (z) and the time (t); however, due to the assumption (5) of perfect solid mixing, solid concentration is considered uniform throughout the reactor and time dependent only.

Rate per particle = $-r_A$ (g mole A consumed/time)

$$\text{Rate per gram of ash} = -R_A = \frac{-r_A}{\frac{4}{3}\pi R^3 \rho_p} = -r_A g_N \qquad (5\text{-}15a)$$

According to the pseudo-homogeneous model,

$$-R_A = k_v C_{As} W^m \qquad (5\text{-}16)$$

or
$$-r_A = (\tfrac{4}{3}\pi R^3 \rho_p) k_v C_{As} W^m \qquad (5\text{-}17)$$

also,
$$-r_A = 4\pi R^2 k_m (C_{Ab} - C_{As}) \qquad (5\text{-}4)$$

Equating equations (5-17) and (5-4) gives the unknown concentration C_{As} in terms of the known bulk concentration C_{Ab}.

$$C_{As} = \left[\frac{1}{(1 + \frac{R\rho_p W^m}{3} \frac{k_v}{k_m})} \right] C_{Ab} \qquad (5\text{-}18)$$

Using equations (5-16) and (5-18),

$$-R_A = k_v \frac{W^m C_{Ab}}{(1 + \frac{R\rho_p W^m}{3} \frac{k_v}{k_m})} \qquad (5\text{-}19)$$

If one considers making a mass balance for A over the small element Δz shown in Figure 5.5 below and follows the usual procedure of letting this element tend to zero, (Smith, (1970)), then

$$u \frac{\partial C_{Ab}}{\partial z} + \epsilon \frac{\partial C_{Ab}}{\partial t} + (-R_A)\rho_B = 0 \qquad (5\text{-}20)$$

subject to the conditions

at $t = 0$ and $0 \leq z \leq L$, $C_{Ab} = 0$

at $t \geq 0$ and $z = 0$, $C_{Ab} = C_{Ao}$

at $t \rightarrow$ large and $0 \leq z \leq L$, $C_{Ab} = C_{Ao}$

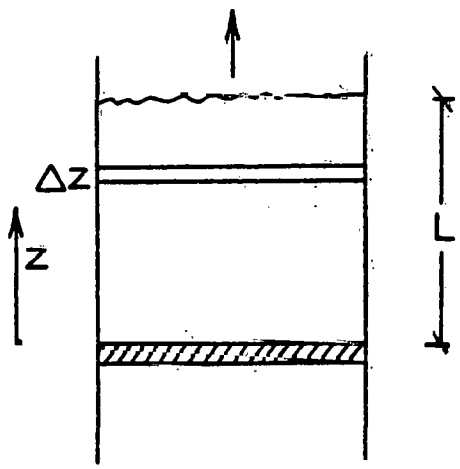

Figure 5.5 Reactor mass balance.

When the time for the conversion of the solid reactant is large in relation to the gas residence time in the reactor, the process as a whole may be assumed to occur in a psuedo-steady-state manner. In this case, the transient term in equation (5-20) may be dropped. This is a very commonly adopted practice in the treatment of multiparticle gas-solid reaction systems. Two of the many specific references

that may be cited are, Natesan and Philbrook (1970), and Doraiswamy et al. (1959). These workers used fluidized-beds in their studies. The transient term in equation (5-20) may also be dropped for many gas-solid reactions carried out in packed-beds (Gidaspow et al. (1975)) as justified by Ozawa (1969).

The pseudo-steady mass balance for A, for the fluidized-bed then becomes,

$$u \frac{dC_{Ab}}{dz} + (-R_A)\rho_B = 0 \qquad (5\text{-}21)$$

Substitution of equation (5-19) in (5-21) gives,

$$u \frac{dC_{Ab}}{dz} + \frac{k_v C_{Ab} \rho_B W^m}{1 + \frac{R\rho_p W^m}{3} \frac{k_v}{k_m}} = 0 \qquad (5\text{-}22)$$

Equation (5-22) may be solved for a specified value of W to express C_{Ab} as a function of z. The time dependency is obtained by a macroscopic balance on the particles in the reactor later.

It is advantageous at this point to introduce some dimensionless variables. A dimensionless time variable is defined as the ratio of the cumulative moles of A passed through the reactor at time t, to the total moles of A needed to saturate the bed. In terms of measurable variables,

$$\tau = \frac{utC_{Ao}}{(1-\varepsilon)LM_o\rho_p} = \frac{QC_{Ao}t}{M_o q} \qquad (5\text{-}23)$$

$$d\tau = \frac{QC_{Ao}}{M_o q}\, dt \qquad (5\text{-}23a)$$

Other variables are,

Y = dimensionless gas phase concentration of A

$$= \frac{C_{Ab}}{C_{Ao}}$$

X = dimensionless concentration of B in the solid

$$= \frac{W}{W_o}$$

Z = dimensionless reactor position

$$= \frac{z}{L}$$

These dimensionless variables are now introduced into equation (5-22). Thus,

$$-\frac{dY}{dZ} = \frac{X^m Y}{\frac{u}{Lk_v W_o{}^m \rho_B} + \frac{uR\rho_p}{3Lk_m \rho_B} X^m} \qquad (5\text{-}24)$$

Defining,

$$K_k = \frac{u}{Lk_v W_o{}^m \rho_B} = \frac{u}{Lk_v W_o{}^m (1-\varepsilon)\rho_p} \qquad (5\text{-}25)$$

$$K_m = \frac{uR\rho_p}{3Lk_m \rho_B} = \frac{uR}{3Lk_m(1-\varepsilon)} \qquad (5\text{-}26)$$

Substituting these in equation (5-24) gives

$$-\frac{dY}{dZ} = \frac{X^m Y}{K_m X^m + K_k} \qquad (5\text{-}27)$$

with boundary conditions,

at $\tau = 0$, $Z \geq 0$, $X = 1$

at $\tau = 0$, $Z \geq 0$, $Y = 0$

at $\tau \geq 0$, $Z = 0$, $Y = 1$

It should be noted that K_k is the kinetic parameter and K_m the mass transfer parameter.

For constant X, equation (5-27) may be integrated to get the steady-state gas phase concentration profile as follows.

$$-\int_1^Y \frac{dY}{Y} = \frac{X^m}{K_m X^m + K_k)} \int_0^Z dZ$$

$$Y = EXP[-\frac{X^m Z}{K_m X^m + K_k}] \qquad (5\text{-}28)$$

Macroscopic mass balance for the solids in the reactor:

Since the solids are assumed to be in a perfectly mixed state, the solid concentration W (or X) is a function of time only as pointed out earlier; therefore, a macroscopic mass balance for the whole reactor may be made for a small time interval Δt during which the concentration profile in the reactor is assumed to be unchanging.

Moles of B consumed during $\Delta t = -\Delta N_B = -\Delta(qXW_0)$

$$= -qW_0\Delta X \qquad (5\text{-}29)$$

Input of A into the reactor during $\Delta t = QC_{Ao}\Delta t$

Output of A from the reactor during $\Delta t =$

$$Y|_{Z=1} QC_{Ao}\Delta t$$

Moles A consumed $= -\Delta N_A = QC_{Ao}\Delta t[1-Y|_{Z=1}]$ (5.29a)

Using equation (5-28) in the expression above,

$$-\Delta N_A = QCA_o \Delta t[1-EXP[-\frac{X^m}{K_m X^m+K_k}]] \qquad (5\text{-}30)$$

Since $\Delta N_A = 1/b\Delta N_B$,

$$-\Delta N_A = -1/b\Delta N_B = -\frac{1}{b} qW_o \Delta X \qquad (5.30a)$$

Therefore,

$$-\frac{1}{b}qW_o\Delta X = QC_{Ao}\Delta t[1-EXP[-\frac{X^m}{K_m X^m+K_k}]]$$

Rearranging,

$$-\frac{\Delta X}{\Delta t} = \frac{bQC_{Ao}}{qW_o}[1 - EXP(-\frac{X^m}{K_m X^m+K_k})] \qquad (5\text{-}31)$$

Noting that $W_o = bM_o$, using dimensionless time as defined in equation (5-23) and letting Δt tend to zero we have the following expression.

$$\frac{dX}{d\tau} = EXP(-\frac{X^m}{K_m X^m+K_k}) - 1 \qquad (5\text{-}32)$$

Equation (5-32) expresses the change of solid concentration of reactant B with time. Equations (5-28) and (5-32) are together numerically solved using Fourth Order Runge-Kutta procedure. The computer program for this is listed in Appendix E as Model 1. The result is discussed in Chapter 6.

5.3.2.2 Unreacted-core models:

Reactor gas phase mass balance given by equation (5-20) applies here also. Reaction rate per particle ac-

cording to this model was developed in Section 5.2.2.1 and is given by equation (5-12).

$$-r_A = \frac{4\pi r_c^2 k_s C_{Ab}}{1 + Da(1-\frac{r_c}{R})\frac{r_c}{R} + \frac{Da}{Bi}\frac{r_c^2}{R^2}} \qquad (5\text{-}12)$$

Rate per mass of ash, $-R_A = \frac{-r_A}{\frac{4}{3}\pi R^3 \rho_p} = -r_A g_N$ (5-15a)

Using equations (5-12) and (5-15a) in equation (5-21) and putting $P = \frac{r_c}{R}$ one obtains,

$$u\frac{dC_{Ab}}{dz} + \frac{4\pi r_c^2 k_s g_N \rho_B C_{Ab}}{(1+Da(1-P)P+\frac{Da}{Bi}P^2)} = 0 \qquad (5\text{-}33)$$

Transformation of equation (5-33) by using previously defined dimensionless variables gives,

$$-\frac{dY}{dz} = \frac{YP^2}{K_u(1+Da(1-P)P+\frac{Da}{Bi}P^2)} \qquad (5\text{-}34)$$

where $K_u = \frac{Ru}{3Lk_s(1-\varepsilon)}$

Equation (5-34) may be integrated to give the instantaneous reactor concentration profile. The result is

$$Y = EXP[-\frac{P^2 Z}{K_u(1+Da(1-P)P+\frac{Da}{Bi}P^2)}] \qquad (5\text{-}35)$$

Macroscopic reactor mass balance for the solids is given by equating equations (5-29), (5-29a) and (5-30a) developed earlier. Therefore,

$$-\frac{1}{b}qW_o\Delta X = QC_{Ao}\Delta t[1-Y|_{Z=1}] \qquad (5\text{-}31a)$$

Substituting equation (5-35) in (5-31a) and rearranging,

$$-\frac{\Delta X}{\Delta t} = \frac{bQC_{Ao}}{qW_o}\left[1 - EXP\left(-\frac{P^2}{K_u I}\right)\right] \qquad (5\text{-}36)$$

where $I = [1+Da(1-P)P+ \frac{Da}{Bi}P^2]$

Taking limits as $\Delta t \to 0$, equation (5-36) becomes,

$$-\frac{dX}{dt} = -\frac{bQCA_o}{qW_o}\left[EXP\left(-\frac{P^2}{IK_u}\right)-1\right] \qquad (5\text{-}37)$$

Use of dimensionless time defined by equation (5-23) in the above equation gives,

$$\frac{dX}{d\tau} = EXP\left[-\frac{P^2}{K_u[1+Da(1-P)P+\frac{Da}{Bi}P^2]}\right] - 1 \qquad (5\text{-}38)$$

Equations (5-35) and (5-38) may be solved together to obtain the breakthrough curve. A Fourth Order Runge-Kutta procedure is used for numerical solution. The computer program is listed in Appendix E. Results are discussed in Chapter 6.

The model equations (5-34), (5-35) and (5-38) may be greatly simplified for the special cases of surface reaction or product-layer diffusion controlling the overall rate process.

Chemical reaction controlling:

In this case external mass transfer resistance is negligible. Also, the diffusion resistance through the product layer is small. Therefore $Da \to 0$ and $\frac{Da}{Bi} \to 0$.

Then equations (5-34), (5-35) and (5-38) reduce to,

$$-\frac{dY}{dZ} = \frac{P^2 Y}{K_u} \tag{5-39}$$

$$Y = EXP(-\frac{P^2 Z}{K_u}) \tag{5-40}$$

$$\frac{dX}{d\tau} = EXP(-\frac{P^2}{K_u}) - 1 \tag{5-41}$$

Equations (5-40) and (5-41) may be solved together to obtain the breakthrough curve.

Diffusion through product-layer controlling:

For this situation, K_u, $K_u \frac{Da}{Bi}$ are small. Then the model equations simplify to,

$$-\frac{dY}{dZ} = \frac{YP}{K_D(1-P)} \tag{5-42}$$

$$Y = EXP(-\frac{PZ}{K_D(1-P)}) \tag{5-43}$$

$$\frac{dX}{d\tau} = EXP(-\frac{P}{K_D(1-P)}) - 1 \tag{5-44}$$

$$\text{where } K_D = K_u\ Da = \frac{R^2 u}{3LD_e(1-\varepsilon)} \tag{5-45}$$

Equations (5-42) and (5-44) together give the breakthrough curve. Results are explained in Chapter 6.

CHAPTER 6

RESULTS AND DISCUSSIONS

6.1 Preliminary Fluidization Runs:

Fluidization studies were conducted at room temperatures on ash particles of mesh size (U.S.) -35+45, -45+70, -70+80, -80+120, and -120+170 to determine the appropriate particle sizes for the process studies. The "quality" of fluidization and the minimum fluidizing velocity for each size range were observed. Based on these observations, particles of mesh size -70+80 (0.01935 cm), -80+120 (0.0151 cm) and -120+170 (0.01065 cm) were selected as suitable candidates. Apparent densities of the particles were also determined by water displacement in a specific gravity bottle. Table 6.1 lists the results. The minimum fluidizing velocity listed is the velocity at which particle movement was noticed for the first time on increasing the fluid velocity. Air was the fluidizing medium used for these tests.

The minimum fluidizing velocity was also determined at 1000°F with nitrogen as the fluidizing medium. The results are listed in Table 6.2.

Since a fluidized-bed is not suitable for particles exhibiting high rates of decrepitation, attrition characteristics of the ash particles were examined. Ash samples of

Table 6.1

PRELIMINARY FLUIDIZATION RESULTS
(ROOM CONDITIONS)

Ash	Average Size (cm)	Apparent Density (gms/cm^3)	Minimum Fluidizing Velocity (cm/sec)	Bed Porosity at Minimum Fluidization	Pressure Drop Δp/cm at minimum fluidization (cms H_2O/cm bed)
Western Kentucky	0.01935	2.835	6.37	0.596	1.08
	0.0151	2.814	3.98	0.615	1.01
	0.01065	2.868	1.75	0.625	0.979
Montana	0.01935	2.051	6.37	0.706	0.575
	0.0151	2.085	3.98	0.717	0.525
	0.01065	2.051	1.75	0.680	0.585
Elkhorn	0.01935	2.272	6.37	0.74	0.453

Table 6.2

MINIMUM FLUIDIZING VELOCITY
at 1000°F (1 atm)

Ash	Average Size (cm)	Minimum Fluidizing Velocity (cm/sec)
Western Kentucky	0.01935	3.37
	0.0151	2.42
	0.1065	1.70
Elkhorn	0.01935	3.23
Montana	0.01935	3.23

known particle size distribution were weighed and fluidized at room temperatures for a period of about 10 days. Then the particles were weighed and examined for change of size distribution, but no significant weight loss or decrepitation were noticed. The ash particles used for the high-temperature process studies were also examined for weight loss due to decrepitation and, no significant weight loss was noticed even after about 40 cycles. Forty cycles of operation is equivalent to about 150 hours of continued operation.

During actual process studies using simulated low-BTU gas, good fluidization was achieved for all ash particles at temperatures of 900°F and 1000°F. Fluidization became poor at 1200°F and was worse at 1400°F. Increasing the temperature beyond 1000°F seemed to promote particle adhesion (not fusion) which could cause poor fluidization. Nevertheless, particles did not seem to adhere during the associated regeneration runs. For fear of permanently damaging the stabilized particles, only a limited number of runs were performed at 1400°F.

6.2 General discussion of process studies:

Figure 6.1 shows a typical time vs. concentration of H_2S+COS curve obtained from the experiments. The experimental procedure was outlined in Chapter 4. The ordinate on Figure 6.1 is the ratio of COS+H_2S concentration in the exit stream to the inlet H_2S concentration (C_{Ao}).

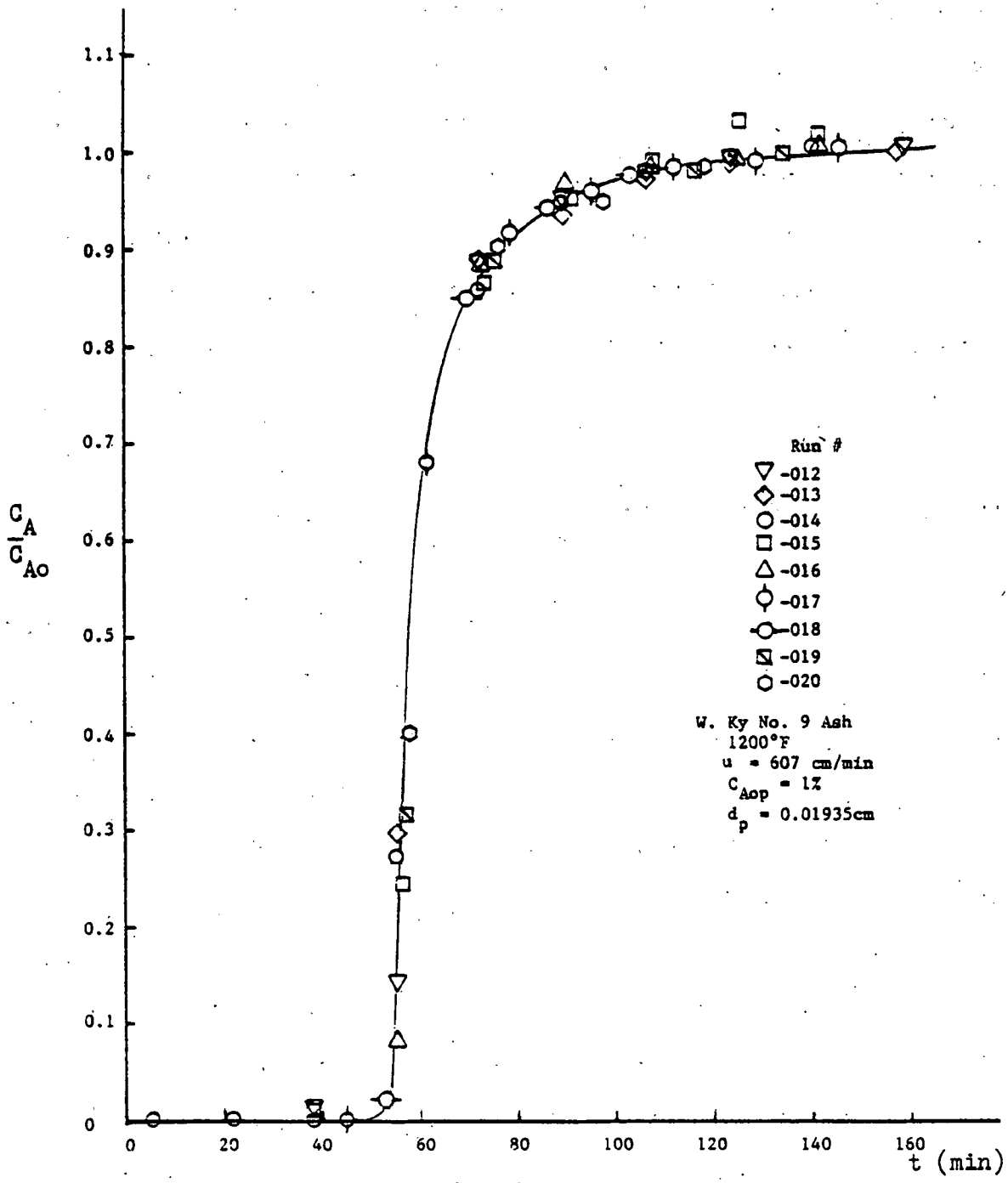

Figure 6.1 Reproducibility of rate data.

In general, the concentration of the sulfur gases in the exit stream was not in measurable levels prior to breakthrough. After the breakthrough occurs, the unabsorbed H_2S elutes the bed partly as COS. The H_2S and COS concentrations may be directly added due to the reasons to be discussed in Section 6.3. The excellent reproducibility of the rate data is apparent from Figure 6.1. The data obtained from nine different runs conducted at the same experimental conditions are plotted in this figure.

The lowest detection level of thermal conductivity detectors is generally about 50 ppm (0.005 vol. %). The integrator used was programmed to ignore peaks of concentration less than about 0.001%. Therefore, the H_2S removal efficiencies attained prior to breakthrough were greater than about 99.5%.

The sulfided ash from each run was regenerated using air at bed temperatures of 1000°F or greater. Regeneration temperatures of above 1200°F were avoided to prevent fusion of ash particles due to the high exothermic heat of reaction of the oxidation step. Regeneration reaction was very rapid, and produced sharp oxygen breakthrough curves as illustrated in Figure 6.1(a).

All the process studies were done with the same nominal low-BTU gas composition--49% N_2, 20% CO, 10% H_2, 17% CO_2, 3% CH_4 and 1 to 1.5% H_2S. Western Kentucky No. 9, Montana Rosebud and Elkhorn No. 3 ashes were studied.

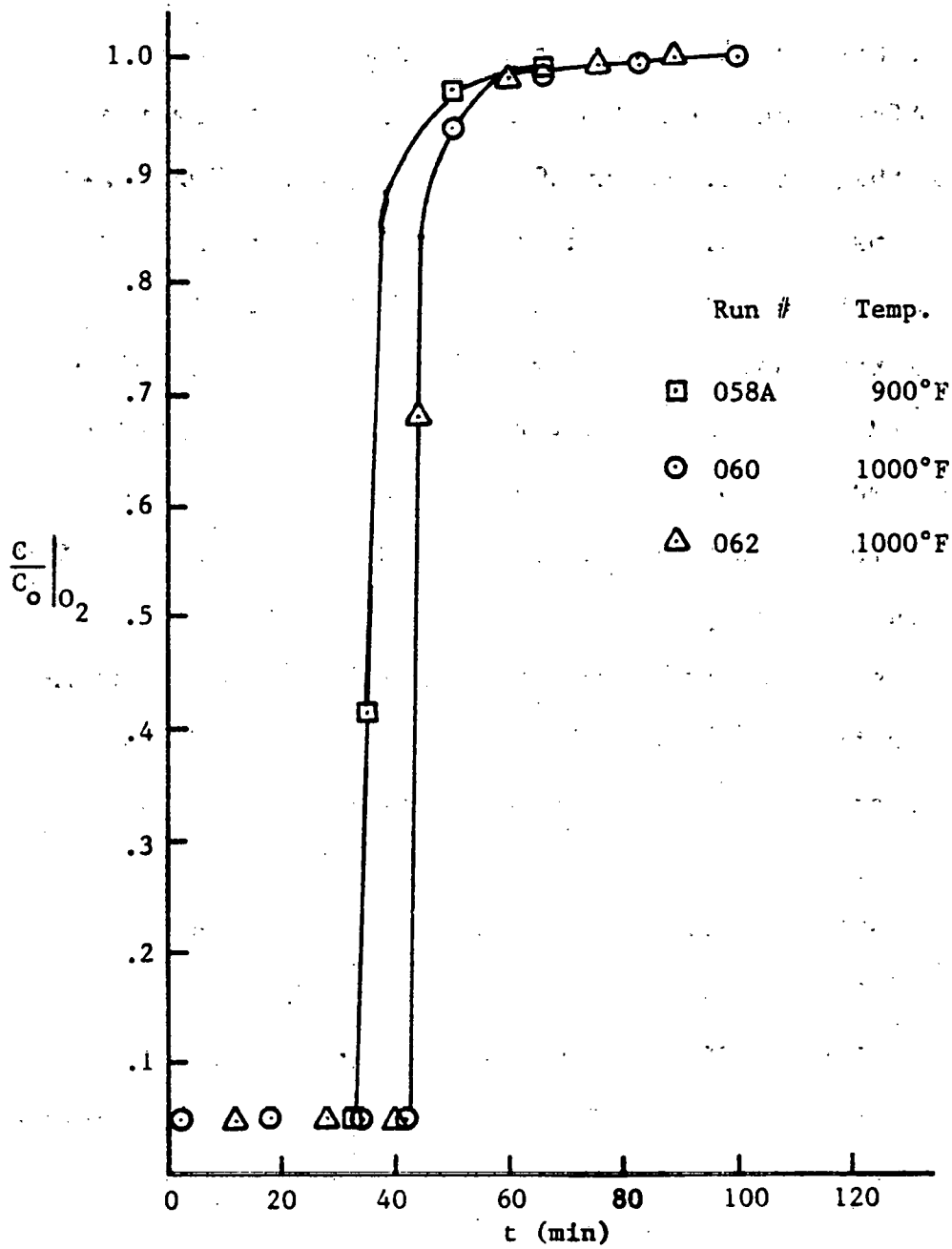

Figure 6.1(a) Regeneration breakthrough curves for W. Ky. No. 9 Ash. Q = 440 SCC/min, Inlet O_2 concentration = 3.0 vol. %, d_p = 0.0151cm.

The as-received mineral analyses of these ashes are given in Appendix A. It should be noted that the Fe_2O_3 content is about 22% for Western Kentucky ash, 8% for Montana ash and 9.5% for Elkhorn ash.

A total of 120 desulfurization and 8 regeneration runs were made. Tables B-1 to B-6 in Appendix B give representative data obtained for six selected runs. The compositions of all the gases are included in these tables. The data from other runs are presented in Appendix C in a reduced form.

6.2.1 Ash capacity and sorption-efficiency results:

The ash capacity of the bed is defined as follows:

Ash capacity in (g mole H_2S/gm ash) = M_o

$$= \frac{QC_{Ao}}{q} \int_0^{t_E} \left(1 - \frac{C_A}{C_{Ao}}\right) dt \qquad (6\text{-}1)$$

Here, t_E is the time at which the outlet H_2S+COS concentration reaches, for all practical purposes, a constant value. Nevertheless, after time t_E, the desulfurization reaction may still be proceeding at a very low rate that is difficult to detect. For this reason, the ash capacity calculated from equation (6-1) may be lower than the theoretical capacity obtained from the Fe_2O_3 content of the ash and the reaction stoichiometry. In fact, the experimental capacities obtained were considerably lower than the theoretical capacity. This is discussed in detail in Section 6.2.1.3.

The gas-chromatographically measured concentration of H_2S+COS, C_o, at t_E generally exceeded the measured inlet H_2S concentration C_{Ao} by about 2 to 3%. This was probably due to error associated with the separation of the overlapped H_2S and COS peaks. To avoid use of a C_A/C_{Ao} value greater than unity at bed saturation, C_A/C_o was used instead of C_A/C_{Ao} in equation (6-1). This correction, however, causes little change in the calculated values of the ash capacity or the breakthrough efficiency. A similar approach was used by Fieldes and Davidson (1978) in their study of the reaction of SO_2 with limestone in a batch fluidized-bed.

As pointed out in Chapter 5, it is convenient to deal with the breakthrough curve plotted in nondimensional form. The dimensionless time τ was defined in that chapter by the relation (5-23). A computer program was set up to calculate the ash capacity and convert the raw data into dimensionless variables C_A/C_o and τ. Raw data for a few representative runs are presented in Appendix B. The computer program for data conversion is listed in Appendix D and the converted data are given in Appendix C. The program uses the trapezoidal rule to calculate τ. The definition of τ has a special physical significance which is explained below.

In theory, if the sorption rate were infinite, all the input sorbate gas that can be absorbed would be sorbed

at the instant of breakthrough, and of course that instant also corresponds to the time of bed saturation as illustrated in Figure 6.2. This behavior is termed perfect sorption and is approached in practice by systems with very high reaction rates. In many practical situations, however, the breakthrough starts before all the solid reactant is consumed, i.e., when $\tau < 1.0$ and the curve has a finite slope. For these situations one may define a sorption efficiency as the value of τ at which C_A/C_{A_o} is equal to a specified value. In this work, this value of C_A/C_{A_o} is arbitrarily selected as 0.1. Sorption efficiency, $\tau_{0.1}$, is an indication of the average reaction rate prior to breakthrough and hence may be used to evaluate the effect of different variables on the performance of the process. An explanation of the average reaction rate may be appropriate at this point. The reaction rate (defined per unit mass of the reactant solid) for gas-solid reactions varies with solid conversion due to depletion of the solid reactant and possible changes in control regimes. It is for this reason that the term "average reaction rate" was used above. To present an example here, the dimensionless breakthrough curves for runs conducted at three different temperatures but the same H_2S concentration and fluid mass velocity are compared in Figure 6.3. It may be noted that temperature significantly affects the efficiency. The efficiency increases with temperature in

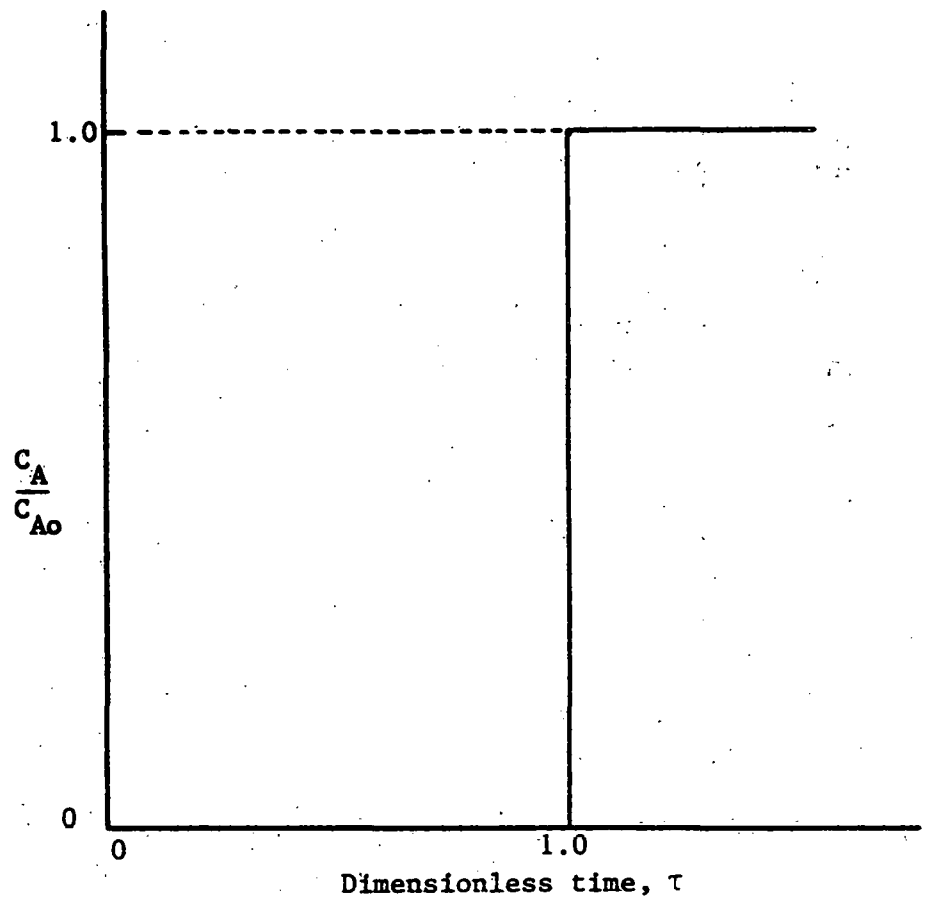

Figure 6.2 Perfect Sorption.

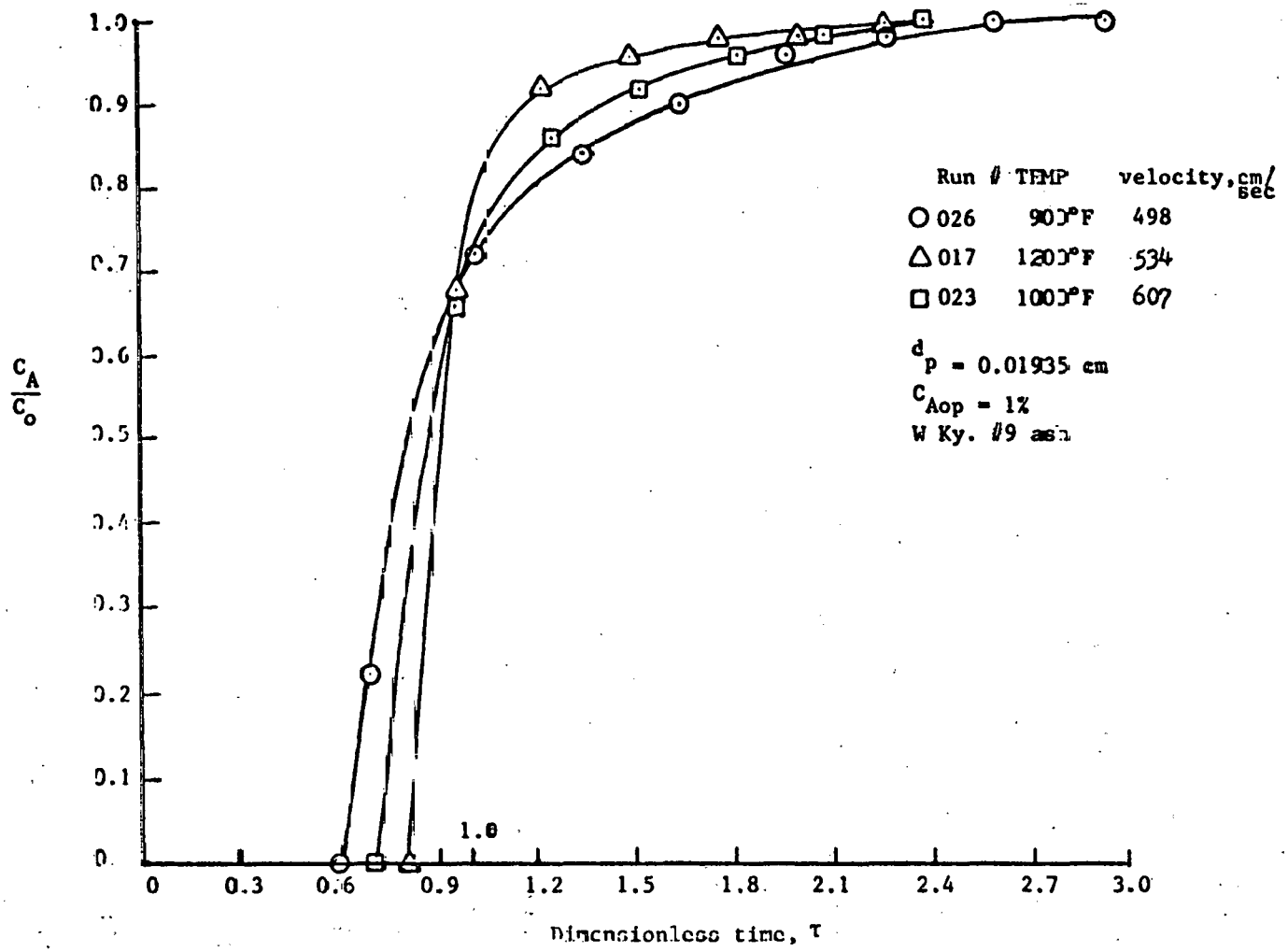

Figure 6.3 Effect of temperature on desulfurization.

spite of the fact that the increased linear velocity (note that the mass velocity is the same) due to temperature increases fluid bypassing which in turn reduces the overall reaction rate. The effect of fluid velocity on reaction rate is considered in more detail in Section 6.4. It will also be shown in Section 6.4 that external mass transfer which is velocity dependent is not a factor.

6.2.1.1 Initial increase of capacity and efficiency of fresh ash:

It was found that the H_2S capacity and efficiency of the fresh ash initially increased with the number of desulfurization-regeneration cycles before stabilizing at a constant value. The stabilized capacity and efficiency increased with temperature; this will be discussed in Section 6.2.1.3. Figure 6.4(a) illustrates the capacity increase with the number of cycles; Figure 6.4(b) shows the change in efficiency. The first cycle values reported are the ones obtained after the very first desulfurization run. The first four cycles were conducted at 1200°F, the next four at 1000°F and the last two again at 1200°F. The capacity (cc H_2S at STP/gm. ash) and efficiency increased from 18.6 and 0.546 respectively to 23.9 and 0.825 during the first four cycles. The change of temperature to 1000°F for the fifth cycle then caused the capacity and efficiency to drop to 16.9 and 0.570. This decrease might have been partly due to the effect discussed later in

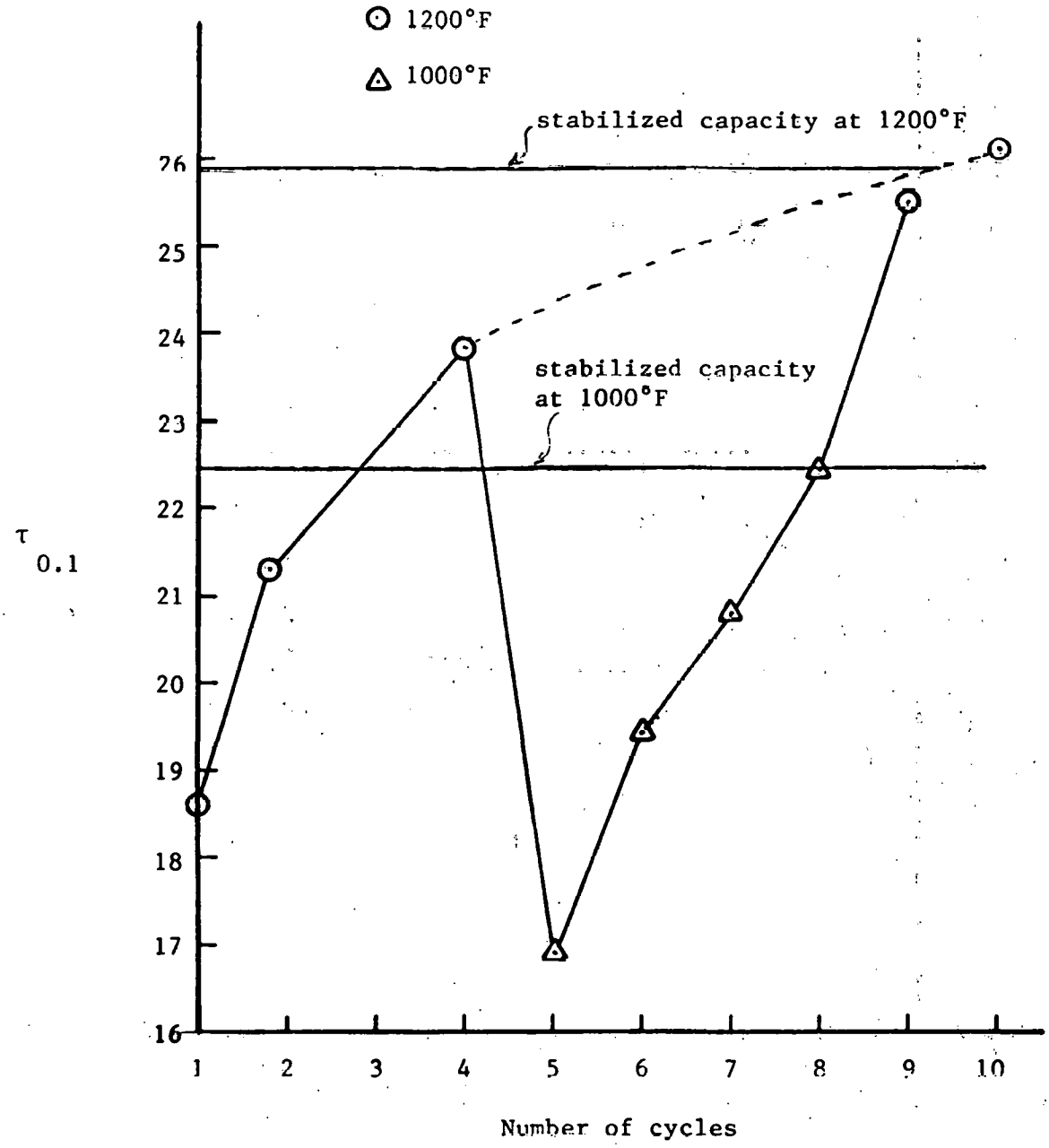

Figure 6.4(a) Initial increase of H_2S capacity with number of cycles. Run Nos. (040-049), Western Ky. No. 9 Ash; d_p = 0.0151cm..

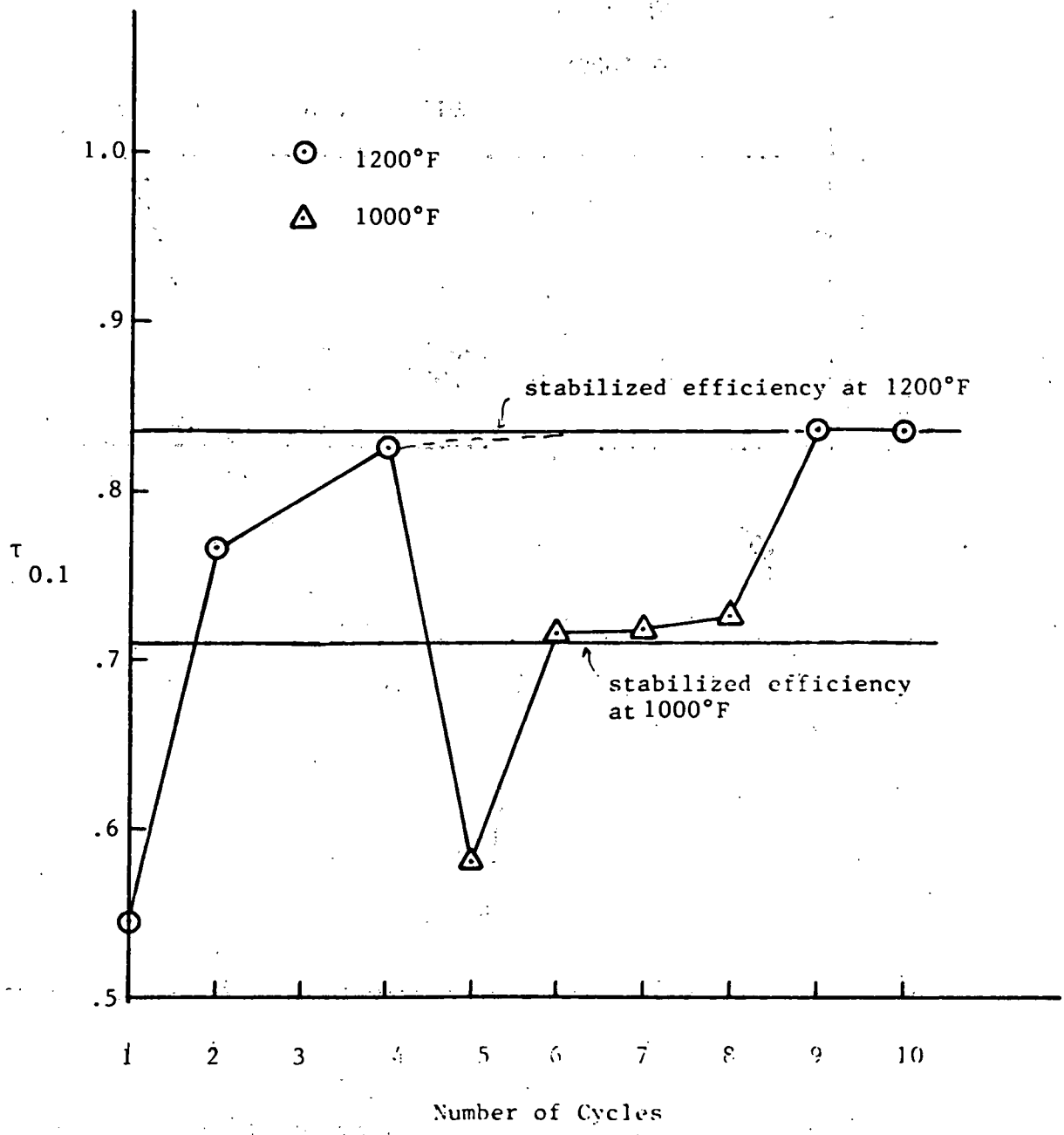

Figure 6.4(b) Initial increase of sorption efficiency with number of cycles, Run Nos. (040-049) (Western Ky. #9 Ash, d_p = 0.0151cm).

Section 6.2.1.2. During the next three cycles at 1000°F, capacity and efficiency again increased reaching the constant values for 1000°F of about 22.5 and 0.72 respectively at the eighth cycle. The stabilized ash capacities and efficiencies are later presented in Table 6.4. The change of reaction temperature to 1200°F for the ninth cycle increased the capacity and efficiency to the constant values for 1200°F of about 26.0 and 0.835. If all the runs discussed above had been conducted at 1200°F, it appears that the ash might have stabilized after six cycles. In Figures 6.4(a)and 6.4(b)the broken line represents the extrapolation of the values if the temperature had been kept the same as the previous cycle. The cycles reported in this section are only the stabilization cycles. More runs were conducted on this ash; these results will be discussed later in this chapter. The stabilized values shown as horizontal lines in Figures 6.4(a)and 6.4(b)are based on these further tests.

Schrodt (1977b) reported that the ash capacity and efficiency for the fresh ash initially increased for his packed-bed runs in much the same fashion as for the fluidized-bed runs discussed above. Schrodt, using EDAX scans on ash particles, showed that this phenomenon is caused by progressive migration of iron towards the particle surface. Turkdogan (1968) explained the growth rate of ferrous sulfide on iron based on iron migration phenomenon. In a

sulfidation study which utilized gas mixtures containing hydrogen sulfide at high temperatures, Sorrel and Hoyt (1956) report that the specific diffusion processes involved during the scaling of steels are the inward migration of sulfur through the scale formed and additionally, cationic diffusion outward. These last two studies support Schrodt's conclusion.

6.2.1.2 Change in capacity and sorption efficiency of stabilized ash immediately following a temperature reduction:

Surprisingly, it was also found, at least for the Western Kentucky stabilized ash, that a temperature reduction after a series of runs at a higher temperature caused the capacity and efficiency to fall below the normal stabilized values for the lower temperature. However, after a few runs at the lower temperature, the capacity and efficiency again returned to their normal values. Such an effect was not noticed when switching from a lower temperature series to runs at higher temperatures. Table 6.3 and Figure 6.5 show the effect described above. Attention is called here to the fact that the capacity and efficiency values reported in Table 6.3 are for the stabilized ashes; already quite a few cycles have been completed with these ashes. The efficiency and capacity values reported in Table 6.3 are for the operation at the lower temperature indicated in column 5. For example, Runs 021-024 were conducted at 1000°F on the stabilized ash from a 1200°F

Table 6.3

EFFICIENCY AND CAPACITY CHANGE
ON REDUCTION OF TEMPERATURE FOR
WESTERN KENTUCKY #9 ASH

Run #	Particle diam (dp) (cm)	Total # of cycles previously completed on this ash	Source temp. of ash (°F)	New processing Temp. (°F)	Efficiency	H_2S capacity (SCC/gm ash)
021	0.01935	20	1200	1000	.579	21.35
022	"	--	"	"	.630	23.90
023	"	--	"	"	.729	26.29
024	"	--	"	"	.729	26.59
050	0.0151	10	1200	1000	.576	19.36
051	"	--	"	"	.700	19.42
052	"	--	"	"	.705	22.46
053	"	--	"	"	.705	22.18
055	0.0151	15	1000	900	.636	20.25
056	"	--	"	"	.663	22.31
057	"	--	"	"	.663	22.12
058	"	--	"	"	.663	22.23
118	0.0151	20	1400	1000	.654	22.90
119	"	--	"	"	.657	24.34
120	"	--	"	"	.666	26.93
121	"	--	"	"	.708	27.00
122	"	--	"	"	.700	28.25

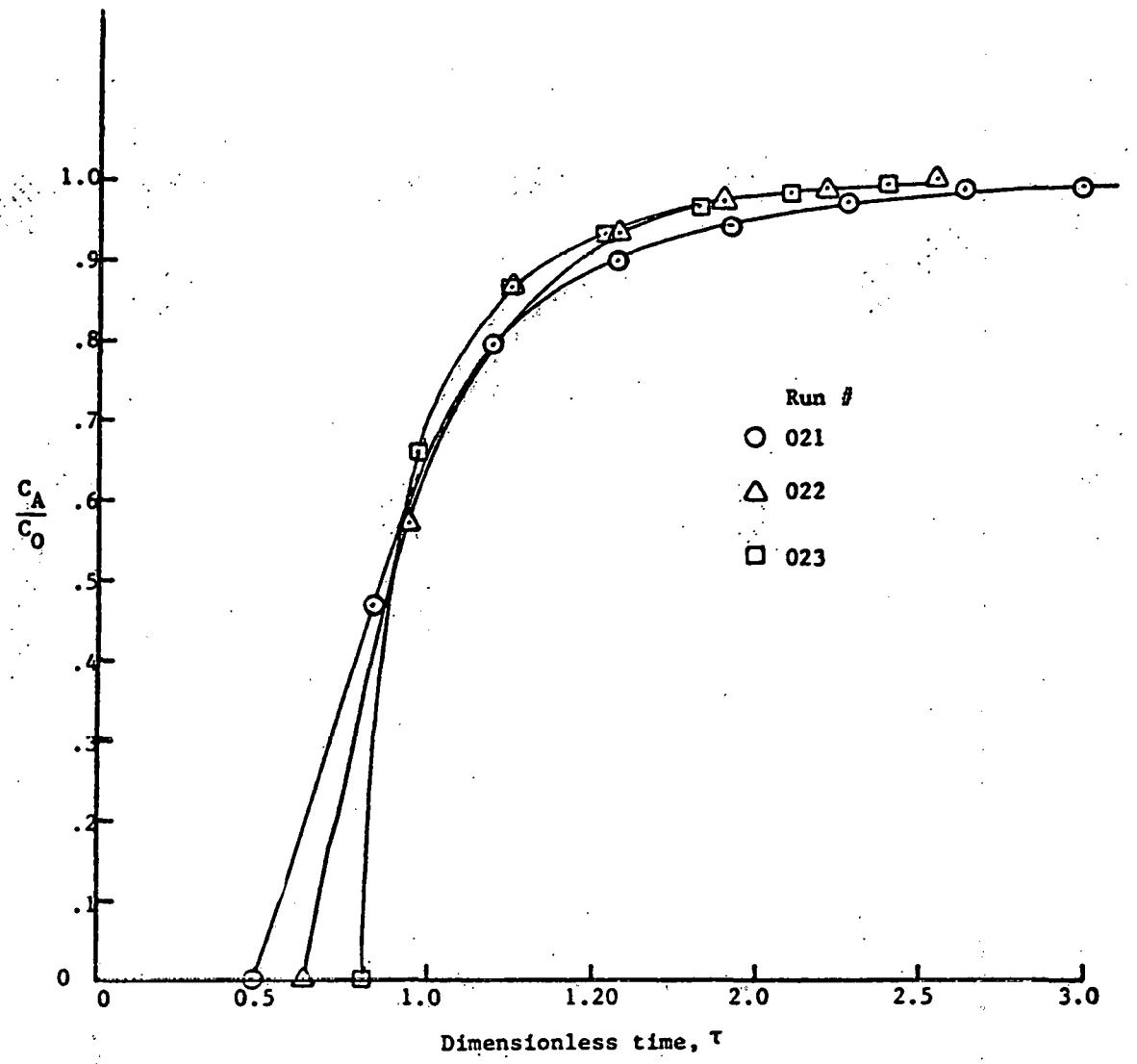

Figure 6.5 Efficiency and capacity change on reduction of temperature for Western Ky. No. 9 Ash. Q = 600 SCC/min, C_{Aop} = 1.0%, d_p = 0.01935cm, temp. = 1000°F.

run. The efficiency and capacity were found to increase from 0.579 and 21.35 respectively to the stable values of 0.729 and 26.30 in about three cycles. The series, Runs 118-122 for 1400-1200°F change, required four cycles for restabilization. The series, Runs 055-058 for 1000-900°F change, required only two cycles. It therefore appears that the extent of the phenomenon described here depends on the magnitude of the temperature change in the investigated range of 900°F-1400°F. Such a phenomenon was not reported by Schrodt for his packed-bed studies.

The low values of efficiency and ash capacity obtained, immediately following a high temperature run, may be due to a change in pore structure. The work of Hasatani and Wen (1977), discussed in Chapter 3, shows that at higher desulfurization temperatures the degree of iron oxide reduction is greater. Further, it is to be noted that the densities of the iron oxides increase as follows: $Fe > FeO > Fe_3O_4 > Fe_2O_3 > FeS$. Due to these facts temperature may, in some fashion, influence the minimum free energy state for the iron oxide sorbent grains dispersed in the particle resulting in structural changes. Regeneration temperature could not have been a factor since it was always carried out above 1000°F. It is suggested here that a previous higher temperature operation, after regeneration, leaves a Fe_2O_3 with a denser structure which requires a few cycles for adjustment to a more porous structure at

the lower temperature. Additional work is required for a conclusive explanation of the phenomenon reported in this section.

6.2.1.3 Effect of process variables on capacity of stabilized ash:

The efficiency and capacity obtained for the various runs are listed in Table 6.4.

Capacity:

Inspection of data reveals that ash capacity increased with temperature; no specific trend is obvious with regard to fluid velocity or H_2S inlet concentration. Effect of temperature on ash capacity is displayed in a graphical form in Figure 6.6; ash capacities for the three sizes of Western Kentucky ash are plotted in this figure. A line is drawn through the points for each size to indicate the trend. The smallest particles with a mean size of 0.01065 cm gave the highest capacities; the intermediate-size particles (d_p=0.0151 cm) displayed the lowest ash capacity. It should be mentioned here that the mineral analyses reported in Appendix-A were not carried out on the screened and sized samples used here. The analyses were performed on larger particles used for the packed-bed studies reported by Schrodt (1977a). Therefore, inherent variation of Fe_2O_3 content between the different sized ash samples used in the current study cannot be ruled out. The reader is referred to Chapter 4 for details on ash sample preparation.

Table 6.4

CAPACITY AND BREAKTHROUGH-EFFICIENCY OF STABILIZED ASH

Run #	Mean particle size dp, cm	Temp. °F	Inlet H_2S conc. C_{Aop} Vol. %	Superficial linear velocity, u cm/min.	u/u_{mf}	Capacity SCC H_2S/gm ash	Efficiency $\tau_{0.1}$
W. Ky Ash:							
014	0.01935	1200	1.0091	607	3.00	29.70	0.830
017	"	"	0.9943	"	"	28.62	0.830
019	"	"	0.9915	"	"	29.95	0.830
023	"	1000	0.9931	534	2.64	26.29	0.729
024	"	"	1.0024	"	"	26.59	0.729
026	"	900	0.9993	498	2.47	23.66	0.633
029	"	1000	1.0019	387	1.92	28.21	0.834
048	0.0151	1200	0.9845	436	3.00	25.57	0.833
049	"	"	0.9959	"	"	26.16	0.833
052	"	1000	0.9884	391	2.70	22.46	0.705
053	"	"	0.9937	"	"	22.18	0.705
054	"	"	1.0033	"	"	22.64	0.705
056	"	900	1.0209	364	2.51	22.23	0.663
057	"	"	1.0059	"	"	22.11	0.663
058	"	"	1.0092	"	"	22.23	0.663
061	"	1400	0.9889	487	3.36	27.96	0.865
075	0.01065	1000	1.2248	335	3.28	28.96	0.726
076	"	"	1.2514	"	"	29.11	0.726
077	"	"	1.2462	391	3.83	28.15	0.703
078	"	"	0.9996	"	"	29.41	0.750
080	"	900	1.2535	312	3.06	27.96	0.690

Table 6.4 continued

121	0.0151	1000	1.0101	443	3.06	27.00	0.700
122	"	"	1.00925	"	"	28.25	0.695
123	"	"	1.4112	"	"	30.04	0.669
124	"	"	1.4210	"	"	30.58	0.669
126	"	"	1.0002	573	3.95	29.49	0.699
127	"	"	1.0001	582	4.01	29.89	0.699
Elkhorn Ash:							
095	.01935	1000	0.9904	408	2.12	9.00	0.550
096	"	"	0.9888	"	"	9.75	0.550
Montana Ash:							
111	.01935	1000	1.0145	408	2.12	7.47	0.630
112	"	"	1.0066	"	"	7.96	0.575
113	"	"	1.0003	"	"	7.49	0.600
114	"	"	0.9794	417	2.16	7.05	0.560*

*About 3.2% water vapor included in inlet gas for this run.

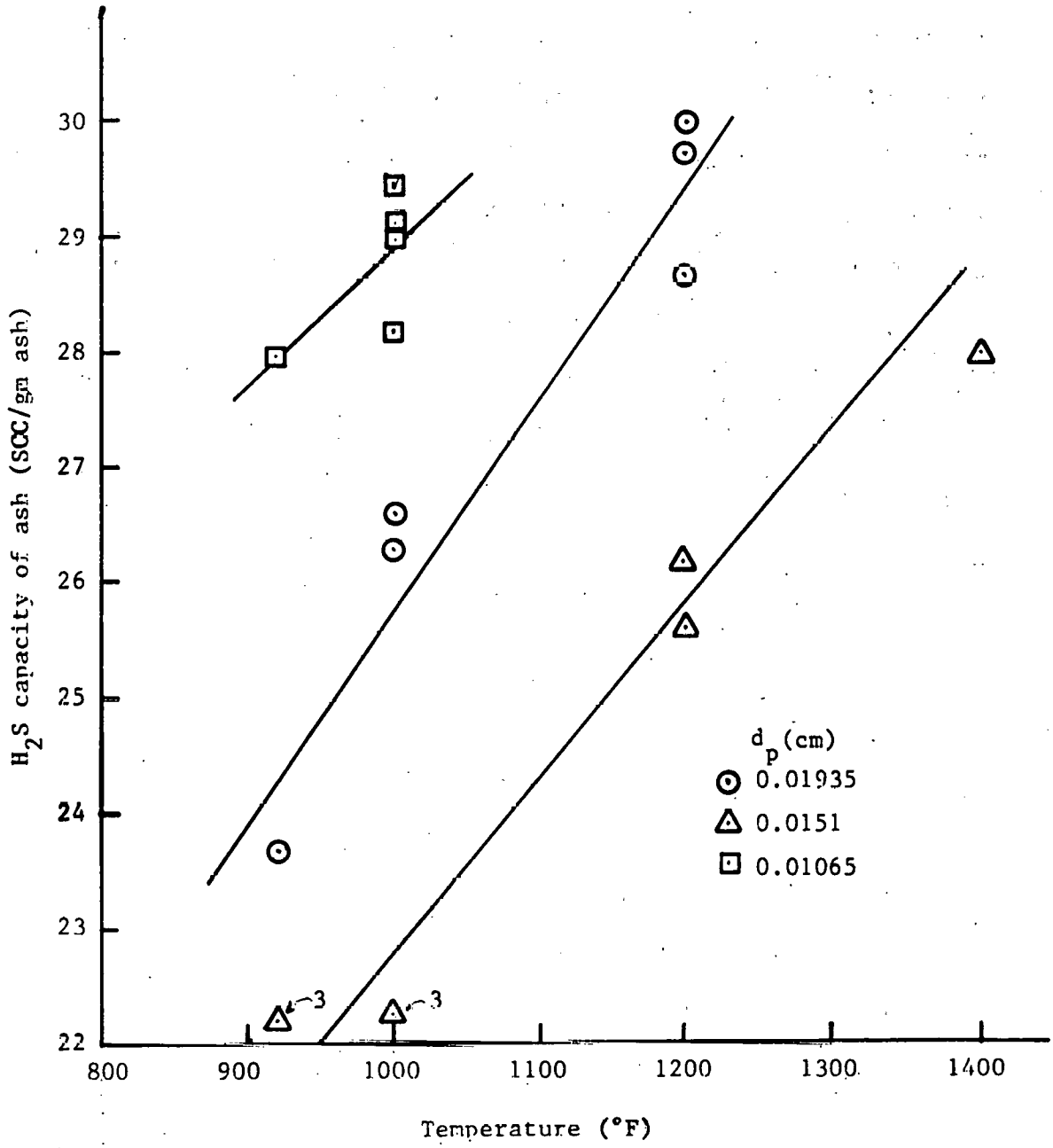

Figure 6.6 Ash capacity vs. temperature for W. Ky. No. 9 Ash.

The fresh ash samples were always stabilized first by making several runs at 1200°F; runs at other temperatures were subsequently performed. It may be noted from Table 6.4 that for the intermediate-size W. Ky. particles, the series, Run Nos. 121-127 gave higher ash capacities at 1000°F as compared to the series, Run Nos. 052-054; the capacities obtained for these series are comparable to the values obtained for the particles of mean size 0.01065 cm. However, efficiency did not change between the two series of runs. These runs are not included in Figure 6.6. The series, Run Nos. 121-127 were carried out after the ash had been run once at 1400°F; in fact this series was the only one conducted after a 1400°F run. It is likely that the 1400°F run had increased the available fraction of iron oxide, thereby increasing the ash capacity at lower temperatures. A few runs at 1400°F were also conducted on the larger (0.01935 cm) W. Ky. particles. Since almost no fluidization could be achieved for these runs, they are not included in the data reported here.

The Montana and Elkhorn ashes gave much lower ash capacities as compared to Western Kentucky ash. This is to be expected since these two ashes contain less Fe_2O_3. Figure 6.7 is a plot of ash capacity vs. Fe_2O_3 content of ash. The W. Ky. series, Run Nos. 014-026 is used in this plot; also the nominal Fe_2O_3 contents reported in Appendix A are used. The solid line is the theoretical capacity

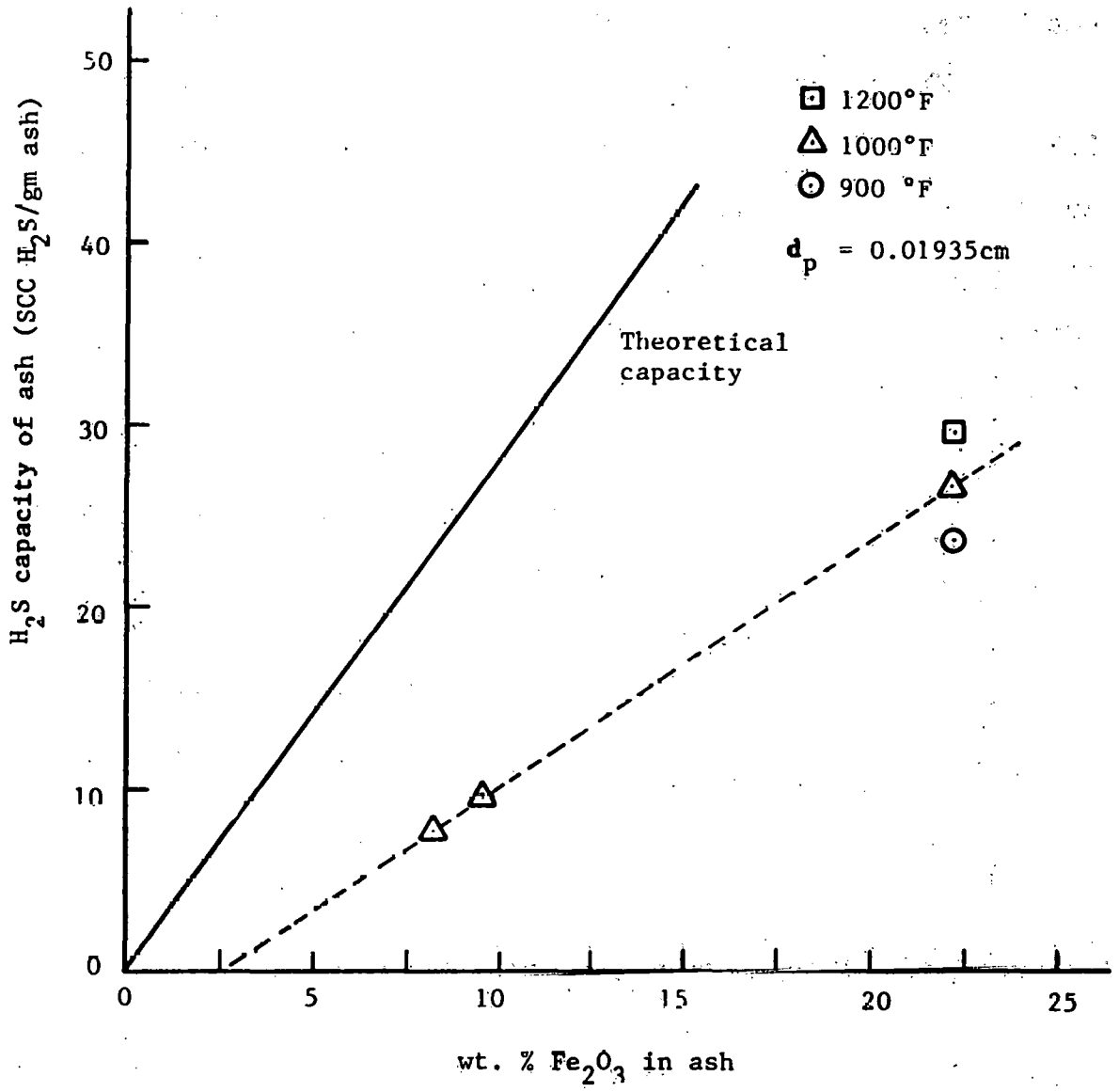

Figure 6.7 Effect of iron oxide concentration on H_2S capacity.

to be expected based on the nominal iron oxide content and stoichiometry. The broken line for 1000°F indicates that the capacity increases approximately linearly with the Fe_2O_3 content. The highest utilization of Fe_2O_3 obtained for the W. Ky. ash was about 48% of theoretical capacity.

The inlet gas for Run No. 114 contained about 3.2% water vapor which seems to reduce the capacity slightly; but the difference is probably not significant. The investigations of Schrodt (1977b) and Hasatani and Wen (1977) show that water vapor has little or no effect on efficiency or capacity.

Breakthrough Efficiency:

Table 6.4 shows that the process variables--temperature, u/u_{mf} ratio, inlet H_2S concentration--affect the efficiency of the process. Since, as explained earlier, efficiency is an indication of average reaction rate, these effects will be discussed in Section 6.4 on reaction rate and kinetic modeling. The reproducibility of efficiency results was very good and well within about 3%.

6.3 Secondary effects:

The tables in Appendix B show the variation of composition of the different gases present in the simulated low-BTU gas during desulfurization; these runs are representative of the desulfurization experiments.

In addition to the H_2S, the compositions of CO, H_2O, CO_2, and H_2 are also found to change during the

course of desulfurization; CH_4 and N_2 remain essentially unchanged. Figure 6.8 illustrates the change in composition of CO, CO_2 and H_2 with time on stream for a representative run (Run #053); concentration of the water vapor formed during the reaction is also shown. Initially the CO_2 concentration increases, CO and H_2 steeply decrease, and high production of water vapor is observed. After approximately 20 minutes, the concentrations of CO, H_2 and CO_2 seem to stabilize at values somewhat different from the respective inlet concentrations. Water vapor concentration reaches a stable value a short time after the H_2S breakthrough has occurred (see Figure 6.9). There seems to be a net increase in CO and decrease in H_2 and CO_2. It is also observed that some of the H_2S is converted to COS; no COS was present in the inlet gas. Figure 6.9 shows the variation of COS and H_2S during the run for Run No. 053. Both COS and H_2S breakthrough at the same time and the concentration of COS seems to increase with that of H_2S. The curve marked (H_2S+COS) is obtained by directly adding the concentrations of H_2S and COS. The concentrations change very little after about 125 minutes; almost all the available iron oxide in the ash is reacted at this point. The final H_2S + COS is equal to the inlet H_2S concentration of 0.9951%. The slight difference may be due to the error involved in processing of the chromatographic peaks of COS and H_2S in exit gas analyses. The direct additivity

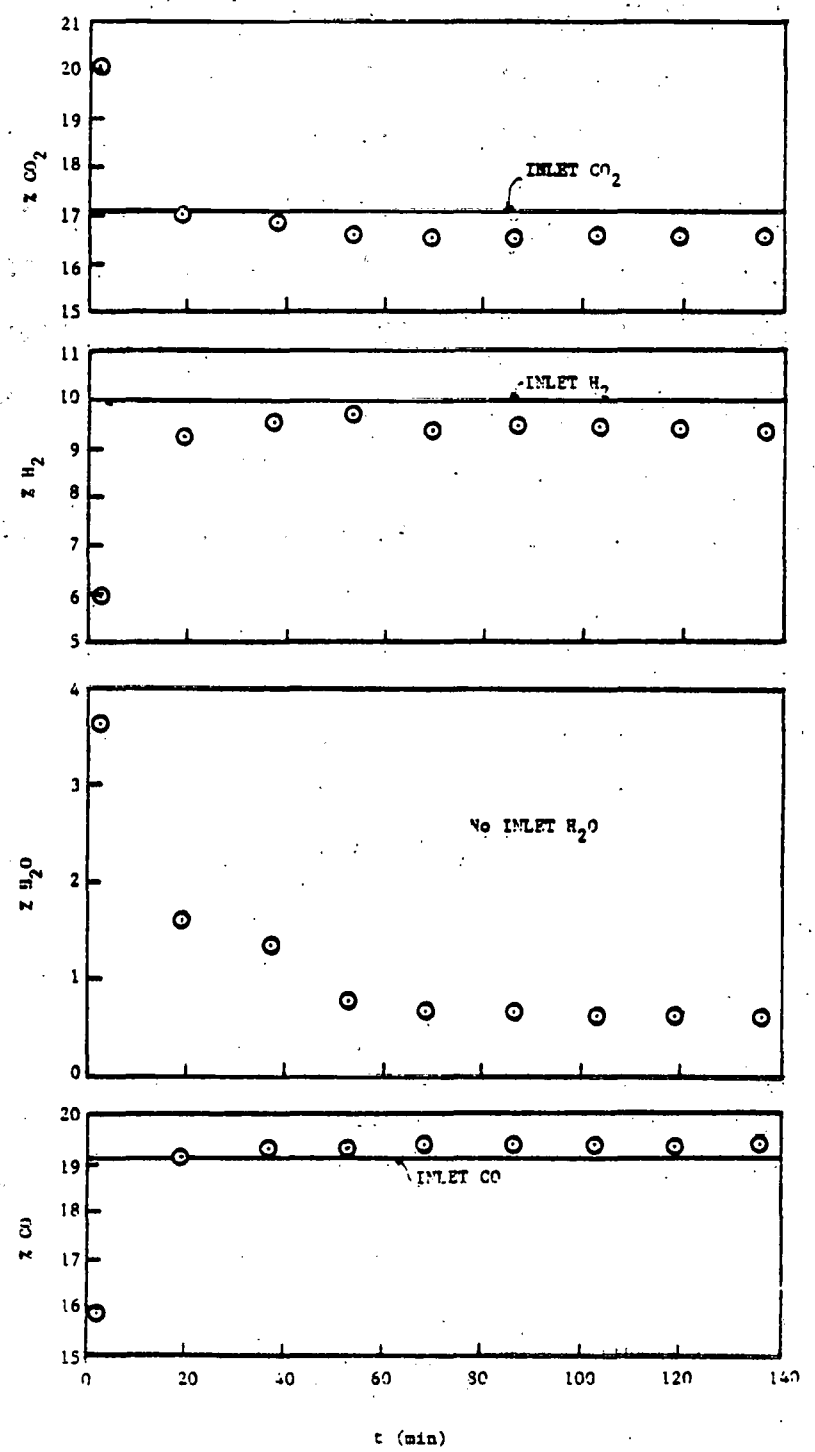

Figure 6.8 Composition change of (exit gas) during desulfurization for W. Ky. No. 9 ash
Run No. 053, 1000°F .

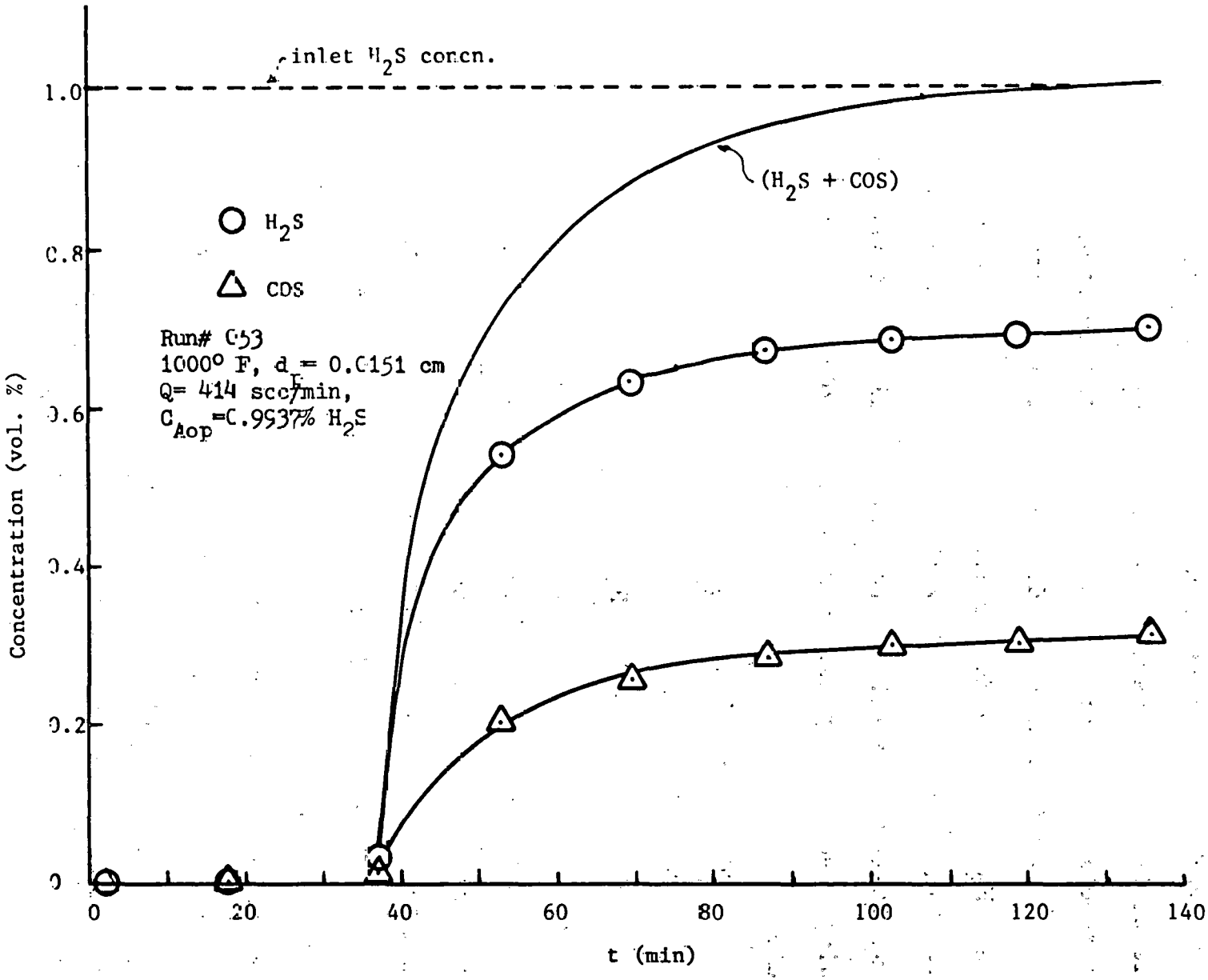

Figure 6.9 Variation of H_2S and COS during desulfurization. W. Ky. No. 9 ash.

of COS and H_2S concentrations is due to the fact that a mole of COS formed requires a mole of H_2S. The COS forming reactions are discussed later in this section.

The initial rapid decrease of the reducing gases CO and H_2 is mainly due to reduction of hematite as discussed in Chapter 3. After the initial period of about 20 minutes the relative rates and equilibria of the following reactions appear to dictate the observed compositions.

$$CO + H_2O = CO_2 + H_2 \qquad (3.16)$$

$$CO + H_2S = COS + H_2 \qquad (3.19)$$

$$CO_2 + H_2S = COS + H_2O \qquad (3.20)$$

Figures 6.10 (a), (b) and (c) are plotted to analyze the extent of these reactions after the initial period in relation with their equilibrium. The ratio of product to reactant concentrations (J_a) is plotted against temperature for Western Kentucky ash of particle size 0.0151 cm. Figure 6.10(a) reveals that the water-gas shift reaction is very close to equilibrium conditions at 1200°F even though the fluid velocity increased with temperature. At 900 and 1000°F, however, the J_a values are far in excess of equilibrium values indicating lower reaction rates. Figure 6.11 is plotted to analyze the catalytic effect of the three different ashes used; the J_a values are plotted as a function of time on stream for Western Kentucky, Montana and Elkhorn ashes. The runs were conducted at 1000°F and

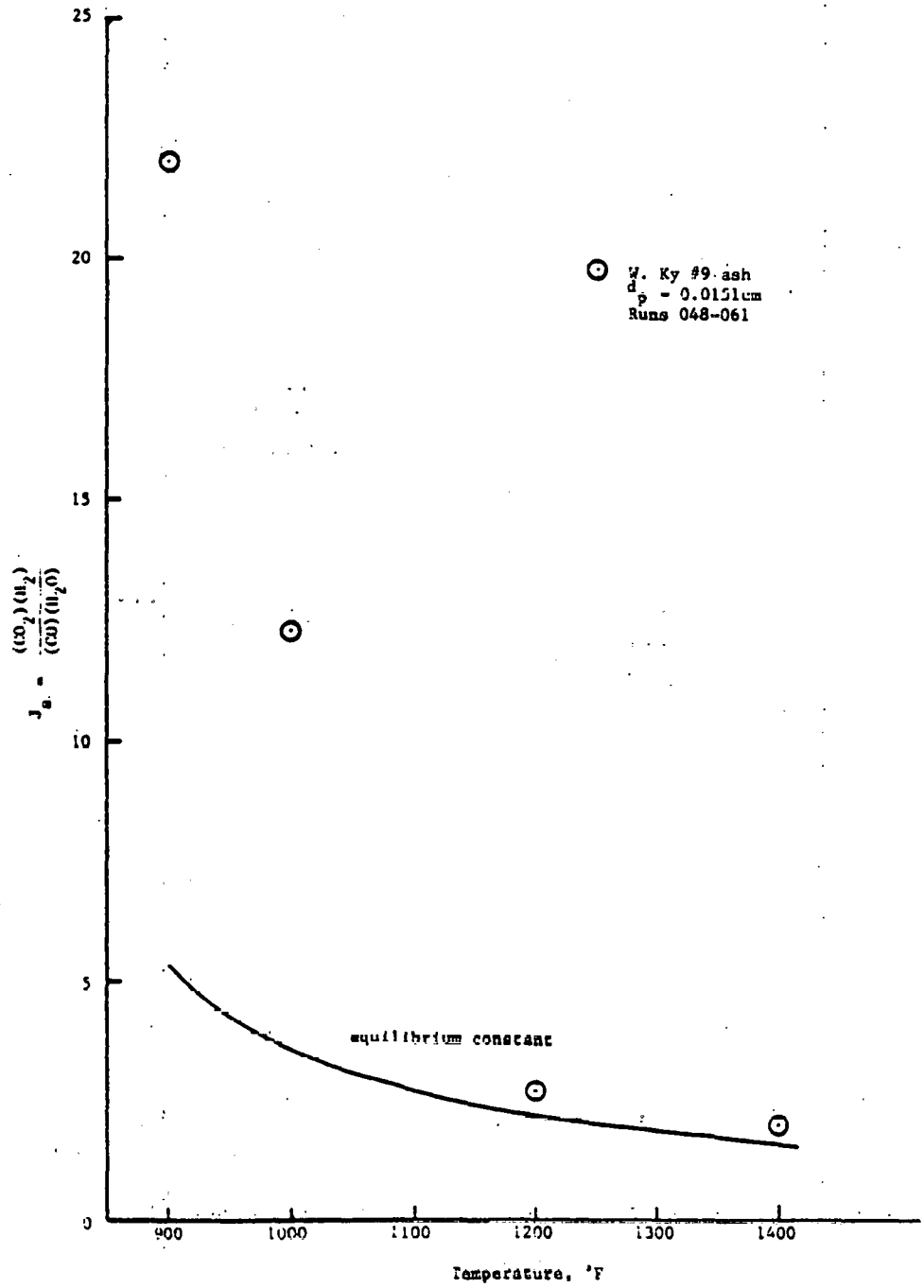

Figure 6.10(a) Check of equilibrium for water gas shift reaction $CO + H_2O = CO_2 + H_2$.

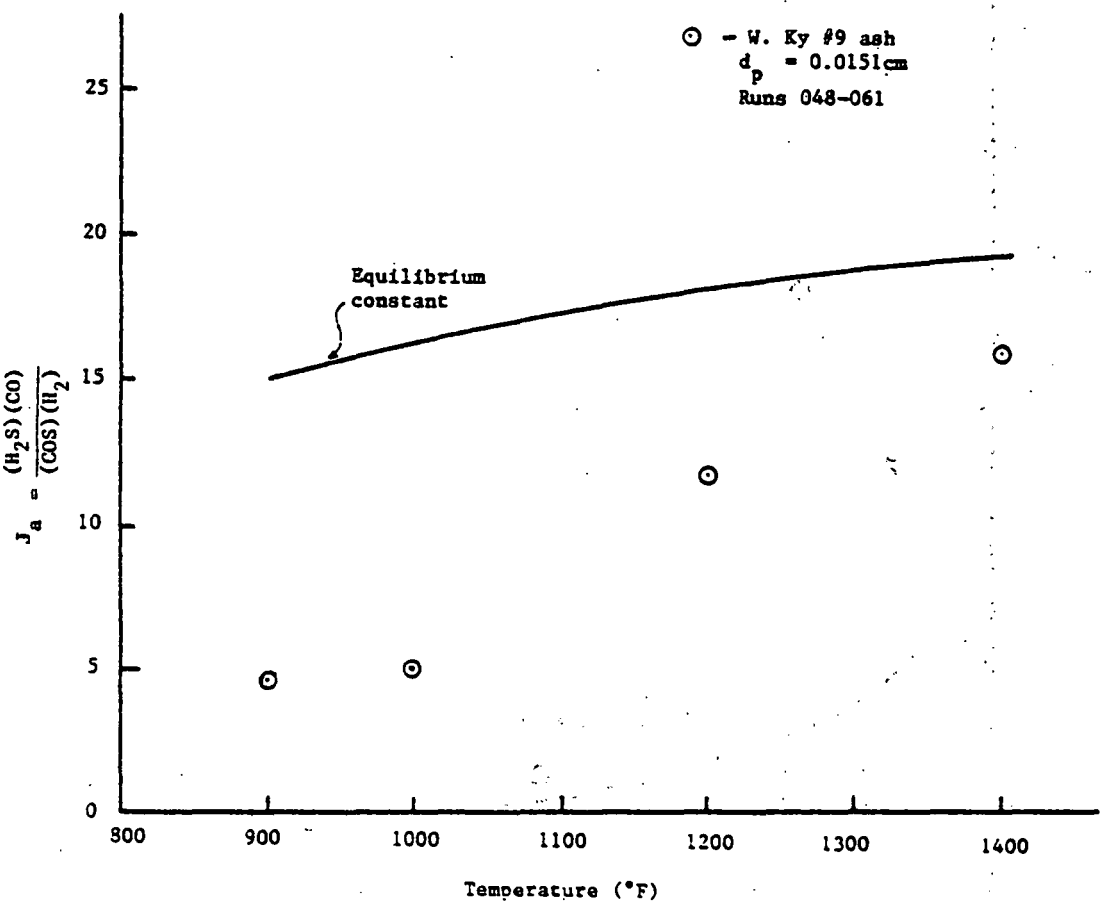

Figure 6.10(b) Check of equilibrium in relation to the COS hydrogenation reaction, $COS + H_2 = H_2S + CO$.

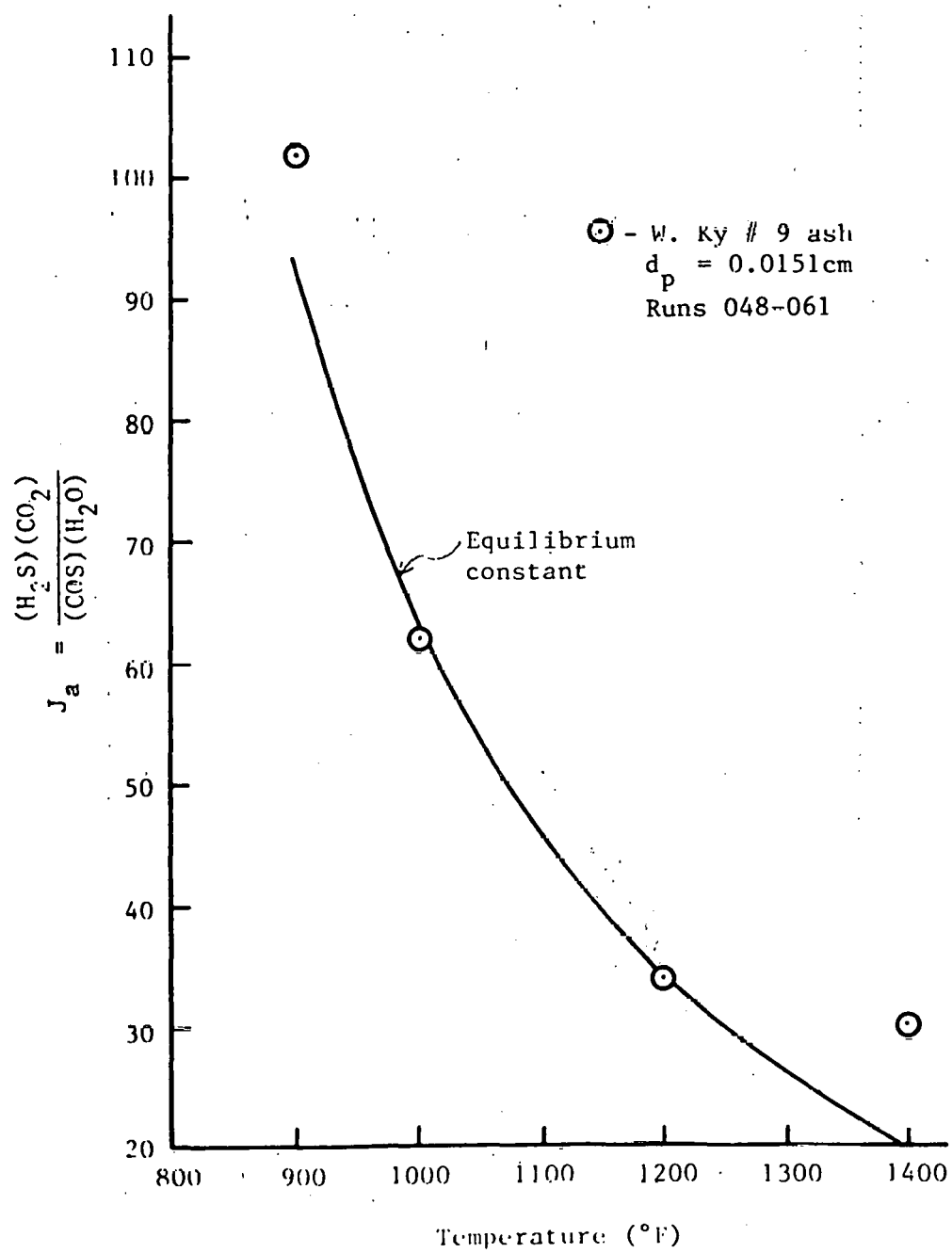

Figure 6.10(c) Check of equilibrium in relation to COS hydrolysis reaction, $COS + H_2O = H_2S + CO_2$.

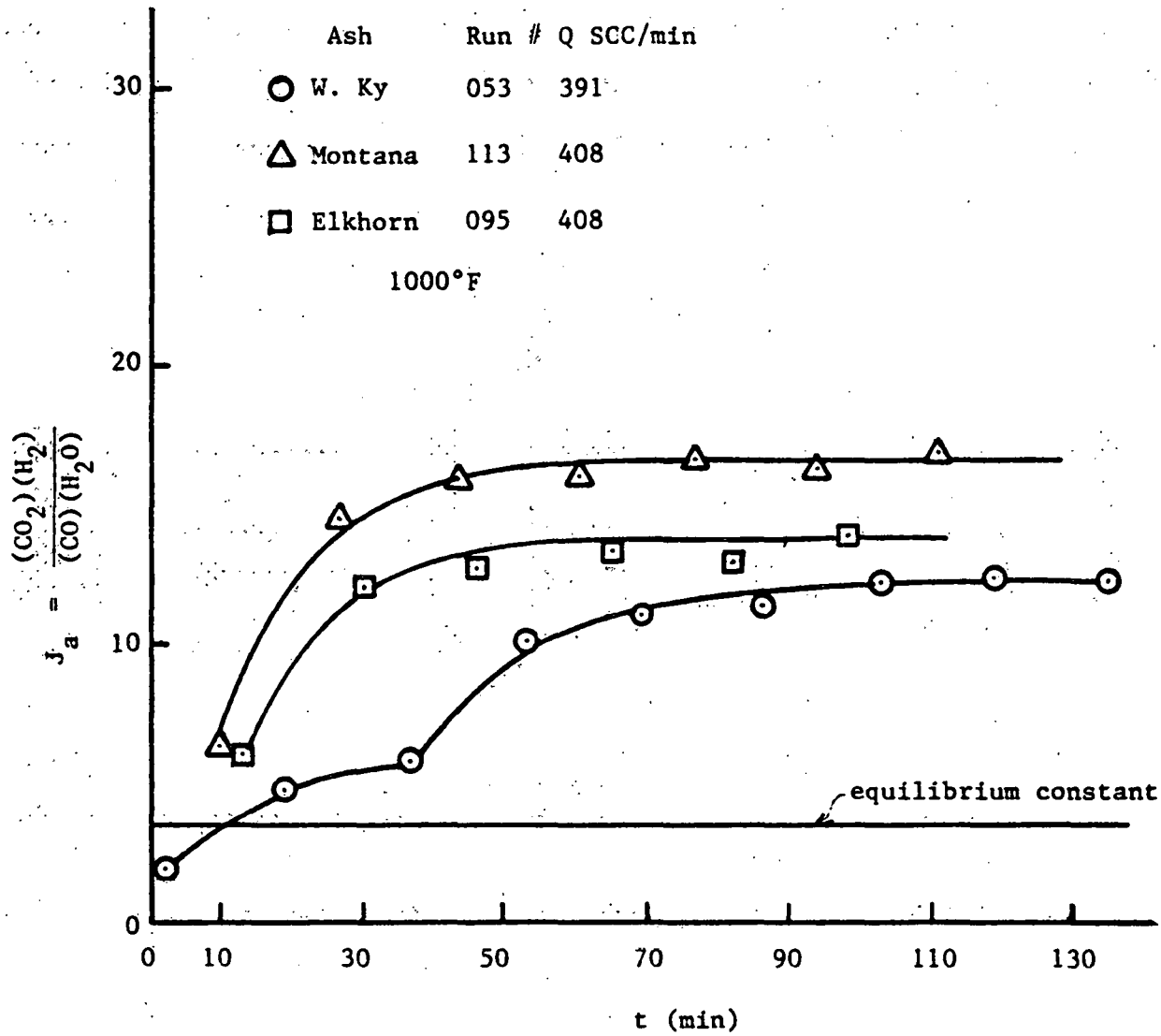

Figure 6.11 Examination of catalytic effect of ash for the reaction, $CO + H_2O = CO_2 + H_2$.

approximately the same fluid velocity and inlet gas compositions. The water-gas shift reaction is closer to equilibrium in the order W. Ky., Elkhorn and Montana. It is interesting to note that the iron oxide content of the ash beds were: W. Ky.>Elkhorn>Montana. While this is not a well-designed test for the catalytic effect of ashes, the intent is to show that the results seem to agree with the findings of Evans (1978) who showed that the iron oxide present in coal ash catalyzes the reverse water-gas shift reaction.

Figure 6.10 c indicates that the reaction (3.20) is rapid enough at most temperatures to reach equilibrium. At 900°F and 1400°F the J_a value is somewhat higher than the equilibrium constant. Figure 6.10(b), on the other hand, indicates that the COS hydrogenation reaction moves closer to equilibrium at higher temperatures with the J_a values below the equilibrium line. Again, the equilibrium is approached at higher temperatures in spite of the fact that the fluid velocity increased with temperature. Therefore as in the case of the water-gas shift reaction, the reaction velocity of COS hydrogenation reaction increases appreciably with temperature.

Figure 6.12 is plotted to check catalytic effects of the ash on the COS-H_2S reactions; the ratio of the concentrations of COS to H_2S (after the ash is saturated) is plotted against temperature. The dissociation of H_2S to

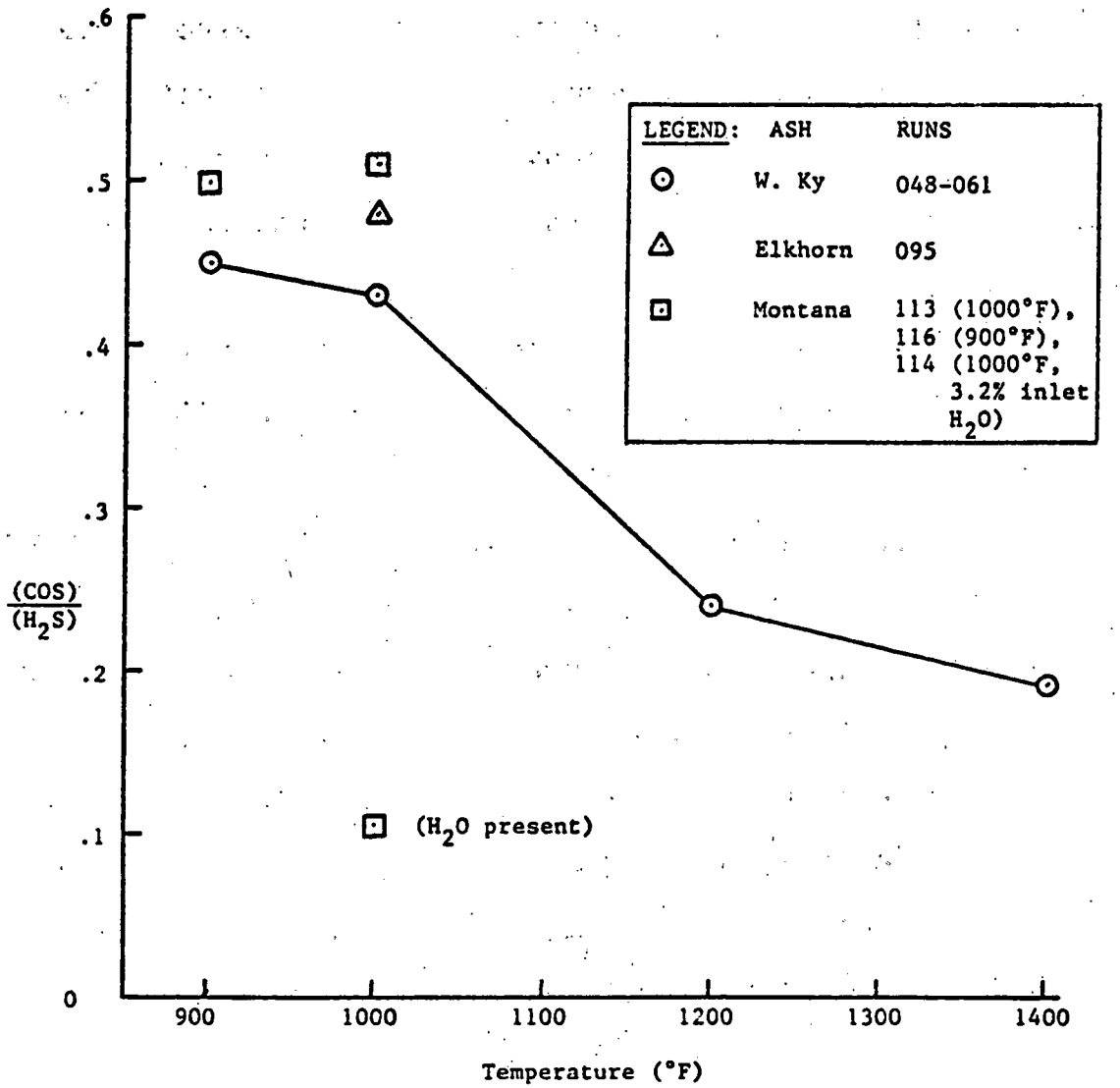

Figure 6.12 Dissociation of H_2S to COS.

form COS reduces with temperature for the Western Kentucky ash with the greatest drop occurring between 1000 and 1200°F. This effect is due to the increased reaction velocities of the reverse water-gas shift reaction. Concentration of water vapor present in the reaction mixture directly affects the formation of COS as evidenced by Run No. 114, where the inlet gas contained about 3.2% water vapor. Montana ash was used for this test. The runs included in Figure 6.12 may be directly compared at a particular temperature since the gas compositions and fluid velocities for these runs were approximately the same. Run No. 095 did not have any inlet water vapor present. It may be seen that the COS to H_2S ratio dropped from 0.510 to about 0.105 due to the water vapor addition. Montana and Elkhorn ashes seem to promote the dissociation of H_2S to a greater extent than the Western Kentucky ash. While the reason for this effect is not conclusively known, the following observations may be made: It was noted while discussing the water gas reaction that Montana and Elkhorn ashes catalyzed the reverse water-gas shift reaction to a lesser extent than Western Kentucky ash. Also, it was noted above that increase of water vapor in the reaction gases (either due to reverse water-gas shift reaction or direct addition) inhibits the formation of COS.

During some runs, when the exit gas was sampled within about 2 minutes from the start of the desulfurization

runs a small concentration (about 0.01%) of a component was detected eluting through G.C. column at the same retention time as SO_2. No such peak was detected, however, after about 3 minutes. In chapter 3 it was mentioned that Bhada and Sage (1970) noticed a small SO_2 spike in the desulfurized gas soon after the run was started. They suggested that this was due to the decomposition of small quantities of iron sulfates formed during the regeneration reaction if carried out below 1000°F. In the current investigations, the regeneration temperature was always above 1000°F; at these temperatures the formation of iron sulfates is not thermodynamically favored. It must, however, be noted that coal ash is an impure material with many minerals present including calcium sulfate; and the explanation may be associated with the reactions of some of these. Since the concentration noted was quite small and disappeared rapidly no detailed investigation of this phenomenon was attempted.

Small amounts of a yellow substance (very likely elemental sulfur) were observed to build up in the cooler sections of the reactor tube after a few runs. Material balance checks between the desulfurization and the following regeneration runs suggest that, within experimental limitations, the sulfur from the sulfided ash is entirely converted to SO_2 during regeneration. For example, the sulfided ash from Run No. 061 was regenerated in Run No.

062, with the following material balance results:

Standard cc of H_2S absorbed in Run No. 061 = 273.5.

Std. cc of O_2 consumed in Run No. 062 = 484.

According to the regeneration reaction (3.26), 1 mole of O_2 produces 4/7 mole of SO_2. Reactions (3.7) and (3.26) indicate that 1 mole of H_2S abosrbed during desulfurization gives 1 mole of SO_2 during regeneration. Therefore,

Std cc of equivalent H_2S from Run No. 062 = $\frac{4}{7}$ X 484

= 278.

Schrodt (1977) and Joshi and Leuenberger (1977) however, reported significant formation of elemental sulfur during regeneration of their packed-beds. The reason for the much smaller amounts of sulfur formed during the current studies may be due to the solid mixing behavior of the fluidized-bed. In the packed-bed, most of the oxygen is initially consumed near the entrance section of the bed. The sulfided ash down stream meets with a very diluted stream of O_2 which may promote the sulfur forming reactions discussed in Chapter 3.

It must be stated in conclusion of this section that the composition of the desulfurized gas will depend upon the temperature of operation, inlet gas composition and the residence time available for the various reactions.

6.4 Discussion of Reaction Rate

A desulfurization rate model is presented in this section for the Western Kentucky ash. The model expresses

the reaction rate as a function of process variables. Only a limited number of runs were performed on Montana and Elkhorn ashes. Rate constants are reported for the conditions studied.

6.4.1 Effect of process variables on reaction rate:

The H_2S breakthrough data for the various runs are given in Appendix-C. The effect of the process variables on the desulfurization reaction are discussed in this section and a predictive rate equation is developed.

It was illustrated in Figure 6.3 that temperature markedly increased the reaction rate which suggests that a chemical phenomenon may be involved. Since the minimum fluidization velocity for any system decreases with particle size, it was anticipated that the ratio u/u_{mf} rather than the absolute value of the velocity would be more meaningful than u in comparing the process results for different particle sizes. It is known that gas-bypassing due to bubbles increases with superficial linear velocity resulting in lower reaction rates; the ratio u/u_{mf} may be used to describe the extent of bypassing. Usually external mass transfer resistance is not important in fluidized-beds (Smith (1970)); this is due to the high external surface area of the small particle sizes usually used and not necessarily because of high mass transfer coefficients. The particles used in the current study are small, the largest size being of diameter 0.01935 cm. The effect of

u/u_{mf} may be qualitatively examined from figure 6.13 where runs 023 and 024 are compared with 029; these runs were conducted at the same conditions with the exception of u/u_{mf}. It may be seen that the efficiency and hence the effective reaction rate increases significantly on reducing the u/u_{mf}.

Figure 6.14 is plotted to examine the effect of inlet H_2S concentration; runs 077 and 078 are compared. A notable decrease in reaction rate due to an increase of inlet H_2S concentration may be observed. Although an explanation for this phenomenon is not known at this point, the facts discussed below may have some relevance.

Joshi and Leuenberger (1977) noticed a drop in efficiency when they increased the inlet H_2S concentration from 0.6 to 1.2% during their packed-bed studies; but, they dismissed the change as not being significant. Schrodt's (1977b) packed-bed data also shows a slight drop of efficiency with an increase of H_2S concentration; however, no definite conclusion can be drawn since the change is not large and might have been due to experimental error. Hasatani and Wen (1977) conducted thermogravimetric analysis of the H_2S absorption reaction of iron oxide sorbents (see chapter 3 for details). They showed that the direct reaction of H_2S with Fe_2O_3 was very much slower in comparison with the corresponding reaction with the reduced oxides (Fe_3O_4, FeO, etc.). It must be noted that during

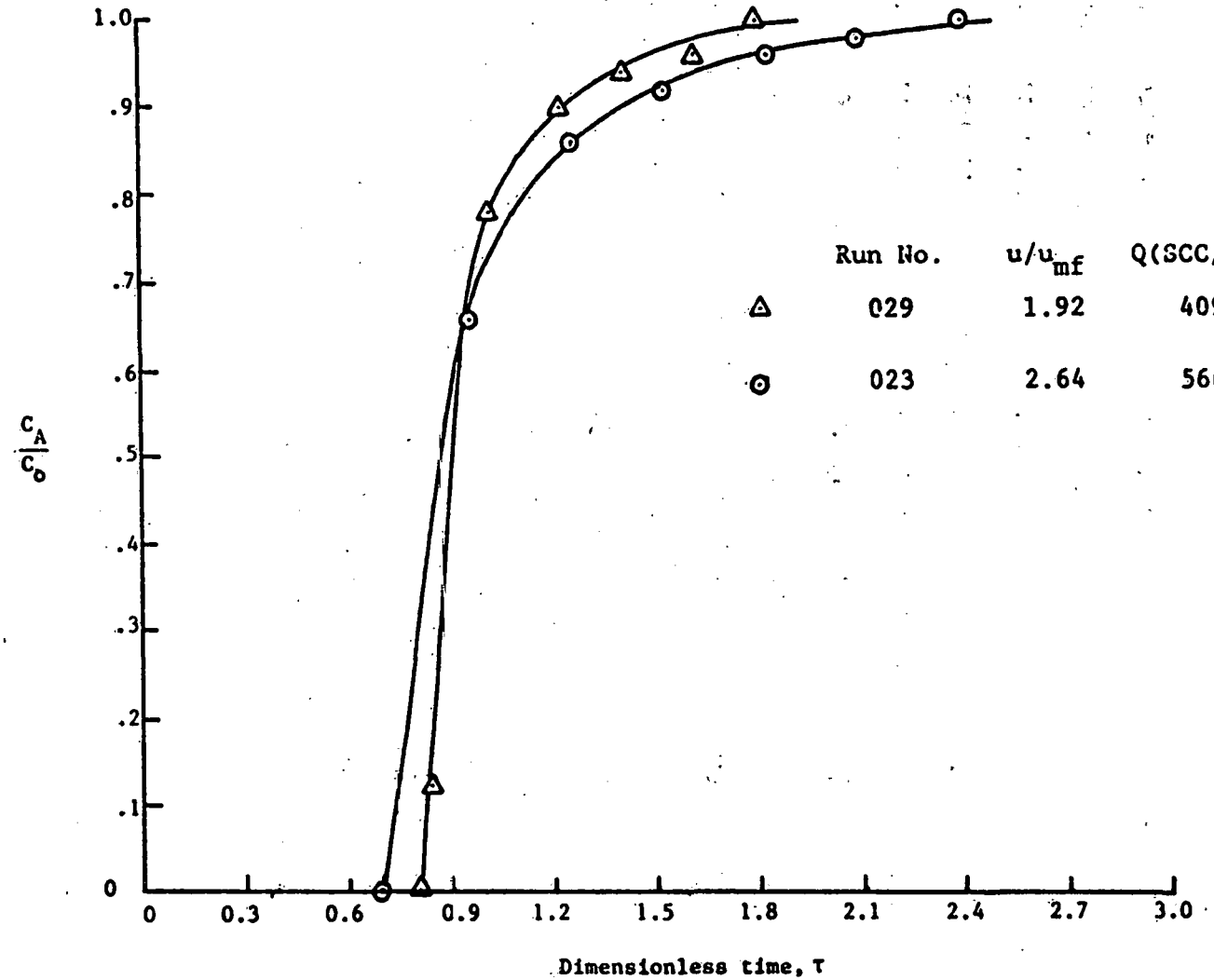

Figure 6.13 Effect of u/u_{mf}.

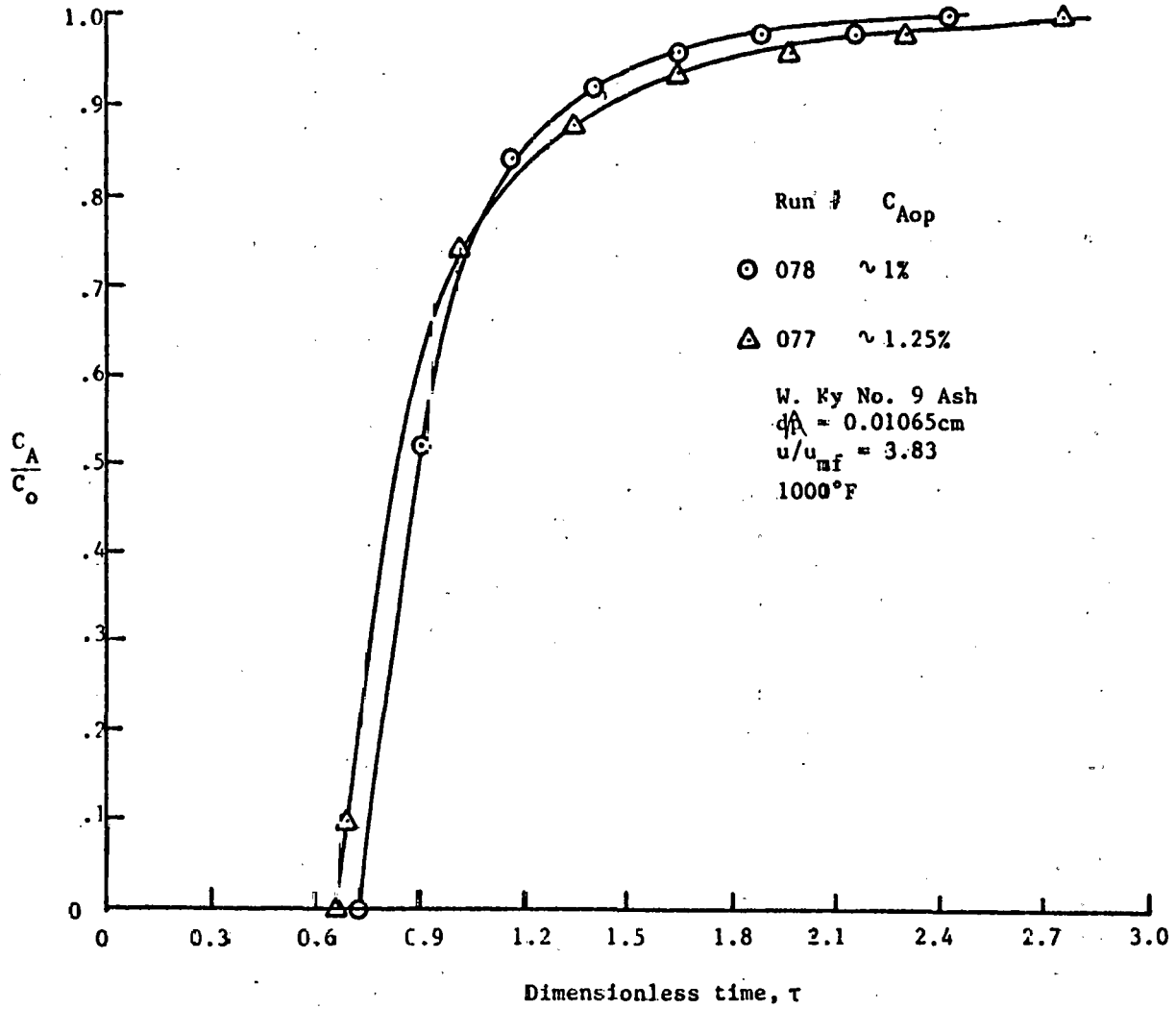

Figure 6.14 Effect of inlet H_2S concentration.

the desulfurization reaction iron oxide reduction by H_2 and CO are also taking place. Therefore, we may have the following competing reactions happening.

(1) Reaction of H_2S with Fe_2O_3

(2) Reaction of H_2S with reduced oxides (Fe_3O_4, FeO, Fe)

(3) Reaction of H_2 and CO with Fe_2O_3 and the reduced oxides.

Schrodt (1977b) suggested that the iron oxide reduction reactions were rapid and preceded the desulfurization reaction. According to this postulate, most of the sulfur absorption takes place due to reaction (2). However, Hasatani and Wen (1977) felt from their studies that desulfurization and iron oxide reduction reactions occurred simultaneously. In addition to this apparent disagreement, the following fundamental differences in the contacting pattern of gas-solid reactors should be kept in mind. In the packed bed reactor, while most of the H_2S is reacting in a zone near the bed entrance, reduction of the downstream section of the bed by CO and H_2 will be relatively unaffected. Thus, in a packed-bed, the H_2S may be viewed as reacting according to reaction (2). Due to the constant motion of the solids in a fluidized-bed, however, this prereduction of Fe_2O_3 does not happen and all three reactions listed above may be occurring simultaneously. It is conceivable that the overall desulfurization rate is decreased by increased inlet H_2S concentration due to the occurrence

of reaction (1). Additional research work is required to explain the finding of this work.

6.4.2. Development of rate model:

A computer program (listed in Appendix-E) was developed to solve the gas-phase and solid-phase mass balances derived in Chapter 5. Each model derived in Chapter 5 was programmed as a subroutine. First, the unreacted core model was tried starting with the special cases of reaction controlling and product-layer controlling. Figure 6.15 shows the breakthrough curves obtained from the case of chemical reaction controlling for different values of the model parameter. It may be seen that these curves are not similar to the experimentally obtained curves. The case of product layer controlling, illustrated in Figure 6.16 also fails to predict the experimental curves. Next, the general unreacted-core model was tested; the curves obtained were similar to the above two cases with only slight variation. Since the unreacted-core models were not successful, attention was focused on pseudo-homogeneous models.

Pseudo-homogeneous model:

Equations (5-28) and (5-32) developed in Chapter 5 were together numerically solved using Fourth Order Runge-Kutta procedure. The computer program for this is listed in Appendix E as Model-1. First, the equations were solved for the case of m = 1. It is recalled here that m is the exponent on solid concentration in the rate equation (5-1).

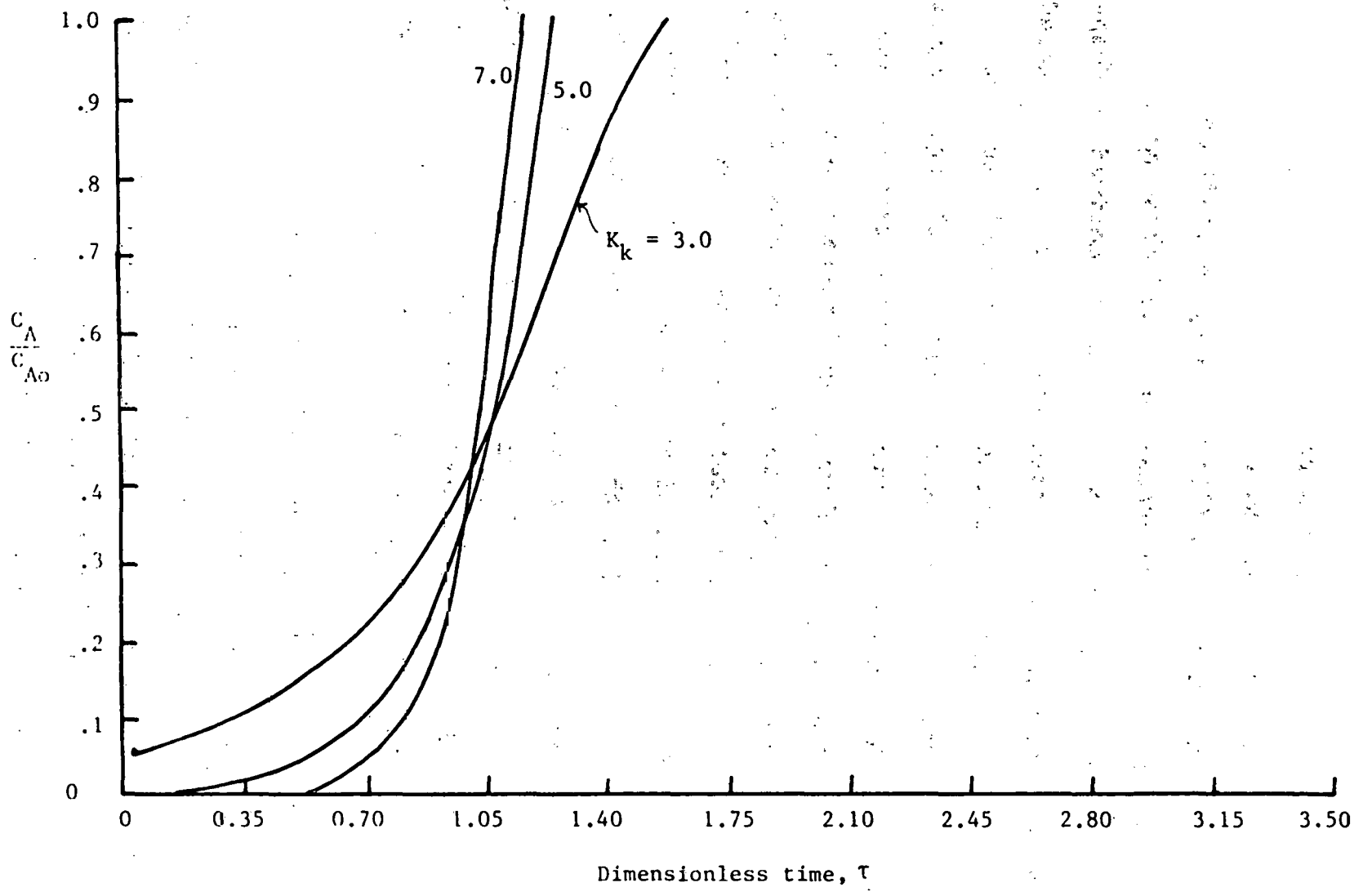

Figure 6.15 Unreacted-core model with reaction rate controlling.

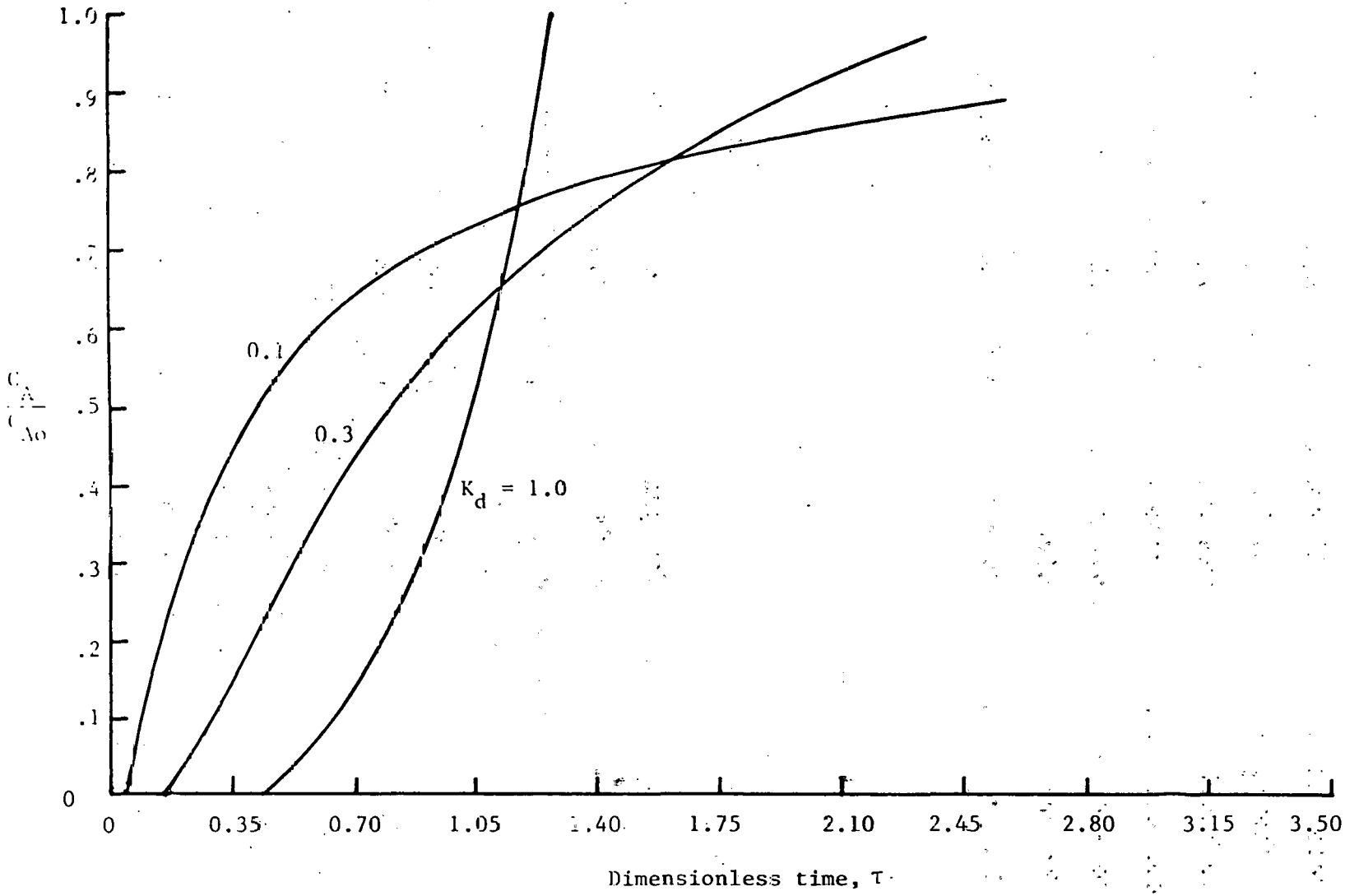

Figure 5.16 Unreacted-core model with product-layer diffusion controlling.

While considerable improvement resulted over the unreacted-core models, result was still not satisfactory. The value of m was then changed to 1.5, 1.75, 2, 2.5 and 3.0 and the predicted breakthrough curves were compared with experimental curves. The curves generated for m=2 were found to match the experimental curves surprisingly well for the Western Kentucky ash particles.

The model parameters are K_k and K_m (see Chapter 5) where

$$K_k = \frac{u}{Lk_v W_o^m \rho_B} \qquad (5\text{-}25)$$

and

$$K_m = \frac{uR\rho_p}{3Lk_m \rho_B} \qquad (5\text{-}26)$$

To estimate the mass transfer parameter K_m, knowledge of the mass transfer coefficient is necessary. The particle Reynolds number as defined by $Re = \frac{d_p u \rho_g}{\mu}$ for the experiments were of the order of 1. A survey of the literature revealed that mass transfer correlations for this range were very sparse. Dwivedi (1977) has presented an exhaustive review of mass transfer correlations for packed and fluidized beds; his review also indicated the difficulty of obtaining reliable values of mass transfer coefficients for Re<1. The following correlation from Kunii and Levenspiel (1969) was finally chosen:

$$\frac{k_m d_p}{D} = 0.374\ Re^{1.18}$$

where D is the molecular diffusion coefficient of gas. For Re = 1.0 the mass transfer coefficient k_m obtained was about 60.0 cm./min. The gas phase diffusivity was estimated from predictive equations (Skelland (1974)). With this value of k_m, the highest encountered K_m value would be about 0.02. The K_m values were varied (for different K_k values) from 0.001 to 0.1; however, the breakthrough curves were not changed. Therefore a standard K_m value of 0.01 was used for simulations.

The kinetic parameter was varied from 0.01 to 0.1 for a K_m value of 0.01 and a series of simulated breakthrough curves were generated. Each experimental breakthrough curve was matched with a simulated curve; the value of the kinetic parameter K_k was thus obtained for each experimental run. The matching for one run is shown in Figure 6.17 as an example. The rest of the graphs and a summary table of K_k values, are included in Appendix-F. The value of the kinetic rate constant k_v may now be calculated from equation (5-25) since the rest of the terms are known. The calculated k_v values for Western Kentucky ash are listed in Table 6.5a. Attention is called here to the fact that the kinetic results are for the stabilized ashes which had been subjected to six or more cycles.

For Montana and Elkhorn ashes a value of m=3 was found to fit the data better. The rate constants are presented in Table 6.5b. Considerable scatter in the data

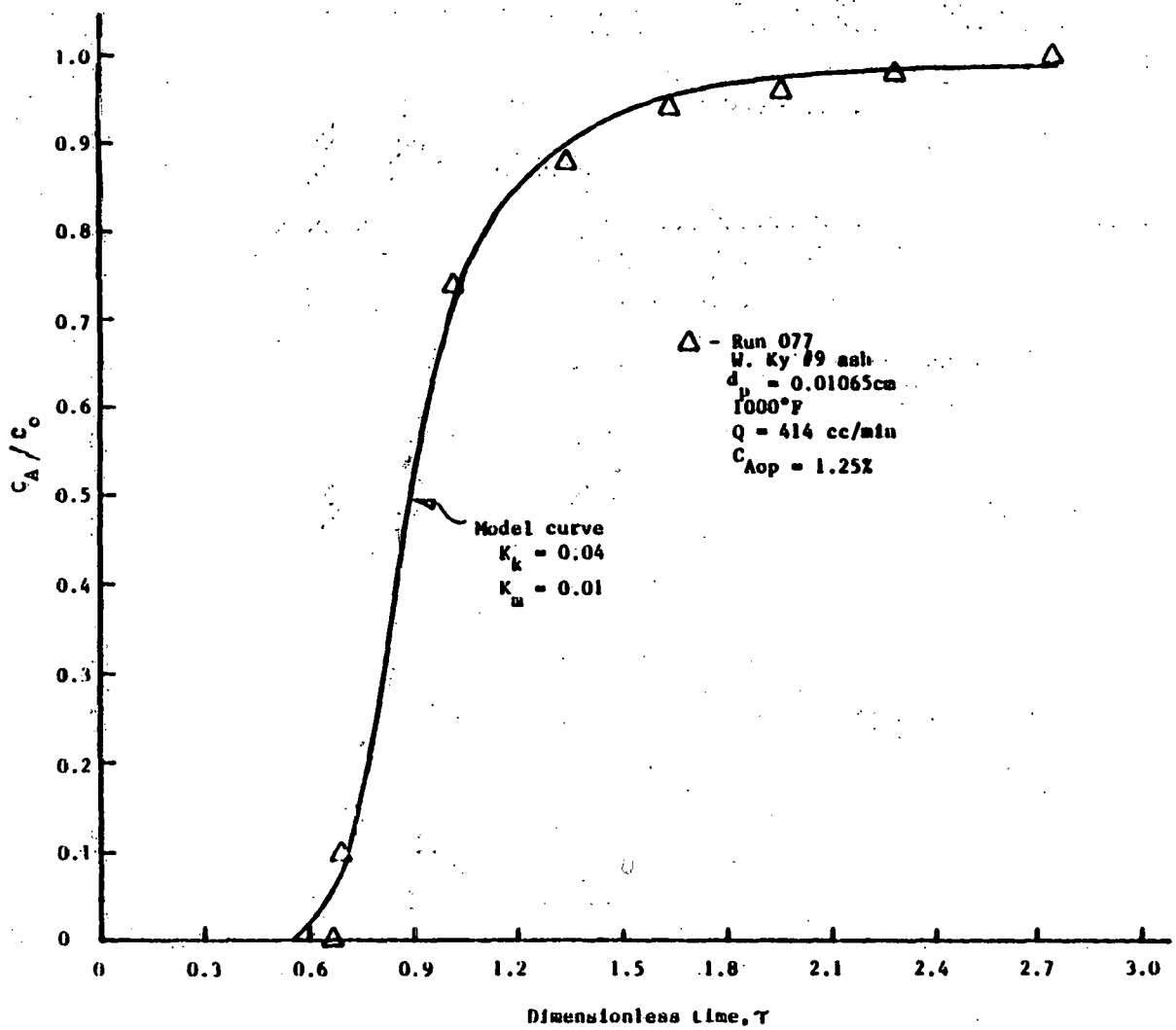

Figure 6.17 Estimation of K_k by curve matching.

Table 6.5a

SUMMARY OF KINETIC CONSTANTS
FOR WESTERN KENTUCKY #9 ASH

Run #	Mean particle size dp, cm	Temp. °F	Inlet H_2S conc. C_{Aop} Vol. %	Volumetric flow rate SCC/min	Superficial linear velocity, u cm/min	u/u_{mf}	weight of ash charged gms	H_2S capacity of ash SCC/gm	$k_v X10^{-9}$*
014	0.01935	1200	1.0091	565	607	3.00	12.49	29.70	24.85
017	"	"	0.9943	"	"	"	"	28.62	26.75
019	"	"	0.9915	"	"	"	"	29.95	24.42
023	"	1000	0.9931	"	534	2.64	"	26.29	11.15
024	"	"	1.0024	"	"	"	"	26.59	10.91
026	"	900	0.9993	"	498	2.47	"	23.66	7.24
029	"	1000	1.0019	409	387	1.92	"	28.21	18.87
048	0.151	1200	0.9845	407	436	3.00	9.78	25.57	33.12
049	"	"	0.9959	"	"	"	"	26.16	31.63
052	"	1000	0.9834	414	391	2.70	"	22.46	14.27
053	"	"	0.9937	"	"	"	"	22.18	14.64
054	"	"	1.0033	"	"	"	"	22.64	14.06
056	"	900	1.0209	"	364	2.51	"	22.23	8.64
057	"	"	1.0059	"	"	"	"	22.11	8.73
058	"	"	1.0092	"	"	"	"	22.23	8.64
061	"	1400	0.9889	405	487	3.36	"	27.96	44.60
122	"	1000	1.0093	469	443	3.06	9.81	28.25	9.39
123	"	"	1.4112	"	"	"	"	30.04	7.02
124	"	"	1.4210	"	"	"	"	30.58	6.77
126	"	"	1.0002	607	573	3.95	"	29.49	10.08
127	"	"	1.0001	617	582	4.01	"	29.89	9.97

Table 6.5a continued

075	0.01065	1000	1.2248	354	335	3.28	9.58	28.96	7.50
076	"	"	1.2514	"	"	"	"	29.11	7.42
077	"	"	1.2462	414	391	3.83	"	28.15	8.54
078	"	"	0.9996	"	"	"	"	29.41	9.30
080	"	900	1.2535	354	312	3.06	"	27.95	5.25

*units - (gm ash) $(cm^3)/(g\ mole\ Fe_2O_3)^2$ (min)

Table 6.5b

SUMMARY OF KINETIC CONSTANTS
FOR ELKHORN AND MONTANA ASHES

Run #	Mean particle size dp (cm)	Temp. °F	Inlet H_2S conc. C_{Aop} Vol. %	Volumetric flow rate SCC/min	Superficial linear velocity, u cm/min	u/u_{mf}	weight of ash charged gms	H_2S capacity of ash SCC/gm	$k_v X10^{-14}$*
Elkhorn Ash:									
095	0.01935	1000	0.9904	432	408	2.12	9.77	9.00	4.62
096	"	"	0.9888	"	"	"	"	9.75	3.66
Montana Ash:									
111	0.01935	1000	1.0145	432	408	2.12	9.57	7.47	9.66
112	"	"	1.0066	"	"	"	"	7.96	7.96
113	"	"	1.0003	"	"	"	"	7.49	9.58
114+	"	"	0.9794	"	417	2.16	"	7.05	11.69

*units - (gm ash) $(cm^3)/(g\ mole\ Fe_2O_3)^3$ (min)

+About 3.2% water vapor included in inlet gas for this run.

for these two ashes may be observed. This is due to the quicker and sharper breakthroughs obtained with these beds.

The kinetic constants for Western Kentucky ash were statistically analyzed to check for the effect of the operating variables. The temperature effect was expressed by the Arrhenius relation. The following correlation was found to give the best fit to the data:

$$k_v = k_o(C_{Aop})^{\bar{a}} \left(\frac{u}{u_{mf}}\right)^{\bar{b}} e^{-\frac{E}{RT}} \qquad (6\text{-}2)$$

Here, C_{Aop} is the inlet concentration of H_2S expressed in volume %, k_o the pre-exponential, E the Arrhenius activation energy, R the gas constant, T the absolute temperature and $\bar{a}$ & $\bar{b}$ the correlation constants.

The result of the statistical analysis is shown in Table 6.6. The overall analysis-of-variance table breaks down the total sum of squares for the dependent variable into the portion attributed to the model, and the portion that the model does not account for, which is attributed to error. The mean square term is the sum of squares divided by the degrees of freedom (DF). The mean square for error (MS(ERROR)) is an estimate of σ^2, the variance of the true residuals. The model F value tests how well the model as a whole (after adjusting for the mean) accounts for the dependent variable's behavior; it is obtained by dividing MS(MODEL) by MS(ERROR). If the significance

TABLE 6.6

STATISTICAL ANALYSIS OF RATE DATA
FOR WESTERN KENTUCKY ASH

S T A T I S T I C A L A N A L Y S I S S Y S T E M

GENERAL LINEAR MODELS PROCEDURE

DEPENDENT VARIABLE: EY

SOURCE	DF	SUM OF SQUARES	MEAN SQUARE	F VALUE	PR > F	R-SQUARE	C.V.
MODEL	3	7.97050735	2.65683578	183.16	0.0001	0.961504	0.5183
ERROR	22	0.31911813	0.01450537		STD DEV		EY MEAN
CORRECTED TOTAL	25	8.28962548			0.12043824		23.23838421

SOURCE	DF	TYPE I SS	F VALUE	PR > F	DF	TYPE IV SS	F VALUE	PR > F
XT	1	6.44858340	444.01	0.0001	1	5.27435561	363.61	0.0001
Z	1	0.84586387	58.31	0.0001	1	0.36081911	24.87	0.0001
W	1	0.62606008	43.16	0.0001	1	0.62606008	43.16	0.0001

PARAMETER	ESTIMATE	T FOR H0: PARAMETER=0	PR > |T|	STD ERROR OF ESTIMATE
INTERCEPT	30.84487069	70.98	0.0001	0.43458657
XT	-5496.01367112	-19.07	0.0001	288.22224753
Z	-0.78745841	-4.99	0.0001	0.15798757
W	-1.48108951	-6.57	0.0001	0.22544349

probability, labeled PR>F, is small, it indicates significance; in our case, the obtained value of 0.0001 indicates very high significance. The R-SQUARE value measures how much variation in the dependent variable can be accounted for by the model R-SQUARE, which can range from 0 to 1, is the ratio of the sum of squares for the model divided by the sum of squares for the corrected total. In general the larger the value of R-SQUARE, the better the model's fit. The value of 0.961504 in the present case indicates that the chosen model accounts for over 96% variation in the dependent variable.

Parameter estimates: The intercerpt and coefficients are also given in Table 6.6. The intercept ($\ln k_o$) estimate is 30.84487, XT (-E/R) is -5496.01, Z (coefficient $\bar{b}$) is -0.787958, and W (coefficient $\bar{a}$) is -1.48109. The table also gives the results of the t-test for each parameter. PR>|T| gives the probability of getting a larger value of t if the parameter is really equal to zero (null hypothesis). Thus, a very small value for this probability indicates that the value of the parameter is not likely to equal zero, and therefore that the independent variable contributes significantly to the model. Table 6.6 shows that PR>|T| for each parameter is 0.0001 (a very small value) which indicates that the independent variables chosen do contribute significantly to the model. Figure 6.18 is the plot of residual vs. predicted k_v values.

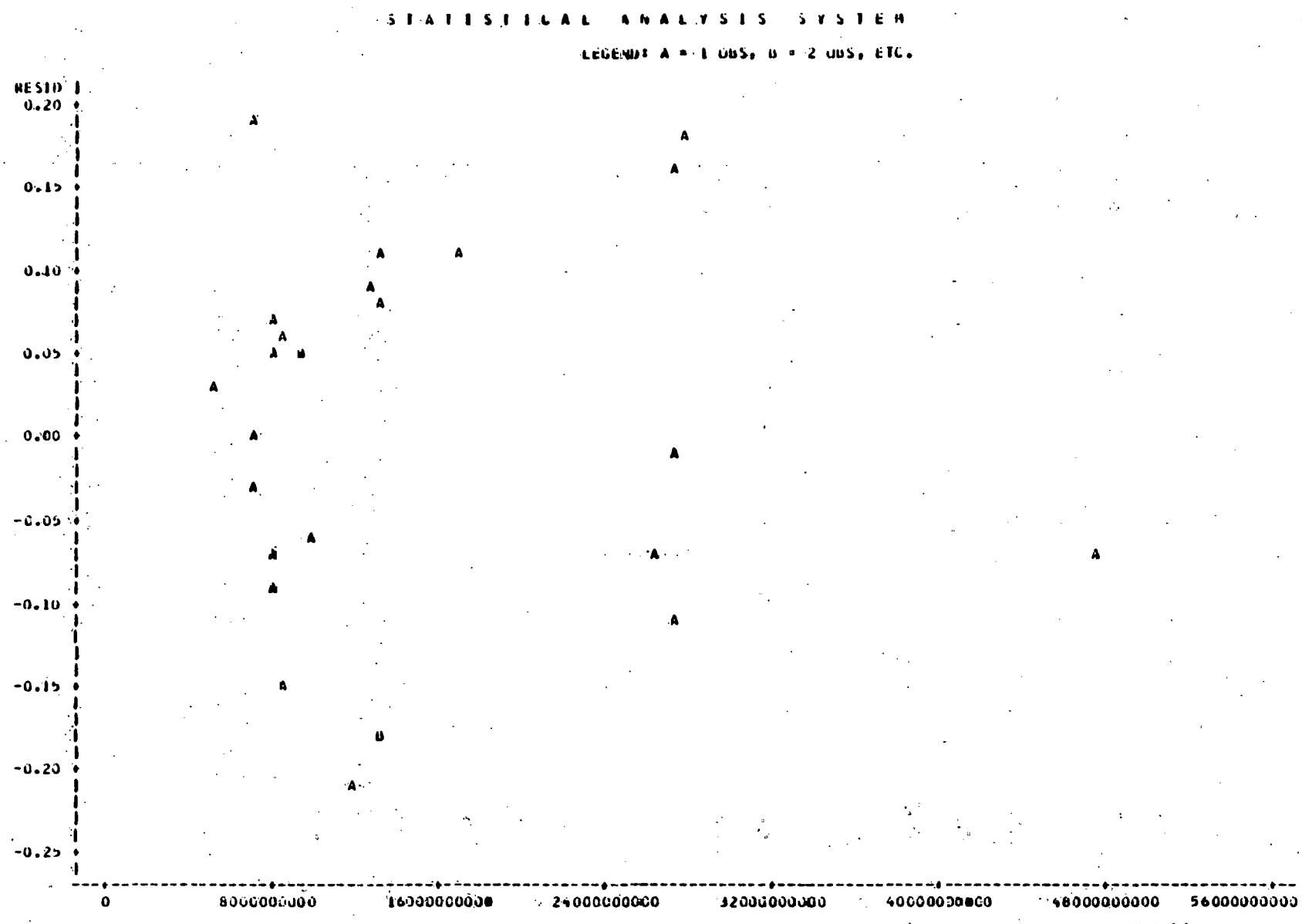

Figure 6.18 Plot of predicted rate constants vs. residuals

It may be noted that the scatter is quite random with no apparent trend. Reasonable agreement of observed vs. predicted values of k_v is evident in Figure 6.19. It is, therefore, concluded that the model given by equation (6-2) is a good mathematical representation of the desulfurization reaction phenomenon taking place in a fluidized bed within the range of variables used. The values of the parameters to be used in equation (6-2) are summarized below along with the units.

Parameter	Units	Value
k_o (pre exponential)	$\frac{(\text{gm ash})(\text{cm}^3)}{(\text{gm mole } Fe_2O_3)^2(\text{min})}$	2.4875×10^{13}
E (Arrhenius constant)	cal/g mole	10882
$\overline{a}$	(dimensionless)	-1.48108951
$\overline{b}$	(dimensionless)	-0.78795841

The proper rate equation is,

$$-R_A = k_v C_A W^2 \qquad (6\text{-}3)$$

where, $-R_A$ = H_2S reacted g mole/(min)(gm ash)

6.4.3 Comparison of rate data with the results of other investigators:

The kinetics of the desulfurization reaction reported in the literature was reviewed in Chapter 3. The activation energies reported by different investigators are summarized in Table 6.7.

The reported values of the activation energy range from 1800 to 11800. This is rather typical of heterogeneous

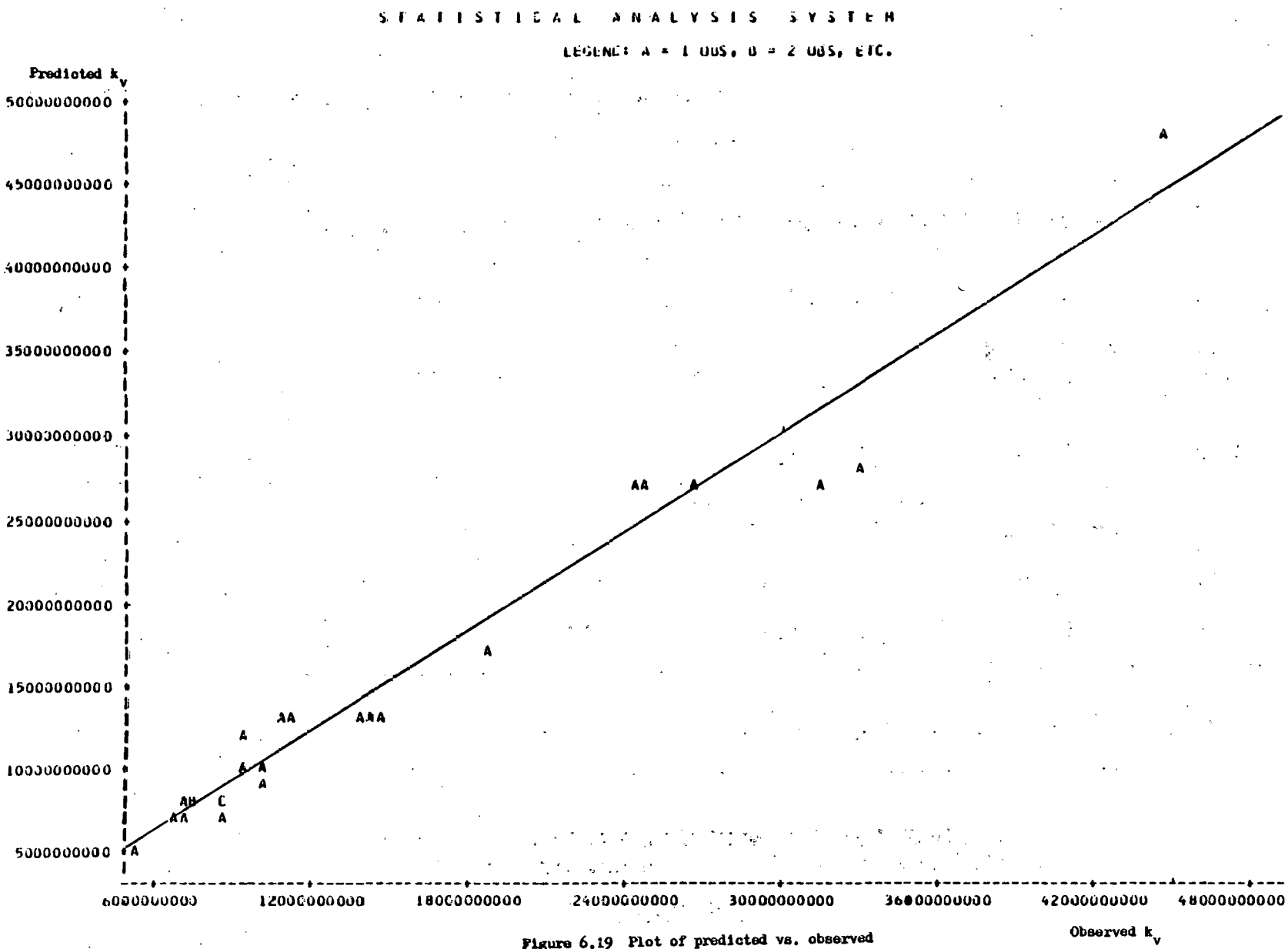

Figure 6.19 Plot of predicted vs. observed values of rate constant.

Table 6.7

COMPARISON OF REPORTED ACTIVATION ENERGIES
FOR THE IRON-OXIDE-HYDROGEN SULFIDE REACTION

Reference	System	Approximate particle size (cm)	Temperature range (°K)	E (cal/g mole)
This work	Fluidized-bed	0.01-0.02	755- 922	10882
Schrodt (1978)	Fixed-bed	0.124	755-1033	2740
Air Products Leuenberger (1976)	Fixed-bed	.159-0.635 diam. cylindrical pellets	755-1088	7771
Hasatani and Wen[a] (1977)	TGA	.007-0.02	900-1135	2650
Gavrilova (1973)	*	.05-0.1	628- 783 873-1073	11800 1800
Brandon[b]	TGA	crushed powder	573- 873	9972

a - E values reported are for sulfurization of iron oxide pre-reduced by H_2 and CO.

b - no reducing gases (CO, H_2) were used.

* - multi-particle system, possibly with TGA.

gas-solid reacting systems (Wen (1968), Szekely et al. (1976)) and is generally due to the difficulty in uncoupling the associated complex transport processes from the chemical phenomena. Even for the seemingly uncomplicated case of the single particle system, as explained by Levenspiel (1972), the difference in the time vs. solid conversion curves for the cases of shell diffusion and chemical reaction as the controlling steps is not great which complicates the interpretation of rate data. The value of the apparent activation energy is generally used as an indication of the probable regime of control. Many gas-solid reaction systems exhibit an intrinsic activation energy greater than 8000 cal/g mole. Intraparticle and gas-film diffusional resistances on the other hand show a much smaller temperature dependence with typical values of apparent activation energies of about 1500 and 500 respectively.

Referring to Table 6.7 and based on the above arguments, the E value of 10882 cal/g mole obtained for this work suggests a probable chemical regime. It should be noted that Hasatani and Wen (1977) reported their E value for a pre-reduced system; also they conducted their experiments at a higher temperature range of 900-1135°K, compared to 755-922°K for this work. It is interesting to note that Gavrilova (1973) obtained a value of 1800 cal/g mole in this temperature range and a value of 11800 for 628-783°K. He suggested a shift from chemical to intra-

particle diffusional control as the temperature was increased above 873°K. The values obtained by Leuenberger (1976) and Brandon (1973) also suggest a chemical phenomenon. It should be noted, however, that Brandon conducted his experiments in the absence of reducing gases H_2 and CO. Hasatani and Wen (1976) showed that at 1113°K the direct reaction of H_2S with Fe_2O_3 was much slower when compared to the system where the reducing gases were present. Therefore, Brandon's values may not be used for direct comparison. The E value of 2740 cal/gmole reported by Schrodt suggests a mixed (kinetic + diffusional) regime.

Generally, for small particles as used in the present study (0.01-0.02 cm) intraparticle resistance should be small at least for lower solid conversions. This reasoning and the E value of 10882 cal/g mole suggest that a chemical process may be involved in the current study.

The direct comparison of the values of the pre-exponential k_o is not possible since the rate equations are different. Figure 6.20 compares the actual reaction rates vs. solid conversion predicted by Schrodt (1978) and equation (6-3) for a constant H_2S concentration of 0.2 X 10^{-6} g mole/cm^3. The comparison is presented here only for the sake of completeness. The fluidized-bed generally gives only the apparent kinetics. Nevertheless, it is interesting to note that the absolute reaction velocities

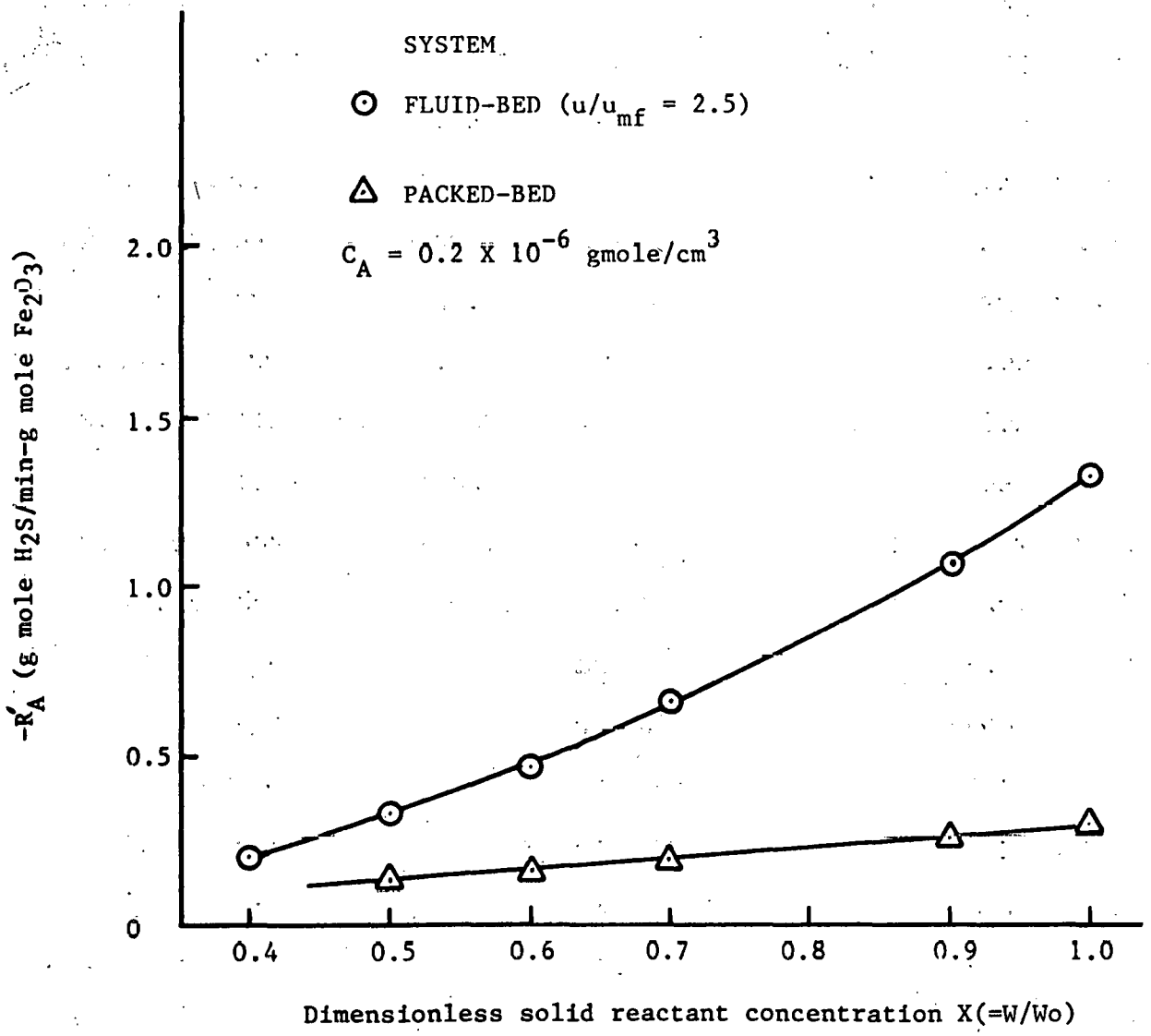

Figure 6.20 Comparison of absolute reaction rates predicted for packed-bed and fluidized-bed studies.

predicted by the two independent investigations are of the same order of magnitude for lower X values. A fundamental difference between a packed bed and a fluid bed must be noted at this point. Unlike the former, the breakthrough curve obtained in the fluid bed is representative of the solid that is partially converted. This is due to the continuous mixing action of the solids in a fluidized system. The solids mixing behavior results in uniform solid-reactant concentration in the reactor. In contrast, a traveling reaction zone develops in a packed bed and the breakthrough curve represents the reaction across this zone. The point of breakthrough in the fluidized system is determined by the average reaction rate during the period before breakthrough. Due to these facts, the fluid-bed reaction model represented by equation (6-3) gives only the average reaction rate prior to breakthrough and as such it is not proper to compare the instantaneous reaction rates prevailing in this period with those obtained for the packed bed. However, it appears that these average rates may be somewhat higher for the fluidized bed probably due to the smaller particle sizes used.

6.5 Continuous desulfurization-regeneration system:

A computer program (listed in Appendix G) was developed for a continuous-system pictured by Figure 6.21. When the inlet gas conditions and reactor operating temperatures are specified, the program calculates the material and energy

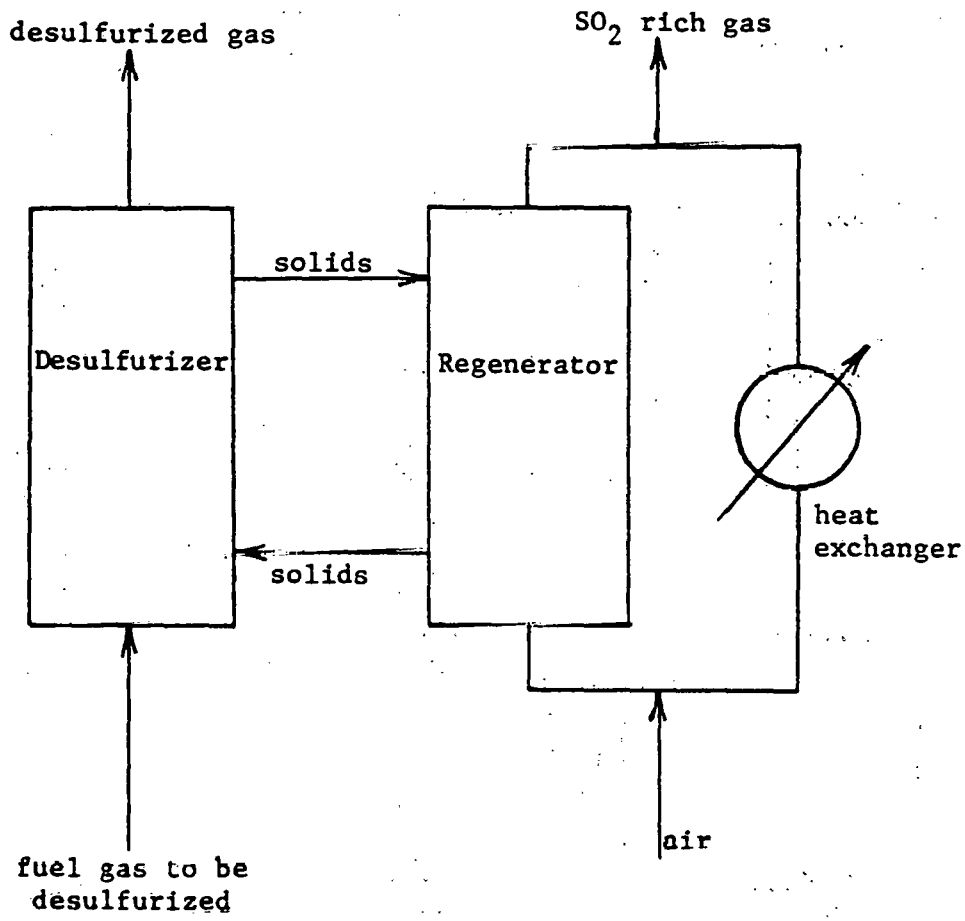

Figure 6.21 Continuous desulfurization-regeneration fluid-bed system.

balances for the system. The comment section of the program is self-explanatory. The global rate equation developed in this chapter is used for the desulfurizer. Since the regeneration rate is very fast (as suggested by the sharp breakthrough curves) an external mass transfer coefficient is programmed-in for the regenerator.

An example on the use of the program is also included in Appendix-G. The following input variables are required: Adsorber-flow rate of inlet gas, operating pressure, inlet fuel gas temperature, inlet gas composition and estimated atmospheric heat loss; regenerator-temperature of inlet air, operating temperature and pressure, gas temperature at the heat-exchanger exit and estimated heat loss to atmosphere. The user also supplies the required H_2S outlet concentration in the fuel gas, solid conversions in adsorber and regenerator. The user can then ask the program to print out the material and energy balances by supplying different values of solids circulation rate. The program is capable of calculating heat capacities and heat of reaction as a function of temperature. By a trial and error procedure, the program calculates the adsorber bed temperature. The fuel gas is assumed to reach thermal equilibrium with the solids before it leaves the adsorber. Gas flow rates and compositions are calculated; gas circulation rate and heat-exchanger heat load are also calculated. Reactor volumes for both the adsorber and the regenerator are

printed out along with the complete energy balance. The example print-out given in Appendix-G illustrates the working of the program adequately.

CHAPTER 7

CONCLUSIONS AND SIGNIFICANCE

The results obtained in this study have demonstrated the feasibility of using coal ash in a fluidized bed mode as the sorbent for low-BTU fuel gas desulfurization. The fluidized system offers the very attractive possibility of continuous, steady-state operation of a coupled desulfurization-regeneration process. H_2S removal efficiencies of over 99% are achievable. Ash attrition and replacement rates in a commercial plant should be minimal.

The H_2S capacity of coal ash was found to increase with the process temperature and the inherent iron oxide content of the ash. H_2S capacities of up to 30 SCC/gm of ash were obtained with the Western Kentucky #9 ash.

The regeneration reaction with air is very rapid, and it appears that mass transport may be the rate controlling phenomenon. Future work in the area of regeneration is required to determine the optimum conditions for the recovery of sulfur from the spent sorbent in the elemental form. The fluidized-bed should prove especially suitable for temperature control of the highly exothermic regeneration reaction.

Iron oxide reduction, water-gas shift reaction and other reactions also occur during desulfurization. Future research work on the reactions of iron oxide and organic sulfur compounds is highly desirable.

For the particles studied ($d_p \leq 0.2$ mm) chemical reaction probably controls the rate. The rate was found to increase significantly with temperature. Gas bypassing in the form of bubbles was found to increase with flow rate, resulting in lower reaction rates. The activation energy for the desulfurization reaction was found to be 10882 cal/mole. Particle size was not found to significantly affect the rate for the range of particles studied.

NOMENCLATURE

$\bar{a}$	index in equation (6-2)
A,B	reactants
b,e,s	stoichiometric constants for B, E and S
$\bar{b}$	index in equation (6-2)
Bi	Biot number for mass transfer, $= \frac{k_m R}{D_e}$
C_o	outlet concentration (H_2S + COS) at time t_E, gmole/cm^3
C_{Ao}	inlet concentration of H_2S, gmole/cm^3
C_{Ab}	bulk concentration of reactant A, gmole/cm^3
C_{Ac}	reactant$_3$concentration at reaction interface, gmole/cm^3
C_{As}	reactant$_3$concentration at particle surface, gmole/cm^3
C_{Aop}	reactant concentration at inlet, vol. %
d_p	mean particle diameter, cm
D	molecular diffusion coefficient of gas, cm^2/min
Da	Damkohler number, $= \frac{k_s R}{D_e}$
D_e	effective diffusion coefficient in a porous structure, cm^2/sec
E'	product in reaction (5-2)
E	activation energy, cal/gmole

g_N number of particles/gm of ash

ΔG free energy change, kcal

$-\Delta H$ heat of reaction, kcal

I $= 1 + Da(1-P)P + \frac{Da}{Bi} p^2$

J_a nonequilibrium ratio of concentrations defined similar to equilibrium constant, dimensionless

k_o preexponential in equation (6-1), $\frac{(gm\ ash)(cm^3)}{(g\ mole\ Fe_2O_3)^n (min)}$

where, n = 2 for W. Ky. ash

n = 3 for Montana & Elkhorn ash

k_m mass transfer coefficient, cm/min

k_s rate constant based on surface

k_v rate constant based on volume, units same as defined for k_o

K_D kinetic parameter for unreacted-core model product-layer diffusion controlling, $= K_u Da$

K_k kinetic parameter for pseudo-homogeneous model, $= \frac{u}{Lk_v W_o^m (1-\varepsilon)\rho_p}$

K_m mass transfer parameter, $= \frac{uR}{3Lk_m(1-\varepsilon)}$

K_u kinetic parameter for the general case of the unreacted-core model, $= \frac{Ru}{3Lk_s(1-\varepsilon)}$

L bed length, cm

m reaction order with respect to solid

M_o sorbent H_2S capacity, g mole H_2S/gm ash

n reaction order with respect to sorbate gas

N_A, N_B	moles of reactants A and B
P	$= r_c/R$
q	mass of ash charged, gms
Q	total volumetric flow rate of gas, cm^3/min
r	particle radius (variable), cm
r_c	radius of unreacted-core, cm
$-r_A$	rate per particle, g mole/min
R	outer radius of particle, cm
$-R_A$	rate per gram of ash, g mole/(gm ash)(min)
S	cross-sectional area of raector, cm^2
t	time on stream, min
t_E	bed saturation time, min
u	superficial linear velocity of gas, cm/min
u_{mf}	minimum fluidizing velocity in nitrogen, cm/min
W	solid reactant (Fe_2O_3) concentration, g mole/gm ash
W_o	initial Fe_2O_3 concentration of particle, g mole/gm ash
X	dimensionless solid concentration, $\frac{W}{W_o}$
X_c	solid conversion = 1 - X
Y	dimensionless sorbate concentration in gas, $= \frac{C_A}{C_{Ao}}$, $\frac{C_A}{C_o}$
z	position along length of reactor, cm
Z	dimensionless reactor position, $= \frac{z}{L}$

Greek symbols:

Δ	difference or change
ε	bed porosity, vol/vol
ρ_s	bulk density of solid, gm/cm^3
ρ_g	gas density, gm/cm^3
ρ_p	particle density, gm/cm^3
σ^2	variance
τ	dimensionless time, $\frac{QC_{Ao}t}{M_o q} = \frac{utC_{Ao}}{(1-\varepsilon)LM_o\rho_p}$
$\tau_{0.1}$	sorption efficiency

APPENDIX A

MINERAL ANALYSES OF GASIFIER ASHES

WESTERN KENTUCKY NO. 9 GASIFIER ASH

Source: MERC Fixed-bed gasifier

Mineral Analysis, Wt. %

P_2O	0.13	MgO	1.16
SiO_2	45.37	SO_3	1.51
Fe_2O_3	22.14	K_2O	2.03
Al_2O_3	19.18	CaO	6.96
TiO_2	0.18	Na_2O	0.79

KENTUCKY ELKHORN NO. 3 GASIFIER ASH

Source: MERC Fixed-bed gasifier

Mineral Analysis, Wt. %

P_2O_5	0.08	CaO	7.17
SiO_2	45.22	MgO	4.92
Fe_2O_3	9.51	SO_3	0.55
Al_2O_3	28.61	K_2O	1.37
TiO_2	1.16	Na_2O	0.77

MONTANA ROSEBUD GASIFIER ASH

Source: Riley Stoker Co. Gasifier

Mineral Analysis, Wt. %

P_2O_5	0.24	CaO	6.97
SiO_2	49.67	MgO	2.64
Fe_2O_3	8.19	SO_3	0.51
Al_2O_3	27.21	K_2O	1.52
TiO_2	1.44	Na_2O	0.77

APPENDIX B

DATA TABLES SHOWING GAS COMPOSITIONS FOR SELECTED RUNS

Run # 033

Western Kentucky Ash

Temp: 1400°F

d_p: 0.01935 cm

vol. %

Time (min)	H_2	O_2	N_2	CH_4	CO	CO_2	H_2S	COS	H_2O
IN	9.96	.0039	49.25	3.013	20.04	16.74	1.0037	-	-
2.95	1.533	.0077	50.01	3.110	12.44	24.63	.0127	0	8.255
19.66	7.60	.0041	48.85	2.958	22.19	14.15	0	0	4.260
36.41	6.92	.0042	49.45	2.946	22.26	14.54	.0605	0	3.819
53.60	8.34	.0073	48.83	2.919	21.95	14.29	.1267	.0220	3.525
70.29	7.36	.0044	49.55	2.993	22.07	14.61	.3731	.0716	2.967
87.04	7.14	.0069	49.67	2.963	22.14	14.72	.6946	.1376	2.534
103.84	7.14	.0029	49.59	2.977	22.10	14.67	.7926	.1528	2.579
120.48	7.46	.0052	49.55	2.955	21.97	14.74	.8155	.1591	2.357
137.12	7.22	.0043	49.62	2.966	22.04	14.63	.8296	.1608	2.531
153.87	7.43	.0055	49.57	2.961	22.09	14.54	.8338	.1811	2.391

Run #053

Western Kentucky Ash

Temp: 1000°F

d_p = 0.0151 cms

vol. %

Time (min)	H_2	O_2	N_2	CH_4	CO	CO_2	H_2S	COS	H_2O
IN	10.01	.0036	48.85	3.056	20.05	17.08	.9941	-	-
2.10	5.96	.0128	50.34	3.063	16.90	20.09	0	0	3.627
18.78	9.25	.0043	49.92	3.035	20.13	17.04	0	0	1.618
37.19	9.53	.0053	48.88	3.041	20.27	16.88	.0297	.0159	1.361
53.30	9.66	.0046	48.86	3.063	20.29	16.60	.5353	.1994	.7823
69.53	9.38	.0029	49.03	3.042	20.39	16.57	.6296	.2540	.6884
86.56	9.43	.0027	48.97	3.059	20.39	16.53	.6704	.2819	.6683
103.06	9.40	.0035	48.99	3.028	20.38	16.59	.6842	.2949	.6238
119.07	9.39	.0034	49.08	3.019	20.38	16.52	.6903	.3005	.6157
135.73	9.35	.0038	49.06	3.004	20.41	16.55	.7013	.3038	.6181
IN	10.02	.0042	48.87	2.974	20.07	17.06	.9963	-	-
165.58	9.66	.0035	48.76	2.981	20.30	16.73	.6999	.3069	.5628

Run #058

Western Kentucky Ash

Temp: 900°F

d_p = 0.0151 cms

vol. %

Time	H_2	O_2	N_2	CH_4	CO	CO_2	H_2S	COS	H_2O
IN	10.08	.0025	48.85	2.988	20.02	17.07	1.0068	-	-
2.53	7.58	.0109	50.69	3.026	18.21	19.67	0	0	.8211
18.74	9.61	.0035	49.01	2.949	19.94	17.21	0	0	1.284
36.39	9.75	.0028	48.95	2.952	20.07	17.07	.0999	.0401	1.059
52.87	9.77	.0032	48.93	2.961	20.15	16.90	.5569	.2107	.5302
69.58	10.09	.0014	48.78	2.966	20.08	16.76	.6400	.2580	.4276
86.29	9.76	.0027	48.98	2.949	20.16	16.78	.6744	.2849	.4054
103.18	9.94	.0044	48.92	2.932	20.04	16.80	.6862	.3017	.3748
120.27	9.55	.0044	49.09	2.961	20.13	16.87	.6977	.3100	.3750
136.99	9.76	.0031	48.98	2.949	20.12	16.80	.7042	.3158	.3619
154.10	9.47	.0030	49.16	2.941	20.17	16.86	.7103	.3206	.3576
IN	9.81	.0036	48.99	2.942	20.04	17.21	1.0115	-	-

Run #059

Western Kentucky Ash

Temp: 1200°F

d_p = 0.0151 cm

vol. %

Time (min)	H_2	O_2	N_2	CH_4	CO	CO_2	H_2S	COS	H_2O	SO_2
IN	9.92	.0048	49.14	3.063	20.08	16.81	.9943	-	-	
2.85	4.66	.0187	50.58	3.121	16.05	20.93	0	0	4.631	.0126
19.63	7.66	.0036	49.25	3.060	21.08	16.10	0	0	2.857	
36.14	8.35	.0025	49.00	3.051	21.25	15.71	0	0	2.626	
53.70	8.55	.0036	48.97	3.031	21.39	15.71	.0183	0	2.330	
70.16	7.69	.0035	49.30	3.037	21.73	15.33	.7189	.1669	2.037	
86.87	7.89	.0031	49.16	3.021	21.78	15.27	.7767	.1831	1.911	
103.28	8.18	.0027	49.06	3.030	21.67	15.22	.8114	.1982	1.819	
120.36	7.72	.0028	49.35	3.016	21.77	15.26	.8137	.1974	1.872	
IN	10.09	.0040	48.98	2.989	20.01	16.95	.9807	-	-	

Run #095

Elkhorn Ash

Temp: 1000°F

d_p = 0.01935 cm

vol. %

Time (min)	H_2	C_2	N_2	CH_4	CO	CO_2	H_2S	COS	H_2O
IN	9.82	.0162	48.91	3.065	20.12	17.09	.9950	-	-
13.15	9.48	.0127	48.86	3.047	20.08	17.01	.1513	.0513	1.310
29.92	9.47	.0117	48.98	3.038	20.35	16.59	.6463	.2806	.6408
46.34	9.20	.0135	49.18	3.054	20.43	16.59	.6807	.3138	.5949
64.99	9.43	.0109	49.01	3.039	20.38	16.55	.6876	.3226	.5739
81.70	9.13	.0114	49.18	3.045	20.43	16.56	.6990	.3307	.5657
98.51	9.45	.0102	49.04	3.014	20.40	16.50	.6975	.3350	.5549
IN	9.75	.0138	49.05	3.020	20.18	17.02	.9857	-	-

Run #113

Montana Ash

Temp.: 1000°F

d_p = 0.01935cm vol. %

Time (min)	H_2	O_2	N_2	CH_4	CO	CO_2	H_2S	COS	H_2O
IN	9.94	.0126	48.98	3.087	19.96	17.02	1.0003	-	-
9.96	9.37	.0200	49.37	3.022	19.88	17.04	.0196	.0098	1.2780
26.65	9.63	.0143	49.04	3.034	20.20	16.55	.6742	.3183	.5434
43.48	9.64	.0138	49.00	3.024	20.25	16.55	.6958	.3446	.4957
60.48	9.46	.0159	49.15	3.012	20.30	16.54	.6955	.3510	.4830
77.26	9.56	.0145	49.07	3.025	20.29	16.52	.7019	.3562	.4674
94.15	9.32	.0143	49.23	3.021	20.32	16.57	.7038	.3596	.4646
110.95	9.52	.0128	49.16	3.0111	20.30	16.49	.6954	.3625	.4564
IN	9.89	.0119	49.12	2.987	20.04	16.97	.9934	-	-

APPENDIX C

REDUCED DATA

RUN NUMBER: 003 WESTERN KENTUCKY ASH

PARTICLE DIAM., (CMS)	:	0.01935	MASS OF ASH CHARGED, (GMS)	:	12.488
APPARENT PARTICLE DENSITY, (GMS/CC)	:	2.8350	DIAMETER OF COLUMN, (CMS)	:	2.0000
BED TEMPERATURE, (DEG. F)	:	1200.00	BED LENGTH, (CMS)	:	3.556
INLET H2S CONCENTRATION, (VOL. FRACTION)	:	0.0105390	BED POROSITY, (VOID FRACTION), (VOL/VOL)	:	0.59600
VOLUMETRIC FLOW RATE OF GAS AT STAND. CONDITIONS, (CC/MIN)	:	565.57	BULK DENSITY OF BED, (GMS/CC)	:	1.14534
H2S CAPACITY OF ASH, (GM MOL /GM ASH)	:	0.13026E-02	SUPERFICIAL LINEAR VELOCITY, (CMS/MIN)	:	607.52120
(STD. CC/GM ASH)	:	29.178			

TIME (MIN)	TAU	WA (ASH CAPACITY) CC H2S	WA (ASH CONC.) GM MOL FE2O3 /GM ASH	CA/CAO	XB
0.00	0.0000	364.381	0.49120E-03	0.0000	0.00000
4.00	0.0654	340.539	0.45887E-03	0.0000	0.06543
21.00	0.3435	239.210	0.32246E-03	0.0000	0.34352
38.00	0.6216	140.774	0.18975E-03	0.0571	0.61366
55.00	0.8997	78.826	0.10624E-03	0.7202	0.78367
72.00	1.1778	57.056	0.76906E-04	0.8501	0.84342
90.00	1.4722	43.028	0.57994E-04	0.8884	0.88192
107.00	1.7503	32.429	0.43715E-04	0.9024	0.91100
161.30	2.6336	9.843	0.13265E-04	0.9324	0.98397
190.00	3.1080	0.000	0.00000E 00	1.0000	1.00000

RUN NUMBER: 004 WESTERN KENTUCKY ASH

PARTICLE DIAM., (CMS)	:	0.01935	MASS OF ASH CHARGED, (GMS)	:	12.486
APPARENT PARTICLE DENSITY, (GMS/CC)	:	2.8350	DIAMETER OF COLUMN, (CMS)	:	2.0000
BED TEMPERATURE, (DEG. F)	:	1200.00	BED LENGTH, (CMS)	:	3.556
INLET H2S CONCENTRATION, (VOL. FRACTION)	:	0.0108270	BED POROSITY, (VOID FRACTION), (VOL/VOL)	:	0.59600
VOLUMETRIC FLOW RATE OF GAS AT STAND. CONDITIONS, (CC/MIN)	:	565.57	BULK DENSITY OF BED, (GMS/CC)	:	1.14534
			SUPERFICIAL LINEAR VELOCITY, (CMS/MIN)	:	607.52120
H2S CAPACITY OF ASH, (GM MOL /GM ASH)	:	0.11882E-02			
(STD. CC/GM ASH)	:	25.616			

TIME (MIN)	TAU	WA (ASH CAPACITY) CC H2S	WM (ASH CONC.) GM MOL FE2O3 /GM ASH	CA/CAO	XB
0.00	0.0000	337.392	0.59411E-03	0.0000	0.00000
3.00	0.0553	314.021	0.56327E-03	0.0000	0.05527
20.00	0.3684	209.923	0.37521E-03	0.0000	0.36845
55.00	1.0132	56.106	0.10028E-03	0.5646	0.83121
72.00	1.3264	24.158	0.43180E-04	0.8216	0.92732
89.00	1.6396	10.730	0.19178E-04	0.9204	0.96772
105.00	1.9343	4.455	0.79620E-05	0.9515	0.98660
135.00	2.4870	0.000	0.00000E 00	1.0000	1.00000

RUN NUMBER: 005 WESTERN KENTUCKY ASH

PARTICLE DIAM., (CMS)	:	0.01935	MASS OF ASH CHARGED, (GMS)	:	12.488
APPARENT PARTICLE DENSITY, (GMS/CC)	:	2.8350	DIAMETER OF COLUMN, (CMS)	:	2.0000
BED TEMPERATURE, (DEG. F)	:	1200.00	BED LENGTH, (CMS)	:	3.556
INLET H2S CONCENTRATION, (VOL. FRACTION)	:	0.0102530	BED POROSITY, (VOID FRACTION), (VOL/VOL)	:	0.59600
VOLUMETRIC FLOW RATE OF GAS AT STAND. CONDITIONS, (CC/MIN)	:	565.57	BULK DENSITY OF BED, (GMS/CC)	:	1.14534
			SUPERFICIAL LINEAR VELOCITY, (CMS/MIN)	:	607.52120
H2S CAPACITY OF ASH, (GM MOL /GM ASH)	:	0.10551E-02			
(STD. CC/GM ASH)	:	23.634			

TIME (MIN)	TAU	WA (ASH CAPACITY) CC H2S	WM (ASH CONC.) GM MOL FE2O3 /GM ASH	CA/CAO	XB
0.00	0.0000	295.155	0.52755E-03	0.0000	0.00000
3.00	0.0589	277.758	0.49646E-03	0.0000	0.05894
20.00	0.3929	179.179	0.32026E-03	0.0000	0.39293
37.00	0.7269	80.599	0.14406E-03	0.0000	0.72692
54.00	1.0609	20.924	0.37400E-04	0.7893	0.92911
71.00	1.3949	7.350	0.13137E-04	0.9353	0.97510
88.00	1.7289	2.801	0.50060E-05	0.9724	0.99051
129.00	2.4165	0.000	0.00000E 00	1.0000	1.00000

RUN NUMBER: 006 WESTERN KENTUCKY ASH

PARTICLE DIAM., (CMS)	:	0.01935	MASS OF ASH CHARGED, (GMS)	:	12.488
APPARENT PARTICLE DENSITY, (GMS/CC)	:	2.8350	DIAMETER OF COLUMN, (CMS)	:	2.0000
BED TEMPERATURE, (DEG. F)	:	1200.00	BED LENGTH, (CMS)	:	3.556
INLET H2S CONCENTRATION, (VOL. FRACTION)	:	0.0098660	BED POROSITY, (VOID FRACTION), (VOL/VOL)	:	0.59600
VOLUMETRIC FLOW RATE OF GAS AT STAND. CONDITIONS, (CC/MIN)	:	565.57	BULK DENSITY OF BED, (GMS/CC)	:	1.14534
			SUPERFICIAL LINEAR VELOCITY, (CMS/MIN)	:	607.52120
H2S CAPACITY OF ASH, (GM MOL /GM ASH)	:	0.10493E-02			
(STD. CC/GM ASH)	:	23.505			

TIME (MIN)	TAU	WA (ASH CAPACITY) CC H2S	WM (ASH CONC.) GM MOL FE2O3 /GM ASH	CA/CAO	XB
0.00	0.0000	293.534	0.52465E-03	0.0000	0.00000
5.00	0.0950	265.635	0.47479E-03	0.0000	0.09505
22.00	0.4182	170.776	0.30524E-03	0.0000	0.41821
39.00	0.7414	75.918	0.13569E-03	0.0000	0.74137
56.00	1.0645	19.126	0.34185E-04	0.8026	0.93484
73.00	1.3877	5.742	0.12051E-04	0.9363	0.97703
90.00	1.7108	2.493	0.44558E-05	0.9741	0.99151
124.50	2.3667	0.000	0.00000E 00	1.0000	1.00000

RUN NUMBER: 007 WESTERN KENTUCKY ASH

PARTICLE DIAM., (CMS)	:	0.01935	MASS OF ASH CHARGED, (GMS)	:	12.488
APPARENT PARTICLE DENSITY, (GMS/CC)	:	2.8350	DIAMETER OF COLUMN, (CMS)	:	2.0000
BED TEMPERATURE, (DEG. F)	:	1200.00	BED LENGTH, (CMS)	:	3.556
INLET H2S CONCENTRATION, (VOL. FRACTION)	:	0.0100580	BED POROSITY, (VOID FRACTION), (VOL/VOL)	:	0.59600
VOLUMETRIC FLOW RATE OF GAS AT STAND. CONDITIONS, (CC/MIN)	:	565.57	BULK DENSITY OF BED, (GMS/CC)	:	1.14534
			SUPERFICIAL LINEAR VELOCITY, (CMS/MIN)	:	607.52120
H2S CAPACITY OF ASH, (GM MOL /GM ASH)	:	0.10848E-02			
(STD. CC/GM ASH)	:	24.299			

TIME (MIN)	TAU	HA (ASH CAPACITY) CC H2S	HM (ASH CONC.) GM MOL FE2O3 /GM ASH	CA/CAO	XB
0.00	0.0000	303.459	0.54240E-03	0.0000	0.00000
4.00	0.0750	280.705	0.50173E-03	0.0000	0.07498
22.00	0.4124	178.312	0.31871E-03	0.0000	0.41240
39.00	0.7311	82.923	0.14821E-03	0.0272	0.72674
56.00	1.0497	23.750	0.42450E-04	0.7490	0.92174
77.00	1.4434	5.425	0.96966E-05	0.9442	0.98212
94.00	1.7621	1.649	0.29472E-05	0.9777	0.99457
120.00	2.2495	0.000	0.00000E 00	1.0000	1.00000

RUN NUMBER: 008 WESTERN KENTUCKY ASH

PARTICLE DIAM., (CMS)	0.01935	MASS OF ASH CHARGED, (GMS)	12.488
APPARENT PARTICLE DENSITY, (GMS/CC)	2.4350	DIAMETER OF COLUMN, (CMS)	2.0000
BED TEMPERATURE, (DEG. F)	1200.00	BED LENGTH, (CMS)	3.556
INLET H2S CONCENTRATION, (VOL. FRACTION)	0.0101040	BED POROSITY, (VOID FRACTION), (VOL/VOL)	0.59600
VOLUMETRIC FLOW RATE OF GAS AT STAND. CONDITIONS, (CC/MIN)	565.57	BULK DENSITY OF BED, (GMS/CC)	1.14534
		SUPERFICIAL LINEAR VELOCITY, (CMS/MIN)	607.52120
H2S CAPACITY OF ASH, (GM MOL /GM ASH)	0.11832E-02		
(STD. CC/GM ASH)	26.503		

TIME (MIN)	TAU	WA (ASH CAPACITY) CC H2S	WM (ASH CONC.) GM MOL FE2O3 /GM ASH	CA/CAO	XB
0.00	0.0000	330.976	0.59158E-03	0.0000	0.00000
3.00	0.0518	313.832	0.56093E-03	0.0000	0.05180
20.00	0.3453	216.685	0.38730E-03	0.0000	0.34531
37.00	0.6388	119.538	0.21366E-03	0.0000	0.63883
54.00	0.9323	47.596	0.85073E-04	0.5189	0.85619
71.00	1.2259	18.807	0.33615E-04	0.8884	0.94318
88.00	1.5194	10.822	0.19343E-04	0.9472	0.96730
140.00	2.4132	0.733	0.13109E-05	0.9849	0.99778
157.00	2.7067	0.000	0.00000E 00	1.0000	1.00000

RUN NUMBER: 011 WESTERN KENTUCKY ASH

PARTICLE DIAM., (CMS)	:	0.01935	MASS OF ASH CHARGED, (GMS)	:	12.488
APPARENT PARTICLE DENSITY, (GMS/CC)	:	2.8350	DIAMETER OF COLUMN, (CMS)	:	2.0000
BED TEMPERATURE, (DEG. F)	:	1200.00	BED LENGTH, (CMS)	:	3.556
INLET H2S CONCENTRATION, (VOL. FRACTION)	:	0.0097830	BED POROSITY, (VOID FRACTION), (VOL/VOL)	:	0.59600
VOLUMETRIC FLOW RATE OF GAS AT STAND. CONDITIONS, (CC/MIN)	:	565.57	BULK DENSITY OF BED, (GMS/CC)	:	1.14534
			SUPERFICIAL LINEAR VELOCITY, (CMS/MIN)	:	607.52120
H2S CAPACITY OF ASH, (GM MOL /GM ASH)	:	0.11913E-02			
(STD. CC/GM ASH)	:	26.685			

TIME (MIN)	TAU	WA (ASH CAPACITY) CC H2S	WM (ASH CONC.) GM MOL FE2O3 /GM ASH	CA/CAO	XB
0.00	0.0000	333.255	0.59565E-03	0.0000	0.00000
4.00	0.0664	311.123	0.55609E-03	0.0000	0.06641
21.00	0.3487	217.063	0.38797E-03	0.0000	0.34866
38.00	0.6309	123.002	0.21985E-03	0.0000	0.63091
55.00	0.9132	44.716	0.79924E-04	0.3354	0.86582
72.00	1.1954	8.799	0.15727E-04	0.9009	0.97360
89.00	1.4776	2.069	0.36982E-05	0.9560	0.99379
106.00	1.7599	0.000	0.00000E 00	1.0000	1.00000

RUN NUMBER: 012 WESTERN KENTUCKY ASH

PARTICLE DIAM., (CMS)	:	0.01935	MASS OF ASH CHARGED, (GMS)	:	12.488
APPARENT PARTICLE DENSITY, (GMS/CC)	:	2.8350	DIAMETER OF COLUMN, (CMS)	:	2.0000
BED TEMPERATURE, (DEG. F)	:	1200.00	BED LENGTH, (CMS)	:	3.556
INLET H2S CONCENTRATION, (VOL. FRACTION)	:	0.0100150	BED POROSITY, (VOID FRACTION), (VOL/VOL)	:	0.59600
VOLUMETRIC FLOW RATE OF GAS AT STAND. CONDITIONS, (CC/MIN)	:	565.57	BULK DENSITY OF BED, (GMS/CC)	:	1.14534
H2S CAPACITY OF ASH, (GM MOL /GM ASH)	:	0.12972E-02	SUPERFICIAL LINEAR VELOCITY, (CMS/MIN)	:	607.52120
(STD. CC/GM ASH)	:	29.056			

TIME (MIN)	TAU	WA (ASH CAPACITY) CC H2S	WM (ASH CONC.) GM MOL FE2O3 /GM ASH	CA/CAO	XB
0.00	0.0000	362.868	0.64858E-03	0.0000	0.00000
4.00	0.0624	340.211	0.60808E-03	0.0000	0.06244
21.00	0.3278	243.920	0.43598E-03	0.0000	0.32780
38.00	0.5932	148.289	0.26505E-03	0.0137	0.59134
55.00	0.8585	59.576	0.10648E-03	0.1437	0.83582
72.00	1.1239	12.894	0.23046E-04	0.8867	0.96447
89.00	1.3892	5.239	0.93636E-05	0.9543	0.98556
106.00	1.6546	1.917	0.34259E-05	0.9767	0.99472
123.00	1.9200	0.535	0.95652E-06	0.9946	0.99853
158.00	2.4663	0.000	0.00000E 00	1.0000	1.00000

RUN NUMBER: 013 WESTERN KENTUCKY ASH

PARTICLE DIAM., (CMS)	:	0.01935	MASS OF ASH CHARGED, (GMS)	:	12.488
APPARENT PARTICLE DENSITY, (GMS/CC)	:	2.8350	DIAMETER OF COLUMN, (CMS)	:	2.0000
BED TEMPERATURE, (DEG. F)	:	1200.00	BED LENGTH, (CMS)	:	3.556
INLET H2S CONCENTRATION, (VOL. FRACTION)	:	0.0101240	BED POROSITY, (VOID FRACTION), (VOL/VOL)	:	0.59600
VOLUMETRIC FLOW RATE OF GAS AT STAND. CONDITIONS, (CC/MIN)	:	565.57	BULK DENSITY OF BED, (GMS/CC)	:	1.14534
			SUPERFICIAL LINEAR VELOCITY, (CMS/MIN)	:	607.52120
H2S CAPACITY OF ASH, (GM MOL /GM ASH)	:	0.12754E-02			
(STD. CC/GM ASH)	:	28.569			

TIME (MIN)	TAU	WA (ASH CAPACITY) CC H2S	WM (ASH CONC.) GM MOL FE2O3 /GM ASH	CA/CAO	XB
0.00	0.0000	356.775	0.63769E-03	0.0000	0.00000
3.00	0.0481	339.598	0.60699E-03	0.0000	0.04815
20.00	0.3210	242.259	0.43301E-03	0.0000	0.32098
38.00	0.6099	139.194	0.24879E-03	0.0000	0.60986
55.00	0.8827	56.378	0.10077E-03	0.2984	0.84198
72.00	1.1555	16.839	0.30097E-04	0.8892	0.95280
89.00	1.4283	8.215	0.14683E-04	0.9336	0.97697
106.00	1.7012	3.455	0.61755E-05	0.9686	0.99032
123.00	1.9740	1.285	0.22962E-05	0.9868	0.99640
157.00	2.5197	0.000	0.00000E 00	1.0000	1.00000

RUN NUMBER: 014 WESTERN KY. ASH

PARTICLE DIAM., (CMS)	:	0.01935	MASS OF ASH CHARGED, (GMS)	:	12.488
APPARENT PARTICLE DENSITY, (GMS/CC)	:	2.8350	DIAMETER OF COLUMN, (CMS)	:	2.0000
BED TEMPERATURE, (DEG. F)	:	1200.00	BED LENGTH, (CMS)	:	3.556
INLET H2S CONCENTRATION, (VOL. FRACTION)	:	0.0100910	BED POROSITY, (VOID FRACTION), (VOL/VOL)	:	0.59600
VOLUMETRIC FLOW RATE OF GAS AT STAND. CONDITIONS, (CC/MIN)	:	565.57	BULK DENSITY OF BED, (GMS/CC)	:	1.14534
			SUPERFICIAL LINEAR VELOCITY, (CMS/MIN)	:	607.52120
H2S CAPACITY OF ASH, (GM MOL /GM ASH)	:	0.13257E-02			
(STD. CC/GM ASH)	:	29.696			

TIME (MIN)	TAU	WA (ASH CAPACITY) CC H2S	WM (ASH CONC.) GM MOL FE2O3 /GM ASH	CA/CAO	XB
0.00	0.0000	370.854	0.66286E-03	0.0000	0.00000
5.00	0.0769	342.389	0.61185E-03	0.0000	0.07695
21.50	0.3309	248.150	0.44354E-03	0.0000	0.33087
38.00	0.5848	153.982	0.27522E-03	0.0000	0.58479
52.00	0.8002	74.082	0.13241E-03	0.0000	0.80024
55.00	0.8464	59.235	0.10595E-03	0.2703	0.84017
72.00	1.1080	16.799	0.30025E-04	0.8541	0.95470
89.00	1.3696	6.932	0.12389E-04	0.9425	0.98131
106.00	1.6313	2.634	0.47076E-05	0.9689	0.99290
123.00	1.8929	0.563	0.10054E-05	0.9884	0.99848
140.00	2.1545	0.000	0.00000E 00	1.0000	1.00000

RUN NUMBER: 017 WESTERN KY. ASH

PARTICLE DIAM., (CMS)	: 0.01935	MASS OF ASH CHARGED, (GMS)	: 12.488
APPARENT PARTICLE DENSITY, (GMS/CC)	: 2.8350	DIAMETER OF COLUMN, (CMS)	: 2.0000
BED TEMPERATURE, (DEG. F)	: 1200.00	BED LENGTH, (CMS)	: 3.556
INLET H2S CONCENTRATION, (VOL. FRACTION)	: 0.0099430	BED POROSITY, (VOID FRACTION), (VOL/VOL)	: 0.59600
VOLUMETRIC FLOW RATE OF GAS AT STAND. CONDITIONS, (CC/MIN)	: 565.57	BULK DENSITY OF BED, (GMS/CC)	: 1.14534
		SUPERFICIAL LINEAR VELOCITY, (CMS/MIN)	: 607.52120
H2S CAPACITY OF ASH, (GM MOL /GM ASH)	: 0.12777E-02		
(STD. CC/GM ASH)	: 28.620		

TIME (MIN)	TAU	HA (ASH CAPACITY) CC H2S	WM (ASH CONC.) GM MOL FE2O3 /GM ASH	CA/CAO	XB
0.00	0.0000	351.422	0.63885E-03	0.0000	0.00000
11.37	0.1789	293.483	0.52456E-03	0.0000	0.17889
28.05	0.4413	199.684	0.35691E-03	0.0000	0.44132
44.75	0.7041	105.772	0.18905E-03	0.0000	0.70407
52.00	0.8181	65.002	0.11618E-03	0.0000	0.81814
61.50	0.9676	29.727	0.53132E-04	0.6794	0.91683
78.25	1.2311	10.653	0.19040E-04	0.9156	0.97020
95.00	1.4947	4.681	0.83665E-05	0.9576	0.98690
111.75	1.7582	1.869	0.33413E-05	0.9827	0.99477
128.50	2.0217	0.527	0.94256E-06	0.9888	0.99852
145.25	2.2853	0.000	0.00000E 00	1.0000	1.00000

RUN NUMBER: 019 WESTERN KY. ASH

PARTICLE DIAM., (CMS)	:	0.01939	MASS OF ASH CHARGED, (GMS)	:	12.488
APPARENT PARTICLE DENSITY, (GMS/CC)	:	2.8350	DIAMETER OF COLUMN, (CMS)	:	2.0000
BED TEMPERATURE, (DEG. F)	:	1200.00	BED LENGTH, (CMS)	:	3.556
INLET H2S CONCENTRATION, (VOL. FRACTION)	:	0.0099150	BED POROSITY, (VOID FRACTION), (VOL/VOL)	:	0.59600
VOLUMETRIC FLOW RATE OF GAS AT STAND. CONDITIONS, (CC/MIN)	:	565.57	BULK DENSITY OF BED, (GMS/CC)	:	1.14534
H2S CAPACITY OF ASH, (GM MOL /GM ASH)	:	0.13371E-02	SUPERFICIAL LINEAR VELOCITY, (CMS/MIN)	:	607.52120
(STD. CC/GM ASH)	:	29.951			

TIME (MIN).	TAU	WA (ASH CAPACITY) CC H2S	WM (ASH CONC.) GM MOL FE2O3 /GM ASH	CA/CAO	XB
0.00	0.0000	374.041	0.66855E-03	0.0000	0.00000
6.22	0.0933	339.151	0.60621E-03	0.0000	0.09325
23.00	0.3448	245.065	0.43802E-03	0.0000	0.34482
40.13	0.6016	149.007	0.26633E-03	0.0000	0.60163
52.00	0.7796	82.444	0.14736E-03	0.0000	0.77958
57.43	0.8610	56.751	0.10144E-03	0.3124	0.84828
75.10	1.1259	17.008	0.30399E-04	0.8854	0.95453
116.21	1.7422	1.320	0.23595E-05	0.9785	0.99647
133.91	2.0076	0.065	0.11564E-06	0.9962	0.99983
140.00	2.0989	0.000	0.00000E 00	1.0000	1.00000

RUN NUMBER: 021 WESTERN KY. ASH

PARTICLE DIAM., (CMS)	:	0.01935	MASS OF ASH CHARGED, (GMS)	:	12.488
APPARENT PARTICLE DENSITY, (GMS/CC)	:	2.8350	DIAMETER OF COLUMN, (CMS)	:	2.0000
BED TEMPERATURE, (DEG. F)	:	1000.00	BED LENGTH, (CMS)	:	3.556
INLET H2S CONCENTRATION, (VOL. FRACTION)	:	0.0099550	BED POROSITY, (VOID FRACTION), (VOL/VOL)	:	0.61500
VOLUMETRIC FLOW RATE OF GAS AT STAND. CONDITIONS, (CC/MIN)	:	565.57	BULK DENSITY OF BED, (GMS/CC)	:	1.09147
			SUPERFICIAL LINEAR VELOCITY, (CMS/MIN)	:	534.32560
H2S CAPACITY OF ASH, (GM MOL /GM ASH)	:	0.95304E-03			
(STD. CC/GM ASH)	:	21.348			

TIME (MIN)	TAU	WA (ASH CAPACITY) CC H2S	WM (ASH CONC.) GM MOL FE2O3 /GM ASH	CA/CAO	XB
0.00	0.0000	266.603	0.47652E-03	0.0000	0.00000
6.22	0.1314	231.583	0.41392E-03	0.0000	0.13136
22.86	0.4828	137.896	0.24647E-03	0.0000	0.48277
39.73	0.8390	65.296	0.11671E-03	0.4713	0.75508
56.47	1.1926	30.664	0.54807E-04	0.7938	0.88498
74.41	1.5714	15.093	0.26978E-04	0.8979	0.94339
91.21	1.9262	7.489	0.13385E-04	0.9413	0.97191
107.97	2.2802	3.511	0.62759E-05	0.9744	0.98683
124.73	2.6341	1.704	0.30463E-05	0.9873	0.99361
141.49	2.9881	0.634	0.11324E-05	0.9900	0.99762
164.00	3.4634	0.000	0.00000E 00	1.0000	1.00000

RUN NUMBER: 022 WESTERN KY. ASH

PARTICLE DIAM., (CMS)	:	0.01935	MASS OF ASH CHARGED, (GMS)	:	12.488
APPARENT PARTICLE DENSITY, (GMS/CC)	:	2.8350	DIAMETER OF COLUMN, (CMS)	:	2.0000
BED TEMPERATURE, (DEG. F)	:	1800.00	BED LENGTH, (CMS)	:	3.556
INLET H2S CONCENTRATION, (VOL. FRACTION)	:	0.0100290	BED POROSITY, (VOID FRACTION), (VOL/VOL)	:	0.61500
VOLUMETRIC FLOW RATE OF GAS AT STAND. CONDITIONS, (CC/MIN)	:	965.57	BULK DENSITY OF BED, (GMS/CC)	:	1.09147
			SUPERFICIAL LINEAR VELOCITY, (CMS/MIN)	:	534.32560
H2S CAPACITY OF ASH, (GM MOL /GM ASH)	:	0.10671E-02			
(STD. CC/GM ASH)	:	23.902			

TIME (MIN)	TAU	WA (ASH CAPACITY) CC H2S	WM (ASH CONC.) GM MOL FE2O3 /GM ASH.	CA/CAO	XB
0.00	0.0000	298.503	0.53354E-03	0.0000	0.00000
16.05	0.3050	207.466	0.37082E-03	0.0000	0.30498
32.90	0.6252	111.891	0.19999E-03	0.0000	0.62516
49.69	0.9442	43.955	0.78565E-04	0.5733	0.85275
66.35	1.2608	17.237	0.30808E-04	0.8612	0.94226
83.10	1.5791	7.356	0.13148E-04	0.9308	0.97536
99.85	1.8973	2.610	0.46657E-05	0.9693	0.99126
116.62	2.2160	0.575	0.10277E-05	0.9879	0.99807
133.38	2.5345	0.000	0.00000E 00	1.0000	1.00000

RUN NUMBER: 325 WESTERN KY. ASH

PARTICLE DIAM., (CMS)	: 0.01935	MASS OF ASH CHARGED, (GMS)	: 12.488
APPARENT PARTICLE DENSITY, (GMS/CC)	: 2.8350	DIAMETER OF COLUMN, (CMS)	: 2.0000
BED TEMPERATURE, (DEG. F)	: 1000.00	BED LENGTH, (CMS)	: 3.556
INLET H2S CONCENTRATION, (VOL. FRACTION)	: 0.0099310	BED POROSITY, (VOID FRACTION), (VOL/VOL)	: 0.59600
VOLUMETRIC FLOW RATE OF GAS AT STAND. CONDITIONS, (CC/MIN)	: 565.57	BULK DENSITY OF BED, (GMS/CC)	: 1.14534
		SUPERFICIAL LINEAR VELOCITY, (CMS/MIN)	: 534.32560
H2S CAPACITY OF ASH, (GM MOL /GM ASH)	: 0.11737E-02		
(STD. CC/GM ASH)	: 26.290		

TIME (MIN)	TAU	NA (ASH CAPACITY) CC H2S	NM (ASH CONC.) GM MOL FE2O3 /GM ASH	CA/CAO	XB
0.00	0.0000	326.324	0.58684E-03	0.0000	0.00000
4.30	0.0730	304.172	0.54367E-03	0.0000	0.07356
22.90	0.3849	201.949	0.36096E-03	0.0000	0.38491
40.70	0.6963	99.725	0.17825E-03	0.0000	0.69626
56.39	0.9640	40.713	0.72769E-04	0.6573	0.87600
73.00	1.2488	18.278	0.32670E-04	0.8629	0.94433
89.69	1.5343	8.552	0.15286E-04	0.9296	0.97395
106.35	1.8193	5.564	0.64955E-05	0.9642	0.98908
123.10	2.1059	1.100	0.19663E-05	0.9830	0.99665
139.77	2.3911	0.000	0.00000E 00	0.9935	1.00000

RUN NUMBER: 024 WESTERN KY. ASH

PARTICLE DIAM., (CMS)	: 0.01935	MASS OF ASH CHARGED, (GMS)	: 12.488
APPARENT PARTICLE DENSITY, (GMS/CC)	: 2.8350	DIAMETER OF COLUMN, (CMS)	: 2.0000
BED TEMPERATURE, (DEG. F)	: 1000.00	BED LENGTH, (CMS)	: 3.556
INLET H2S CONCENTRATION, (VOL. FRACTION)	: 0.0100240	BED POROSITY, (VOID FRACTION), (VOL/VOL)	: 0.59600
VOLUMETRIC FLOW RATE OF GAS AT STAND. CONDITIONS, (CC/MIN)	: 565.57	BULK DENSITY OF BED, GGMS/CC)	: 1.14534
H2S CAPACITY OF ASH, (GM MOL /GM ASH)	: 0.11869E-02	SUPERFICIAL LINEAR VELOCITY, (CMS/MIN)	: 534.32560
(STD. CC/GM ASH)	: 26.586		

TIME (MIN)	TAU	NA (ASH CAPACITY) CC H2S	NN (ASH CONC.) GM MOL FE2O3 /GM ASH	CA/CAO	XB
0.00	0.0000	532.612	0.59343E-03	0.0000	0.00000
11.39	0.1930	267.066	0.47842E-03	0.0000	0.19381
29.09	0.4960	107.320	0.29906E-03	0.0000	0.44604
41.60	0.7001	99.572	0.17797E-03	0.0000	0.70010
46.05	0.7803	74.329	0.13285E-03	0.2566	0.77613
62.79	1.0919	28.168	0.50383E-04	0.7887	0.91510
79.43	1.3563	13.465	0.24067E-04	0.8999	0.95944
90.79	1.6521	5.978	0.10685E-04	0.9475	0.98200
113.44	1.9370	2.198	0.39282E-05	0.9725	0.99338
130.10	2.2215	0.450	0.80512E-06	0.9909	0.99864
140.83	2.5072	0.000	0.00000E 00	1.0000	1.00000

RUN NUMBER: 026 WESTERN KY.ASH

PARTICLE DIAM., (CMS)	: 0.01935	MASS OF ASH CHARGED, (GMS)	: 12.488
APPARENT PARTICLE DENSITY, (GMS/CC)	: 2.8350	DIAMETER OF COLUMN, (CMS)	: 2.0000
BED TEMPERATURE, (DEG. F)	: 400.00	BED LENGTH, (CMS)	: 3.556
INLET H2S CONCENTRATION, (VOL. FRACTION)	: 0.0099930	BED POROSITY, (VOID FRACTION), (VOL/VOL)	: 0.59600
VOLUMETRIC FLOW RATE OF GAS AT STAND. CONDITIONS, (CC/MIN)	: 565.57	BULK DENSITY OF BED, (GMS/CC)	: 1.14534
H2S CAPACITY OF ASH, (GM MOL /GM ASH)	: 0.10562E-02	SUPERFICIAL LINEAR VELOCITY, (CMS/MIN)	: 497.72600
(STD. CC/GM ASH)	: 23.658		

TIME (MIN)	TAU	HA (ASH CAPACITY) CC H2S	WM (ASH CONC.) GM MOL FE2O3 /GM ASH	CA/CAO	XB
0.00	0.0000	295.457	0.52809E-03	0.0000	0.00000
2.50	0.0478	288.327	0.50284E-03	0.0000	0.04782
19.10	0.3654	187.508	0.33515E-03	0.0000	0.36536
32.00	0.6121	114.601	0.20483E-03	0.0000	0.61212
35.70	0.6830	95.606	0.17088E-03	0.2123	0.67641
55.11	1.0539	43.038	0.76924E-04	0.7155	0.85434
69.88	1.3367	22.266	0.39833E-04	0.8466	0.92457
80.54	1.5554	10.794	0.19292E-04	0.9093	0.96347
103.20	1.9741	4.396	0.78568E-05	0.9548	0.98512
119.65	2.2928	1.361	0.24328E-05	0.9807	0.99539
136.52	2.6115	0.226	0.40364E-06	0.9952	0.99924
153.17	2.9300	0.000	0.00000E 00	1.0000	1.00000

RUN NUMBER: 027 WESTERN KY. ASH

PARTICLE DIAM., (CMS)	:	0.01935	MASS OF ASH CHARGED, (GMS)	:	12.488
APPARENT PARTICLE DENSITY, (GMS/CC)	:	2.8350	DIAMETER OF COLUMN, (CMS)	:	2.0000
BED TEMPERATURE, (DEG. F)	:	900.00	BED LENGTH, (CMS)	:	3.556
INLET H2S CONCENTRATION, (VOL. FRACTION)	:	0.0100610	BED POROSITY, (VOID FRACTION), (VOL/VOL)	:	0.59600
VOLUMETRIC FLOW RATE OF GAS AT STAND. CONDITIONS, (CC/MIN)	:	565.67	BULK DENSITY OF BED, (GMS/CC)	:	1.14534
			SUPERFICIAL LINEAR VELOCITY, (CMS/MIN)	:	497.72800
H2S CAPACITY OF ASH, (GM MOL /GM ASH)	:	0.10536E-02			
(STD. CC/GM ASH)	:	23.601			

TIME (MIN)	TAU	WA (ASH CAPACITY) CC H2S	WM (ASH CONC.) GM MOL FE2O3 /GM ASH	CA/CAO	XB
0.00	0.0000	294.740	0.52681E-03	0.0000	0.00000
5.27	0.1017	264.752	0.47321E-03	0.0000	0.10174
22.54	0.4352	166.483	0.29757E-03	0.0000	0.43515
32.00	0.6178	112.654	0.20135E-03	0.0000	0.61779
43.97	0.8489	65.936	0.11785E-03	0.6282	0.77629
51.04	1.1784	38.365	0.68574E-04	0.8041	0.86983
76.20	1.5097	22.694	0.40562E-04	0.8749	0.92300
94.82	1.8300	12.844	0.22957E-04	0.9168	0.95642
111.58	2.1541	6.545	0.11699E-04	0.9511	0.97779
128.32	2.4773	2.950	0.52722E-05	0.9734	0.98999
145.33	2.8057	0.845	0.15098E-05	0.9831	0.99713
162.40	3.1349	0.000	0.00000E 00	1.0000	1.00000

RUN NUMBER: 029 WESTERN KY.ASH

PARTICLE DIAM., (CMS)	:	0.01935	MASS OF ASH CHARGED, (GMS)	:	12.488
APPARENT PARTICLE DENSITY, (GMS/CC)	:	2.8350	DIAMETER OF COLUMN, (CMS)	:	2.0000
BED TEMPERATURE, (DEG. F)	:	1000.00	BED LENGTH, (CMS)	:	3.556
INLET H2S CONCENTRATION, (VOL. FRACTION)	:	0.0100190	BED POROSITY, (VOID FRACTION), (VOL/VOL)	:	0.59600
VOLUMETRIC FLOW RATE OF GAS AT STAND. CONDITIONS, (CC/MIN)	:	409.23	BULK DENSITY OF BED, (GMS/CC)	:	1.14534
H2S CAPACITY OF ASH, (GM MOL /GM ASH)	:	0.17591E-02	SUPERFICIAL LINEAR VELOCITY, (CMS/MIN)	:	386.62590
(STD. CC/GM ASH)	:	28.204			

TIME (MIN)	TAU	WA (ASH CAPACITY) CC H2S	WM (ASH CONC.) GM MOL FE2O3 /GM ASH	CA/CAO	XB
0.00	0.0000	352.225	0.62956E-03	0.0000	0.00000
0.87	0.0800	324.057	0.57921E-03	0.0000	0.07997
21.51	0.2504	264.032	0.47192E-03	0.0000	0.25039
38.40	0.4470	194.781	0.34815E-03	0.0000	0.44700
55.05	0.6408	-126.514	0.22613E-03	0.0000	0.64081
68.70	0.7997	70.548	0.12609E-03	0.0000	0.79971
71.76	0.8353	58.792	0.10508E-03	0.1260	0.83308
88.37	1.0287	21.243	0.37970E-04	0.7713	0.93969
105.03	1.2226	9.819	0.17550E-04	0.8942	0.97212
121.68	1.4164	4.279	0.76487E-05	0.9435	0.98785
138.34	1.6104	1.175	0.20998E-05	0.9656	0.99666
155.00	1.8043	0.000	0.00000E 00	1.0000	1.00000

RUN NUMBER: 035 WESTERN KY. ASH

PARTICLE DIAM., (CMS)	: 0.01935	MASS OF ASH CHARGED, (GMS)	: 12.488
APPARENT PARTICLE DENSITY, (GMS/CC)	: 2.8350	DIAMETER OF COLUMN, (CMS)	: 2.0000
BED TEMPERATURE, (DEG. F)	: 1000.00	BED LENGTH, (CMS)	: 3.556
INLET H2S CONCENTRATION, (VOL. FRACTION)	: 0.0151160	BED POROSITY, (VOID FRACTION), (VOL/VOL)	: 0.59600
VOLUMETRIC FLOW RATE OF GAS AT STAND. CONDITIONS, (CC/MIN)	: 565.57	BULK DENSITY OF BED, (GMS/CC)	: 1.14534
H2S CAPACITY OF ASH, (GM MOL /GM ASH)	: 0.985935-03	SUPERFICIAL LINEAR VELOCITY, (CMS/MIN)	: 534.32560
(STD. CC/GM ASH)	: 22.085		

TIME (MIN)	TAU	WA (ASH CAPACITY) CC H2S	WM (ASH CONC.) GM MOL FE2O3 /GM ASH	CA/CAO	XB
0.00	0.0000	275.804	0.49296E-03	0.0000	0.00000
2.75	0.0552	252.294	0.45094E-03	0.0000	0.08524
14.03	0.2840	190.116	0.27904E-03	0.0030	0.43396
19.41	0.4017	165.919	0.20719E-03	0.2618	0.57970
36.08	1.1184	43.075	0.85929E-04	0.7861	0.82569
52.95	1.6413	24.307	0.43446E-04	0.8843	0.91167
69.66	2.1593	11.800	0.21092E-04	0.9406	0.95721
86.46	2.6800	4.899	0.87566E-05	0.9603	0.98224
103.16	3.1977	1.145	0.20457E-05	0.9841	0.99585
120.00	3.7197	0.000	0.00000E 00	1.0000	1.00000

RUN NUMBER: 036 WESTERN KY. ASH

PARTICLE DIAM., (CMS)	:	0.01935	MASS OF ASH CHARGED, (GMS)	:	12.488
APPARENT PARTICLE DENSITY, (GMS/CC)	:	2.8350	DIAMETER OF COLUMN, (CMS)	:	2.0000
BED TEMPERATURE, (DEG. F)	:	1000.00	BED LENGTH, (CMS)	:	3.556
INLET H2S CONCENTRATION, (VOL. FRACTION)	:	0.0099720	BED POROSITY, (VOID FRACTION), (VOL/VOL)	:	0.59600
VOLUMETRIC FLOW RATE OF GAS AT STAND. CONDITIONS, (CC/MIN)	:	565.57	BULK DENSITY OF BED, (GMS/CC)	:	1.14534
			SUPERFICIAL LINEAR VELOCITY, (CMS/MIN)	:	534.32560
H2S CAPACITY OF ASH, (GM MOL /GM ASH)	:	0.98128E-03			
(STD. CC/GM ASH)	:	21.981			

TIME (MIN)	TAU	WA (ASH CAPACITY) CC H2S	WM (ASH CONC.) GM MOL FE2O3 /GM ASH	CA/CAO	X8
0.00	0.0000	274.504	0.49064E-03	0.0000	0.00000
7.22	0.1483	233.784	0.41786E-03	0.0000	0.14834
25.38	0.5214	131.364	0.23480E-03	0.0000	0.52145
43.62	0.8962	58.691	0.10490E-03	0.5871	0.78619
60.54	1.2438	30.220	0.54015E-04	0.8162	0.88991
77.25	1.5872	16.489	0.29472E-04	0.8924	0.93993
94.10	1.9333	8.621	0.15409E-04	0.9420	0.96859
110.75	2.2754	4.081	0.72939E-05	0.9613	0.98513
127.61	2.6218	1.466	0.26204E-05	0.9837	0.99466
144.35	2.9658	0.347	0.62096E-06	0.9926	0.99873
161.00	3.3079	0.000	0.00000E 00	1.0000	1.00000

RUN NUMBER: 037 WESTERN KY. ASH

PARTICLE DIAM., (CMS)	:	0.01935	MASS OF ASH CHARGED, (GMS)	:	12.488
APPARENT PARTICLE DENSITY, (GMS/CC)	:	2.8350	DIAMETER OF COLUMN, (CMS)	:	2.0000
BED TEMPERATURE, (DEG. F)	:	1000.00	BED LENGTH, (CMS)	:	3.556
INLET H2S CONCENTRATION, (VOL. FRACTION)	:	0.0099970	BED POROSITY, (VOID FRACTION), (VOL/VOL)	:	0.59600
VOLUMETRIC FLOW RATE OF GAS AT STAND. CONDITIONS, (CC/MIN)	:	565.57	BULK DENSITY OF BED, (GMS/CC)	:	1.14534
H2S CAPACITY OF ASH, (GM MOL /GM ASH)	:	0.11760E-02	SUPERFICIAL LINEAR VELOCITY, (CMS/MIN)	:	534.32560
(STD. CC/GM ASH)	:	26.342			

TIME (MIN)	TAU	WA (ASH CAPACITY) CC H2S	WM (ASH CONC.) GM MOL FE2O3 /GM ASH	CA/CAO	XB
0.00	0.0000	328.973	0.58800E-03	0.0000	0.00000
6.70	0.1152	291.091	0.52029E-03	0.0000	0.11515
41.96	0.7212	91.731	0.16396E-03	0.0000	0.72116
56.61	1.0073	33.488	0.59855E-04	0.7626	0.89821
75.32	1.2945	16.784	0.29999E-04	0.8838	0.94898
92.18	1.5843	8.286	0.14810E-04	0.9379	0.97481
108.85	1.8708	3.738	0.66813E-05	0.9656	0.98864
125.81	2.1623	1.288	0.23023E-05	0.9833	0.99608
142.86	2.4553	0.242	0.43288E-06	0.9950	0.99926
160.00	2.7499	0.000	0.00000E 00	1.0000	1.00000

RUN NUMBER: 040 WESTERN KY. ASH

PARTICLE DIAM., (CMS)	0.01510	MASS OF ASH CHARGED, (GMS)	9.781
APPARENT PARTICLE DENSITY, (GMS/CC)	2.8360	DIAMETER OF COLUMN, (CMS)	2.0000
BED TEMPERATURE, (DEG. F)	1200.00	BED LENGTH, (CMS)	3.048
INLET H2S CONCENTRATION, (VOL. FRACTION)	0.0099650	BED POROSITY, (VOID FRACTION), (VOL/VOL)	0.61500
VOLUMETRIC FLOW RATE OF GAS AT STAND. CONDITIONS, (CC/MIN)	326.47	BULK DENSITY OF BED, (GMS/CC)	1.09186
		SUPERFICIAL LINEAR VELOCITY, (CMS/MIN)	350.68260
H2S CAPACITY OF ASH, (GM MOL /GM ASH)	0.82941E-03		
(STD. CC/GM ASH)	18.579		

TIME (MIN)	TAU	WA (ASH CAPACITY) CC H2S	WM (ASH CONC.) GM MOL FE2O3 /GM ASH	CA/CAO	XB
0.00	0.0000	181.714	0.41471E-03	0.0000	0.00000
29.63	0.5305	89.398	0.20402E-03	0.0846	0.50803
47.34	0.8475	48.610	0.11094E-03	0.4995	0.73249
64.03	1.1463	26.451	0.60366E-04	0.6843	0.85444
80.75	1.4457	13.726	0.31324E-04	0.8478	0.92447
97.61	1.7475	7.533	0.16735E-04	0.9191	0.95965
114.43	2.0486	3.979	0.90798E-05	0.9583	0.97811
130.55	2.3372	2.080	0.47472E-05	0.9693	0.98855
146.60	2.6246	0.665	0.15179E-05	0.9765	0.99634
164.00	2.9361	0.000	0.00000E 00	1.0000	1.00000

RUN NUMBER: 041 WESTERN KY. ASH

PARTICLE DIAM., (CMS)	:	0.01510	MASS OF ASH CHARGED, (GMS)	:	9.781
APPARENT PARTICLE DENSITY, (GMS/CC)	:	2.8360	DIAMETER OF COLUMN, (CMS)	:	2.0000
BED TEMPERATURE, (DEG. F)	:	1200.00	BED LENGTH, (CMS)	:	3.048
INLET H2S CONCENTRATION, (VOL. FRACTION)	:	0.0100200	BED POROSITY, (VOID FRACTION), (VOL/VOL)	:	0.61500
VOLUMETRIC FLOW RATE OF GAS AT STAND. CONDITIONS, (CC/MIN)	:	406.47	BULK DENSITY OF BED, (GMS/CC)	:	1.09186
			SUPERFICIAL LINEAR VELOCITY, (CMS/MIN)	:	436.62470
H2S CAPACITY OF ASH, (GM MOL /GM ASH)	:	0.97428E-03			
(STD. CC/GM ASH)	:	21.824			

TIME (MIN)	TAU	WA (ASH CAPACITY) CC H2S	WM (ASH CONC.) GM MOL FE2O3 /GM ASH	CA/CAO	XB
0.00	0.0000	213.452	0.48714E-03	0.0000	0.00000
4.89	0.0933	193.535	0.44168E-03	0.0000	0.09331
21.50	0.4102	125.885	0.28729E-03	0.0000	0.41024
39.03	0.7447	55.462	0.12657E-03	0.0273	0.74017
55.85	1.0657	15.605	0.35614E-04	0.8091	0.92689
71.88	1.3715	6.586	0.15030E-04	0.9146	0.96915
88.41	1.6870	2.351	0.53657E-05	0.9596	0.98899
104.85	2.0006	0.496	0.11328E-05	0.9850	0.99767
121.10	2.3107	0.000	0.00000E 00	1.0000	1.00000

RUN NUMBER: 042 WESTERN KY. ASH

PARTICLE DIAM., (CMS)	:	0.01510	MASS OF ASH CHARGED, (GMS)	:	9.781
APPARENT PARTICLE DENSITY, (GMS/CC)	:	2.8360	DIAMETER OF COLUMN, (CMS)	:	2.0000
BED TEMPERATURE, (DEG. F)	:	1200.00	BED LENGTH, (CMS)	:	3.048
INLET H2S CONCENTRATION, (VOL. FRACTION)	:	0.0099720	BED POROSITY, (VOID FRACTION), (VOL/VOL)	:	0.61500
VOLUMETRIC FLOW RATE OF GAS AT STAND. CONDITIONS, (CC/MIN)	:	406.47	BULK DENSITY OF BED, (GMS/CC)	:	1.09186
H2S CAPACITY OF ASH, (GM MOL /GM ASH)	:	0.97526E-03	SUPERFICIAL LINEAR VELOCITY, (CMS/MIN)	:	436.62470
(STD. CC/GM ASH)	:	21.846			

TIME (MIN)	TAU	HA (ASH CAPACITY) CC H2S	HM (ASH CONC.) GM MOL FE2O3 /GM ASH	CA/CAO	XB
0.00	0.0000	213.668	0.48763E-03	0.0000	0.00000
2.86	0.0543	202.076	0.46118E-03	0.0000	0.05426
19.18	0.3639	135.925	0.31021E-03	0.0000	0.36385
35.62	0.6757	69.288	0.15813E-03	0.0000	0.67572
51.76	0.9819	22.279	0.50845E-04	0.5629	0.89573
68.39	1.2974	4.797	0.10948E-04	0.9184	0.97755
84.42	1.6015	1.353	0.30886E-05	0.9756	0.99367
101.17	1.9192	0.345	0.78771E-06	0.9947	0.99838
117.20	2.2233	0.089	0.20201E-06	0.9974	0.99959
134.00	2.5420	0.000	0.00000E 00	1.0000	1.00000

RUN NUMBER: 043 WESTERN KY. ASH

PARTICLE DIAM., (CMS)	:	0.01510	MASS OF ASH CHARGED, (GMS)	:	9.781
APPARENT PARTICLE DENSITY, (GMS/CC)	:	2.8360	DIAMETER OF COLUMN, (CMS)	:	2.0000
BED TEMPERATURE, (DEG. F)	:	1200.00	BED LENGTH, (CMS)	:	3.048
INLET H2S CONCENTRATION, (VOL. FRACTION)	:	0.0101390	BED POROSITY, (VOID FRACTION), (VOL/VOL)	:	0.61500
VOLUMETRIC FLOW RATE OF GAS AT STAND. CONDITIONS, (CC/MIN)	:	406.47	BULK DENSITY OF BED, (GMS/CC)	:	1.09186
			SUPERFICIAL LINEAR VELOCITY, (CMS/MIN)	:	436.62470
H2S CAPACITY OF ASH, (GM MOL /GM ASH)	:	0.10665E-02			
(STD. CC/GM ASH)	:	23.890			

TIME (MIN)	TAU	WA (ASH CAPACITY) CC H2S	WM (ASH CONC.) GM MOL FE2O3 /GM ASH	CA/CAO	XB
0.00	0.0000	233.666	0.23327E-03	0.0000	0.00000
8.63	0.1522	198.099	0.45210E-03	0.0000	0.15221
27.18	0.4794	121.650	0.27763E-03	0.0000	0.47938
45.42	0.8011	47.497	0.10840E-03	0.0271	0.79673
61.44	1.0836	9.980	0.22776E-04	0.8364	0.95729
77.68	1.3701	2.571	0.58675E-05	0.9422	0.98900
94.11	1.6589	0.336	0.69838E-06	0.9909	0.99869
110.43	1.9457	0.000	0.00000E 00	1.0000	1.00000

RUN NUMBER: 044 WESTERN KY. ASH

PARTICLE DIAM., (CMS)	:	0.01510	MASS OF ASH CHARGED, (GMS)	:	9.781
APPARENT PARTICLE DENSITY, (GMS/CC)	:	2.8360	DIAMETER OF COLUMN, (CMS)	:	2.0000
BED TEMPERATURE, (DEG. F)	:	1000.00	BED LENGTH, (CMS)	:	3.048
INLET H2S CONCENTRATION, (VOL. FRACTION)	:	0.0099800	BED POROSITY, (VOID FRACTION), (VOL/VOL)	:	0.61500
VOLUMETRIC FLOW RATE OF GAS AT STAND. CONDITIONS, (CC/MIN)	:	413.83	BULK DENSITY OF BED, (GMS/CC)	:	1.09186
H2S CAPACITY OF ASH, (GM MOL /GM ASH)	:	0.75560E-03	SUPERFICIAL LINEAR VELOCITY, (CMS/MIN)	:	390.96970
(STD. CC/GM ASH)	:	16.925			

TIME (MIN)	TAU	WA (ASH CAPACITY) CC H2S	WM (ASH CONC.) GM MOL FE2O3 /GM ASH	CA/CAO	XB
0.00	0.0000	165.543	0.37780E-03	0.0000	0.00000
3.48	0.0868	151.171	0.34500E-03	0.0000	0.08682
20.00	0.4990	82.943	0.18929E-03	0.0000	0.49897
34.88	0.8702	38.799	0.88548E-04	0.5634	0.76562
51.31	1.2801	18.052	0.41199E-04	0.8251	0.89095
67.23	1.6773	9.271	0.21159E-04	0.9078	0.94399
83.28	2.0777	4.393	0.10025E-04	0.9450	0.97347
99.51	2.4826	1.755	0.40053E-05	0.9763	0.98940
118.00	2.9439	0.407	0.92933E-06	0.9884	0.99754
135.00	3.3680	0.000	0.00000E 00	1.0000	1.00000

RUN NUMBER: 045 WESTERN KY. ASH

PARTICLE DIAM., (CMS)	:	0.01510	MASS OF ASH CHARGED, (GMS)	:	9.781
APPARENT PARTICLE DENSITY, (GMS/CC)	:	2.8360	DIAMETER OF COLUMN, (CMS)	:	2.0000
BED TEMPERATURE, (DEG. F)	:	1000.00	BED LENGTH, (CMS)	:	3.048
INLET H2S CONCENTRATION, (VOL. FRACTION)	:	0.0101180	BED POROSITY, (VOID FRACTION), (VOL/VOL)	:	0.61500
VOLUMETRIC FLOW RATE OF GAS AT STAND. CONDITIONS, (CC/MIN)	:	413.83	BULK DENSITY OF BED, (GMS/CC)	:	1.09186
H2S CAPACITY OF ASH, (GM MOL /GM ASH)	:	0.86789E-03	SUPERFICIAL LINEAR VELOCITY, (CMS/MIN)	:	390.96970
(STD. CC/GM ASH)	:	19.441			

TIME (MIN)	TAU	WA (ASH CAPACITY) CC H2S	WM (ASH CONC.) GM MOL FE2O3 /GM ASH	CA/CAO	XB
0.00	0.0000	190.145	0.43395E-03	0.0000	0.00000
11.47	0.2525	142.118	0.32434E-03	0.0000	0.25258
30.26	0.6663	63.442	0.14479E-03	0.0000	0.66635
46.33	1.0202	19.826	0.45247E-04	0.7036	0.89573
62.27	1.3712	6.561	0.14973E-04	0.8989	0.96549
77.28	1.7018	2.275	0.51913E-05	0.9647	0.98804
94.33	2.0772	0.490	0.11181E-05	0.9853	0.99742
110.25	2.4278	0.000	0.00000E 00	1.0000	1.00000

RUN NUMBER: 046 WESTERN KY. ASH

PARTICLE DIAM., (CMS)	:	0.01510	MASS OF ASH CHARGED, (GMS)	:	9.781
APPARENT PARTICLE DENSITY, (GMS/CC)	:	2.8360	DIAMETER OF COLUMN, (CMS)	:	2.0000
BED TEMPERATURE, (DEG. F)	:	1000.00	BED LENGTH, (CMS)	:	3.048
INLET H2S CONCENTRATION, (VOL. FRACTION)	:	0.0099180	BED POROSITY, (VOID FRACTION), (VOL/VOL)	:	0.61500
VOLUMETRIC FLOW RATE OF GAS AT STAND. CONDITIONS, (CC/MIN)	:	413.83	BULK DENSITY OF BED, (GMS/CC)	:	1.09186
			SUPERFICIAL LINEAR VELOCITY, (CMS/MIN)	:	390.96970
H2S CAPACITY OF ASH, (GM MOL /GM ASH)	:	0.92964E-03			
(STD. CC/GM ASH)	:	20.824			

TIME (MIN)	TAU	WA (ASH CAPACITY) CC H2S	WM (ASH CONC.) GM MOL FE2O3 /GM ASH	CA/CAO	XB
0.00	0.0000	203.673	0.46482E-03	0.0000	0.00000
19.86	0.4002	122.160	0.27879E-03	0.0000	0.40021
35.68	0.7230	60.087	0.13713E-03	0.1119	0.70498
52.42	1.0564	21.792	0.49734E-04	0.7599	0.89300
68.53	1.3810	10.138	0.23137E-04	0.8876	0.95022
84.58	1.7044	3.874	0.88415E-05	0.9222	0.98098
100.66	2.0289	0.663	0.15137E-05	0.9806	0.99674
117.34	2.3646	0.000	0.00000E 00	1.0000	1.00000

RUN NUMBER: 047 WESTERN KY. ASH

PARTICLE DIAM., (CMS)	:	0.01510	MASS OF ASH CHARGED, (GMS)	:	9.781
APPARENT PARTICLE DENSITY, (GMS/CC)	:	2.8360	DIAMETER OF COLUMN, (CMS)	:	2.0000
BED TEMPERATURE, (DEG. F)	:	1000.00	BED LENGTH, (CMS)	:	3.048
INLET H2S CONCENTRATION, (VOL. FRACTION)	:	0.0100100	BED POROSITY, (VOID FRACTION), (VOL/VOL)	:	0.61500
VOLUMETRIC FLOW RATE OF GAS AT STAND. CONDITIONS, (CC/MIN)	:	413.83	BULK DENSITY OF BED, (GMS/CC)	:	1.09186
			SUPERFICIAL LINEAR VELOCITY, (CMS/MIN)	:	390.96970
H2S CAPACITY OF ASH, (GM MOL /GM ASH)	:	0.10027E-02			
(STD. CC/GM ASH)	:	22.460			

TIME (MIN)	TAU	WA (ASH CAPACITY) CC H2S	WM (ASH CONC.) GM MOL FE2O3 /GM ASH	CA/CAO	XB
0.00	0.0030	219.670	0.50133E-03	0.0000	0.00000
2.81	0.0530	208.030	0.47476E-03	0.0000	0.05299
20.20	0.3809	135.993	0.31036E-03	0.0000	0.38092
38.37	0.7236	64.330	0.14581E-03	0.0958	0.70715
55.69	1.0502	23.803	0.54324E-04	0.7745	0.89164
72.51	1.3674	11.979	0.27339E-04	0.8861	0.94547
89.42	1.6862	5.521	0.12599E-04	0.9295	0.97487
106.08	2.0004	1.542	0.35195E-05	0.9552	0.99298
122.70	2.3136	0.000	0.00000E 00	1.0000	1.00000

RUN NUMBER: 048 WESTERN KY. ASH

PARTICLE DIAM., (CMS)	:	0.01510	MASS OF ASH CHARGED, (GMS)	:	9.781
APPARENT PARTICLE DENSITY, (GMS/CC)	:	2.8360	DIAMETER OF COLUMN, (CMS)	:	2.0000
BED TEMPERATURE, (DEG. F)	:	1200.00	BED LENGTH, (CMS)	:	3.048
INLET H2S CONCENTRATION, (VOL. FRACTION)	:	0.0098450	BED POROSITY, (VOID FRACTION), (VOL/VOL)	:	0.61500
VOLUMETRIC FLOW RATE OF GAS AT STAND. CONDITIONS, (CC/MIN)	:	406.47	BULK DENSITY OF BED, (GMS/CC)	:	1.09186
			SUPERFICIAL LINEAR VELOCITY, (CMS/MIN)	:	436.62470
H2S CAPACITY OF ASH, (GM MOL /GM ASH)	:	0.11414E-02			
(STD. CC/GM ASH)	:	25.568			

TIME (MIN)	TAU	WA (ASH CAPACITY) CC H2S	WM (ASH CONC.) GM MOL FE2O3 /GM ASH	CA/CAO	XB
0.00	0.0000	250.073	0.57071E-03	0.0000	0.00000
3.41	0.0546	236.427	0.53957E-03	0.0000	0.05457
20.10	0.3216	169.638	0.38715E-03	0.0000	0.32165
47.95	0.7673	58.189	0.13280E-03	0.0000	0.76731
51.00	0.8161	45.984	0.10494E-03	0.0000	0.81612
63.98	1.0239	14.374	0.32804E-04	0.7829	0.94252
80.61	1.2899	5.174	0.11807E-04	0.9406	0.97931
97.46	1.5596	1.961	0.44747E-05	0.9641	0.99216
113.58	1.8175	0.406	0.92672E-06	0.9877	0.99838
130.06	2.0810	0.000	0.00000E 00	1.0000	1.00000

RUN NUMBER: 049 WESTERN KY. ASH

PARTICLE DIAM., (CMS)	: 0.01510	MASS OF ASH CHARGED, (GMS)	: 9.781
APPARENT PARTICLE DENSITY, (GM/CC)	: 2.8360	DIAMETER OF COLUMN, (CMS)	: 2.0000
BED TEMPERATURE, (DEG. F)	: 1200.00	BED LENGTH, (CMS)	: 3.048
INLET H2S CONCENTRATION, (VOL. FRACTION)	: 0.0099590	BED POROSITY, (VOID FRACTION), (VOL/VOL)	: 0.61500
VOLUMETRIC FLOW RATE OF GAS AT STAND. CONDITIONS, (CC/MIN)	: 406.47	BULK DENSITY OF BED, (GMS/CC)	: 1.09186
H2S CAPACITY OF ASH, (GM MOL /GM ASH)	: 0.11682E-02	SUPERFICIAL LINEAR VELOCITY, (CMS/MIN)	: 436.62470
(STD. CC/GM ASH)	: 26.167		

TIME (MIN)	TAU	WA (ASH CAPACITY) GC H2S	WM (ASH CONC.) GM-MOL FE2O3 /GM ASH	CA/CAO	XB
0.00	0.0000	255.934	0.58609E-03	0.0000	0.00000
34.60	0.5508	135.060	0.26259E-03	0.0000	0.55043
51.00	0.8067	49.481	0.11293E-03	0.0000	0.80666
52.67	0.8381	43.056	0.98263E-04	0.0992	0.83177
69.22	1.0948	8.122	0.18535E-04	0.8579	0.96827
85.42	1.3511	2.174	0.49605E-05	0.9607	0.99151
101.55	1.6062	0.456	0.10413E-05	0.9867	0.99822
118.50	1.8743	0.000	0.00000E 00	1.0000	1.00000

RUN NUMBER: 050 WESTERN KY. ASH

PARTICLE DIAM., (CMS)	:	0.01510	MASS OF ASH CHARGED, (GMS)	:	9.781
APPARENT PARTICLE DENSITY, (GMS/CC)	:	2.8360	DIAMETER OF COLUMN, (CMS)	:	2.0000
BED TEMPERATURE, (DEG. F)	:	1000.00	BED LENGTH, (CMS)	:	3.048
INLET H2S CONCENTRATION, (VOL. FRACTION)	:	0.0100310	BED POROSITY, (VOID FRACTION), (VOL/VOL)	:	0.61500
VOLUMETRIC FLOW RATE OF GAS AT STAND. CONDITIONS, (CC/MIN)	:	413.83	BULK DENSITY OF BED, (GMS/CC)	:	1.09186
			SUPERFICIAL LINEAR VELOCITY, (CMS/MIN)	:	390.96970
H2S CAPACITY OF ASH, (GM MOL /GM ASH)	:	0.86420E-03			
(STD. CC/GM ASH)	:	19.358			

TIME (MIN)	TAU	WA (ASH CAPACITY) CC H2S	WM (ASH CONC.) GM MOL FE2O3 /GM ASH	CA/CAO	XB
0.00	0.0000	189.337	0.43210E-03	0.0000	0.00000
3.52	0.0772	174.725	0.39875E-03	0.0000	0.07717
20.53	0.4501	104.114	0.23761E-03	0.0000	0.45011
40.22	0.8818	44.246	0.10098E-03	0.5351	0.76631
57.39	1.2583	21.046	0.48031E-04	0.8139	0.88884
74.09	1.6244	11.251	0.25676E-04	0.9035	0.94058
90.92	1.9934	5.812	0.13263E-04	0.9408	0.96931
107.97	2.3672	2.372	0.54131E-05	0.9620	0.98747
125.10	2.7428	0.505	0.11532E-05	0.9859	0.99733
141.89	3.1109	0.000	0.00000E 00	1.0000	1.00000

RUN NUMBER: 051 WESTERN KY. ASH

PARTICLE DIAM., (CMS)	:	0.01510	MASS OF ASH CHARGED, (GMS)	:	9.781
APPARENT PARTICLE DENSITY, (GMS/CC)	:	2.8360	DIAMETER OF COLUMN, (CMS)	:	2.0000
BED TEMPERATURE, (DEG. F)	:	1000.00	BED LENGTH, (CMS)	:	3.048
INLET H2S CONCENTRATION, (VOL. FRACTION)	:	0.0100370	BED POROSITY, (VOID FRACTION), (VOL/VOL)	:	0.61500
VOLUMETRIC FLOW RATE OF GAS AT STAND. CONDITIONS, (CC/MIN)	:	413.83	BULK DENSITY OF BED, (GMS/CC)	:	1.09186
H2S CAPACITY OF ASH, (GM MOL /GM ASH)	:	0.86709E-03	SUPERFICIAL LINEAR VELOCITY, (CMS/MIN)	:	390.96970
(STD. CC/GM ASH)	:	19.423			

TIME (MIN)	TAU	WA (ASH CAPACITY) CC H2S	WM (ASH CONC.) GM MOL FE2O3 /GM ASH	CA/CAO	XB
0.00	0.0000	189.969	0.43355E-03	0.0000	0.00000
2.29	0.0501	180.457	0.41184E-03	0.0000	0.05007
19.08	0.4172	110.718	0.25268E-03	0.0000	0.41718
37.84	0.8274	47.457	0.10831E-03	0.3763	0.75019
54.89	1.2002	18.687	0.42647E-04	0.8112	0.90163
71.18	1.5563	8.970	0.20472E-04	0.9016	0.95278
87.22	1.9070	4.067	0.92812E-05	0.9512	0.97859
119.95	2.6227	0.247	0.56292E-06	0.9926	0.99870
136.00	2.9736	0.000	0.00000E 00	1.0000	1.00000

RUN NUMBER 052 WESTERN KY. ASH

PARTICLE DIAM., (CMS)	:	0.01510	MASS OF ASH CHARGED, (GMS)	:	9.781
APPARENT PARTICLE DENSITY, (GMS/CC)	:	2.8360	DIAMETER OF COLUMN, (CMS)	:	2.0000
BED TEMPERATURE, (DEG. F)	:	1000.00	BED LENGTH, (CMS)	:	3.048
INLET H2S CONCENTRATION, (VOL. FRACTION)	:	0.0098840	BED POROSITY, (VOID FRACTION), (VOL/VOL)	:	0.61500
VOLUMETRIC FLOW RATE OF GAS AT STAND. CONDITIONS, (CC/MIN)	:	413.83	BULK DENSITY OF BED, (GMS/CC)	:	1.09186
			SUPERFICIAL LINEAR VELOCITY, (CMS/MIN)	:	390.96970
H2S CAPACITY OF ASH, (GM MOL /GM ASH)	:	0.10027E-02			
(STD. CC/GM ASH)	:	22.461			

TIME (MIN)	TAU	WA (ASH CAPACITY) CC H2S	WM (ASH CONC.) GM MOL FE2O3 /GM ASH	CA/CAO	XB
0.00	0.0000	219.687	0.50137E-03	0.0000	0.00000
2.49	0.0421	210.443	0.48027E-03	0.0000	0.04208
14.00	0.3538	141.971	0.32401E-03	0.0000	0.35376
35.00	0.6517	76.527	0.17465E-03	0.0000	0.65166
36.03	0.6706	72.370	0.16516E-03	0.0270	0.67058
52.18	0.9715	30.238	0.69010E-04	0.6974	0.86236
60.84	1.2817	15.321	0.34966E-04	0.8648	0.93026
65.30	1.5826	8.525	0.18999E-04	0.9235	0.96211
101.40	1.8879	4.387	0.10012E-04	0.9591	0.98003
135.92	2.5307	0.497	0.11347E-05	0.9858	0.99774
153.04	2.8494	0.000	0.00000E 00	1.0000	1.00000

RUN NUMBER: 053 WESTERN KY. ASH

PARTICLE DIAM., (CMS)	: 0.01510	MASS OF ASH CHARGED, (GMS)	: 9.781
APPARENT PARTICLE DENSITY, (GMS/CC)	: 2.6360	DIAMETER OF COLUMN, (CMS)	: 2.0000
BED TEMPERATURE, (DEG. F)	: 1000.00	BED LENGTH, (CMS)	: 3.048
INLET H2S CONCENTRATION, (VOL. FRACTION)	: 0.0059370	BED POROSITY, (VOID FRACTION), (VOL/VOL)	: 0.61500
VOLUMETRIC FLOW RATE OF GAS AT STAND. CONDITIONS, (CC/MIN)	: 413.83	BULK DENSITY OF BED, (GMS/CC)	: 1.09186
		SUPERFICIAL LINEAR VELOCITY, (CMS/MIN)	: 390.96970
H2S CAPACITY OF ASH, (GM MOL /GM ASH)	: 0.99006E-03		
(STD. CC/GM ASH)	: 22.177		

TIME (MIN)	TAU	WA (ASH CAPACITY) CC H2S	WM (ASH CONC.) GM MOL FE2O3 /GM ASH	CA/CAO	XB
0.00	0.0000	210.910	0.49503E-03	0.0000	0.00000
2.10	0.0396	208.274	0.47532E-03	0.0000	0.03981
10.78	0.1960	139.682	0.31878E-03	0.0000	0.35604
30.00	0.6829	68.869	0.15717E-03	0.0000	0.68250
37.19	0.7051	64.067	0.14626E-03	0.0454	0.70455
53.30	1.0105	23.556	0.53760E-04	0.7310	0.89140
69.53	1.3182	10.545	0.24065E-04	0.8791	0.95139
86.56	1.6410	4.470	0.10200E-04	0.9474	0.97939
103.06	1.9538	1.806	0.41226E-05	0.9741	0.99167
119.07	2.2574	0.486	0.11101E-05	0.9858	0.99776
135.73	2.5732	0.000	0.00000E 00	1.0000	1.00000

RUN NUMBER: 054 WESTERN KY. ASH

PARTICLE DIAM., (CMS)	:	0.01510	MASS OF ASH CHARGED, (GMS)	:	9.781
APPARENT PARTICLE DENSITY, (GMS/CC)	:	2.8360	DIAMETER OF COLUMN, (CMS)	:	2.0000
BED TEMPERATURE, (DEG. F)	:	1000.00	BED LENGTH, (CMS)	:	3.048
INLET H2S CONCENTRATION, (VOL. FRACTION)	:	0.0100330	BED POROSITY, (VOID FRACTION), (VOL/VOL)	:	0.61500
VOLUMETRIC FLOW RATE OF GAS AT STAND. CONDITIONS, (CC/MIN)	:	413.83	BULK DENSITY OF BED, (GMS/CC)	:	1.09186
			SUPERFICIAL LINEAR VELOCITY, (CMS/MIN)	:	390.96970
H2S CAPACITY OF ASH, (GM MOL/GM ASH)	:	0.10103E-02			
(STD. CC/GM ASH)	:	22.631			

TIME (MIN)	TAU	WA (ASH CAPACITY) CC H2S	WM (ASH CONC.) GM MOL FE2O3 /GM ASH	CA/CAO	XB
0.00	0.0000	221.350	0.50516E-03	0.0000	0.00000
11.02	0.2067	175.595	0.40074E-03	0.0000	0.20671
30.00	0.6753	71.879	0.16404E-03	0.0000	0.67527
45.14	0.8467	42.605	0.97233E-04	0.4572	0.80752
61.32	1.1502	18.001	0.41082E-04	0.8103	0.91868
78.03	1.4036	8.094	0.18471E-04	0.9041	0.96344
96.09	1.8455	2.303	0.52559E-05	0.9589	0.98960
114.54	2.1481	0.462	0.10553E-05	0.9862	0.99791
130.66	2.4512	0.000	0.00000E 00	1.0000	1.00000

RUN NUMBER: 055 WESTERN KY. ASH

PARTICLE DIAM., (CMS)	:	0.01510	MASS OF ASH CHARGED, (GMS)	:	9.781
APPARENT PARTICLE DENSITY, (GMS/CC)	:	2.8360	DIAMETER OF COLUMN, (CMS)	:	2.0000
BED TEMPERATURE, (DEG. F)	:	900.00	BED LENGTH, (CMS)	:	3.048
INLET H2S CONCENTRATION, (VOL. FRACTION)	:	0.0100480	BED POROSITY, (VOID FRACTION), (VOL/VOL)	:	0.61500
VOLUMETRIC FLOW RATE OF GAS AT STAND. CONDITIONS, (CC/MIN)	:	413.83	BULK DENSITY OF BED, (GMS/CC)	:	1.09186
H2S CAPACITY OF ASH, (GM MOL /GM ASH)	:	0.90415E-03	SUPERFICIAL LINEAR VELOCITY, (CMS/MIN)	:	364.19090
(STD. CC/GM ASH)	:	20.253			

TIME (MIN)	TAU	WA (ASH CAPACITY) CC H2S	WM (ASH CONC.) GM MOL FE2O3 /GM ASH	CA/CAO	XB
0.00	0.0000	198.068	0.45207E-03	0.0000	0.00000
19.26	0.4043	118.002	0.26930E-03	0.0000	0.40430
35.37	0.7425	62.160	0.14191E-03	0.3334	0.68610
51.39	1.0788	31.405	0.71671E-04	0.7426	0.84146
67.40	1.4148	18.210	0.41559E-04	0.8610	0.90807
83.64	1.7557	10.552	0.24082E-04	0.9122	0.94673
99.94	2.0979	5.852	0.13355E-04	0.9491	0.97046
116.65	2.4487	2.801	0.63934E-05	0.9631	0.98586
133.36	2.7994	0.752	0.17155E-05	0.9779	0.99621
149.72	3.1429	0.000	0.00000E 00	1.0000	1.00000

RUN NUMBER: 056 WESTERN KY. ASH

PARTICLE DIAM., (CMS)	: 0.01510	MASS OF ASH CHARGED, (GMS)	: 9.781
APPARENT PARTICLE DENSITY, (GMS/CC)	: 2.8360	DIAMETER OF COLUMN, (CMS)	: 2.0000
BED TEMPERATURE, (DEG. F)	: 900.00	BED LENGTH, (CMS)	: 3.048
INLET H2S CONCENTRATION, (VOL. FRACTION)	: 0.0102090	BED POROSITY, (VOID FRACTION), (VOL/VOL)	: 0.61500
VOLUMETRIC FLOW RATE OF GAS AT STAND. CONDITIONS, (CC/MIN)	: 413.83	BULK DENSITY OF BED, (GMS/CC)	: 1.09186
		SUPERFICIAL LINEAR VELOCITY, (CMS/MIN)	: 364.19090
H2S CAPACITY OF ASH, (GM MOL /GM ASH)	: 0.99246E-03		
(STD. CC/GM ASH)	: 22.231		

TIME (MIN)	TAU	WA (ASH CAPACITY) CC H2S	WM (ASH CONC.) GM MOL FE2O3 /GM ASH	CA/CAO	XB
0.00	0.0000	217.439	0.49624E-03	0.0000	0.00000
14.03	0.2726	158.165	0.36096E-03	0.0000	0.27260
32.09	0.6352	79.330	0.18105E-03	0.0000	0.63516
49.39	0.9596	32.098	0.73253E-04	0.6611	0.85238
66.21	1.2864	15.068	0.34388E-04	0.8596	0.93070
82.80	1.6086	7.432	0.16960E-04	0.9225	0.96582
99.59	1.9355	3.222	0.73526E-05	0.9588	0.98518
116.30	2.2597	1.143	0.26078E-05	0.9823	0.99474
132.96	2.5834	0.259	0.59183E-06	0.9926	0.99881
149.55	2.9057	0.000	0.00000E 00	1.0000	1.00000

RUN NUMBER: 057 WESTERN KENTUCKY ASH

PARTICLE DIAM., (CMS)	:	0.01510	MASS OF ASH CHARGED, (GMS)	:	9.781
APPARENT PARTICLE DENSITY, (GMS/CC)	:	2.8360	DIAMETER OF COLUMN, (CMS)	:	2.0000
BED TEMPERATURE, (DEG. F)	:	900.00	BED LENGTH, (CMS)	:	3.048
INLET H2S CONCENTRATION, (VOL. FRACTION)	:	0.0100590	BED POROSITY, (VOID FRACTION), (VOL/VOL)	:	0.61500
VOLUMETRIC FLOW RATE OF GAS AT STAND. CONDITIONS, (CC/MIN)	:	413.83	BULK DENSITY OF BED, (GMS/CC)	:	1.09186
H2S CAPACITY OF ASH, (GM MOL /GM ASH)	:	0.98731E-03	SUPERFICIAL LINEAR VELOCITY, (CMS/MIN)	:	364.19090
(STD. CC/GM ASH)	:	22.116			

TIME (MIN)	TAU	NA (ASH CAPACITY) CC H2S	WM (ASH CONC.) GM MOL FE2O3 /GM ASH	CA/CAO	XB
0.00	0.0000	216.306	0.49365E-03	0.0000	0.00000
1.71	0.0329	209.188	0.47741E-03	0.0000	0.03291
17.92	0.3449	141.710	0.32341E-03	0.0000	0.34486
35.96	0.6935	74.940	0.17103E-03	0.0000	0.65355
50.27	0.9674	30.086	0.68662E-04	0.6787	0.86091
66.78	1.2852	14.358	0.32767E-04	0.8636	0.93362
84.47	1.6256	6.644	0.15163E-04	0.9269	0.96928
101.10	1.9456	2.646	0.60394E-05	0.9576	0.98777
117.47	2.2607	0.749	0.17089E-05	0.9867	0.99654
134.12	2.5811	0.000	0.00000E-00	0.9917	1.00000

RUN NUMBER 058 WESTERN KY. ASH

PARTICLE DIAM., (CMS)	:	0.01510	MASS OF ASH CHARGED, (GMS)	:	9.781
APPARENT PARTICLE DENSITY, (GMS/CC)	:	2.8360	DIAMETER OF COLUMN, (CMS)	:	2.0000
BED TEMPERATURE, (DEG. F)	:	900.00	BED LENGTH, (CMS)	:	3.048
INLET H2S CONCENTRATION, (VOL. FRACTION)	:	0.0100920	BED POROSITY, (VOID FRACTION), (VOL/VOL)	:	0.61500
VOLUMETRIC FLOW RATE OF GAS AT STAND. CONDITIONS, (CC/MIN)	:	413.83	BULK DENSITY OF BED, (GMS/CC)	:	1.09186
			SUPERFICIAL LINEAR VELOCITY, (CMS/MIN)	:	364.19090
H2S CAPACITY OF ASH, (GM MOL /GM ASH)	:	0.99229E-03			
(STD. CC/GM ASH)	:	22.227			

TIME (MIN)	FA	WA (ASH CAPACITY) CC H2S	WM (ASH CONC.) GM MOL FE2O3 /GM ASH	CA/CAO	XB
0.00	0.0000	217.399	0.49615E-03	0.0000	0.00000
2.53	0.0400	208.833	0.47203E-03	0.0000	0.04860
18.74	0.3600	139.134	0.31753E-03	0.0000	0.36001
32.00	0.5147	83.755	0.19114E-03	0.0000	0.61474
36.39	0.5991	66.865	0.15214E-03	0.1358	0.69335
52.87	1.0157	28.129	0.64197E-04	0.7444	0.87061
69.58	1.3367	14.709	0.33569E-04	0.8710	0.93234
86.29	1.6577	7.779	0.17754E-04	0.9304	0.96422
103.16	1.9822	3.847	0.87790E-05	0.9581	0.98231
120.07	2.3105	1.545	0.35258E-05	0.9774	0.99289
136.99	2.6317	0.382	0.87247E-06	0.9893	0.99824
154.10	2.9604	0.000	0.00000E 00	1.0000	1.00000

RUN NUMBER: 059 WESTERN KY. ASH

PARTICLE DIAM., (CMS)	:	0.01510	MASS OF ASH CHARGED, (GMS)	:	9.781
APPARENT PARTICLE DENSITY, (GMS/CC)	:	2.8350	DIAMETER OF COLUMN, (CMS)	:	2.0000
BED TEMPERATURE, (DEG. F)	:	1200.00	BED LENGTH, (CMS)	:	3.048
INLET H2S CONCENTRATION, (VOL. FRACTION)	:	0.0092030	BED POROSITY, (VOID FRACTION), (VOL/VOL)	:	0.61500
VOLUMETRIC FLOW RATE OF GAS AT STAND. CONDITIONS, (CC/MIN)	:	406.47	BULK DENSITY OF BED, (GMS/CC)	:	1.09186
			SUPERFICIAL LINEAR VELOCITY, (CMS/MIN)	:	436.02470
H2S CAPACITY OF ASH, (GM MOL /GM ASH)	:	0.11016E-02			
(STD. CC/GM ASH)	:	24.677			

TIME (MIN)	TAU	WA (ASH CAPACITY) CC H2S	WM (ASH CONC.) GM MOL FE2O3 /GM ASH	CA/CAO	XB
0.00	0.0000	241.358	0.55082E-03	0.0000	0.00000
2.85	0.0442	230.700	0.52650E-03	0.0000	0.04416
19.63	0.3041	867.950	0.33329E-03	0.0000	0.30414
36.14	0.5599	106.210	0.24239E-03	0.0000	0.55995
53.70	0.8320	41.138	0.93884E-04	0.0181	0.82956
70.16	1.0870	7.105	0.16214E-04	0.8761	0.97056
86.87	1.3460	1.650	0.37646E-05	0.9493	0.99317
103.28	1.6002	0.048	0.10931E-06	0.9985	0.99980
120.36	1.8648	0.000	0.00000E 00	1.0000	1.00000

RUN NUMBER: 061 WESTERN KY. ASH

PARTICLE DIAM., (CMS)	:	0.01510	MASS OF ASH CHARGED, (GMS)	:	9.781
APPARENT PARTICLE DENSITY, (GMS/CC)	:	2.8360	DIAMETER OF COLUMN, (CMS)	:	2.0000
BED TEMPERATURE, (DEG. F)	:	1400.00	BED LENGTH, (CMS)	:	3.048
INLET H2S CONCENTRATION, (VOL. FRACTION)	:	0.0098890	BED POROSITY, (VOID FRACTION), (VOL/VOL)	:	0.61500
VOLUMETRIC FLOW RATE OF GAS AT STAND. CONDITIONS, (CC/MIN)	:	404.64	BULK DENSITY OF BED, (GMS/CC)	:	1.09186
H2S CAPACITY OF ASH, (GM MOL /GM ASH)	:	0.12485E-02	SUPERFICIAL LINEAR VELOCITY, (CMS/MIN)	:	867.01660
(STD. CC/GM ASH)	:	27.965			

TIME (MIN)	TAU	WA (ASH CAPACITY) CC. H2S	WM (ASH CONC.) GM MOL FE2O3 /GM ASH	CA/CAO	XB
0.00	0.0000	273.521	0.62423E-03	0.0000	0.00000
23.65	0.3460	178.887	0.40825E-03	0.0000	0.34598
40.36	0.5904	112.254	0.25618E-03	0.0069	0.58960
57.08	0.8350	46.363	0.10581E-03	0.0234	0.83049
73.78	1.0794	9.086	0.20735E-04	0.8609	0.96678
90.48	1.3237	3.028	0.69112E-05	0.9578	0.98893
107.22	1.5680	1.083	0.24705E-05	0.9841	0.99604
123.89	1.8124	0.276	0.62905E-06	0.9917	0.99899
140.58	2.0554	0.000	0.000000E 00	1.0000	1.00000

PUN NUMBER: 075 WESTERN KY. ASH

PARTICLE DIAM., (CMS)	:	0.01065	MASS OF ASH CHARGED, (GMS)	:	9.578
APPARENT PARTICLE DENSITY, (GMS/CC)	:	2.9500	DIAMETER OF COLUMN, (CMS)	:	2.0000
BED TEMPERATURE, (DEG. F)	:	1000.00	BED LENGTH, (CMS)	:	3.175
INLET H2S CONCENTRATION, (VOL. FRACTION)	:	0.0122480	BED POROSITY, (VOID FRACTION), (VOL/VOL)	:	0.62500
VOLUMETRIC FLOW RATE OF GAS AT STAND. CONDITIONS, (CC/MIN)	:	354.06	BULK DENSITY OF BED, (GMS/CC)	:	1.10625
H2S CAPACITY OF ASH, (GM MOL /GM ASH)	:	0.12928E-02	SUPERFICIAL LINEAR VELOCITY, (CMS/MIN)	:	334.49630
(STD. CC/GM ASH)	:	28.958			

TIME (MIN)	TAU	WA (ASH CAPACITY) CC H2S	WM (ASH CONC.) GM MOL FE2O3 /GM ASH	CA/CAO	XB
0.00	0.0000	247.352	0.64539E-03	0.0000	0.00000
2.85	0.0446	224.992	0.61758E-03	0.0000	0.04456
20.50	0.3215	138.194	0.43860E-03	0.0000	0.32146
42.31	0.6615	43.875	0.21378E-03	0.0000	0.66153
59.20	0.9256	10.781	0.95044E-04	0.5502	0.85296
76.54	1.1967	18.242	0.42514E-04	0.8503	0.93423
93.30	1.4588	10.236	0.23856E-04	0.9294	0.96309
110.10	1.7214	5.829	0.13585E-04	0.9496	0.97848
126.90	1.9841	2.933	0.68368E-05	0.9709	0.98942
143.60	2.2464	1.039	0.24210E-05	0.9774	0.99625
165.00	2.5798	0.000	0.00000E 00	1.0000	1.00000

RUN NUMBER: 076 WESTERN KY. ASH

PARTICLE DIAM., (CMS)	:	0.01065	MASS OF ASH CHARGED, (GMS)	:	9.578
APPARENT PARTICLE DENSITY, (GMS/CC)	:	2.9500	DIAMETER OF COLUMN, (CMS)	:	2.0000
BED TEMPERATURE, (DEG. F)	:	1000.00	BED LENGTH, (CMS)	:	3.175
INLET H2S CONCENTRATION, (VOL. FRACTION)	:	0.0125140	BED POROSITY, (VOID FRACTION), (VOL/VOL)	:	0.62500
VOLUMETRIC FLOW RATE OF GAS AT STAND. CONDITIONS, (CC/MIN)	:	354.06	BULK DENSITY OF BED, (GMS/CC)	:	1.10625
			SUPERFICIAL LINEAR VELOCITY, (CMS/MIN)	:	334.49630
H2S CAPACITY OF ASH, (GM MOL /GM ASH)	:	0.1299BE-02			
(STD. CC/GM ASH)	:	29.116			

TIME (MIN)	FAU	WA (ASH CAPACITY) CC H2S	WM (ASH CONC.) GM MOL FE2O3 /GM ASH	CA/CAO	XB
0.00	0.0000	270.860	0.64990E-03	0.0000	0.00000
4.87	0.0774	257.283	0.59961E-03	0.0000	0.07738
43.50	0.6911	86.127	0.20072E-03	0.0000	0.69115
45.10	0.7166	79.311	0.18484E-03	0.0772	0.71559
64.01	1.0170	28.383	0.66149E-04	0.7071	0.89822
81.42	1.2936	12.616	0.29403E-04	0.8841	0.95476
98.10	1.5587	6.198	0.14445E-04	0.9422	0.97777
114.82	1.8243	2.846	0.66327E-05	0.9673	0.98979
132.44	2.1043	0.766	0.17843E-05	0.9794	0.99725
149.22	2.3709	0.000	0.00000E 00	1.0000	1.00000

RUN NUMBER: 077 WESTERN KY. ASH

PARTICLE DIAM., (CMS)	:	0.01065	MASS OF ASH CHARGED, (GMS)	:	9.578
APPARENT PARTICLE DENSITY, (GMS/CC)	:	2.9500	DIAMETER OF COLUMN, (CMS)	:	2.0000
BED TEMPERATURE, (DEG. F)	:	1000.00	BED LENGTH, (CMS)	:	3.175
INLET H2S CONCENTRATION, (VOL. FRACTION)	:	0.0124620	BED POROSITY, (VOID FRACTION), (VOL/VOL)	:	0.62500
VOLUMETRIC FLOW RATE OF GAS AT STAND. CONDITIONS, (CC/MIN)	:	413.83	BULK DENSITY OF BED, (GMS/CC)	:	1.10625
			SUPERFICIAL LINEAR VELOCITY, (CMS/MIN)	:	390.96970
H2S CAPACITY OF ASH, (GM MOL /GM ASH)	:	0.125708E-02			
(STD. CC/GM ASH)	:	28.156			

TIME (MIN)	TAU	WA (ASH CAPACITY) CC H2S	WM (ASH CONC.) GM MOL FE2O3 /GM ASH	CA/CAO	XB
0.00	0.0000	269.674	0.628849E-03	0.0000	0.00000
4.68	0.0895	245.538	0.572246-03	0.0000	0.08950
20.76	0.3970	162.611	0.379898E-03	0.0000	0.39701
34.00	0.6502	94.330	0.219846-03	0.0000	0.65021
36.77	0.7032	80.749	0.188196-03	0.0986	0.70057
53.26	1.0185	31.497	0.734066-04	0.7431	0.88320
69.95	1.3377	15.638	0.364466-04	0.8884	0.94201
86.63	1.6561	8.164	0.190266-04	0.9375	0.96973
103.35	1.9764	3.983	0.928196-05	0.9657	0.98523
121.06	2.3151	1.389	0.323706-05	0.9775	0.99465
145.00	2.7729	0.000	0.000006 00	1.0000	1.00000

RUN NUMBER: 078 WESTERN KY. ASH

PARTICLE DIAM., (CMS)	:	0.01065	MASS OF ASH CHARGED, (GMS)	:	9.578
APPARENT PARTICLE DENSITY,(GMS/CC)	:	2.9500	DIAMETER OF COLUMN, (CMS)	:	2.0000
BED TEMPERATURE, (DEG. F)	:	1000.00	BED LENGTH, (CMS)	:	3.175
INLET H2S CONCENTRATION, (VOL. FRACTION)	:	0.0099960	BED POROSITY, (VOID FRACTION), (VOL/VOL)	:	0.62500
VOLUMETRIC FLOW RATE OF GAS AT STAND. CONDITIONS, (CC/MIN)	:	413.83	BULK DENSITY OF BED, (GMS/CC)	:	1.10625
H2S CAPACITY OF ASH, (GM MOL /GM ASH)	:	0.13026E-02	SUPERFICIAL LINEAR VELOCITY, (CMS/MIN)	:	390.96970
(STD. CC/GM ASH)	:	29.178			

TIME (MIN)	TAU	WA (ASH CAPACITY) CC H2S	WM (ASH CONC.) GM MOL FE2O3 /GM ASH	CA/CAO	XB
0.00	0.0000	279.454	0.65129E-03	0.0000	0.00000
4.56	0.0675	260.591	0.60732E-03	0.0000	0.06750
22.95	0.3397	184.518	0.43003E-03	0.0000	0.33972
45.95	0.6802	89.375	0.20829E-03	0.0000	0.68018
48.00	0.7105	80.895	0.18853E-03	0.0000	0.71053
61.99	0.9176	38.220	0.89074E-04	0.5252	0.86323
78.70	1.1650	16.256	0.37886E-04	0.8393	0.94183
95.04	1.4157	7.998	0.18639E-04	0.9250	0.97138
112.56	1.6662	3.847	0.89646E-05	0.9564	0.98623
129.55	1.9177	1.641	0.38236E-05	0.9808	0.99413
147.97	2.1903	0.437	0.10179E-05	0.9876	0.99844
165.00	2.4424	0.000	0.00000E 00	1.0000	1.00000

RUN NUMBER: 060 WESTERN KY. ASH

PARTICLE DIAM., (CMS)	:	0.01065	MASS OF ASH CHARGED, (GMS)	:	9.578
APPARENT PARTICLE DENSITY, (GMS/CC)	:	2.9500	DIAMETER OF COLUMN, (CMS)	:	2.0000
BED TEMPERATURE, (DEG. F)	:	900.00	BED LENGTH, (CMS)	:	3.175
INLET H2S CONCENTRATION, (VOL. FRACTION)	:	0.0125350	BED POROSITY, (VOID FRACTION), (VOL/VOL)	:	0.62500
VOLUMETRIC FLOW RATE OF GAS AT STAND. CONDITIONS, (CC/MIN)	:	354.06	BULK DENSITY OF BED, (GMS/CC)	:	1.10625
			SUPERFICIAL LINEAR VELOCITY, (CMS/MIN)	:	311.58560
H2S CAPACITY OF ASH, (GM MOL /GM ASH)	:	0.12480E-02			
(STD. CC/GM ASH)	:	27.955			

TIME (MIN)	TAU	WA (ASH CAPACITY) CC H2S	WM (ASH CONC.) GM MOL FE2O3 /GM ASH	CA/CAO	XB
0.00	0.0000	267.746	0.62400E-03	0.0000	0.00000
17.22	0.2654	191.324	0.44589E-03	0.0000	0.28543
33.41	0.5536	119.471	0.27843E-03	0.0000	0.55379
40.50	0.6813	88.005	0.20510E-03	0.0000	0.67131
49.30	0.8172	56.585	0.13187E-03	0.3910	0.78866
65.30	1.0824	27.450	0.63974E-04	0.7884	0.89748
82.00	1.3592	15.417	0.35931E-04	0.8869	0.94242
98.75	1.6368	8.612	0.20070E-04	0.9300	0.96784
115.40	1.9128	4.488	0.10460E-04	0.9584	0.98324
132.19	2.1911	1.989	0.46344E-05	0.9745	0.99257
149.36	2.4757	0.529	0.12336E-05	0.9872	0.99802
166.00	2.7517	0.000	0.00000E 00	1.0000	1.00000

RUN NUMBER: 081 WESTERN KY. ASH

PARTICLE DIAM., (CMS)	:	0.01065	MASS OF ASH CHARGED, (GMS)	:	9.578
APPARENT PARTICLE DENSITY, (GMS/CC)	:	2.9500	DIAMETER OF COLUMN, (CMS)	:	2.0000
BED TEMPERATURE, (DEG. F)	:	900.00	BED LENGTH, (CMS)	:	3.175
INLET H2S CONCENTRATION, (VOL. FRACTION)	:	0.0125480	BED POROSITY, (VOID FRACTION), (VOL/VOL)	:	0.62500
VOLUMETRIC FLOW RATE OF GAS AT STAND. CONDITIONS, (CC/MIN)	:	354.06	BULK DENSITY OF BED, (GMS/CC)	:	1.10625
H2S CAPACITY OF ASH, (GM MOL /GM ASH)	:	0.11900E-02	SUPERFICIAL LINEAR VELOCITY, (CMS/MIN)	:	311.58560
(STD. CC/GM ASH)	:	26.656			

TIME (MIN)	TAU	WA (ASH CAPACITY) CC H2S	WM (ASH CONC.) GM MOL FE2O3 /GM ASH	CA/CAO	XB
0.00	0.0000	255.308	0.59501E-03	0.0000	0.00000
13.15	0.2286	195.886	0.45886E-03	0.0000	0.22883
34.00	0.5916	104.256	0.24298E-03	0.0000	0.59165
46.45	0.8076	57.250	0.13342E-03	0.5150	0.77576
65.00	1.1311	31.468	0.73339E-04	0.7921	0.87674
81.70	1.4211	19.319	0.45025E-04	0.8804	0.92433
98.39	1.7121	11.982	0.27926E-04	0.9217	0.95307
116.21	2.0222	6.943	0.16182E-04	0.9510	0.97280
180.00	3.1322	0.000	0.00000E 00	1.0000	1.00000

RUN NUMBER: 095 ELKHORN ASH

PARTICLE DIAM., (CMS)	:	0.01935	MASS OF ASH CHARGED, (GMS)	:	9.768
APPARENT PARTICLE DENSITY, (GMS/CC)	:	2.1000	DIAMETER OF COLUMN, (CMS)	:	2.0000
BED TEMPERATURE, (DEG. F)	:	1000.00	BED LENGTH, (CMS)	:	3.048
INLET H2S CONCENTRATION, (VOL. FRACTION)	:	0.0090480	BED POROSITY, (VOID FRACTION), (VOL/VOL)	:	0.70000
VOLUMETRIC FLOW RATE OF GAS AT STAND. CONDITIONS, (CC/MIN)	:	432.22	BULK DENSITY OF BED, (GMS/CC)	:	0.63000
			SUPERFICIAL LINEAR VELOCITY, (CMS/MIN)	:	406.34640
H2S CAPACITY OF ASH, (GM MOL /GM ASH)	:	0.40212E-03			
(STD. CC/GM ASH)	:	9.008			

TIME (MIN)	TAU	WA (ASH CAPACITY) CC H2S	WM (ASH CONC.) GM MOL FE2O3 /GM ASH	CA/CAO	XB
0.00	0.0000	87.985	0.20106E-03	0.0000	0.00000
11.59	0.5112	43.011	0.98288E-04	0.0000	0.51115
13.15	0.5845	37.191	0.84988E-04	0.1962	0.57730
29.92	1.3299	7.479	0.17090E-04	0.8977	0.91500
46.34	2.0597	3.012	0.68840E-05	0.9632	0.96576
64.99	2.8887	0.883	0.20172E-05	0.9784	0.98997
81.70	3.6334	0.089	0.20280E-06	0.9973	0.99899
96.51	4.2926	0.000	0.00000E 00	1.0000	1.00000

RUN NUMBER: 096 ELKHORN ASH

PARTICLE DIAM., (CMS)	:	0.01935	MASS OF ASH CHARGED, (GMS)	:	9.768
APPARENT PARTICLE DENSITY, (GMS/CC)	:	2.1000	DIAMETER OF COLUMN, (CMS)	:	2.0000
BED TEMPERATURE, (DEG. F)	:	1000.00	BED LENGTH, (CMS)	:	3.048
INLET H2S CONCENTRATION, (VOL. FRACTION)	:	0.0098880	BED POROSITY, (VOID FRACTION), (VOL/VOL)	:	0.70000
VOLUMETRIC FLOW RATE OF GAS AT STAND. CONDITIONS, (CC/MIN)	:	432.22	BULK DENSITY OF BED, (GMS/CC)	:	0.63000
			SUPERFICIAL LINEAR VELOCITY, (CMS/MIN)	:	408.34640
H2S CAPACITY OF ASH, (GM MOL /GM ASH)	:	0.43508E-03			
(STD. CC/GM ASH)	:	9.746			

TIME (MIN)	TAU	WA (ASH CAPACITY) CC H2S	WM (ASH CONC.) GM MOL FE2O3 /GM ASH	CA/CAO	XB
0.00	0.0000	95.196	0.21754E-03	0.0000	0.00000
11.50	0.5163	46.047	0.10523E-03	0.0000	0.51629
13.70	0.6151	37.815	0.86415E-04	0.2490	0.60276
30.35	1.3626	7.807	0.17842E-04	0.9076	0.91799
47.50	2.1325	2.985	0.68204E-05	0.9608	0.96865
64.60	2.8993	1.067	0.24372E-05	0.9848	0.98680
83.19	3.7600	0.206	0.46976E-06	0.9948	0.99784
102.25	4.5905	0.000	0.00000E 00	1.0000	1.00000

RUN NUMBER: 111 MONTANA ASH

PARTICLE DIAM., (CMS)	:	0.01935	MASS OF ASH CHARGED, (GMS)	:	9.573
APPARENT PARTICLE DENSITY, (GMS/CC)	:	2.0510	DIAMETER OF COLUMN, (CMS)	:	2.0000
BED TEMPERATURE, (DEG. F)	:	1000.00	BED LENGTH, (CMS)	:	3.556
INLET H2S CONCENTRATION, (VOL. FRACTION)	:	0.0101450	BED POROSITY, (VOID FRACTION), (VOL/VOL)	:	0.70600
VOLUMETRIC FLOW RATE OF GAS AT STAND. CONDITIONS, (CC/MIN)	:	432.22	BULK DENSITY OF BED, (GMS/CC)	:	0.60299
			SUPERFICIAL LINEAR VELOCITY, (CMS/MIN)	:	408.34640
RES. CAPACITY OF ASH, (GM MOL /GM ASH)	:	0.33327E-03			
(STD. CC/GM ASH)	:	7.455			

TIME (MIN)	TAU	WA (ASH CAPACITY) CC H2S	WM (ASH CONC.) GM MOL FE2O3 /GM ASH	CA/CAO	XB
0.00	0.0000	31.463	0.16563E-03	0.0000	0.00000
9.50	0.5829	29.806	0.69501E-04	0.0000	0.58291
10.61	0.6510	25.374	0.59166E-04	0.1788	0.64493
17.72	1.0873	10.203	0.23792E-04	0.8480	0.85722
20.94	1.2850	5.979	0.13941E-04	0.9430	0.91634
23.76	1.4581	2.693	0.62793E-05	0.9679	0.96232
26.90	1.6508	0.927	0.21609E-05	0.9851	0.98703
27.79	1.7054	0.186	0.43464E-06	0.9948	0.99739
94.05	5.7708	0.000	0.00000E 00	1.0000	1.00000

RUN NUMBER: 112 MONTANA ASH

PARTICLE DIAM., (CMS)	:	0.01935	MASS OF ASH CHARGED, (GMS)	:	9.573
APPARENT PARTICLE DENSITY, (GMS/CC)	:	2.0510	DIAMETER OF COLUMN, (CMS)	:	2.0000
BED TEMPERATURE, (DEG. F)	:	1000.00	BED LENGTH, (CMS)	:	3.556
INLET H2S CONCENTRATION, (VOL. FRACTION)	:	0.0100660	BED POROSITY, (VOID FRACTION), (VOL/VOL)	:	0.70600
VOLUMETRIC FLOW RATE OF GAS AT STAND. CONDITIONS, (CC/MIN)	:	432.22	BULK DENSITY OF BED, (GMS/CC)	:	0.60299
			SUPERFICIAL LINEAR VELOCITY, (CMS/MIN)	:	408.34640
H2S CAPACITY OF ASH, (GM MOL /GM ASH)	:	0.35538E-03			
(STD. CC/GM ASH)	:	7.961			

TIME (MIN)	TAU	WA (ASH CAPACITY) CC H2S	WM (ASH CONC.) GM MOL FE2O3 /GM ASH	CA/CAO	XB
0.00	0.0000	79.205	0.17769E-03	0.0000	0.00000
9.50	0.5424	34.873	0.81314E-04	0.0000	0.54238
10.45	0.5966	31.102	0.72522E-04	0.1755	0.59186
17.72	1.0117	15.659	0.36512E-04	0.8480	0.79452
27.18	1.5518	10.923	0.25471E-04	0.9219	0.85666
44.00	2.5121	6.525	0.15215E-04	0.9579	0.91437
60.68	3.4644	3.938	0.91828E-05	0.9708	0.94832
77.35	4.4179	2.158	0.50320E-05	0.9802	0.97168
94.10	5.3725	0.870	0.20297E-05	0.9844	0.98858
119.75	6.8364	0.000	0.00000E 00	1.0000	1.00000

RUN NUMBER: 113 MONTANA ASH

PARTICLE DIAM., (CMS)	0.01438	MASS OF ASH CHARGED, (GMS)	9.573
APPARENT PARTICLE DENSITY, (GMS/CC)	2.0510	DIAMETER OF COLUMN, (CMS)	2.0000
BED TEMPERATURE, (DEG. F)	1000.00	BED LENGTH, (CMS)	3.556
INLET H2S CONCENTRATION, (VOL. FRACTION)	0.0100030	BED POROSITY, (VOID FRACTION), (VOL/VOL)	0.70600
VOLUMETRIC FLOW RATE OF GAS AT STAND. CONDITIONS, (CC/MIN)	432.22	BULK DENSITY OF BED, (GMS/CC)	0.60299
H2S CAPACITY OF ASH, (GM MOL /GM ASH)	0.33413E-03	SUPERFICIAL LINEAR VELOCITY, (CMS/MIN)	408.34640
(STD. CC/GM ASH)	7.485		

TIME (MIN)	TAU	WA (ASH CAPACITY) CC H2S	WM (ASH CONC.) GM MOL FE2O3 /GM ASH	CA/CAO	XB
0.00	0.0000	71.649	0.16107E-03	0.0000	0.00000
5.50	0.5735	30.575	0.71294E-04	0.0000	0.57326
9.96	0.6010	28.614	0.66720E-04	0.0277	0.60064
17.72	1.0693	9.753	0.22742E-04	0.8480	0.86387
26.69	1.6082	5.531	0.12898E-04	0.9333	0.92280
43.46	2.6257	2.319	0.54069E-05	0.9784	0.96764
60.48	3.6495	0.941	0.21935E-05	0.9841	0.98687
77.26	4.6628	0.183	0.42568E-06	0.9950	0.99745
94.15	5.6813	0.000	0.00000E 00	1.0000	1.00000

RUN NUMBER: 114 / MONTANA ASH (WATER VAPOR)

PARTICLE DIAM., (CMS)	:	0.01935	MASS OF ASH CHARGED, (GMS)	:	9.573
APPARENT PARTICLE DENSITY, (GMS/CC)	:	2.0510	DIAMETER OF COLUMN, (CMS)	:	2.0000
BED TEMPERATURE, (DEG. F)	:	1000.00	BED LENGTH, (CMS)	:	3.556
INLET H2S CONCENTRATION, (VOL. FRACTION)	:	0.0097940	BED POROSITY, (VOID FRACTION), (VOL/VOL)	:	0.70600
VOLUMETRIC FLOW RATE OF GAS AT STAND. CONDITIONS, (CC/MIN)	:	441.42	BULK DENSITY OF BED, (GMS/CC)	:	0.60299
			SUPERFICIAL LINEAR VELOCITY, (CMS/MIN)	:	417.03440
H2S CAPACITY OF ASH, (GM MOL /GM ASH)	:	0.31488E-03			
(STD. CC/GM ASH)	:	7.053			

TIME (MIN)	TAU	WA (ASH CAPACITY) CC H2S	WM (ASH CONC.) GM MOL FE2O3 /GM ASH	CA/CAO	XB
0.00	0.0000	67.520	0.15744E-03	0.0000	0.00000
9.50	0.5083	26.449	0.61673E-04	0.0000	0.60828
10.57	0.6040	23.017	0.53670E-04	0.1750	0.65911
17.72	1.1346	7.495	0.17476E-04	0.8480	0.88900
27.50	1.7608	3.252	0.75820E-05	0.9513	0.95184
44.26	2.6339	0.984	0.22938E-05	0.9861	0.98543
77.60	4.9302	0.000	0.00000E 00	1.0000	1.00000

RUN NUMBER: 118 WESTERN KY. ASH

PARTICLE DIAM., (CMS)	:	0.01510	MASS OF ASH CHARGED, (GMS)	:	9.809
APPARENT PARTICLE DENSITY, (GMS/CC)	:	2.8360	DIAMETER OF COLUMN, (CMS)	:	2.0000
BED TEMPERATURE, (DEG. F)	:	1000.00	BED LENGTH, (CMS)	:	3.048
INLET H2S CONCENTRATION, (VOL. FRACTION)	:	0.0098510	BED POROSITY, (VOID FRACTION), (VOL/VOL)	:	0.61500
VOLUMETRIC FLOW RATE OF GAS AT STAND. CONDITIONS, (CC/MIN)	:	469.81	BULK DENSITY OF BED, (GMS/CC)	:	1.09186
H2S CAPACITY OF ASH, (GM MOL /GM ASH)	:	0.10223E-02	SUPERFICIAL LINEAR VELOCITY, (CMS/MIN)	:	443.09930
(STD. CC/GM ASH)	:	22.900			

TIME (MIN)	TAU	WA (ASH CAPACITY) CC H2S	WM (ASH CONC.) GM MOL FE2O3 /GM ASH	CA/CAO	XB
0.00	0.0000	224.621	0.51116E-03	0.0000	0.00000
11.58	0.2382	171.119	0.38941E-03	0.0000	0.23819
33.26	0.6841	78.736	0.17918E-03	0.1554	0.64947
49.77	1.0237	35.689	0.81672E-04	0.7212	0.84022
66.61	1.3701	19.737	0.44915E-04	0.8636	0.91213
83.45	1.7165	11.311	0.25740E-04	0.9198	0.94964
100.30	2.0631	6.231	0.14180E-04	0.9497	0.97226
117.15	2.4096	3.148	0.71646E-05	0.9711	0.98598
133.95	2.7552	1.313	0.29871E-05	0.9816	0.99416
150.80	3.1018	0.293	0.66632E-06	0.9922	0.99870
167.05	3.4360	0.000	0.00000E 00	1.0000	1.00000

RUN NUMBER: 119 WESTERN KY. ASH

PARTICLE DIAM., (CMS)	:	0.01510	MASS OF ASH CHARGED, (GMS)	:	9.809
APPARENT PARTICLE DENSITY, (GMS/CC)	:	2.8360	DIAMETER OF COLUMN, (CMS)	:	2.0000
BED TEMPERATURE, (DEG. F)	:	1000.00	BED LENGTH, (CMS)	:	3.048
INLET H2S CONCENTRATION, (VOL. FRACTION)	:	0.0098330	BED POROSITY, (VOID FRACTION), (VOL/VOL)	:	0.61500
VOLUMETRIC FLOW RATE OF GAS AT STAND. CONDITIONS, (CC/MIN)	:	469.01	BULK DENSITY OF BED, (GMS/CC)	:	1.09186
			SUPERFICIAL LINEAR VELOCITY, (CMS/MIN)	:	443.09930
H2S CAPACITY OF ASH, (GM MOL /GM ASH)	:	0.10864E-02			
(STD. CC/GM ASH)	:	24.335			

TIME (MIN)	TAU	WA (ASH CAPACITY) CC H2S	WM (ASH CONC.) GM MOL FE2O3 /GM ASH	CA/CAO	XB
0.00	0.0000	238.698	0.54320E-03	0.0000	0.00000
11.98	0.2315	183.449	0.41747E-03	0.0000	0.23146
31.42	0.6071	93.796	0.21345E-03	0.0000	0.60705
48.34	0.9340	38.562	0.87754E-04	0.5843	0.83845
67.95	1.3128	13.646	0.31054E-04	0.8647	0.94283
84.84	1.6392	5.923	0.13479E-04	0.9370	0.97519
101.62	1.9634	2.216	0.50439E-05	0.9672	0.99071
117.45	2.2692	0.687	0.15634E-05	0.9909	0.99712
139.50	2.6952	0.107	0.24439E-06	0.9977	0.99955
159.75	3.0865	0.000	0.00000E 00	1.0000	1.00000

RUN NUMBER: 120 WESTERN KY. ASH

PARTICLE DIAM., (CMS)	:	0.01510	MASS OF ASH CHARGED, (GMS)	:	9.809
APPARENT PARTICLE DENSITY, (GMS/CC)	:	2.8360	DIAMETER OF COLUMN, (CMS)	:	2.0000
BED TEMPERATURE, (DEG. F)	:	1000.00	BED LENGTH, (CMS)	:	3.048
INLET H2S CONCENTRATION, (VOL. FRACTION)	:	0.0100810	BED POROSITY, (VOID FRACTION), (VOL/VOL)	:	0.61500
VOLUMETRIC FLOW RATE OF GAS AT STAND. CONDITIONS, (CC/MIN)	:	469.01	BULK DENSITY OF BED, (GMS/CC)	:	1.09186
			SUPERFICIAL LINEAR VELOCITY, (CMS/MIN)	:	443.09930
H2S CAPACITY OF ASH, (GM MOL /GM ASH)	:	0.12020E-02			
(STD. CC/GM ASH)	:	26.925			

TIME (MIN)	TAU	WA (ASH CAPACITY) CC H2S	WM (ASH CONC.) GM MOL FE2O3 /GM ASH	CA/CAO	XB
0.00	0.0000	254.095	0.60100E-03	0.0000	0.00000
12.47	0.2232	205.136	0.46682E-03	0.0000	0.22325
34.25	0.6132	102.158	0.23248E-03	0.0000	0.61318
50.35	0.9014	45.200	0.10286E-03	0.5035	0.82885
67.08	1.2009	19.136	0.43548E-04	0.8375	0.92754
83.92	1.5024	9.339	0.21253E-04	0.9164	0.96464
100.13	1.7926	4.331	0.98550E-05	0.9529	0.98360
116.80	2.0911	1.588	0.36135E-05	0.9775	0.99399
136.25	2.4393	0.282	0.64226E-06	0.9941	0.99893
156.50	2.8018	0.000	0.00000E 00	1.0000	1.00000

RUN NUMBER: 121 WESTERN KY. ASH

PARTICLE DIAM., (CMS)	:	0.01510	MASS OF ASH CHARGED, (GMS)	:	9.809
APPARENT PARTICLE DENSITY, (GMS/CC)	:	2.8360	DIAMETER OF COLUMN, (CMS)	:	2.0000
BED TEMPERATURE, (DEG. F)	:	1000.00	BED LENGTH, (CMS)	:	3.048
INLET H2S CONCENTRATION, (VOL. FRACTION)	:	0.0101040	BED POROSITY, (VOID FRACTION), (VOL/VOL)	:	0.61500
VOLUMETRIC FLOW RATE OF GAS AT STAND. CONDITIONS, (CC/MIN)	:	469.01	BULK DENSITY OF BED, (GMS/CC)	:	1.09186
			SUPERFICIAL LINEAR VELOCITY, (CMS/MIN)	:	443.09930
H2S CAPACITY OF ASH, (GM MOL /GM ASH)	:	0.12055E-02			
(STD. CC/GM ASH)	:	27.003			

TIME (MIN)	TAU	WA (ASH CAPACITY) CC H2S	WM (ASH CONC.) GM MOL FE2O3 /GM ASH	CA/CAO	XB
0.00	0.0000	264.862	0.60274E-03	0.0000	0.00000
13.10	0.2344	202.783	0.46147E-03	0.0000	0.23438
36.37	0.6507	92.509	0.21052E-03	0.0000	0.65073
53.15	0.9510	36.914	0.84004E-04	0.6017	0.86063
69.89	1.2503	15.651	0.35616E-04	0.8619	0.94091
86.63	1.5500	7.352	0.16731E-04	0.9290	0.97224
103.36	1.8493	3.257	0.74126E-05	0.9677	0.98770
121.32	2.1706	1.079	0.24546E-05	0.9811	0.99593
139.57	2.4972	0.132	0.30002E-06	0.9970	0.99950
158.15	2.8296	0.000	0.00000E 00	1.0000	1.00000

RUN NUMBER: 122 WESTERN KY. ASH

PARTICLE DIA., (CMS)	:	0.01910	MASS OF ASH CHARGED, (GMS)	:	9.809
APPARENT PARTICLE DENSITY, (GMS/CC)	:	2.8360	DIAMETER OF COLUMN, (CMS)	:	2.0000
BED TEMPERATURE, (DEG. F)	:	1000.00	BED LENGTH, (CMS)	:	3.048
INLET H2S CONCENTRATION, (VOL. FRACTION)	:	0.0100925	BED POROSITY, (VOID FRACTION), (VOL/VOL)	:	0.61500
VOLUMETRIC FLOW RATE OF GAS AT STAND. CONDITIONS, (CC/MIN)	:	469.01	BULK DENSITY OF BED, (GMS/CC)	:	1.09186
H2S CAPACITY OF ASH, (GM MOL /GM ASH)	:	0.12613E-02	SUPERFICIAL LINEAR VELOCITY, (CMS/MIN)	:	443.09930
(STD. CC/GM ASH)	:	28.253			

TIME (MIN)	TAU	WA (ASH CAPACITY) CC H2S	WM (ASH CONC.) GM MOL FE2O3 /GM ASH	CA/CAO	XB
0.00	0.0000	271.129	0.63966E-03	0.0000	0.00000
21.00	0.3601	178.347	0.40358E-03	0.0000	0.36006
38.50	0.6576	94.890	0.21594E-03	0.0000	0.65760
46.66	0.6965	85.111	0.19369E-03	0.0872	0.69288
57.89	0.9851	35.249	0.80215E-04	0.6872	0.87281
74.62	1.2745	17.293	0.39353E-04	0.8604	0.93760
91.40	1.5612	8.874	0.20194E-04	0.9276	0.96798
108.14	1.8471	4.440	0.10105E-04	0.9605	0.98398
125.08	2.1364	1.826	0.41563E-05	0.9743	0.99341
141.71	2.4205	0.410	0.93227E-06	0.9897	0.99852
158.52	2.7076	0.000	0.00000E 00	1.0000	1.00000

RUN NUMBER: 123 WESTERN KY. ASH

PARTICLE DIAM., (CMS)	:	0.01510	MASS OF ASH CHARGED, (GMS)	:	9.809
APPARENT PARTICLE DENSITY, (GMS/CC)	:	2.8360	DIAMETER OF COLUMN, (CMS)	:	2.0600
BED TEMPERATURE, (DEG. F)	:	1000.00	BED LENGTH, (CMS)	:	3.048
INLET H2S CONCENTRATION, (VOL. FRACTION)	:	0.0141122	BED POROSITY, (VOID FRACTION), (VOL/VOL)	:	0.61500
VOLUMETRIC FLOW RATE OF GAS AT STAND. CONDITIONS, (CC/MIN)	:	469.01	BULK DENSITY OF BED, (GMS/CC)	:	1.09186
H2S CAPACITY OF ASH, (GM MOL /GM ASH)	:	0.13409E-02	SUPERFICIAL LINEAR VELOCITY, (CMS/MIN)	:	443.09930
(STD. CC/GM ASH)	:	30.037			

TIME (MIN)	TAU	WA (ASH CAPACITY) CC H2S	WM (ASH CONC.) GM MOL FE2O3 /GM ASH	CA/CAO	XB
0.00	0.0000	294.621	0.67046E-03	0.0000	0.00000
10.51	0.2361	225.058	0.51216E-03	0.0000	0.23611
28.50	0.6403	105.986	0.24119E-03	0.0000	0.64026
34.55	0.7762	73.287	0.16678E-03	0.3668	0.75125
50.68	1.1385	30.503	0.69414E-04	0.8317	0.89647
67.12	1.5079	16.814	0.38264E-04	0.9167	0.94293
83.16	1.8682	9.792	0.22282E-04	0.9510	0.96677
99.69	2.2441	5.313	0.12090E-04	0.9681	0.98197
116.61	2.6197	2.590	0.58948E-05	0.9827	0.99121
133.46	2.9986	0.940	0.21390E-05	0.9877	0.99661
150.30	3.3765	0.126	0.28779E-06	0.9977	0.99957
166.94	3.7506	0.000	0.00000E 00	1.0000	1.00000

RUN NUMBER: 124 WESTERN KY. ASH

PARTICLE DIAM., (CMS)	:	0.02510	MASS OF ASH CHARGED, (GMS)	:	9.809
APPARENT PARTICLE DENSITY, (GMS/CC)	:	2.6360	DIAMETER OF COLUMN, (CMS)	:	2.0000
BED TEMPERATURE, (DEG. F)	:	1000.00	BED LENGTH, (CMS)	:	3.048
INLET H2S CONCENTRATION, (VOL. FRACTION)	:	0.0142100	BED POROSITY, (VOID FRACTION), (VOL/VOL)	:	0.61500
VOLUMETRIC FLOW RATE OF GAS AT STAND. CONDITIONS, (CC/MIN)	:	469.01	BULK DENSITY OF BED, (GMS/CC)	:	1.09186
			SUPERFICIAL LINEAR VELOCITY, (CMS/MIN)	:	443.09930
H2S CAPACITY OF ASH, (GM MOL /GM ASH)	:	0.13651E-02			
(STD. CC/GM ASH)	:	30.579			

TIME (MIN)	TAU	WA (ASH CAPACITY) CC H2S	WM (ASH CONC.) GM MOL FE2O3 /GM ASH	CA/CAO	XB
0.00	0.0000	299.942	0.68257E-03	0.0000	0.00000
10.43	0.2311	230.630	0.52484E-03	0.0000	0.23108
28.56	0.6333	110.001	0.25033E-03	0.0000	0.63326
30.31	0.6735	98.803	0.22484E-03	0.1435	0.67059
40.52	1.0334	40.703	0.92627E-04	0.7809	0.86430
53.27	1.4056	22.686	0.52082E-04	0.8999	0.92370
86.00	1.9776	13.760	0.31314E-04	0.9364	0.95412
96.90	2.1531	7.938	0.18063E-04	0.9602	0.97354
113.08	2.5254	4.275	0.97289E-05	0.9743	0.98575
130.41	2.8977	1.861	0.42352E-05	0.9824	0.99379
147.13	3.2594	0.441	0.10029E-05	0.9921	0.99853
163.67	3.6411	0.000	0.00000E 00	1.0000	1.00000

RUN NUMBER: 126 WESTERN KY. ASH

PARTICLE DIAM., (CMS)	:	0.01510	MASS OF ASH CHARGED, (GMS)	:	9.809
APPARENT PARTICLE DENSITY, (GMS/CC)	:	2.8360	DIAMETER OF COLUMN, (CMS)	:	2.0000
BED TEMPERATURE, (DEG. F)	:	1000.00	BED LENGTH, (CMS)	:	3.048
INLET H2S CONCENTRATION, (VOL. FRACTION)	:	0.0100020	BED POROSITY, (VOID FRACTION), (VOL/VOL)	:	0.61500
VOLUMETRIC FLOW RATE OF GAS AT STAND. CONDITIONS, (CC/MIN)	:	606.95	BULK DENSITY OF BED, (GMS/CC)	:	1.09186
			SUPERFICIAL LINEAR VELOCITY, (CMS/MIN)	:	573.42260
H2S CAPACITY OF ASH, (GM MOL /GM ASH)	:	0.131675-02			
(STD. CC/GM ASH)	:	29.495			

TIME (MIN)	TAU	WA (ASH CAPACITY) CC H2S	WM (ASH CONC.) GM MOL FE2O3 /GM ASH	CA/CAO	XB
0.00	0.0000	289.305	0.65837E-03	0.0000	0.00000
9.08	0.1905	234.183	0.53292E-03	0.0000	0.19053
32.00	0.6715	95.041	0.21628E-03	0.0000	0.67148
32.64	0.6891	90.116	0.20507E-03	0.0681	0.68851
46.96	1.0278	33.340	0.75871E-04	0.7730	0.88476
65.11	1.3663	17.284	0.39560E-04	0.9011	0.93991
84.89	1.7175	9.586	0.21860E-04	0.9415	0.96756
98.07	2.0579	4.906	0.11164E-04	0.9675	0.98304
114.00	2.4089	2.448	0.55714E-05	0.9841	0.99154
134.27	2.8179	0.699	0.15906E-05	0.9883	0.99758
191.40	3.1702	0.000	0.00000E 00	1.0000	1.00000

RUN NUMBER: 127 WESTERN KY. ASH

PARTICLE DIAM., (CMS)	:	0.01510	MASS OF ASH CHARGED, (GMS)	:	9.809
APPARENT PARTICLE DENSITY, (GMS/CC)	:	2.8360	DIAMETER OF COLUMN, (CMS)	:	2.0000
BED TEMPERATURE, (DEG. F)	:	1000.00	BED LENGTH, (CMS)	:	3.048
INLET H2S CONCENTRATION, (VOL. FRACTION)	:	0.01000C10	BED POROSITY, (VOID FRACTION), (VOL/VOL)	:	0.61500
VOLUMETRIC FLOW RATE OF GAS AT STAND. CONDITIONS, (CC/MIN)	:	616.15	BULK DENSITY OF BED, (GMS/CC)	:	1.09186
			SUPERFICIAL LINEAR VELOCITY, (CMS/MIN)	:	582.11080
H2S CAPACITY OF ASH, (GM MOL /GM ASH)	:	0.13343E-02			
(STD. CC/GM ASH	:	29.889			

TIME (MIN)	TAU	WA (ASH CAPACITY) CC H2S	WM (ASH CONC.) GM MOL FE2O3 /GM ASH	CA/CAO	XB
0.00	0.0000	295.169	0.66716E-03	0.0000	0.00000
19.25	0.4046	174.548	0.39721E-03	0.0000	0.40462
32.09	0.6726	95.981	0.21842E-03	0.0000	0.67261
39.08	0.7584	73.680	0.16767E-03	0.2259	0.74868
52.80	1.1098	25.065	0.57039E-04	0.8304	0.91450
69.04	1.4511	12.421	0.28265E-04	0.9169	0.95763
85.86	1.8047	6.026	0.13713E-04	0.9597	0.97945
102.60	2.1565	2.797	0.63659E-05	0.9777	0.99046
118.52	2.4995	1.028	0.23390E-05	0.9871	0.99649
136.14	2.8625	0.168	0.38280E-06	0.9967	0.99943
152.69	3.2094	0.000	0.00000E 00	1.0000	1.00000

APPENDIX D

COMPUTER PROGRAM FOR DATA REDUCTION

This program converts the raw breakthrough data and generates the data sheets presented in Appendix C. The raw data is read in using data cards. The raw breakthrough data is read in as time on stream (min) vs. (C_A/C_o). The program uses the trapezoidal rule to evaluate the area under the curve (ash H_2S capacity) defined by equation (6-1). The important variables used in the program are defined below:

INPUT VARIABLES

T(I)	raw time, min
Y(I)	C_A/C_o
DP	particle diameter, cm
RHOP	particle density, gm/CC
TEMP	desulfurization temperature, °F
VOR	volumetric flow rate of fluid at room conditions, CC/min
CAO	inlet H_2S concentration, vol. %
AM	weight of ash charged, gms
DCOL	diameter of reactor, cm
BL	bed length at minimum fluidization, cm
EPSB	bed porosity at minimum fluidization
NDP	number of data points
NSET	number of data sets

OTHER VARIABLES

RHOB	bulk density of bed, gms/CC
VO	volumetric flow rate of fluid at standard conditions, SCC/min
SLV	superficial linear velocity, cm/min
SCAP	capacity of ash bed, g mole H_2S/gm ash
SCAPV	capacity of ash bed, SCC H_2S/ gm ash
TAU(I)	dimensionless time
WA(I)	remaining H_2S capacity of whole bed, SCC H_2S

WM(I)	ash bed Fe_2O_3 concentration, g mole/ gm ash
XB(I)	solid conversion

```
    $JOB
 1        REAL KM,KK
 2        DIMENSION HEAD1(20)
 3        DIMENSION TAU(20), WM(20),XB(20),WA(20),RTAU(20),RY(20),RB(20)
 4        DIMENSION T(20),Y(20)
 5        DIMENSION WMG(250),XBG(250),RBG(250)
 6        DIMENSION S(10),INDEX(10)
 7        DIMENSION TIME(250),W(250),CONC(250)
 8        COMMON/FDATA/ TAU,WM,XB,WA
 9        COMMON/PLOT1/TIME,W,CONC,N,Z
10        COMMON/EXDATA/T,Y, CAO,VO,NDP,AM
11        COMMON /PARAM/  KM,KK
12        WRITE(6,102)
13   102  FORMAT (1H1)
14        NSET=10
15        NSET=2
16        NSET=1
17        NSET=70
18        DO 55 JK=1,NSET
19        READ (5,101) HEAD1
20   101  FORMAT(20A4)
21        WRITE(6,201) HEAD1
22   201  FORMAT(51X,20A4,/)
23   8    CONTINUE
24        READ (5,100) NDP,(T(I),Y(I),I=1,NDP)
25   100  FORMAT(I10,7F10.5,/,(8F10.5))
26        READ(5,104)DP,RHOP,TEMP,VOR,CAO,AM,DCOL,BL,EPSB
27   104  FORMAT( 8F10.5)
28        RHOB=(1.0-EPSB)*RHOP
29        VO=VOR*(460.0+32.0)/(460.0+75.0)
30        SLV =(VO*(460.0+TEMP)/(460.0+32.0)) / ((3.141/4.0)*(DCOL**2))
31        CALL EDATA
32        SCAP = WM(1)/0.5
33        SCAPV=WA(1)/AM
34        WRITE(6,1005) DP,AM,RHOP,DCOL,TEMP,BL,CAO,EPSB,RHOB,VO,SLV,SCAP,
         $SCAPV
35   1005 FORMAT(////,T2,'PARTICLE DIAM., (CMS)',T42,':',F14.5,T70,
         7   'MASS OF ASH CHARGED, (GMS)',T110,':',F14.3,//,
         1T2,'APPARENT PARTICLE DENSITY,(GMS/CC)',T42,':',F14.4 ,T70,
         0   'DIAMETER OF COLUMN, (CMS)',T110,':',F14.4,//,
         2T2,'BED TEMPERATURE, (DEG. F)',T42,':',F14.2,T70,
         9'BED LENGTH, (CMS)',T110,':',F14.3,//,
         6T2,'INLET H2S CONCENTRATION, (MOL - FRACTION)',T42,':',F14.7,T70,
         1   'BED POROSITY, (VOID FRACTION), (VOL/VOL)',T110,':',F14.5,//,
         3T2,'VOLUMETRIC FLOW RATE OF GAS AT',T70,
         2   'BULK DENSITY OF BED, (GMS/CC)',T110,':',F14.5,/,
         4T4,'STAND.  CONDITIONS, (CC/MIN)',T42,':',E14.2,/,T70,
         $'SUPERFICIAL LINEAR VELOCITY, (CMS/MIN)',T110,':',F14.5,/,T2,
         $ 'H2S CAPACITY OF ASH, (GM MOL /GM ASH)',T42,':',E14.5,/,
         $T23,'(STD. CC/GM ASH )',T42,':',F14.3,/,
         $///)
36        WRITE(6,1002)
37   1002 FORMAT (////,T5,'TIME (MIN)',T21,'TAU',T31,'WA (ASH CAPACITY)',
         $T51,'WM (ASH CONC.)',T70,'CA/CAO',T85,'XB',/,T35, 'CC H2S',T51,
         $'GM MOL FE2O3',/,T51,'/GM ASH',//)
38        DO 56 J=1,NDP
39        WRITE(6,1001) T(J),TAU(J),WA(J),WM(J),Y(J),XB(J)
40   1001 FORMAT(T5,F6.2,T21,F6.4,T34,F10.3,T48, E14.5,T70,F6.4,T80 ,F10.5
         $,/)
41   56   CONTINUE
42        CALL SCALER(2.8,0.0,1.0,0.0)
```

```
      CALL BOX
      CALL PLOTEM ('O',TAU,Y,NDP)
      CALL GRAPH ('DIMENSIONLESS TIME',18,'CA/CAO',6)
      WRITE(6,201) HEAD1
      WRITE(6,202)
202   FORMAT(///////)
      CONTINUE
55    CONTINUE
      STOP
       END

      SUBROUTINE EDATA
      COMMON/FDATA/ TAU,WM,XB,WA
      COMMON/EXDATA/T,Y, CAO,VO,NDP,AM
      DIMENSION T(20),Y(20)
      DIMENSION TAU(20), WM(20),XB(20),WA(20)
      DIMENSION Q(20),Y1(20),DELX(20),WC(20),TM(20)
      DO 10 J=1,NDP
10    CONTINUE
      DO 9 J=1,NDP
      FAO = VO*CAO
      TM(J) = T(J)*VO
      Y1(J) = (1.0-Y(J))*CAO
9     CONTINUE
      SUM = 0.0
      K=NDP-1
      DO 11 J= 1,K
      DELX(J) = TM(J+1)-TM(J)
      WC(J) = DELX(J)*((Y1(J) + Y1(J+1)) /2.0)
      Q(J) = SUM+ WC(J)
      SUM = Q(J)
11    CONTINUE
      DO 12 J= 1,NDP
      WAO = SUM
       WA(1) = WAO
      Q(NDP)=WAO
      WA(J+1) = WAO-Q(J)
      TAU(J) = TM(J)*CAO/WAO
      WM(J)=(WA(J)*0.5)/(22400.0*AM)
      XB(J) = (WAO-WA(J))/WAO
12    CONTINUE
      CONTINUE
      RETURN
      END

$ENTRY
```

APPENDIX E

COMPUTER PROGRAMS FOR MODELS

Computer Program for the Pseudo-homogeneous Model

This program solves equation (5-32) using the Fourth Order Runge-Kutta numerical routine. The Fe_2O_3 concentration of the solid is thus obtained as a function of time. These values are then put in equation (5-28) to obtain the corresponding exit H_2S concentrations. The two subroutines MODEL 1 and FUNC contain the Runge-Kutta routine. The important variables are as follows:

DELT	increment in dimensionless time
KM	the mass transfer parameter K_m
KK	the kinetic parameter K_k
SI	the index m in rate equation (5-1)
YO	initial solid Fe_2O_3 concentration (at time 0)
TO	initial time (= 0)
TIME(I)	dimensionless time,
CONC(I)	dimensionless exit H_2S concentration
W	dimensionless solid Fe_2O_3 concentration
Z	dimensionless reactor position

In the program listed, the breakthrough curves were simulated for various values of KK and SI = 2, 3 and 1. The required KK values were read in from data cards.

```
    $JOB          ,TIME=(2,0)
 1          REAL KM,KK
 2          DIMENSION HEAD1(20)
 3          DIMENSION T(20),Y(20)
 4          DIMENSION TIME(250),W(250),CONC(250)
 5          COMMON/PLOT1/TIME,W,CONC,N,Z
 6          COMMON/EXDATA/T,Y, CAO,VO,NDP
 7          COMMON /PARAM/  KM,KK,SI
 8          WRITE(6,102)
 9    102   FORMAT (1H1)
10          Z = 1.0
11          DELT = 0.01
12          KM=0.01
13           NK=18
14          SI = 2.0
15    57    CONTINUE
16          DO 58 JK=1,NK
17          READ,KK
18          TO=0.0
19          YO=1.0
20          CALL MODEL1(TO,YO,DELT)
21          CALL SCALER(2.8,0.0,1.0,0.0)
22          CALL BOX
23          CALL PLOTEM ('+',TIME,CONC,N)
24          CALL GRAPH ('DIMENSIONLESS TIME',18,'CA/CAO        ',13)
25          WRITE(6,50002) KM,KK,SI
26    50002  FORMAT(///,2X,'KM=',F10.5,3X,'KK=',F10.5,3X,'SI=',F10.5,////)
      CONTINUE
27    58    CONTINUE
28          SI=3.0
29          NK=2
30          DO 60 JK=1,NK
31          READ,KK
32          TO=0.0
33          YO=1.0
34          CALL MODEL1(TO,YO,DELT)
35          CALL SCALER(2.8,0.0,1.0,0.0)
36          CALL BOX
37          CALL PLOTEM ('+',TIME,CONC,N)
38          CALL GRAPH ('DIMENSIONLESS TIME',18,'CA/CAO        ',13)
39          WRITE(6,50002) KM,KK,SI
40    60     CONTINUE
41          SI=1.0
42          NK=6
43          DO 61 JK=1,NK
44          READ,KK
45          TO=0.0
46          YO=1.0
47          CALL MODEL1(TO,YO,DELT)
48          CALL SCALER(2.8,0.0,1.0,0.0)
49          CALL BOX
50          CALL PLOTEM ('+',TIME,CONC,N)
51          CALL GRAPH ('DIMENSIONLESS TIME',18,'CA/CAO        ',13)
52          WRITE(6,50002) KM,KK,SI
53    61    CONTINUE
54          STOP
55           END

56          SUBROUTINE MODEL1(TO,CAO,DELT)
57          REAL KM,KK
58          DIMENSION TIME(250),W(250),CONC(250)
```

```
59          COMMON/PLOT1/TIME,W,CONC,N,Z
60          COMMON /PARAM/  KM,KK,SI
61          N=1
62    10    CONTINUE
63          T= TO
64          CA=CAO
65          CALL FUNC (CA,T,F)
66          AK1 = F*DELT
67          CA = CAO +(AK1/ 2.0)
68          T = TO + (DELT/2.0)
69          CALL FUNC (CA,T,F)
70          AK2 = F*DELT
71          CA = CAO + (AK2/2.0)
72          CALL FUNC (CA,T,F)
73          AK3 = F*DELT
74          T = TO + DELT
75          CA = CAO + AK3
76          CALL FUNC (CA,T,F)
77          AK4 = F* DELT
78          DELCA = (1.0/6.0) * (AK1 + 2.0*AK2 + 2.0*AK3 + AK4)
79          CAO = CAO  + DELCA
80           TO = TO + DELT
81          Y = EXP ((-(CA**SI)*Z) / (KM*(CA**SI) + KK))
82          TIME(N)=TO
83          CONC(N) = Y
84          W(N) =CAO
85          IF (Y.GE.1.0)  GO TO 20
86          IF (TO. GE . 2.5 ) GO TO 20
87          IF (N.EQ.250) GO TO 20
88          N=N+1
89          GO TO 10
90    20    CONTINUE
91          RETURN
92          END

93          SUBROUTINE FUNC (CA, T, F)
94          REAL KM,KK
95          COMMON /PARAM/  KM,KK,SI
96          F = EXP(((-(CA**SI)) / (KM*(CA**SI) + KK))) -1.0
97          RETURN
98           END

      $ENTRY
```

Computer Program for Unreacted-core Models and Other Unsuccessful Models

This program solves the unreacted-core models discussed in Chapter 5. The models are programmed in as subroutines. The MODEL 1 listed is the program for the special case of m = 1 in the pseudo-homogeneous model. MODEL 2 is another special case of the pseudo-homogeneous model with m = 1 and chemical reaction controlling ($K_k >> K_m$); with these assumptions, equation (5-32) is solved explicitly to obtain

$$\tau = 1 - X + K_k \ln \frac{1 - EXP(-1/K_k)}{1 - EXP(-X/K_k)}$$

MODEL 2 thus solves this equation together with equation (5-28) with m = 1 to obtain the breakthrough curves. MODEL 5 solves the general case of the unreacted-core model; equation (5-38) is solved using the Fourth Order Runge-Kutter numerical routine together with equation (5-35) to obtain the breakthrough curves. The special case of chemical reaction controlling is solved by MODEL 3; equations (5-41) and (5-40) are solved. MODEL 4 solves the special case of diffusion through product-layer controlling; equations (5-44) and (5-43) are solved in this case.

Some of the important variables used in the programs are listed below:

DELT	increment in dimensionless time
KM	the mass transfer parameter K_m
KK	the kinetic parameter K_k
KD	the diffusion parameter K_D
DA	Damkohler number
BI	Biot number for mass transfer
YO	initial Fe_2O_3 concentration of solid at time = 0
TO	initial time (=0)
CONC(I)	dimensionless exit H_2S concentration
TIME(I)	dimensionless time, τ
W	dimensionless solid Fe_2O_3 concentration
Z	dimensionless reactor position

```
0001: $JOB
0002:       REAL KM,KK,KD
0003:       DIMENSION TIME(250),W(250),CONC(250)
0004:       COMMON/PLOT1/TIME,W,CONC,N,Z
0005:       COMMON/PARAM4/KD
0006:       COMMON /PARAM5/KK,DA,BI
0007:       WRITE(6,102)
0008: 102   FORMAT (1H1)
0009: 8     CONTINUE
0010:       Z = 1.0
0011:       DELT = 0.01
0012:       TO=0.0
0013:       YO = 1.0
0014:       KM=0.2
0015:       KK = 0.1
0016:        DA = 50.0
0017:       BI = 1000.0
0018:       CALL MODEL5  (TO,YO,DELT)
0019:       CALL SCALER(3.5,0.0,1.0,0.0)
0020:       CALL BOX
0021:       CALL PLOTEM ('+',TIME,CONC,N)
0022:       CALL PLOTEM ('W',TIME,W,N)
0023:       CALL GRAPH ('DIMENSIONLESS TIME',18,'CONCENTRATION',13)
0024:       WRITE(6,202)
0025: 202   FORMAT(///////)
0026: 50    CONTINUE
0027:       CONTINUE
0028:       STOP
0029:        END
0030:       SUBROUTINE MODEL1(TO,CA0,DELT)
0031:       REAL KM,KK
0032:       DIMENSION TIME(250),W(250),CONC(250)
0033:       COMMON/PLOT1/TIME,W,CONC,N,Z
0034:       COMMON/PARAM/KM,KK
0035:       N=1
0036: 10    CONTINUE
0037:       T= TO
0038:       CA=CA0
0039:       CALL FUNC (CA,T,F)
0040:       AK1 = F*DELT
0041:       CA = CA0 +(AK1/ 2.0)
0042:       T = TO + (DELT/2.0)
0043:       CALL FUNC (CA,T,F)
0044:       AK2 = F*DELT
0045:       CA = CA0 + (AK2/2.0)
0046:       CALL FUNC (CA,T,F)
0047:       AK3 = F*DELT
0048:       T = TO + DELT
0049:       CA = CA0 + AK3
0050:       CALL FUNC (CA,T,F)
0051:       AK4 = F* DELT
0052:       DELCA = (1.0/6.0) * (AK1 + 2.0*AK2 + 2.0*AK3 + AK4)
0053:       CA0 = CA0  + DELCA
0054:        TO = TO + DELT
0055:       Y = EXP ((-CA*Z) / ( KM*CA + KK))
0056:       TIME(N)=TO
0057:       CONC(N) = Y
0058:       W(N) =CA0
0059:       IF (Y.GE.1.0)  GO TO 20
0060:       IF (TO. GE . 2.5 ) GO TO 20
```

```
0061:       IF (N.EQ.250) GO TO 20
0062:       N=N+1
0063:       GO TO 10
0064: 20    CONTINUE
0065:       RETURN
0066:       END
0067:       SUBROUTINE MODEL2
0068:       REAL KM,KK
0069:       DIMENSION TIME(250),W(250),CONC(250)
0070:       COMMON/PLOT1/TIME,W,CONC,N,Z
0071:       COMMON /PARAM/  KM,KK
0072:       W(1) = 1.0
0073:       DO 21 N=1,120
0074:       IF(W(N).GE.0.0) GO TO 21
0075:       TIME(N) = 1.0 -W(N) +KK*ALOG((1.0-(EXP(-1.0/KK))))
0076:      $- KK*ALOG(1.0-(EXP(-W(N)/KK)))
0077:       CONC(N) = EXP((-W(N)*Z) / (KM*W(N) + KK))
0078:       W(N+1) = W(N)-0.01
0079: 21    CONTINUE
0080:       RETURN
0081:       END
0082:       SUBROUTINE FUNC (CA, T, F)
0083:       REAL KM,KK
0084:       COMMON /PARAM/  KM,KK
0085:       F =  EXP(( -CA ) / (KM*CA + KK))) -1.0
0086:       RETURN
0087:        END
0088:       SUBROUTINE MODEL3 (T0,CA0,DELT)
0089:       REAL KM,KK
0090:       DIMENSION TIME(250),W(250),CONC(250)
0091:       COMMON/PLOT1/TIME,W,CONC,N,Z
0092:       COMMON/PARAM/KM,KK
0093:       N=1
0094: 10    CONTINUE
0095:       T= T0
0096:       CA=CA0
0097:       CALL FUNC2(CA,T,F)
0098:       AK1 = F*DELT
0099:       CA = CA0 +(AK1/ 2.0)
0100:       T = T0 + (DELT/2.0)
0101:       CALL FUNC2(CA,T,F)
0102:       AK2 = F*DELT
0103:       CA = CA0 + (AK2/2.0)
0104:       CALL FUNC2(CA,T,F)
0105:       AK3 = F*DELT
0106:       T = T0 + DELT
0107:       CA = CA0 + AK3
0108:       CALL FUNC2(CA,T,F)
0109:       AK4 = F* DELT
0110:       DELCA = (1.0/6.0) * (AK1 + 2.0*AK2 + 2.0*AK3 + AK4)
0111:       CA0 = CA0  + DELCA
0112:        T0 = T0 + DELT
0113:       Y = EXP(-KK*(CA**0.666667)*Z)
0114:       TIME(N)=T0
0115:       CONC(N) = Y
0116:       W(N) =CA0
0117:       WRITE (6,100) N,TIME(N),CONC(N),W(N)
0118: 100   FORMAT (I4,3F15.5)
0119:       IF ( W(N).LE. 0.0001) GO TO 20
0120:       IF (Y.GE.1.0)  GO TO 20
```

```
0121:       IF (TO. GE . 2.5 ) GO TO 20
0122:       IF (N.EQ.250) GO TO 20
0123:       N=N+1
0124:       GO TO 10
0125: 20    CONTINUE
0126:       RETURN
0127:       END
0128:       SUBROUTINE FUNC2 (W ,T,F)
0129:       REAL KK
0130:       COMMON /PARAM/ KM,KK
0131:       F = EXP (-KK*(W**0.66667)) -1.0
0132:       RETURN
0133:       END
0134:       SUBROUTINE MODEL4 (T0,CA0,DELT)
0135:       REAL KM,KK,KD
0136:       DIMENSION TIME(250),W(250),CONC(250)
0137:       COMMON/PLOT1/TIME,W,CONC,N,Z
0138:       COMMON/PARAM4/KD
0139:       N=1
0140: 10    CONTINUE
0141:       T= T0
0142:       CA=CA0
0143:       CALL FUNC4(CA,T,F)
0144:       AK1 = F*DELT
0145:       CA = CA0 +(AK1/ 2.0)
0146:       T = T0 + (DELT/2.0)
0147:       CALL FUNC4(CA,T,F)
0148:       AK2 = F*DELT
0149:       CA = CA0 + (AK2/2.0)
0150:       CALL FUNC4(CA,T,F)
0151:       AK3 = F*DELT
0152:       T = T0 + DELT
0153:       CA = CA0 + AK3
0154:       CALL FUNC4(CA,T,F)
0155:       AK4 = F* DELT
0156:       DELCA = (1.0/6.0) * (AK1 + 2.0*AK2 + 2.0*AK3 + AK4)
0157:       CA0 = CA0  + DELCA
0158:        T0 = T0 + DELT
0159:       Y = EXP ((KD*Z) / (1.0-(CA**(-0.33333))))
0160:       TIME(N)=T0
0161:       CONC(N) = Y
0162:       W(N) =CA0
0163:       WRITE (6,100) N,TIME(N),CONC(N),W(N)
0164: 100   FORMAT (I4,3F15.5)
0165:       IF ( W(N).LE. 0.002 ) GO TO 20
0166:       IF (Y.GE.1.0) GO TO 20
0167:       IF (T0. GE . 2.5 ) GO TO 20
0168:       IF (N.EQ.250) GO TO 20
0169:       N=N+1
0170:       GO TO 10
0171: 20    CONTINUE
0172:       RETURN
0173:       END
0174:       SUBROUTINE FUNC4 (W,T,F)
0175:       REAL KM,KK,KD
0176:       COMMON/PARAM4/KD
0177:       F = (EXP(KD/(1.0-(W**(-0.3333))))) - 1.0
0178:       RETURN
0179:       END
0180:       SUBROUTINE MODEL5 (T0,CA0,DELT)
```

```
0181:       REAL KM,KK,KD
0182:       DIMENSION TIME(250),W(250),CONC(250)
0183:       COMMON/PLOT1/TIME,W,CONC,N,Z
0184:       COMMON/PARAM4/KD
0185:       COMMON /PARAMS/KK,DA,BI
0186:       N=1
0187: 10    CONTINUE
0188:       T= T0
0189:       CA=CA0
0190:       CALL FUNCS(CA,T,F)
0191:       AK1 = F*DELT
0192:       CA = CA0 +(AK1/ 2.0)
0193:       T = T0 + (DELT/2.0)
0194:       CALL FUNCS(CA,T,F)
0195:       AK2 = F*DELT
0196:       CA = CA0 + (AK2/2.0)
0197:       CALL FUNCS(CA,T,F)
0198:       AK3 = F*DELT
0199:       T = T0 + DELT
0200:       CA = CA0 + AK3
0201:       CALL FUNCS(CA,T,F)
0202:       AK4 = F* DELT
0203:       DELCA = (1.0/6.0) * (AK1 + 2.0*AK2 + 2.0*AK3 + AK4)
0204:       CA0 = CA0  + DELCA
0205:        T0 = T0 + DELT
0206:       P = CA**0.33333
0207:       ETA = 1.0 + (DA*(1.0-P)*P) + (DA/BI)*(P*P)
0208:       Y = EXP( -(P*P)*Z / (KK*ETA))
0209:       TIME(N)=T0
0210:       CONC(N) = Y
0211:       W(N) =CA0
0212:       WRITE (6,100) N,TIME(N),CONC(N),W(N)
0213: 100   FORMAT (I4,3F15.5)
0214:       IF ( W(N).LE. 0.02)   GO TO 20
0215:       IF (Y.GE.1.0)  GO TO 20
0216:       IF (T0. GE . 2.5 ) GO TO 20
0217:       IF (N.EQ.250) GO TO 20
0218:       N=N+1
0219:       GO TO 10
0220: 20    CONTINUE
0221:       RETURN
0222:       END
0223:       SUBROUTINE FUNCS (W ,T,F)
0224:       REAL KM,KK,KD
0225:       COMMON/PARAM4/KD
0226:       COMMON /PARAMS/KK,DA,BI
0227:       P = W**0.3333
0228:       ETA = 1.0 + (DA*(1.0-P)*P) + (DA/BI)*(P*P)
0229:       F = EXP(-P*P/(KK*ETA)) - 1.0
0230:       RETURN
0231:       END
0232: $STOP
0233: /*
```

APPENDIX F

SUMMARY OF MODEL PARAMETERS AND DETERMINATION OF MODEL PARAMETERS BY CURVE MATCHING

Summary of Model Parameters*

Run #	K_k
Western Ky. Ash	
014	0.014
017	0.014
019	0.014
023	0.035
024	0.035
026	0.062
029	0.013
048	0.013
049	0.013
052	0.035
053	0.035
054	0.035
056	0.055
057	0.055
058	0.055
061	0.009
122	0.038
123	0.045
124	0.045
126	0.042
127	0.042
075	0.035
076	0.035
077	0.038
078	0.032
080	0.050
Elkhorn Ash	
095	0.035
096	0.035
Montana Ash	
111	0.03
112	0.03
113	0.03
114	0.03

* See Tables 6.5(a) and (b) for process conditions

m = 2 for W. Ky Ash and m = 3 for Elkhorn and Montana Ashes.

$K_m = 0.01$

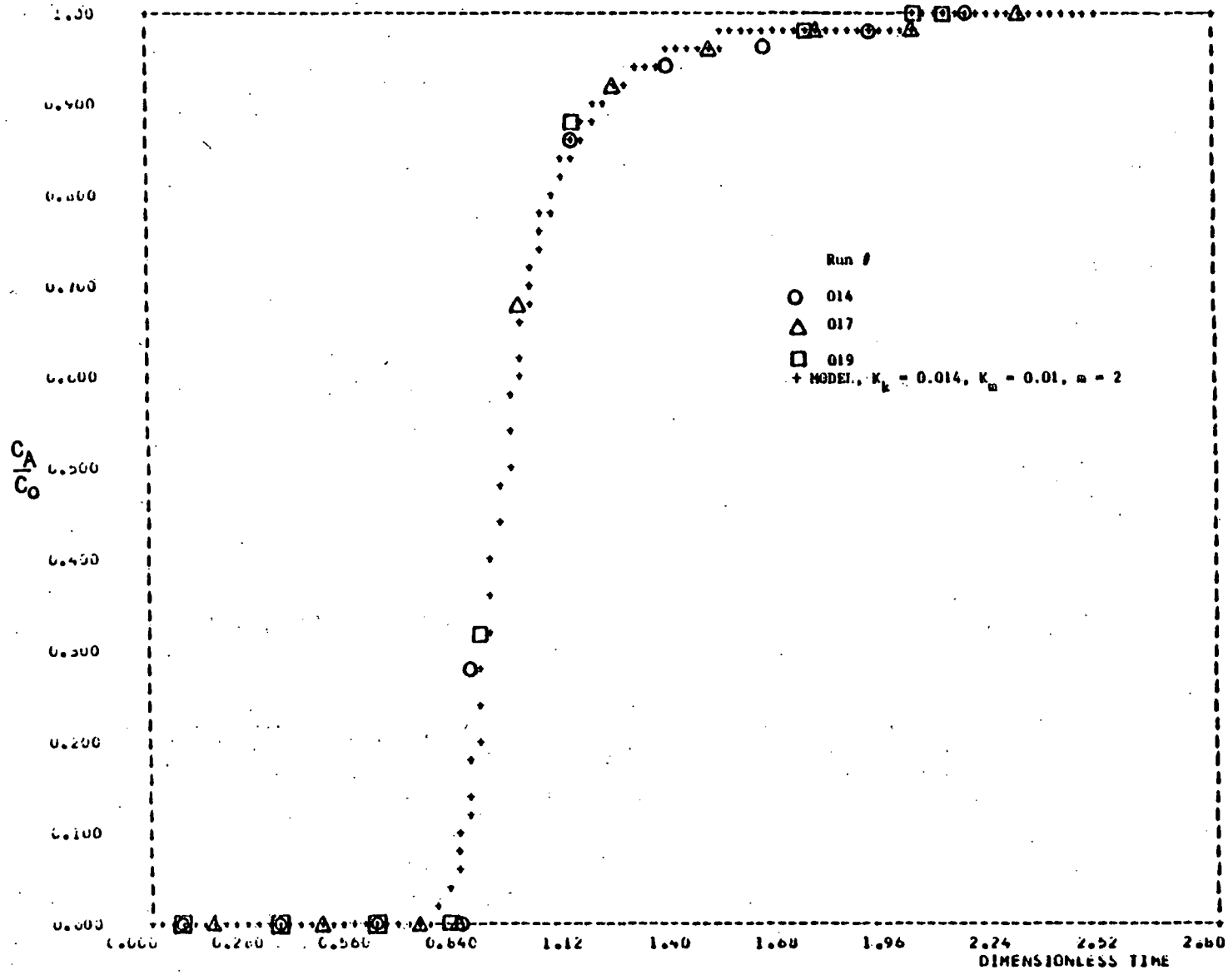
Run #
014
017
019
+ MODEL, K_k = 0.014, K_m = 0.01, m = 2
$\frac{C_A}{C_o}$
0.640
1.12
1.40
1.68
1.96
2.24
2.52
2.80
DIMENSIONLESS TIME

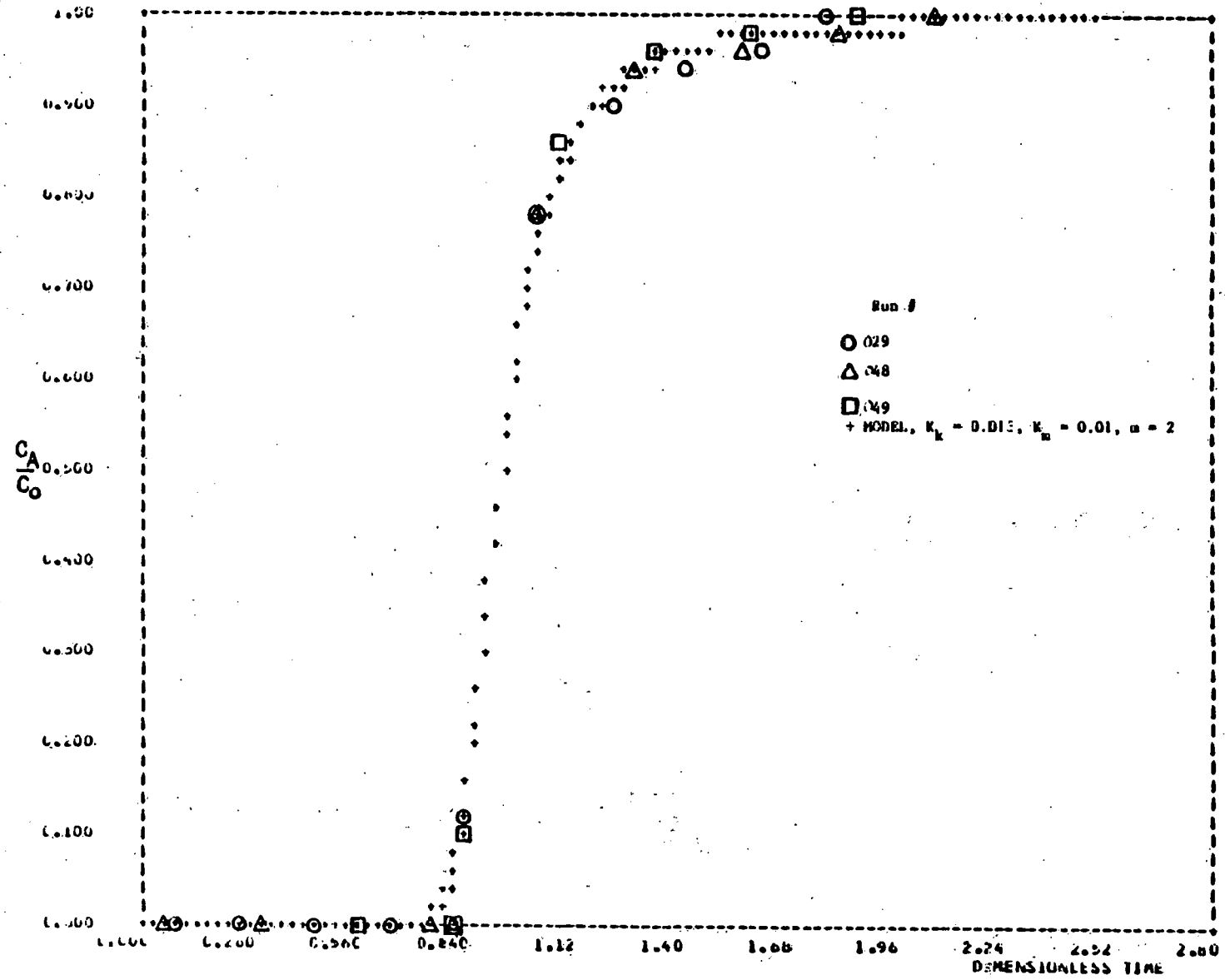
Run #
029
048
049
+ MODEL, K_k = 0.015, K_m = 0.01, n = 2
$\frac{C_A}{C_o}$
DIMENSIONLESS TIME
1.40
1.68
1.96
2.24
2.52
2.80

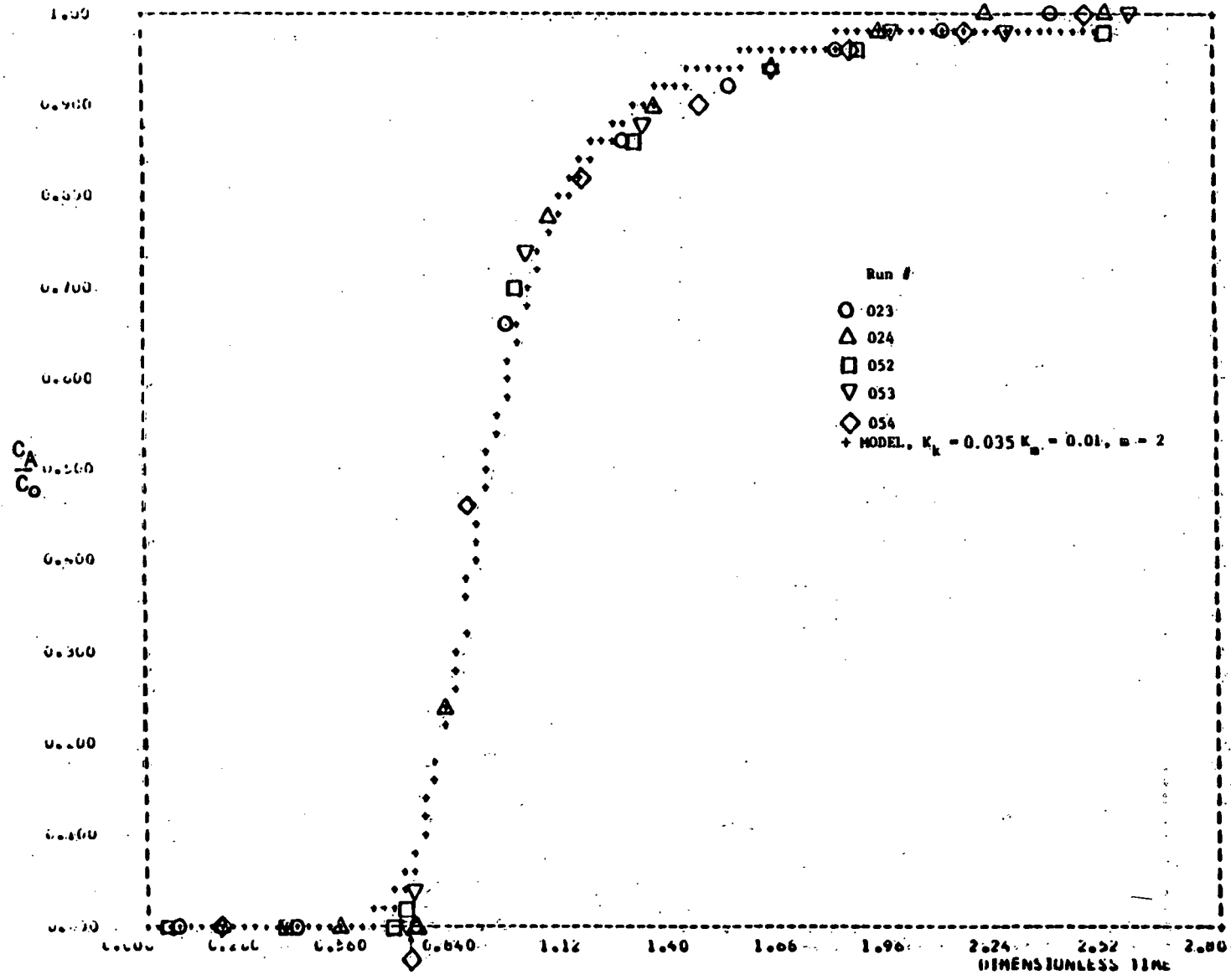
C/Co
1.00
0.900
0.800
0.700
0.600
0.500
0.400
0.300
0.200
0.100
0.000
0.280
0.560
0.840
1.12
1.40
1.68
1.96
2.24
2.52
2.80
DIMENSIONLESS TIME
Run #
023
024
052
053
054
+ MODEL, $K_k = 0.035$ $K_m = 0.01$, $n = 2$

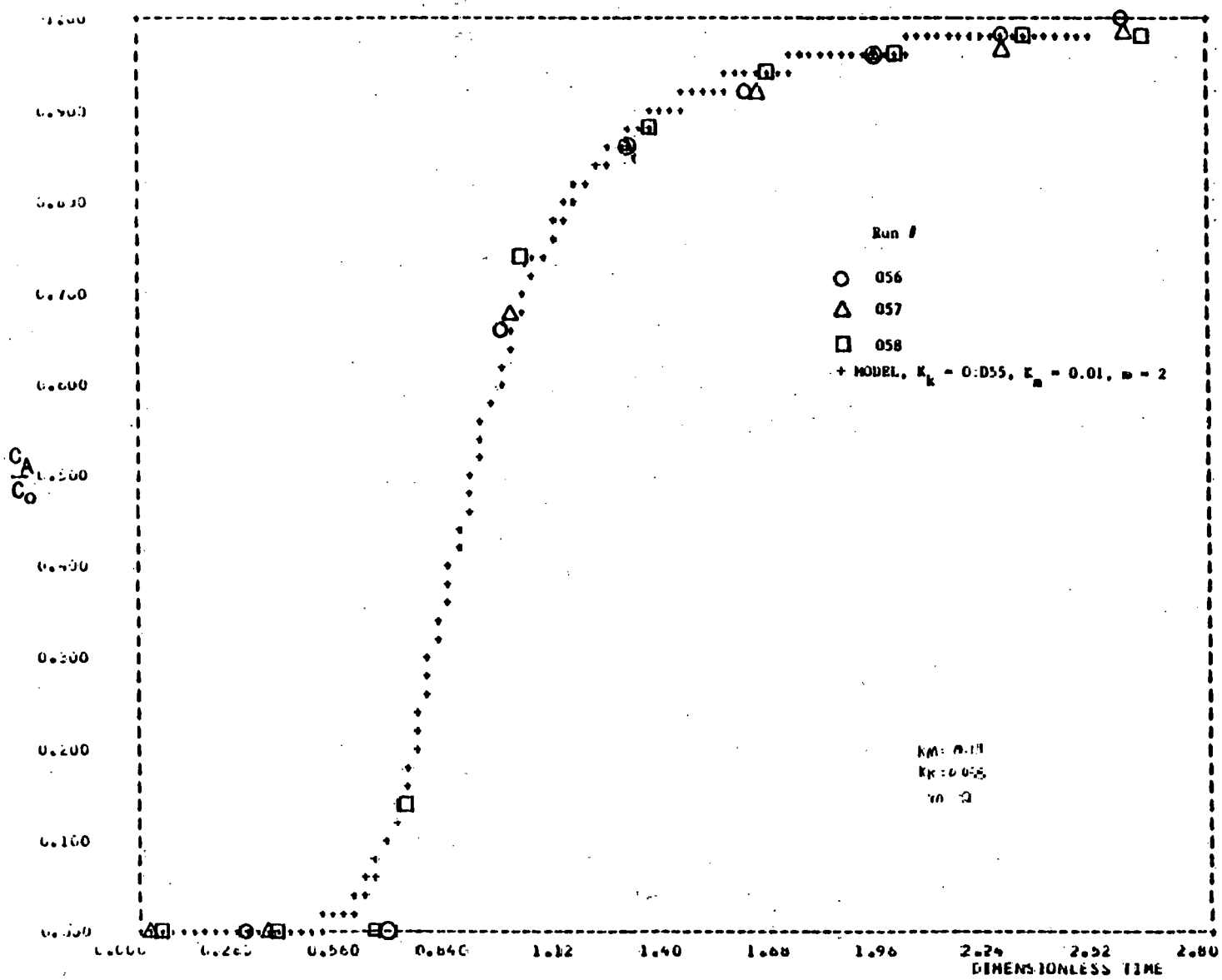
Run #
056
057
058
+ MODEL, K_k = 0.055, K_m = 0.01, n = 2
$\frac{C_A}{C_o}$
0.560
0.840
1.12
1.40
1.68
1.96
2.24
2.52
2.80
DIMENSIONLESS TIME

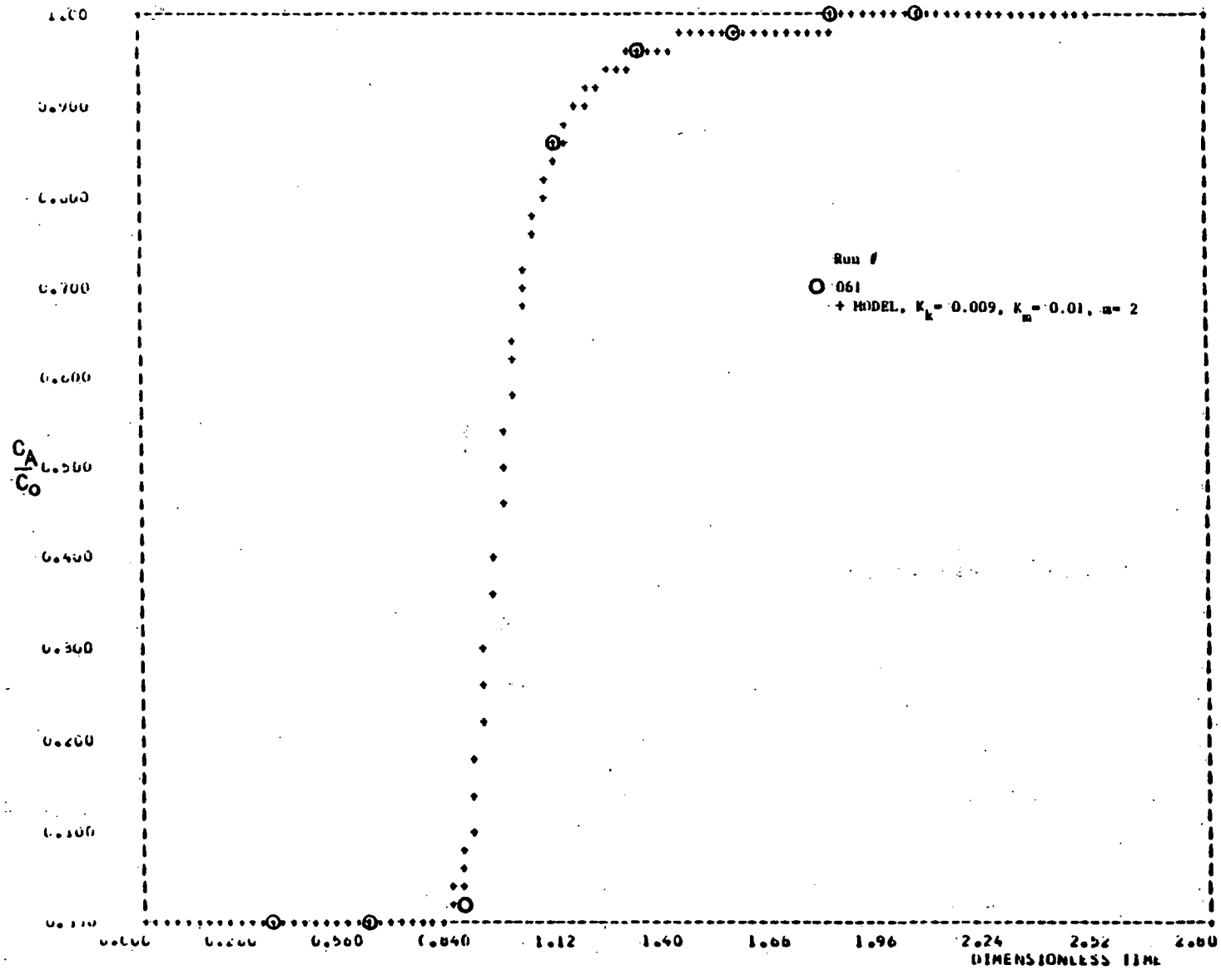
Run #
O 061
+ MODEL, K_k= 0.009, K_m= 0.01, n= 2
$\frac{C_A}{C_o}$
0.840
1.12
1.40
1.68
1.96
2.24
2.52
DIMENSIONLESS TIME

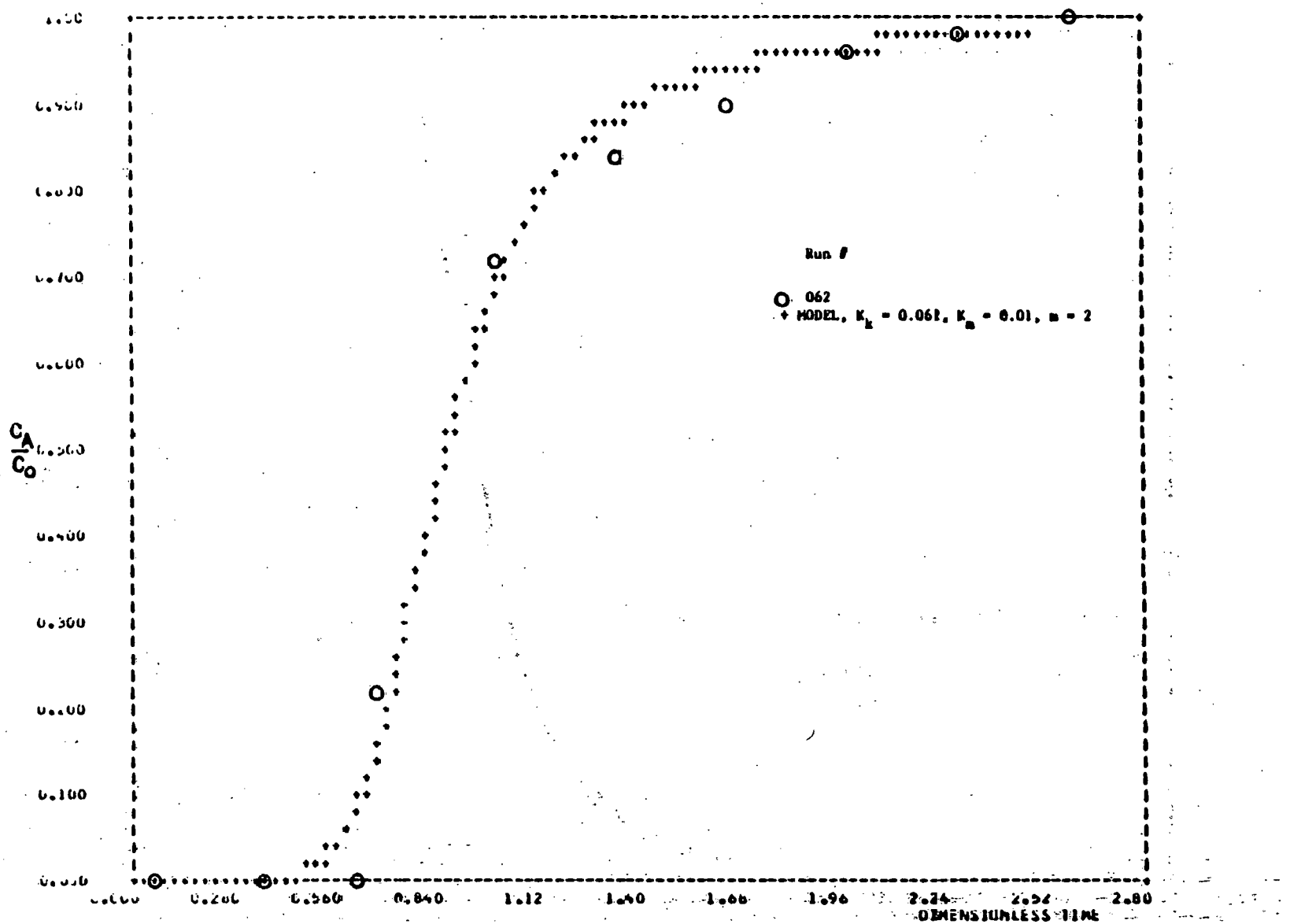
Run #
062
MODEL, K_k = 0.061, K_m = 0.01, n = 2
C_A/C_o
0.300
0.100
0.840
1.12
1.40
1.96
2.24
2.80
DIMENSIONLESS TIME

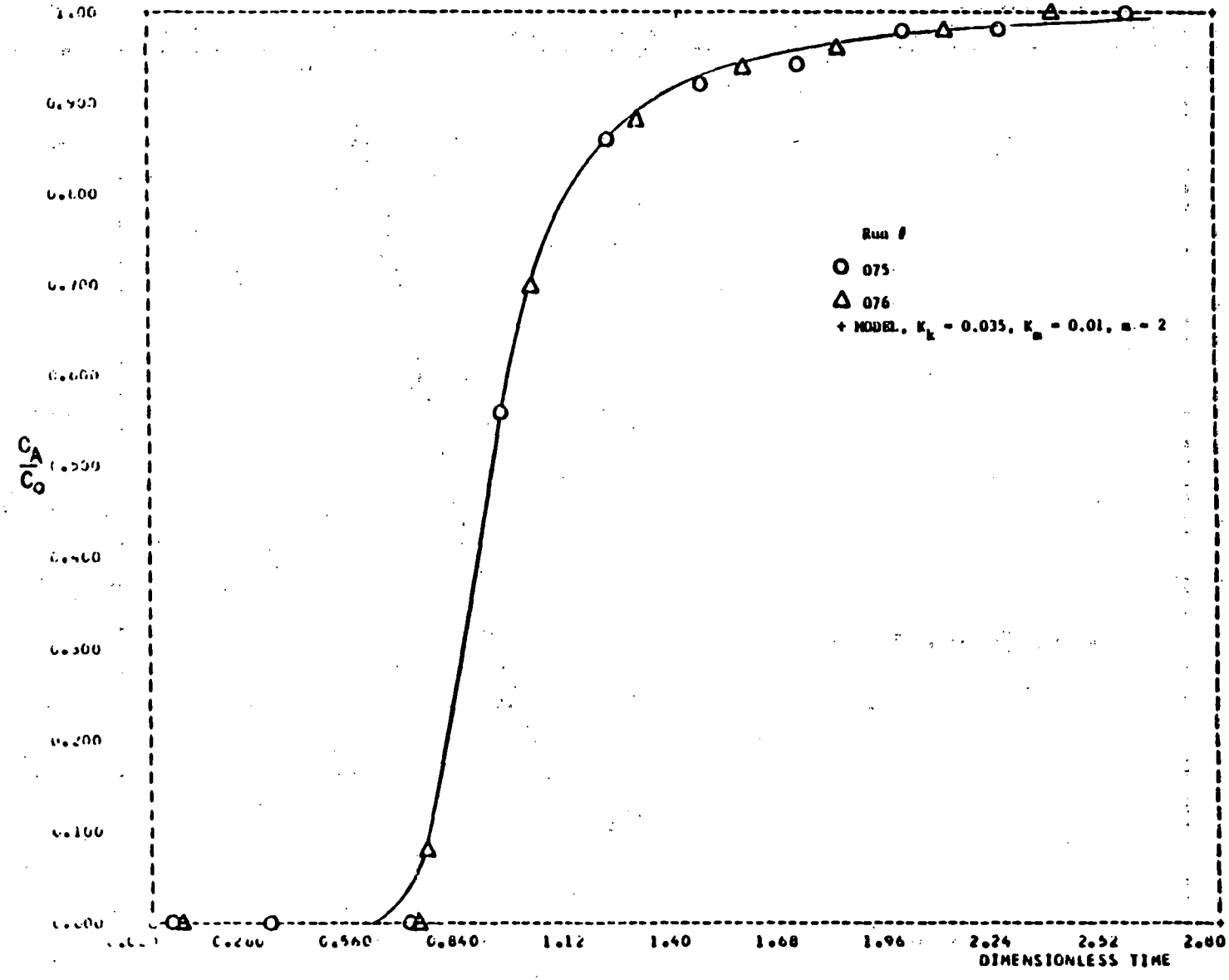
Run #
075
076
+ MODEL, K_k = 0.035, K_m = 0.01, n = 2
C_A/C_o
0.840
1.12
1.40
1.68
1.96
2.24
2.52
2.80
DIMENSIONLESS TIME

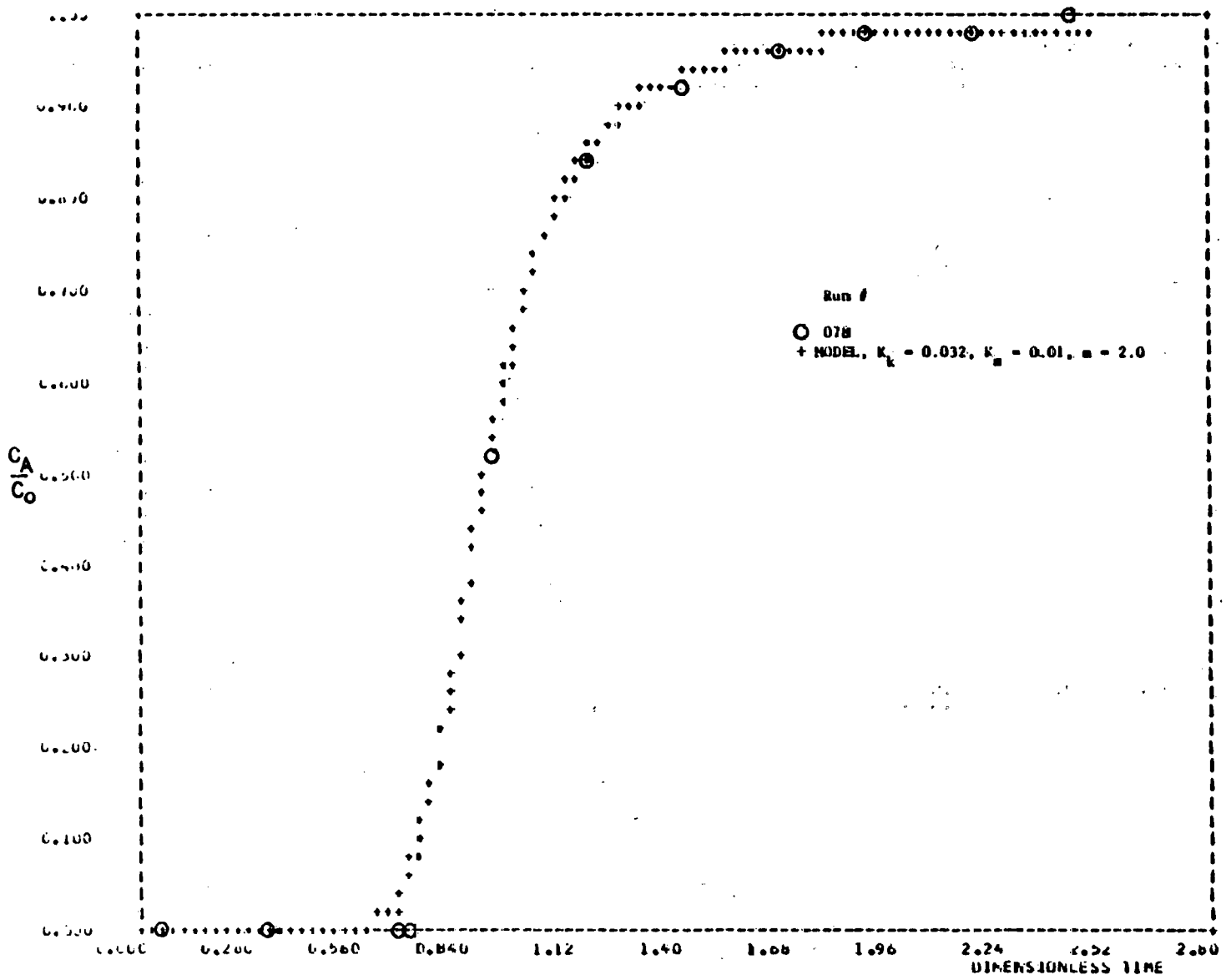
Run #
078
+ MODEL, K_k = 0.032, K_a = 0.01, n = 2.0
$\frac{C_A}{C_o}$
0.200
0.560
0.840
1.12
1.40
1.68
1.96
2.24
2.52
2.80
DIMENSIONLESS TIME

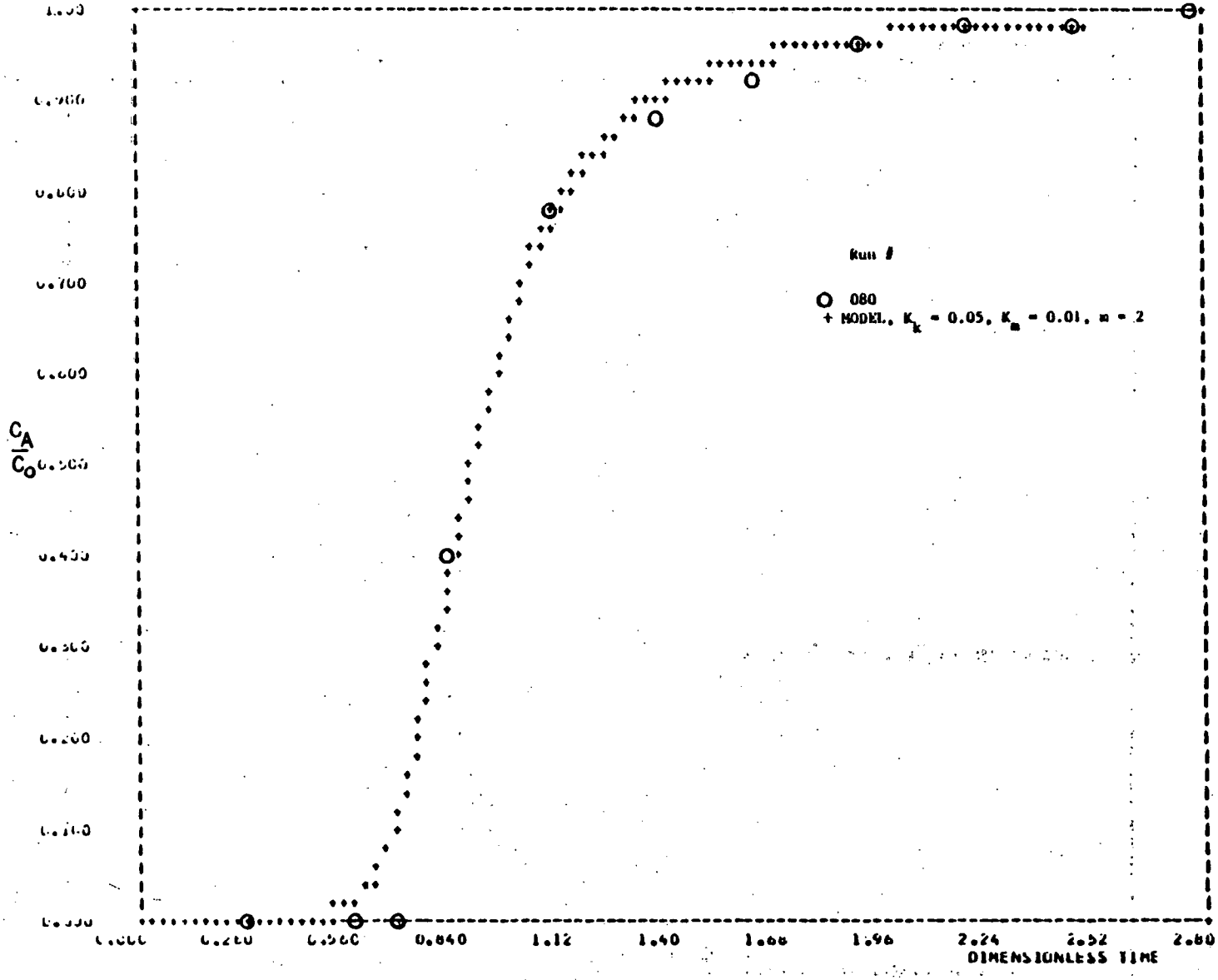
Run #
080
+ MODEL, K_k = 0.05, K_m = 0.01, n = 2
$\frac{C_A}{C_o}$
0.840
1.12
1.40
1.68
1.96
2.24
2.52
2.80
DIMENSIONLESS TIME

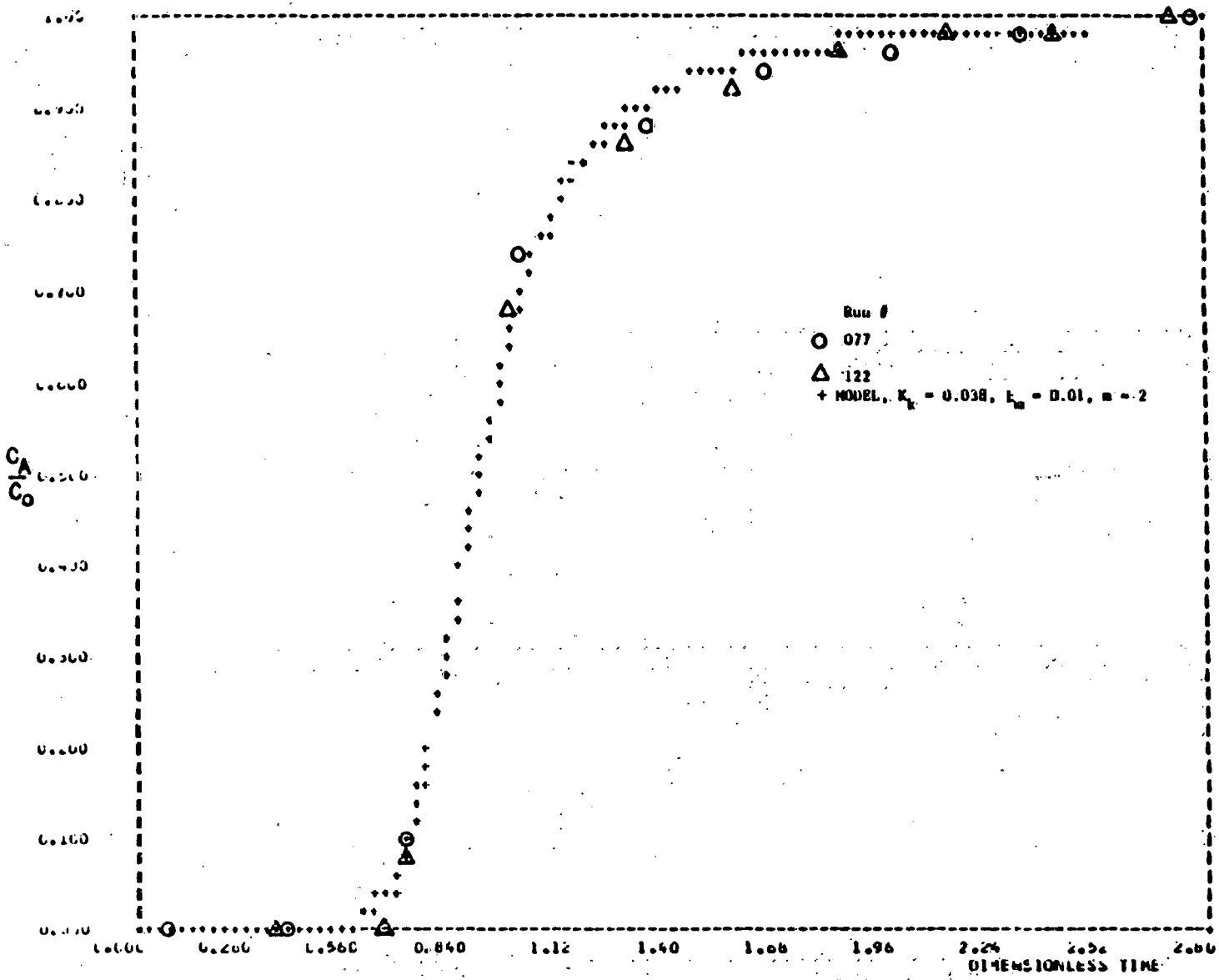
Run #
077
122
+ MODEL, K_L = 0.038, L_m = 0.01, m = 2
$\frac{C_A}{C_o}$
0.200
0.560
0.840
1.12
1.40
1.68
1.96
2.24
DIMENSIONLESS TIME

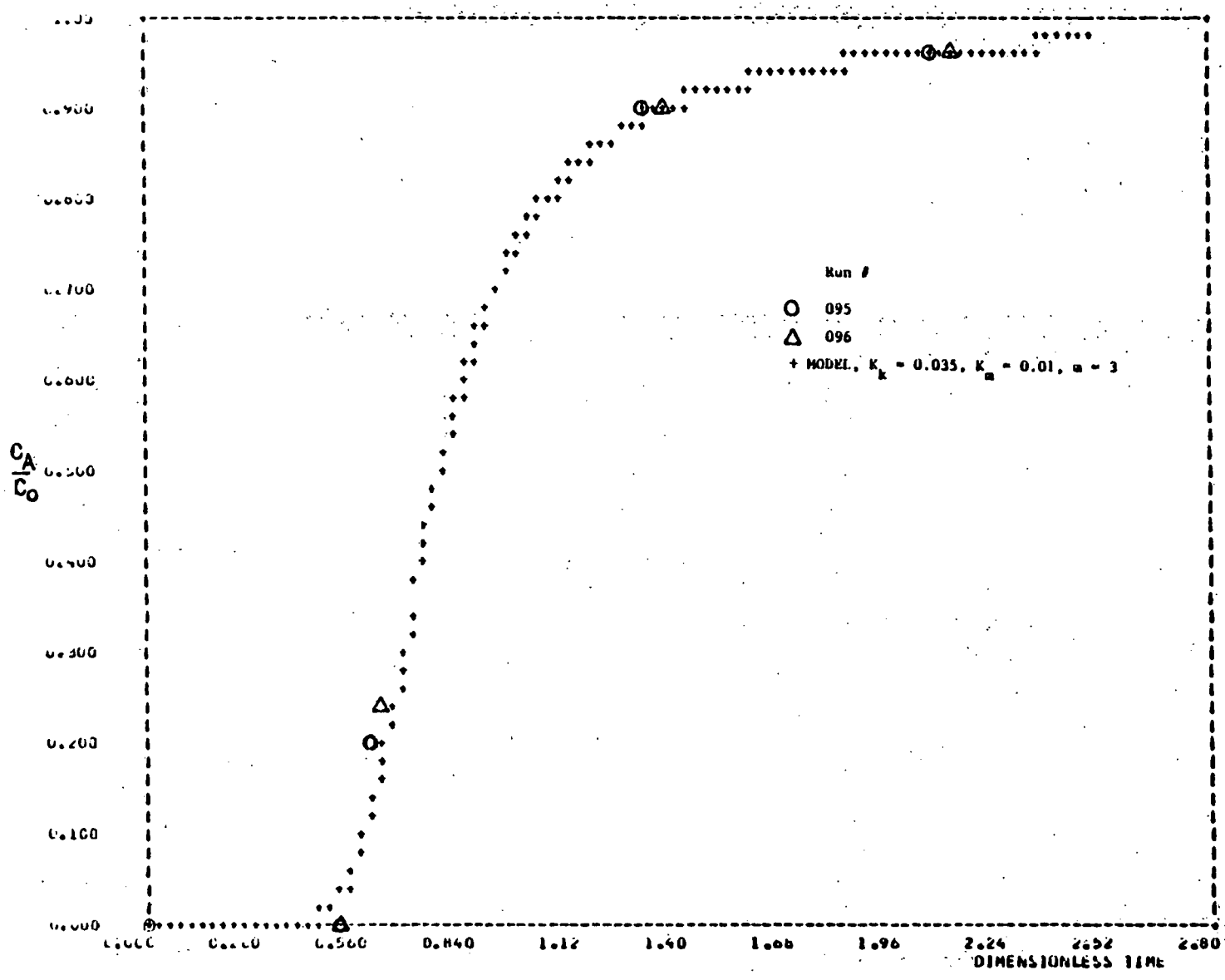
Run #
095
096
+ MODEL, K_k = 0.035, K_m = 0.01, n = 3
$\frac{C_A}{C_o}$
0.800
0.600
0.400
0.200
0.100
0.840
1.12
1.40
1.96
2.24
2.80
DIMENSIONLESS TIME

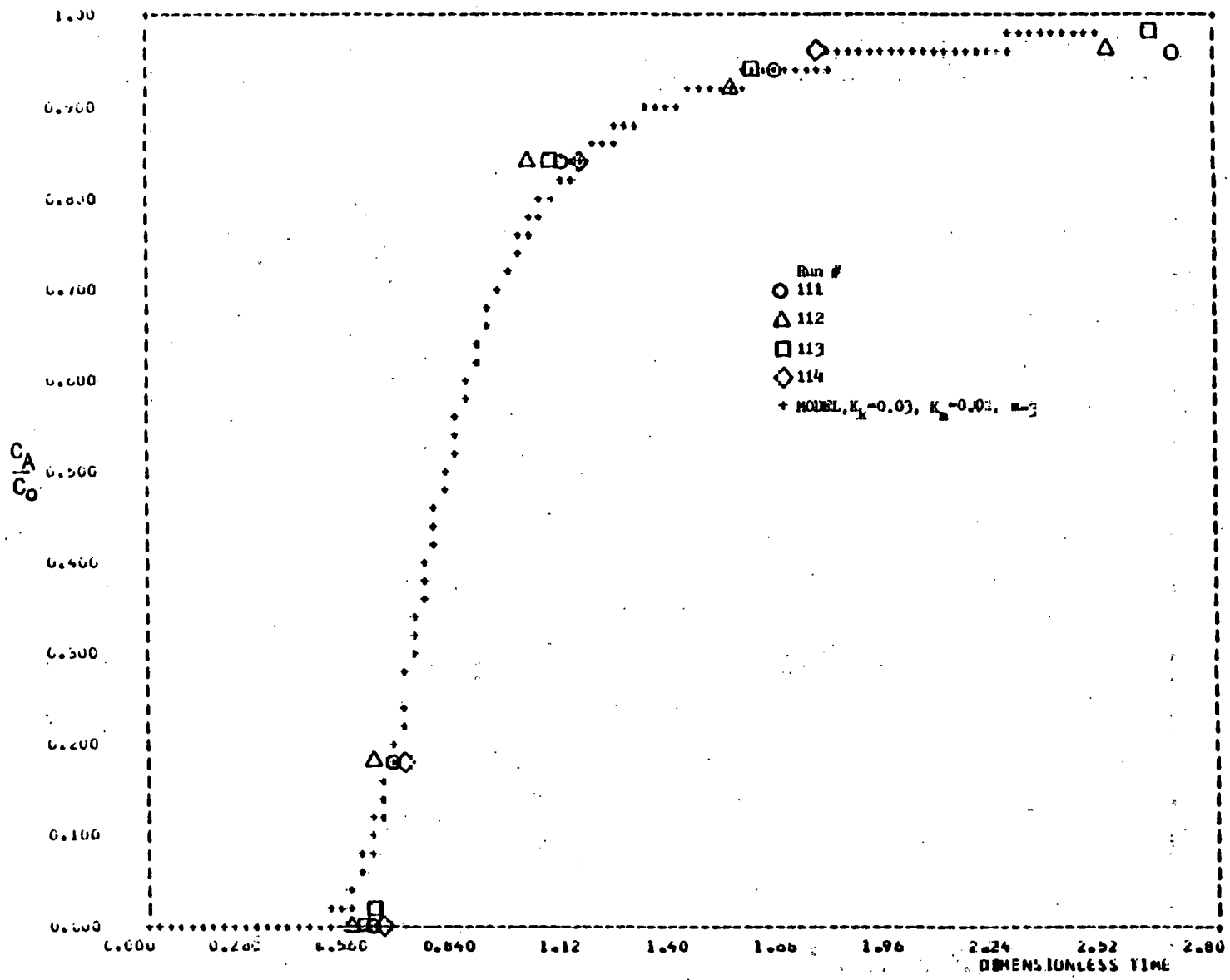
Run #
111
112
113
114
+ MODEL, K_k=0.03, K_a=0.0
$\frac{C_A}{C_o}$
0.800
0.700
0.600
0.500
0.400
0.300
0.200
0.100
0.000
0.000
0.560
0.840
1.12
1.40
1.68
1.96
2.24
2.52
2.80
DIMENSIONLESS TIME

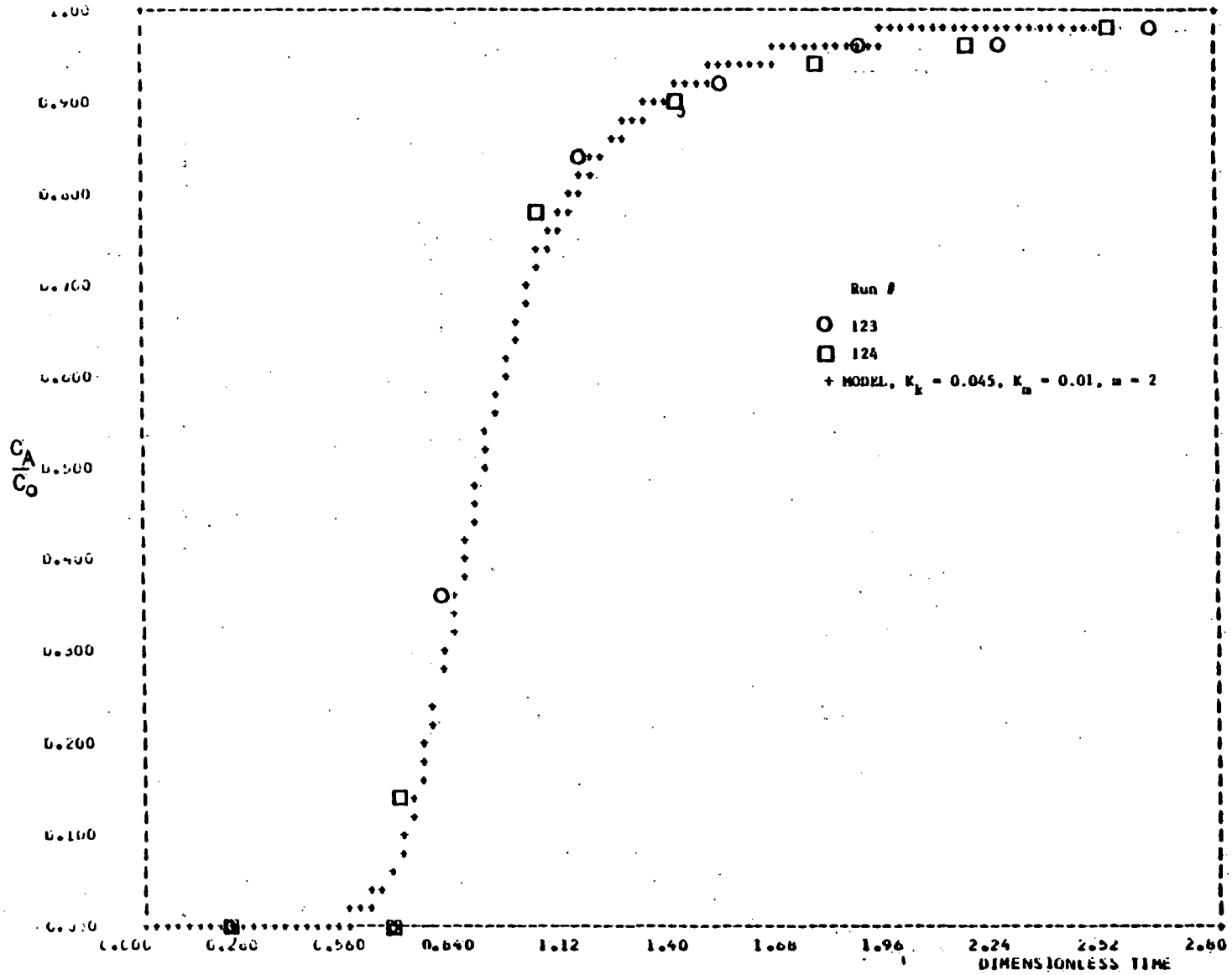
Run #
123
124
+ MODEL, K_k = 0.045, K_m = 0.01, m = 2
C_A/C_o
0.500
0.400
0.300
0.200
0.100
0.560
0.640
1.12
1.40
1.68
1.96
2.24
2.52
2.80
DIMENSIONLESS TIME

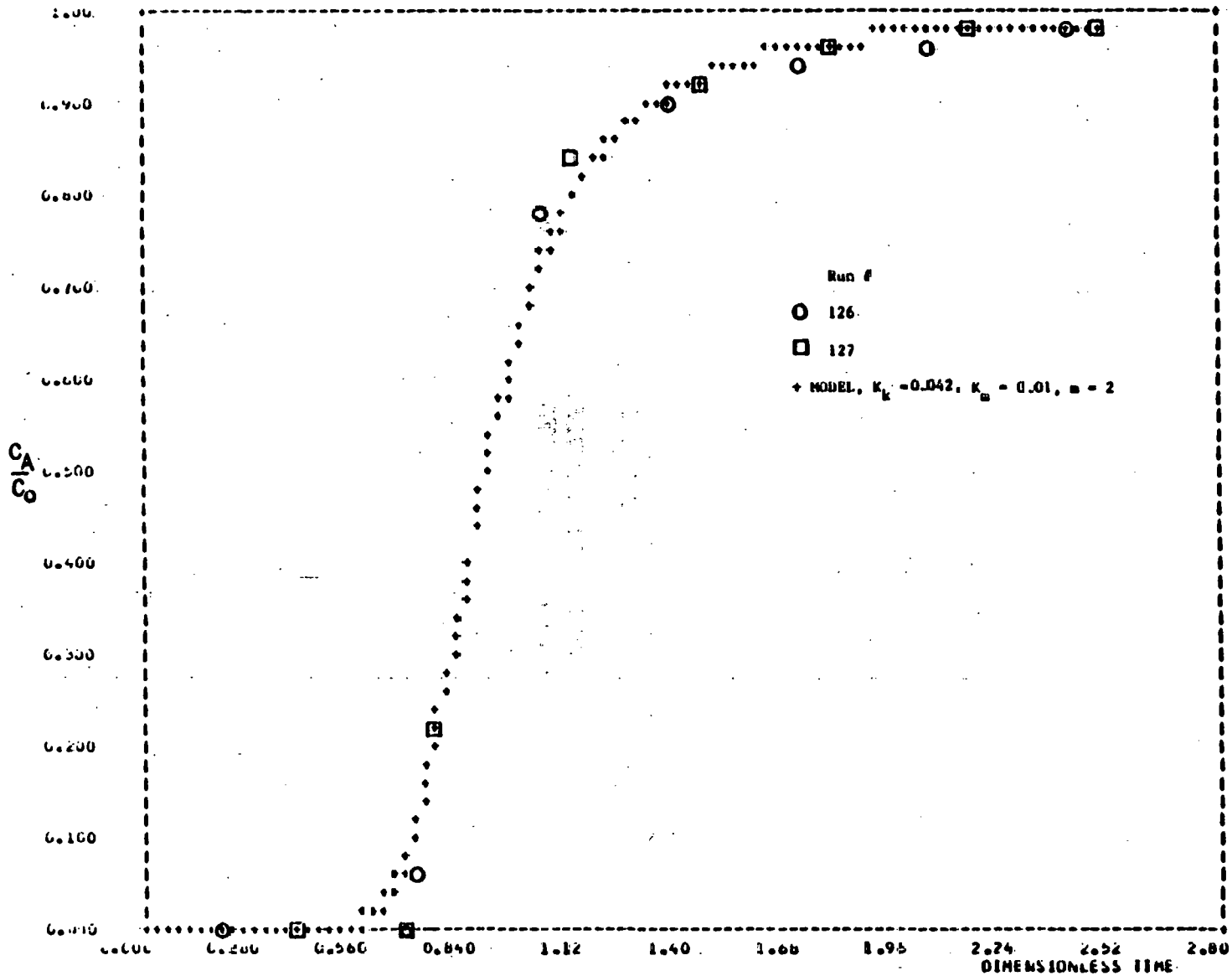
Run #
126
127
+ MODEL, K_k =0.042, K_m = 0.01, n = 2
C_A/C_o
0.400
0.300
0.200
0.100
0.560
0.840
1.12
1.40
1.68
1.96
2.24
2.52
2.80
DIMENSIONLESS TIME

APPENDIX G

CONTINUOUS DESULFURIZER-REGENERATOR COMPUTER SIMULATION

```
$JOB            ,TIME=(2,0)
C
C               TITLE
C
C               HOT-GAS DESULFURIZATION AND REGENERATION IN
C               A COUPLED, FLUIDIZED-BED , CONTINUOUS
C               ADSORPTION-REGENERATION SYSTEM
C
C
C               THIS PROGRAM IS ESSENTIALLY A MATERIAL AND ENERGY
C               BALANCE ON A CONTINUOUSLY OPERATING FLUIDIDIZED-BED, COUPLED
C               DESULFURIZATION-REGENERATION REACTORS.  BASED ON
C               THE INPUT DATA THE PROGRAM PREDICTS THE SOLID AND GAS
C               CONCENTRATIONS AND TEMPERATURES PREVAILING IN SUCH A SYSTEM.  IT
C               ALSO PREDICTS THE REACTOR SIZE NEEDED ASSUMING A PLUG FLOW MODEL
C               FOR GAS FLOW AND USING THE INPUT RATE PARAMETERS.
C
C
C
C
C
C     C         INPUT
C
C               SYMBOL      DESCRIPTION                                    COLUMN
C
C               WFI         MASS   FLOW RATE OF INLET GAS TO ADSORBER,
C                           LB MOLES/HR                                    1 - 10
C               AYI         H2S CONCN. OF ADSORBER INLET GAS
C     C                     MOLE FRACTION                                  21-30
C     C         ATI         TEMPERATURE OF ADSORBER INLET GAS, DEG F.      31-40
C     C         AYO         DESIRED ADSORBER OUTLET CONCENTRATIONOF
C     C                     H2S, MOLE FRACTION                             41-50
C     C         APR         OPERATING PRESSURE OF ADSORBER, PSIG.          51-60
C
C     C         CARD # 2
C
C     C         HR(1)       STANDARD HEAT OF REACTION OF ADSORPTION
C     C                     REACTION, CALORIES / 2 GM. MOLES OF FES        1-10
C     C         HR(2)       STANDARD HEAT OF REACTION FOR REGENERATION
C     C                     REACTION WITH OXYGEN,  CALS. / GM. MOLES FE2O3 21-30
C
C     C         CARD # 3
C     C         HO          SOLID SORBATE FES CAPACITY, LB MOLE/LB ASH-    1 - 10
C
C
C     C         CARD # 4
C
C     C         RYN2A       NITROGEN CONCENTRATION IN REGENERATOR INLET GAS
C     C                     BEFORE MIXING WITH RECYCLED GAS,MOLE FRACTION  1-  10
C     C         RYO2A       OXYGEN CONCENTRATION AT SAME LOCATION,
C     C                     MOLE FRACTION.                                 11 - 20
C     C         RYIA        SULFUR DIOXIDE CONCENTRATION AT SAME LOCATION,
C     C                     MOLE FRACTION.                                 21 -30
C     C         RTA         GAS TEMPERATURE AT SAME LOCATION, DEG F        31 - 40
C     C         RTS         TEMPERATURE OF  REGENERATOR BED, DEG F         41 - 50
C     C         RPR         REGENERATOR PRESSURE, PSIG                      51-60
C
C     C         CARD # 5
C
```

```
C     C     THE         DESIRED  GAS TEMP. AT EXIT OF HEAT EXCHANGER,
C     C                 DEG F.                                          1 - 10
C     C     EXAIR       EXCESS AIR OR OXYGEN PROVIDED AS A PERCENTAGE
C     C                 OF THE THEORETICAL AMOUNT NEEDED.               11 - 20
C
C     C     CARD # 6
C
C     C     YN2         NITROGEN CONCENTRATION IN INLET GAS TO ADSORBER,
C     C                 MOLE FRACTION.                                  1 - 10
C     C     YCO2        CARBODIOXIDE CONCENTRATION AT SAME LOCATION,
C     C                 MOLE FRACTION.                                  11 - 20
C     C     YCO         CARBON MONOXIDE CONCENTRATION AT SAME LOCATION,
C     C                 MOLE FRACTION.                                  21 - 30
C     C     YH2         HYDROGEN CONCENTRATION AT SAME LOCATION,
C     C                 MOLE FRACTION                                   31 - 40
C     C     YCH4        METHANE CONCENTRATION AT SAME LOCATION
C     C                 MOLE FRACTION.                                  41 - 50
C     C     YH2O        WATER VAPOR CONCENTRATION AT SAME LOCATION,
C     C                 MOLE FRACTION.                                  51 - 60
C     C     AYI         H2S CONCENTRATION AT SAME LOCATION, MOLE FRACTION 61 - 70
C
C     C     CARD # 7
C
C     C     C(1,1)      COEFFICIENTS IN THE CORRELATION FOR
C     C     C(1,2)      HEAT  CAPACITY OF FE2O3                         11 - 20
C     C     C(1,3)      CPG = C(J,1) + C(J,2)*T + C(J,3)*T*T            21 - 30
C     C                 WHERE T IS IN DEG K
C
C     C     CARD # 8
C
C     C     C(2,1)      SAME AS ABOVE, FOR H2S                           1- 10
C     C     C(2,2)                                                      11 - 20
C     C
C     C     C(2,3)                                                      21 - 30
C
C     C     CARD # 9
C
C     C     C(3,1)      SAME AS ABOVE, FOR H2                            1 - 10
C     C     C(3,2)                                                      11 - 20
C     C     C(3,3)                                                      21 - 30
C
C     C     CARD # 10
C
C     C     C(4,1)      SAME AS ABOVE  , FOR FES                         1 - 10
C     C     C(4,2)                                                      11 - 20
C     C     C(4,3)                                                      21 - 30
C
C     C     CARD # 11
C
C     C     C(5,1)      SAME AS ABOVE, FOR H2O                           1 - 10
C     C     C(5,2)                                                      11 - 20
C     C     C(5,3)                                                      21 - 30
C
C     C     CARD # 12
C
C     C     C(6,1)      SAME AS ABOVE, FOR SO2                           1 - 10
C     C     C(6,2)                                                      11 - 20
C     C     C(6,3)                                                      21 - 30
C
C     C     CARD # 13
```

```
C
C     C(7,1)      SAME AS ABOVE, FOR O2                                1 - 10
C     C(7,2)                                                           11 - 20
C     C(7,3)                                                           21 - 30
C
C     CARD # 14
C
C     RHOP        APPARANT DENSITY OF ASH, LBS./CFT.                   1 - 10
C     POROS       BED POROSITY                                         11-20
C
C     CARD # 15
C
C     SCON(1)     DESIRED SOLID CONVERSION IN ADSORBER,
C                 FRACTION                                             1 - 10
C     SCON(2)     SAME AS ABOVE, IN REGENERATOR, FRACTION              11 - 20
C
C     CARD # 16
C
C     RU1         HEAT LOST TO ATMOSPHERE PER LB MOLE OF GAS
C                 PROCESSED IN THE REGENERATOR, BTU                    1-10
C     AQ1         THE SAME IN THE ADSORBER                             11-20
C     CARD # 17
C
C     UMF         MINIMUM FLUIDIZING VEL. OF ASH, FT/HR                1-10
C                  AT 1000 F.
C     UOVUMF      RATIO OF ACTUAL SUPERFICIAL LINEAR VELOCITY
C                 TO THE MINIMUM FLUIDIZING VELOCITY AT 1000 F         11-20
C     CPS         HEAT CAPACITY OF THE SOLID, BTU/LB F                 21-30
C
C     CARD # 18
C
C     W           SPECIFIED FLOW RATE OF SOLIDS, LB/HR                 1-10
C
C
C     NOMENCLATURE
C
C     THE FOLLOWING IS A LIST OF IMPORTANT CONSTANT AND VARIABLE NAMES
C
C     SYMBOLS     DESCRIPTION                                  UNITS
C
C     AFO         GAS MASS VELOCITY AT ADSORBER OUTLET         LB MOLES/HR
C     W           ASH FLOW RATE                                LBS/HR
C     ATO         GAS TEMP. AT ADSORBER OUTLET                 DEG F
C     RTS         TEMP. OF SOLIDS  IN REGENERATOR              DEG F
C     ATS         TEMP. OF SOLIDS IN ADSORBER                  DEG F
C     RTI         TEMP. OF GAS AT REGENERATOR INLET            DEG F
C     RYI         SO2 CONCN. AT REGENERATOR INLET              MOLE FRACTION
C     RFI         GAS MASS VELOCITY AT REGENERATOR INLET       LB MOLES/HR
C     RFO         GAS MASS VELOCITY AT REGENERATOR OUTLET      LB MOLES/HR
C     RYO         SO2 CONCN. AT REGENERATOR OUTLET             MOLE FRACTION
C     RTO         GAS TEMP. AT REGENERATOR OUTLET              DEG F
C     RFS         MASS VELOCITY OF GAS LEAVING REGENERATOR
C                 AT RECYCLE BRANCH                            LB MOLES/HR
C     RYS         SO2 CONCN. AT REGENERATOR RECYCLE POINT      MOLE FRACTION
C     RTS         GAS TEMP. AT REGENERATOR RECYCLE POINT       DEG F
C     RRA         FRACTION OF GAS LEAVING REGENERATOR
```

```
C     C                    THAT IS RECYCLED                          FRACTION
C     C     SR             AMOUNT OF H2S ADSORBED                    LB MOLES/HR
C
C
C
C
C     C     CALC1          SUBROUTINE FOR CALCULATING HEAT CAPACITY OF
C     C                    GAS  IN THE ADSORBER
C
C     C     CALC2          SUBROUTINE FOR CALCULATING HEAT CAPACITY OF GASIN THE
C     C                    REGENERATOR
C
C     C     COMP           SUBROUTINE FOR CALCULATING GAS COMPOSITIONS
C
C     C     HEAT           SUBROUTINE FOR CALCULATING HEAT OF REACTION  FOR
C     C                    BOTH THE ADSORPTION AND REGENERATION REACTIONS
C     C                    AT ANY TEMPERATURE
C
C     C     ASIZE          SUBROUTINE FOR CALCULATING THE REACTOR SIZE
C     C                    NEEDED FOR ADSORPTION
C
C     C     RSIZE          SUBROUTINE FOR CALCULATING THE REACTOR SIZE
C     C                    NEEDED FOR REGENERATION
C
C
C
C
C
      REAL MO
      COMMON C(7,3)
      COMMON CON(2)
      COMMON DEL
      COMMON/SIZE/RHOP,POROS,SCON
      DIMENSION MR(2),DEL(2,3),DELT(2)
      DIMENSION VOL(2)
      DIMENSION AZ(2)
      DIMENSION SAREA(2),DIA(2)
      DIMENSION SCON(2)
      READ, AFI,AYI,ATI,AYO,APR
      READ, MR(1),MR(2)
      READ,MO
      READ,KYN2A,KYO2A,RYIA,RTA,RTS,RPR
      READ, THE,EXAIR
      READ, YN2,YCO2,YCO,YH2,YCH4,YH2O,AYI
      READ, ((C(J,I),I=1,3),J=1,7)
      READ , RHOP,POROS
      READ, SCON(1), SCON(2)
      READ, AQ1, RQ1
      READ,UMF,QQVUMF,CPS
      READ,W
      ATS = ATI
      ATO = RTS
       RTI = THE
      ATO = ATI
      AFO = (AFI*(1.0-AYI)) /(1.0-AYO)
      SR= AFI*AYI -AFO*AYO
      XO = SCON(1)*MO
      XI = XO - (SR/W)
      IF (XI.GT.0.0)  GO TO 12
      WRITE (6,1003) XI
1003  FORMAT (////////,2X,'RES CONCN OF INCOMING',/, 2X,
```

```
     1 'ASH TO ADSORBER (XI) = ',E16.5,' LB MOLES/LB ASH',/,2X,'XI IS
     2NEGATIVE SINCE ASH FLOW RATE (W) IS TOO LOW.  CHOOSE A HIGHER
     3VALUE OF W',//////)
34         GO TO 104
35   12    CONTINUE
36         WRITE(6,1002)
37   1002  FORMAT('1',58X,'I N P U T  D A T A',/,59X,'*****************')
38         WRITE(6,1000) AFI,APR,ATS,ATI,AQ1,YN2,YCO2,YCO,YH2,YCH4,AYI,YH2O
39   1000  FORMAT(////,2X,'ADSORBER CONDITIONS(INPUT DATA):',//,4X,
     1'FLOW RATE OF INLET GAS (AFI) =', F6.2,'LB. MOLES / HR.',/,4X,
     2'PRESSURE, (APR) = ',F8.1,' PSIG',/,4X,
     3'TEMP. OF BED, (ATS) =', F8.1,' F',/,4X,
     4'TEMP. OF INLET GAS,(ATI) =',F8.1,' F',/ ,4X,
     C'HEAT LOSS TO ATMOSPHERE,(AQ1)=' , F12.1,'BTU/LB MOLE GAS',//6X,
     5'INLET GAS COMPOSITION:',/,18X,'MOLE FRCN.',/,12X,
     7'N2    ',F7.4,/,12X,'CO2   ',F7.4,/,12X,'CO    ',F7.4,/,12X,
     8'H2    ',F7.4,/,12X,'CH4   ',F7.4,/,12X,'H2S   ',F7.4,/,12X,
     9'H2O   ',F7.4,//)
40         WRITE(6,1001)RTA,RPR,RTS, THE,RQ1
41   1001  FORMAT(//,2X,'REGENERATOR CONDITIONS (INPUT DATA):',//,4X,
     1'TEMP. OF INLET AIR,(RTA), = ',F8.1,' F',/,4X,
     2'BED PRESSURE, (RPR)= ',F8.1,' PSIG',/,4X,
     3'TEMP. OF BED,(RTS) = ',F8.1,' F',/,4X,
     4'GAS TEMP. AT HEAT EXCHANGER EXIT, (THE) = ',F8.1,' F',/,4X,
     5'HEAT LOSS TO ATMOSPHERE, (RQ1)= ',F12.1,' BTU/LB MOLE GAS',//)
42         HR(1) = -12704.0
43         HR(2) =-1.6490.0
44         S= 298.0
45         DO 10 I=1,3
46         DEL(1,I) = 2.0*C(4,I) + 3.0*C(5,I) - C(1,I) - 2.0*C(2,I)- C(3,I)
47         DEL(2,I)=    + 0.5*C(1,I) - C(4,I) - 1.75*C(7,I) + C(6,I)
48   10    CONTINUE
49         DO 11 K=1,2
50         DELT(K) = DEL(K,1)*S + (DEL(K,2)/2.0)*S*S + (DEL(K,3)/3.0)*S*S*S
51         CON(K) = HR(K) - DELT(K)
52   11    CONTINUE
53         CALL COMP (YN2,YCO2,YCO,YH2,YCH4,AYI, YH2O,AFI,AFO,
     1YN2O,YCO2O,YCOO,YH22,YCH4O,YH2OO)
54         CALL CALC1 (YN2,YCO2,YCO,YH2,YCH4,AYI ,YH2O,ATI,ACPGI)
55         CALL CALC2 (RYN2A,RYO2A,RYIA,RTA,RCPGA)
56         TO = 32.0
57   49     CONTINUE
58         RRA = 0.0
59         DO 103 NZ=1,2
60         STEP = 0.1
61   30    CONTINUE
62         DO 100 I= 1,10
63         AFA = 8.3333*SR
64         RFO = (SR*0.75 -RFA) /(RRA-1.0 )
65         AFI = RRA*RFO + RFA
66         RFS = RFO*(1.0- RRA)
67         RYO2O = 0.0
68         RYN2O = (RFA*0.79) / RFS
69         RYN2 = (RRA*RFO*RYN2O + RFA*0.79) /RFI
70         RYO2 = (RFA*0.21) / RFI
71         RYO = SR / RFS
72         RYI = (RRA*RFO+RYO) / RFI
73         AQ=AQ1*AFI
74         AQ=RQ1*RFI
75         AEQ1 = AFI*ACPGI*(ATI-TO)
76         CALL HEAT (ATS,RTS,AHX,RHR)
```

```
      CALL CALC1 (YN20,YCO20,YCOO,YH22,YCH40,AYO,YH20O,ATO,ACPGO)
      CALL CALC2 (RYN2,RYO2,RYI,RTI,RCPGI)
      CALL CALC2 (RYN20,RYO20,RYO,RTO,RCPGO)
      CALL CALC2 (RYN20,RYO20,RYO,THE,RCPGH)
      AMRA = AMR*SR
      RMRR= RMR*SR
      ATO = (( AFI*ACPGI*(ATI-TO) + W*CPS*(RTO-TO) - ( AMR*SR)
     2-AO ) / (AFO*ACPGO + W*CPS) ) +32.0
      ATS = ATO
      RTI = (((RRA*RFO*RCPGH*(THE-TO)) + (RFA*RCPGA*(RTA-TO)))
     2/ (RFI*RCPGI)) +TO
      QHE =(RFO*RRA*RCPGO* (RTO-TO))-(RFO*RRA*RCPGH*(THE-TO))
      AEGO = AFO*ACPGO*(ATO-TO)
      REGI = RFA*RCPGA*(RTA-TO)
      REGO = RFS*RCPGO*(RTO-TO)
      ENIS = W*CPS* (RTS-ATS)
      GEN=-(AMRA+RMRR)
      DENR = REGO-REGI
      DENA= AEGO-AEGI
      ENG = AEGO-AEGI+REGO-REGI +AQ + RQ +QHE
      GIVE =-AMRA + ENIS
      QREMOV =-RMRR -RQ-ENIS-DENR
  100 CONTINUE
      QUANT = ABS(QHE-QREMOV)
      IF (QUANT.LE.0.001*QREMOV) GO TO 101
      IF (QHE.GT.QREMOV) GO TO 102
      RRA = RRA + STEP
      IF (RRA.GE. 1.0) GO TO 101
      GO TO 50
  102 CONTINUE
      RRA = RRA- STEP
      STEP = 0.1*STEP
      IF(STEP.LE.0.0001) GO TO 101
      RRA = RRA +STEP
      GO TO 50
  101 CONTINUE
      CALL        ASIZE (AFI,AYI,ATS,AYO,MO,APR,UMF,UOVUMF,Z,DIAM ,XA)
      DIA(1)=DIAM
      AZ(1)=Z
      SAREA(1) = 3.141 * DIA(1) *AZ(1)
  103 CONTINUE
      WRITE(6,2001)  #
 2001 FORMAT('1', 59X,'R E S U L T S' , /, 60X,'*************',////,
     12X,'ASH FLOW RATE,(W) : = ',F8.2,' LBS. / HR.',///)
      WRITE (6,2000) XI,XO,ATS,ATO,AFO,YN20,YCO20,YCOO,YH22,YCH40,AYO,
     CYH20O,YCOSO
 2000 FORMAT(    2X,'A U S O R B E R :',//,8X,
     A'FES CONCENTRATION IN ASH:', /,16X,'INLET (XI) : ',F10.8,' LB. M',
     1'OLES / LB. ASH',/,16X,'EXIT (XO)  : ',F10.8,' LB. MOLES / LB. A',
     2'SH'
     3,/,8X,'TEMP. OF ASH DEO,(ATS) = ',F8.1,' F',/,8X,
     0'TEMP. OF EXIT GAS, (ATO) = ',F8.1,' F',/,8X,
     2'FLOW RATE OF EXIT GAS, (AFO) = ',F6.2,' LB. MOLES / HR. ',//,8X,
     F'EXIT GAS COMPOSITION :',/,26X,'MOLE FRCN.',/,20X,
     G'N2    ',F7.4,/,20X,'CO2   ',F7.4,/,20X,'CO    ',F7.4,/,20X,
     H'H2    ',F7.4,/,20X,'CH4   ',F7.4,/,20X,'H2S   ',F7.4,/,20X,
     I'H2O   ',F7.4,/,20X,'COS   ',F7.4,//)
      WRITE (6,202) XA,AZ(1),DIA(1)
  202  FORMAT(    ,4X,'FINAL CONVERSION H2S = ',F10.5,/,4X,
     C'BED HEIGHT REQUIRED = ',F14.5, 'FT.',/,4X,
     C'REQUIRED  DIAMETER OF ADSORBER = ',F10.3,' FT.', //)
```

```
      WRITE (6,2002) RTI,RFA,RFO,RFI,RFS
 2002 FORMAT(//,2X,'R E G E N E R A T O R :',//,8X,
     1'TEMP. OF GAS AT BED INLET, (RTI) : = ',F8.1,' F', /,8X,
     2'AIR FLOW RATE, (RFA) = ',F6.2,' LB. MOLES / HR.',/,8X,
     3'GAS FLOW RATE AT BED EXIT, (RFO) = ',F6.2,' LB. MOLES /HR.',/,8X,
     4'GAS FLOW RATE AT BED INLET (RFI) = ',F6.2,' LB. MOLES / HR.',/,8X
     5,'GAS FLOW RATE AT EXIT AFTER RECYCLE BRANCH, (RFS) = ',F6.2,
     6' LB. MOLES / HR.')
      WRITE(6,2003) RYN2,RYN2O,RYO2,RYO2O,RYI, RYO,RH2O, RH2OO
 2003 FORMAT(//,8X,
     C       'GAS COMPOSITION (MOLE FRACTION) : ',/,26X,'BED INLET', 8X,
     1'BED EXIT',/,20X,'N2    ',F7.4,8X,F7.4,/,20X,'O2    ',F7.4,8X,
     2F7.4,/,  20X,'SO2   ',F7.4,8X,F7.4,/,20X,'H2O   ', F7.4,8X,F7.4,/)
      RGU=RYO2O
      RIN=  RYO2
      CALL        RSIZE(RFI,RIN,RTS,RGU,MO,RPR,UMF,UOVUMF,Z,DIAM,XA)
      AZ(2)=Z
      DIA(2)=DIAM
      WRITE (6,702) AA,AZ(2),DIA(2)
  702  FORMAT(    ,4X,'FINAL CONVERSION O2  = ',F10.5,/,4X,
     1'BED HEIGHT REQUIRED = ',F14.5, 'FT.',/,4X,
     2'REQUIRED  DIAMETER OF REGENERATOR',F10.3,' FT.', //)
      WRITE(6,2004) AHRA,ENIS,AQ,DENA
 2004 FORMAT('1',1X,'E N E R G Y  B A L A N C E  :',///,
     1 2A,'ADSORBER :',//,8X,'HEAT GENERATED BY REACTION, (AHRA) = ',
     2F12.1,' BTU / HR. ', /,8X,
     3'HEAT GIVEN UP BY ASH, (ENIS) : ',F12.1,' BTU / HR. ',/,8X,
     4'HEAT LOST TO ATMOSPHERE, (AQ) = ',F12.1,' BTU/ HR.',/,8X,
     5'ENTHALPY GAIN OF GAS, (DENA) = ',F12.1,' BTU / HR.',/,8X)
      WRITE(6,2005) RHRR,ENIS,RQ,DENR,QREMOV,QHE
 2005 FORMAT(///,2X,'REGENERATOR :', //,8X,
     1'HEAT GENERATED BY REACTION, (RHRR) = ',F12.1,' BTU / HR.',/,8X,
     2'HEAT GAINED BY ASH, (ENIS) = ',F12.1,' BTU / HR.',/,8X,
     3'HEAT LOST TO ATMOSPHERE (RQ) = ',F12.1,' BTU / HR.',/,8X,
     4'ENTHALPY GAIN OF GAS (REGEN. + RECYCLE), DENR = ',F12.1,/,8X,
     5'HEAT REQUIRED TO BE REMOVED BY  H.E., (QREMOV) = ',F12.1,
     6' BTU / HR. ',/,8X,'HEAT ACTUALLY REMOVED BY H. E., (QHE) = ',
     7F12.1,' BTU / HR.')
      WRITE(6,2006) GEN,ENG
 2006 FORMAT(///,2X,'TOTAL ENTHALPY BALANCE (ADSORBER + REGEN.) :',//,8X
     1,'TOTAL HEAT GENERATED BY REACTIONS, (GEN) = ' ,F12.1,' BTU / HR.'
     2,/,8X,'ENTHALPY INCREASE OF GASES,(DENA + DENR)    ',/,
     312X,'+ HEAT REMOVED BY HEAT EXCHANGER, (QHE))',/,
     412X,'+ HEAT LOST TO ATMOSPHERE, (AQ+RQ)      )=',F12.1,
     5' BTU / HR.',//////////)
  104 CONTINUE
      STOP
      END

      SUBROUTINE CALC1 ( YN2,YCO2,YCO,YH2,YCH4,YH2S,YH2O,AT,ACPG)
      T=(AT+460.0)/1.8
      YA=0.3224 + 1.250E-05*T -0.001E-06*T*T
      YB= 3.214+10.396E-03*T -3.545E-06*T*T
      YC=6.+20+ 1.005E-03*T -0.196E-06*T*T
      YD = 0.497 -0.200E-05*T + 0.481E-06*T*T
      YE = 3.361 +16.044E-05*T - 4.30E-06*T*T
      YF = 6.802 + 5.13+E-03*T - 0.854E-06*T*T
      ACPG = YN2*YA+YCO2*YB + YCO*YC + YH2*YD + YCH4*YE + YH2S*YF
      RETURN
      END
```

```
      SUBROUTINE CALC2 (RYN2,RYO2,RSO2,RT,RCPG)
      T=(RT+460.0)/1.8
      YA=6.524+1.250E-03*T-0.001E-06*T*T
      YB = 6.104 + 3.102E-03*T -0.923E-06*T*T
      YC = 7.70 + 5.30E-03*T -0.83E-06 *T*T
      RCPG = RYN2*YA + RYO2*YB + RSO2*YC
      RETURN
      END

      SUBROUTINE COMP ( A,B,C,D,E,F,G,AFI,AFO,P,Q,R,S,T,U)
      P= (AFI*A)/AFO
      Q = (AFI*B)/AFO
      R= (AFI*C)/AFO
      S= (AFI*D)/AFO
      T= (AFI*E)/AFO
      U= (AFI*G)/AFO
      RETURN
      END

      SUBROUTINE HEAT (T1,T2,AHRT1,AHRT2)
      DIMENSION HR(2),DEL(2,3),DELT(2),CON(2),AHRT(2),T(2)
      COMMON C(7,3)
      COMMON CON
      COMMON DEL
      T(1) =T1
      T(2) =T2
      DO 12 L= 1,2
      T(L) = (T(L) + 460.0)/1.8
      DELT(L) = DEL(L,1)*T(L) + (DEL(L,2)/2.0)* T(L)* T(L)  +
     U  (DEL(L,3)/3.0)*T(L) * T(L) * T(L)
      AHRT(L) = CON(L) + DELT (L)
      AHRT(L) =(AHRT(L)/251.996)*454.0
12    CONTINUE
      AHRT1 = AHRT(1)/2.0
      AHRT2 = AHRT(2)
      RETURN
      END

      SUBROUTINE ASIZE (AFI,AYI,ATS,AYO,MO,APR,UMF,UOVUMF,Z,DIA  ,XA)
      REAL MO
      DIMENSION SCON(2)
      COMMON/SIZE/RHOP,PUROS,SCON
      A=-0.78796
      B=-1.+810895
      EOVR=5490.0
      RACOND=2.+66E13
      CAOP=AYI*100.0
      U=UOVUMF*UMF
      UCM=(U/60.0)*30.48
      AFE=0.5*MU* SCON(1)
      RHOB=(1.0-PUROS)*RHOP
      RHOBCM=RHOB*0.01602
      XA=(AYI-AYO)/AYI
      T=((ATS-32.0)/1.8)+273.0
      P1=14.7
      P2=APR+14.7
      RACON=RACOND*(UOVUMF**A)*(CAOP**B)*(EXP(-EOVR/T))
      ZCM=-(UCM  *ALOG(1.0-XA))/(RACON*((XFE    )**2.0)*RHOBCM)
      Z=ZCM/30.48
      VOFLOW=(AFI*359.0)*((ATS+460.0)/492.0)*(P1/P2)
      DIA=SQRT((VOFLOW*4.0)/(U*3.141))
```

```
      RETURN
      END

      SUBROUTINE RSIZE(RFI,RIN,RTS,ROU,MO,RPR,UMF,UOVUMF,Z,DIAM,XA)
      DIMENSION SCON(2)
      COMMON/SIZE/RHOP,POROS,SCON
      REAL MO
      T=((RTS-32.0)/1.8)+273.0
      RACON=1.1CEC7*(EXP(-404/T))
      U=UOVUMF*UMF
      UM=U/60.0
      P1=14.7
      P2=RPR*14.7
      XA=0.99
      Z=-(UM*ALOG(1.0-XA))/(RACON*MO*SCON(2))
      VOFLOW=(RFI*359.0)*((RTS+460.0)/492.0)*(P1/P2)
      DIA=SQRT((VOFLOW*4.0)/(UM*3.141))
      RETURN
      END

$ENTRY
```

INPUT DATA
****

ABSORBER CONDITIONS(INPUT DATA):

FLOW RATE OF INLET GAS (AFI) =100.00LB. MOLES / HR.
PRESSURE, (APR) = 0.0 PSIG
TEMP. OF BED, (ATS) = 1000.0 F
TEMP. OF INLET GAS,(ATI) = 1000.0 F
HEAT LOSS TO ATMOSPHERE,(AQ1)= 2.08TU/LB MOLE GAS

INLET GAS COMPOSITION:

	MOLE FRCN.
N2	0.4900
CO2	0.1700
CO	0.2000
H2	0.1000
CH4	0.0300
H2S	0.0100
H2O	0.0000

REGENERATOR CONDITIONS (INPUT DATA):

TEMP. OF INLET AIR,(RTA), = 80.0 F
BED PRESSURE, (RPR)= 0.0 PSIG
TEMP. OF BED,(RTS) = 1200.0 F
GAS TEMP. AT HEAT EXCHANGER EXIT, (THE) = 250.0 F
HEAT LOSS TO ATMOSPHERE, (RQ1)= 2.0 BTU/LB MOLE GAS

RESULTS
****

ASH FLOW RATE,(W) : = 5000.00 LBS. / HR.

ADSORBER :

FES CONCENTRATION IN ASH:
INLET (XI) : 0.00020198 LB. MOLES / LB. ASH
EXIT (XO) : 0.00040000 LB. MOLES / LB. ASH
TEMP. OF ASH BED,(ATS) = 1126.8 F
TEMP. OF EXIT GAS, (ATO) = 1126.8 F
FLOW RATE OF EXIT GAS, (AFO) = 99.01 LB. MOLES / HR.

EXIT GAS COMPOSITION :

	MOLE FRCN.
N2	0.4949
CO2	0.1717
CO	0.2020
H2	0.1010
CH4	0.0303
H2S	0.0001
H2O	0.0000
COS	0.0000

FINAL CONVERSION H2S = 0.99000
BED HEIGHT REQUIRED = 0.46046FT.
REQUIRED DIAMETER OF ADSORBER = 8.586 FT.

REGENERATOR :

TEMP. OF GAS AT BED INLET, (RTI) : = 180.5 F
AIR FLOW RATE, (RFA) = 8.25 LB. MOLES / HR.
GAS FLOW RATE AT BED EXIT, (RFO) = 19.01 LB. MOLES /HR.
GAS FLOW RATE AT BED INLET (RFI) = 19.75 LB. MOLES / HR.
GAS FLOW RATE AT EXIT AFTER RECYCLE BRANCH, (RFS) = 7.51 LB. MOLES / HR.

GAS COMPOSITION (MOLE FRACTION) :

	BED INLET	BED EXIT
N2	0.8355	0.8681
O2	0.0077	0.0000
SO2	0.0766	0.1319
H2O	0.0000	0.0000

FINAL CONVERSION O2 = 0.99000
BED HEIGHT REQUIRED = 0.05407FT.
REQUIRED DIAMETER OF REGENERATOR 8.586 FT.

ENERGY BALANCE :

ADSORBER :

HEAT GENERATED BY REACTION, (AHRA) = 14689.7 BTU / HR.
HEAT GIVEN UP BY ASH, (ENIS) : 98766.2 BTU / HR.
HEAT LOST TO ATMOSPHERE, (AQ) = 200.0 BTU/ HR.
ENTHALPY GAIN OF GAS, (DENA) = 113253.2 BTU / HR.

REGENERATOR :

HEAT GENERATED BY REACTION, (RHRR) = 260506.1 BTU / HR.
HEAT GAINED BY ASH, (ENIS) = 98766.2 BTU / HR.
HEAT LOST TO ATMOSPHERE (RQ) = 39.5 BTU / HR.
ENTHALPY GAIN OF GAS (REGEN. + RECYCLE), DENR = 69602.3
HEAT REQUIRED TO BE REMOVED BY H.E., (QREMOV) = 92098.1 BTU / HR.
HEAT ACTUALLY REMOVED BY H. E., (QHE) = 92086.6 BTU / HR.

TOTAL ENTHALPY BALANCE (ADSORBER + REGEN.) :

TOTAL HEAT GENERATED BY REACTIONS, (GEN) = 275195.8 BTU / HR.
ENTHALPY INCREASE OF GASES, (DENA + DENR))
+ HEAT REMOVED BY HEAT EXCHANGER, (QHE))
+ HEAT LOST TO ATMOSPHERE, (AQ+RQ))= 275181.6 BTU / HR.

APPENDIX H

ROTAMETER CALIBRATION CURVE

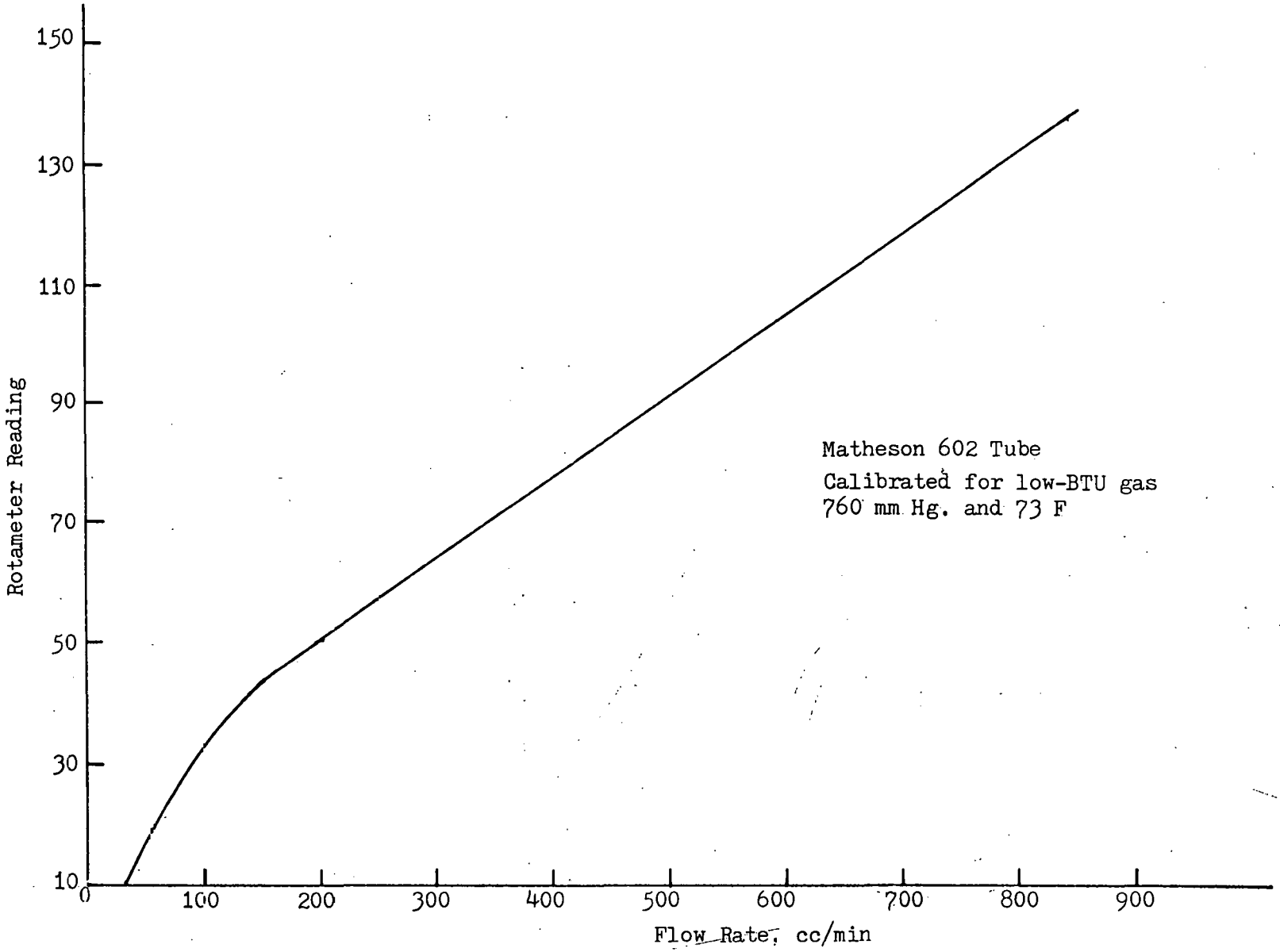

Rotameter Calibration Curve

BIBLIOGRAPHY

Abel, W.T., Schultz, F.W., and Langdon, P.F. "Removal of hydrogen sulfide from hot producer gas by solid absorbents", Publication RI-7947, Bureau of Mines, U.S. Department of the Interior, Morgantown, W.V., 1974.

Attar, A. "Chemistry, thermodynamics and kinetics of reactions of sulfur in coal-gas reactions: A review", Fuel, 57, 201, 1978.

Avedesian, M.M., and Davidson, J.F. "Combustion of carbon particles in a fluidized-bed", Trans. Inst. Chem. Eng., 51, 121, 1973.

Balzhiser, R.E., Samuels, M.R., and Eliassen, J.D. Chemical Engineering Thermodynamics, Prentice-Hall, New Jersey, 1972.

Bhada, R.U., and Sage, W.L. "Desulfurizing fuel via metal oxides", ACS Preprint, 14, 121, 1970.

Bhatia, S.P. The Removal of Organic Sulfur from Town's Gas, Ph.D. Dissertation, University of Aston, England, 1967.

Bhatia, S.J. "Removal of Organic Sulfur from coal gas", Can. J. Chem. Engng, 49, 605, 1971.

Bischoff, K. "Accuracy of the pseudo-steady state approximation for moving-boundary diffusion problems", Chem. Engng. Science, 18, 711, 1963.

Brandon, T.B. The Kinetics of the Reaction of Hydrogen Sulfide with Spherical Particles of Ferric Oxide, M.S. Thesis, Louisiana State University, Baton Rouge, Louisiana, 1973.

Bureau, A.C., and Olden, M.J.F. "Operation of the Frodingham desulfurizing plant at Exeter", The Chemical Engineer, 55, 1967.

Calistru, C., Leonte, C., and Ifrim, L. "Influence of the mass transfer upon the rate of reactions which proceed in systems containing solid phases", Bul. Inst. Politech. Iasi., 11 (1-2), 121, 1965. Cited in CA 1439a, 65, 1966.

Carberry, J.E. Chemical and Catalytic Reaction Engineering, McGraw-Hill Book Co., New York, 1976.

Case, G.D. Chemistry of Hot Gas Cleanup in Coal Gasification and Combustion, Report MERC/SP-7812, Morgantown Energy Research Center, U.S. Department of Energy, Morgantown, W.V., 1978.

Castello, G., and Riccio, M. "GC analysis of fuel gases in iron and steel processes", Fuel, 57, 469, 1978.

Crynes, B.L. Chemical Reactions as a Means of Spearation-Sulfur Removal, 156, Marcel Dekker, New York, 1977.

DeBoer, W. M. Removal of Hydrogen Sulfide from Hot Gas Utilizing a System of Fluidized Gasifier Ash, M.S. Thesis, University of Kentucky, Lexington, KY, 1975.

Doraiswamy, L.K., Bijawat, H.C., and Kunte, M.V. "Chlorination of Ilmenite in a fluidized bed", Chem. Engng. Prog., 55, No. 10, 80, 1959.

Dwivedi, P.N., and Upadhyay, S.N. "Particle-fluid mass transfer in fixed and fluidized beds", Ind. Engng. Chem., Process Design Dev., 16, No. 2, 1977.

Edwards, M.S. "H_2S removal processes for low-BTU coal gas", Report ORNL/TM-6077 prepared for the U.S. Department of Energy, January 1979.

Evans, J., Secondary Factors in the Hot Ash Desulfurization Process, M.S. Thesis, University of Kentucky, Lexington, Ky., 1978.

Farrior, W.L., Poston, A.M., and Oldaker, E.C. "Regenerable iron oxide-silica sorbents for the removal of H_2S from hot producer gas", University of Kentucky Min. Miner. Res. Report IMMR 19-PD-14-76, presented at the Fourth Energy Resource Conference, Lexington, Kentucky, 45, Jan. 1976.

Ferguson, P.A. Hydrogen Sulfide Removal from Gases, Air and Liquids, Noyes Data Corp., Park Ridge, N.J., 1975.

Fields, R.B., and Davidson, J.F. "Reaction of SO_2 with limestone in a fluidized bed; Estimation of kinetic data from a batch experiment", paper offered for presentation at AIChE National Meeting, Miami, Nov. 12-16, 1978.

Ganguly, N.D., and Banerjee, A.V. "Recovery of sulfur from iron pyrite", Ind. Engng. Chem., Process Design Dev., 12, 56, 1973.

Gavrilova, A.A. "Kinetics of the reaction of hydrogen sulfide containing gas with iron oxides", Tr. Inst. Goryuch. Iskop., Moscow, 28(2), 167 (1972).

Gidaspow, D., Leung, L., and Dharia, D. "Design of reaction controlled sorbers for environmental control: removal of nitric oxide with high capacity recuced iron oxide sorbent", A.I.Ch.E. Symposium Series, 71, No. 152, 8, 1975.

Gilliland, E.R., Mason, E.A., and Oliver, R.C. "Gas-flow patterns in beds of fluidized solids", Ind. Engng. Chem. 45, 1177 (1953).

Gray, N.B., Harvey, M.R., and Willis, G.M. "Roasting of sulfides in theory and practice", Proc. Richardson conf. Phys. Chem. Process Metallurgy, Imperial College, London, 1973.

Griffith, R.H., and Morcom, A.R. J. Chem. Soc., 1, 786 (1945).

Haas, L.A., and Khalafalla, S.E. "Formation of surface sulfides on iron through reaction with sulfur", Publication RI-7847, Bureau of Mines, U.S. Department of Interior, 1974.

Hahn, O.J., and Heilig, M.R. "Hot low-BTU gas purification with coal ash", Paper presented at the 172nd ACS National Meeting, San Francisco, California, 1976.

Hamrin, C.E. Jr., and Maa, P.S. "Desulfurization and deagglomeration of Western Kentucky coal using bottom ash", Fuel, 54, 1975.

Hasatani, M., and Wen, C.Y. "Reactivity of iron oxide sorbents for hydrogen sulfide removal from a hot low-BTU gas", Final Report, Contract No. EY-77-X-21-0118, Morgantown Energy Research Center, U.S. Department of Energy, Sept. 1977.

Hilton, G.B. Producer-gas Cleanup Using Gasifier Ash, M.S. Thesis, University of Kentucky, Lexington, Kentucky, 1974.

Jahnig, C.E., Bank, R., Gornowski, E.J., and Cranford, N.J. "Synthesis gas desulfurization", U.S. Patent 2,671,723, Serial No. 151, 482, March 1950.

Jordan, D.G. Chemical Process Development, Part 1, Interscience Publishers, New York, 1968.

Joshi, D.K., and Leuenberger, E.L. "Hot low-BTU producer gas desulfurization in fixed bed of iron oxide-fly ash", Publication FE-2033-19, U.S. ERDA, 1977. Prepared by Air Products and Chemicals, Inc., Marcus Hook, PA, under Contract E(49-18)-2033 and EX-76-C-01-2033, 1977.

Karr, C., Rahfuse, R.V., and Langdon, P.F. "Reactions of iron sulfides in simulated stack gases", J. Appl. Chem. and Biotechnol., 22, 613, 1972.

Kellog, H.H. "A critical review of sulfation equilibria", Trans. Metallug. Soc. AIME, 230, 1622, 1964.

Kertamus, N.J. "Removal of H_2S on oxidized iron", Am. Chem. Soc. Div. Fuel Chem. Prepr., 18 (2), 131, 1973.

Kirklady, J.S., and Ward, R.G. Aspects of Modern Ferrous Metallurgy, University of Toronto Press, Canada, 1964.

Kohl, A.L., and Reisenfeld, F.C. Gas Purification, McGraw-Hill Book Co., Inc., New York, 1960.

Korobeinichev, O.P. "Kinetics of H_2S and COS reactions with bauxite at elevated temperatures", Kinet. Katal. 8 (2) 471, 1967. Cited in CA 76609j, 67, 1967.

Kubaschewski, O., Evans, E.L., and Alcock, C.B. Metallurgical Thermochemistry, Pergamon Press, London, 1967.

Kullerud, G. and Yoder, H.S. "Pyrite stability relations in the Fe-S system", Economic Geology, 54, 533, 1959.

Kunii, D., and Levenspiel, O. Fluidization Engineering, John Wiley & Sons, Inc., New York, 1969.

Leva, M. Fluidization, McGraw-Hill Book Co., New York, 1959.

Levenspiel, O., Chemical Reaction Engineering, John Wiley & Sons, Inc., New York, 1972.

Lewis, P.S., Belt, R.J., and Liberatore, A.J. "Low-BTU fuel gas for power generation", Paper presented at the 1973 Lignite Symposium, University of North Dakota, Grand Forks, N.D., May 1973.

Maa, P.S., Lewis, C.R., and Hamrin, C.E.,Jr., "Sulfur transformation and removal for Western Kentucky coals", Fuel, 54, 62, 1975.

Meyer, J.P., and Edwards, M.S. "A survey of processes for high temperature-high pressure gas purification", Publication ORNL/TM-6178, Oakridge National Laboratory, Oakridge, TN, Nov. 1978.

Meyers, R.A. Coal Desulfurization, Marcek Dekker, Inc., New York, 1977.

Montilo, I.A., Sivakov, E.V., Paikina, R.I., and Kiseleval, L.O. "Study of the reaction of water vapor with iron sulfide at high temperatures", Tr. Ural's k. N-i.i Proekt. In-ta Med. Prom-sti, 18, 175 (1975). Cited in CA 141282q, 84, 1976.

Morrison, G.I. "Hot gas cleanup", Report ICTIS/TR03, IEA Coal Research, London, March 1979.

Natesan, K., and Philbrook, W.O. "Oxidation kinetic studies of zinc sulfide in a fluidized-bed reactor", Met. Trans., 1, 1353, 1970.

Niwa, K., Wada, T., and Shiraishi, Y. "Roasting reaction of ferrous sulfide", Journal of Metals, Trans. AIME, 269, Feb. 1957.

Oldaker, E.C., Poston, A.M., and Farrior, W.L. "Removal of hydrogen sulfide from hot low-BTU gas with iron oxide-fly ash sorbents", Publication MERC/TPR-75/1, Morgantown Energy Research Center, U.S. ERDA, 1975(a).

Oldaker, E.C., Poston, A.M., and Farrior, W.L. "H_2S removal from hot producer gas with a solid fly ash-iron oxide sorbent", Publication MERC/TPR-75/2, Morgantown Energy Research Center, U.S. ERDA, 1975(b).

Oldaker, E.C., Poston, A.m., and Farrior, W.L. "Laboratory evaluation of properties of fly ash-iron oxide absorbents for H_2S removal in hot low-BTU gas". Paper presented at the ACS National Meeting, Chicago, Illinois, 1975(c).

Othmer, D.F. Fluidization, Reinhold Publishing Corp., New York, 1956.

Ozawa, Y. "Regeneration of coked catalyst in adiabotic fixed beds at lower temperatures", Ind. Engng. Chem. Process Design Develop., 8, 378 (1969).

Purcell, J.E., and Ettre, L.S. "Analysis of hydrogen with thermal conductivity detectors", Journal of Gas Chromat., 69, 1965.

Reeve, L. "Desulfurization of coke oven gas at Appleby-Frodingham", J. Inst. Fuel, 31, 319 1958.

Richter, E., and Hoffman, H. "Kinetics of heterogeneous fluid-solid reactions, Intl. Chem. Engng., 17 (2), 1977.

Sands, A.E., and Schmidt, L.D. "Recovery of sulfur from synthesis gas", Ind. Engng. Chem., 42, No. 11, 2277, 1950.

Schrodt, J.T. "Hot gas desulfurization", Report No. ORO-5076-1, University of Kentucky Research Foundation, University of Kentucky, Lexington, Kentucky, Nov. 1976.

Schrodt, J.T. "Hot gas desulfurization", Report No. ORO-5076-2, University of Kentucky Research Foundation, University of Kentucky, Lexington, Kentucky, Feb. 1977(a).

Schrodt, J.T. "Hot gas desulfurization" Report No. ORO-5076-3, University of Kentucky Research Foundation, University of Kentucky, Lexington, Kentucky, Jun. 1977(b).

Schrodt, J.T. "Hot gas desulfurization", Report No. ORU-5076-4, University of Kentucky, Lexington, Kentucky, Dec. 1977(c).

Schrodt, J.T. "Hot gas desulfurization", Report No. ORO-5076-5, University of Kentucky, Lexington, Kentucky, Dec. 1978.

Schrodt, J.T., and Hahn, O.J. "Hot fuel gas desulfurization", Report No. IMMR 15-PD11-76, Institute for Mines and Minerals Research, University of Kentucky, Lexington, Kentucky, May 1976.

Schrodt, J.T., and Best, J.E. "Sulfur recovery from fuel gas desulfurization sorbents", AIChE Symp. Ser., 74 (175), 184, 1978.

Schrodt, J.T., Hilton, G.B., and Rogge, C.A. "High-temperature desulfurization of low-CV fuel gas", Fuel, 54, 269, 1975.

Shakhtahtinskii, G.B., Talybly, A.I., Guliev, A.I., Azizov, E.T., and Veliev, R.A. "Formal kinetics of the fluidized bed roasting of iron sulfide from a Filizchai pyrite concentrate", Dokl. Akad. Nauk. Az. SSR, 30 (6), 33, 1974 cited in CA 62428x, 82, 1975.

Shultz, F.G., Chidester, G.E., and Collect, F.E. "Iron oxide-fly ash sorbent", U.S. Patent 3,579, 293, assigned to the U.S. Secretary of the Interior, 1971.

Shultz, F.G., and Berber, J.S. "Hydrogen sulfide removal from hot producer gas with sintered adsorbents", J. Air Poll. Control Assoc., 20 (2), 93, 1970.

Skelland, A.H.P., Diffusional Mass Transfer, John Wiley & Sons, Inc., New York, 1974.

Sohn, H.Y. and Szekely, J., "Structural model for gas-solid reactions with a moving boundary. III. General dimensionless representation of the irreversible reaction between a porous solid and a reactant gas", Chem. Engng. Sci., 27, 763, 1972.

Smith, J.M. Chemical Engineering Kinetics, McGraw-Hill Book Co., New York, 1970.

Sorrel, G., and Hoyt, W.B. "Collection and correlation of high temperature hydrogen sulfide corrosion data", Corrosion, 12 (5), 33, 1956.

Stone & Webster Engineering Corporation. "Purification of hot fuel gases from coal or heavy oil", Interim Report EPRI 243-2, Nov. 1974.

Szekely, J., Evans, J.W., and Sohn, H.Y. Gas-solid Reactions, Academic Press, New York, 1976.

Turkdogan, E.T. "Iron-sulfur system. Part I: Growth rate of ferrous sulfide on iron and diffusivities of iron in ferrous sulfide", Trans. Met. Soc. AIME, 242, 1665, 1968.

U.S. Bureau of Mines. "Bibliography of processes for removing hydrogen sulfide from industrial gases--Jan. 1950-Dec. 1957", Information Circular 7886, 1959.

Vanyukov, A.V., and Bruek, V.N. "Heterogeneous processes studied by differential thermal analysis", Izv. Vyssh. Ucheb. Zaved., Tsvet. Met., (1), 18, 1973. Cited in CA 70640p, 79, 1973.

Wen, C.Y. "Non-catalytic heterogeneous solid-fluid reaction models", Ind. Engng. Chem., 60 (9), 1968.

Wen, C.Y., Tseng, S.C. and Tone, S. "Reactivity of iron sulfide in sulfur dioxide atmosphere", West Virginia University, Morgantown, WV, 1978. Report prepared for Morgantown Energy Research Center.

Westmoreland, P.R., Gibson, J.B., and Harrison, D.P. "Comparative kinetics of high-temperature reaction between H_2S and selected metal oxides", Environ. Sci. Tech., 10 (7), 659, 1976.

Yates, J.G., "Fluidized-bed reactors", The Chemical Engineer, 671, Nov. 1975.

Zabolotny, E.R., and Kuhr, R.W. "Waste treatment advances: hot gas purification", Chem. Engng. Prog., 72 (10), 69, 1967.

Zabrodsky, S.S. "Hydrodynamics and heat transfer in fluidized beds", The M.I.T. Press, Cambridge, Mass., 1966.

Zahradnik, R.L. "Coal conversion R & D: what the government is doing", Chem. Eng. Prog., 25, June 1976.

Zenz, F.A. and Othmer, D.F. Fluidization and Fluid-particle Systems, Reinhold Publishing Corp., New York, 1960.

Zahuranee, G., and Simkovich, G. "Inert-marker studies during high temperature formation of FeS_2 from FeS_{1+x}", Fuel, 57, 787, 1978.

VITA

The author, Chat Parameswaran Mohan, was born on September 25, 1946 at Koduvayur, Kerala State, India. He attended the Ramakrishna Mission High School at Madras, India and matriculated in April, 1962. He then successfully completed the Pre-University course at Loyola College, affiliated to the University of Madras, Madras in April, 1963. He entered the A. C. College of Technology, University of Madras at Madras in the Fall of 1963 and received the Bachelor of Technology degree in Chemical Engineering in April 1968. After this, he joined the Indian Institute of Science at Bangalore, India in the Fall of 1968 and received the Master of Engineering degree in Chemical Engineering with specialization in Chemical Process and Plant Design in July, 1970. Following graduation, he enrolled in the Speed Scientific School of the University of Louisville, Louisville, Kentucky in the Fall of 1970 and completed his work for the Master of Science degree in Chemical Engineering during the Summer of 1972. He then worked for Corning Glass Works at Louisville, Kentucky as a Process Engineer during the period Sept., 1972-Sept., 1976. During Fall, 1976, he entered the School of Engineering

at the University of Kentucky, Lexington, Kentucky working towards the Doctor of Philosophy degree in Chemical Engineering. Upon completion, he joined the Monsanto Company in Saint Louis, Missouri as a Senior Research Engineer.

*U.S. GOVERNMENT PRINTING OFFICE: 1981-740-145 1295

LEGIBILITY NOTICE

A major purpose of the Technical Information Center is to provide the broadest possible dissemination of information contained in DOE's Research and Development Reports to business, industry, the academic community, and federal, state, and local governments. Non-DOE originated information is also disseminated by the Technical Information Center to support ongoing DOE programs.

Although large portions of this report are not reproducible, it is being made available only in paper copy form to facilitate the availability of those parts of the document which are legible. Copies may be obtained from the National Technical Information Service. Authorized recipients may obtain a copy directly from the Department of Energy's Technical Information Center.